Peptide-loaded, shear sensitive hydrogel as a novel topical delivery system for wound management and repair

Luke Speers MPharm(Hons)

Faculty of Life and Health Sciences

Ulster University

Thesis submitted for the degree of

Doctor of Philosophy

May 2018

I confirm that the word count of this thesis is less than 100,000 words

Declaration

I hereby declare that for 2 years following the date on which the thesis is deposited in the Research Office of the Ulster University, the thesis shall remain confidential with access or copying prohibited. Following expiry of this period I permit

1. The Librarian of the University to allow the thesis to be copied in whole or in part without reference to me on the understanding that such authority applies to the provision of single copies made for study purposes or for inclusion within the stock of another library.
2. The thesis to be made available through the Ulster Institutional Repository and/or EThOS under the terms of the Ulster e-Theses Deposit Agreement which I have signed.

IT IS A CONDITION OF USE OF THIS THESIS THAT ANYONE WHO CONSULTS IT MUST RECOGNISE THAT THE COPYRIGHT RESTS WITH THE UNIVERSITY AND THEN SUBSEQUENTLY TO THE AUTHOR ON THE EXPIRY OF THIS PERIOD AND THAT NO QUOTATION FROM THE THESIS AND NO INFORMATION DERIVED FROM IT MAY BE PUBLISHED UNLESS THE SOURCE IS PROPERLY ACKNOWLEDGED.

This thesis is the sole work of the author and has not been submitted for any previous application for a higher degree.

Luke Speers

Acknowledgements

I would like to express my sincere thanks to my supervisor Professor Paul McCarron for his invaluable help, advice and guidance throughout my PhD. I would also like to thank my secondary supervisors Dr Murtaza Tambuwala and Dr Nigel Ternan for their contributions. Thanks also to the technical staff within the School of Pharmacy and Pharmaceutical science for their help, advice, technical expertise and those all-important words of encouragement when having a bad day. I would also like to express my gratitude to the Department of Employment and Learning (DEL) for funding the work.

To my fellow comrades, of whom there are too many to mention, thank you for making my time as a postgraduate at Coleraine enjoyable and I wish you all every success in your future careers. However, there are two people I must mention, Mr Dean Nicholas and Dr Naomi Todd. Thanks Dean for taking the time to take numerous photographs of hydrogels for various presentations and, indeed, this thesis. Thanks also for the endless discussions on a plethora of topics, including our ventures into community pharmacy. A massive thank you must go to Naomi for taking the time to introduce me to the world of immunofluorescent chemistry and for her help and advice when it came to the completion of this investigation. Not forgetting that eventful day in the 'big smoke!'

Finally, a very special thank you to my parents and wife Sabina for their endless support and encouragement. Sabina, at least now there will be no more 'PhD-talk' to endure.

Summary

The use of pharmaceutically active peptides and proteins has increased significantly over the last 30 years. Topical delivery of growth factors to chronic wounds to enhance wound management and repair have been of particular interest. The aim of the work in this thesis was to evaluate the ability of the PVA-borate hydrogel formulation to deliver biologically active protein payloads. The unique viscoelastic properties of PVA-borate hydrogels are advantageous for application to wounds. The hydrogel can flow into the wound crevasses providing maximal surface area for drug delivery. Yet, they maintain enough cohesive integrity of its cross-linked network to allow for complete and intact removal from the wound, without causing any trauma to newly formed tissue. The ability of the PVA-borate hydrogel to maintain a moist environment and also absorb small volumes of exudate from low exuding wounds also aids wound healing.

Several model payloads (BSA, haemoglobin, trypsin and pepsin) were incorporated into the hydrogel. These proteins where found to change the viscoelastic properties of the PVA-borate hydrogel, but, were released in a sustained manner from the hydrogel without undergoing any degradation. This investigation indicated that the PVA-borate hydrogel is capable of providing a sustained release of protein payloads with certain physical and chemical characteristics.

Insulin-like growth factor-1 (IGF-1) was incorporated into the hydrogel and found not to effect the viscoelastic properties of the hydrogel. *In vitro* release studies confirmed that the hydrogel provided a sustained release of IGF-1, which had maintained its biological activity and not experienced any degradation.

Cell culture studies confirmed that IGF-1-loaded PVA-borate hydrogels can stimulate fibroblast and keratinocyte migration and proliferation. Therefore, the

work in this thesis demonstrates that IGF-1-loaded hydrogels may have a beneficial use in the management and repair of chronic and recalcitrant wounds.

Abbreviations

3D	3-dimensional
ABI	Ankle-brachial index
ALS	Acid labile subunit
ANOVA	Analysis of variance
BCA	Bicinchoninic acid
BMP	Bone morphogenic proteins
BSA	Bovine serum albumin
CBD	Collagen-binding domain
CVD	Chronic venous disease
CVI	Chronic venous insufficiency
DMSO	Dimethyl sulfoxide
ED_{50}	Median effective dose
ECM	Extracellular matrix
EGF	Epidermal growth factor
ELISA	Enzyme-linked immunosorbent assay
EPUAP	European Pressure Ulcer Advisory Panel
ERK	Extracellular signal-regulated kinases
FDA	Food and Drug Administration
FGF	Fibroblast growth factor
FGFR	Fibroblast growth factor receptor
g	Grams
G’	Storage modulus (elastic solid-like component)
G”	Loss modulus (viscous liquid-like component)
GH	Growth hormone

Hb	Haemoglobin
HCEC	Human corneal epithelial cells
HCl	Hydrochloric acid
HER	Human epidermal growth factor receptor
Hrs	Hours
HSPG	Heparan sulphate proteoglycans
ICU	Intensive care unit
IGF	Insulin-like growth factor
IGFBP	Insulin-like growth factor binding protein
IgG	Immunoglobulin G
IgM	Immunoglobulin M
IL	Interleukin
IRS-1	Insulin receptor substrate-1
JAK-STAT	Janus tyrosine kinase-signal transducers and activators of transcription
JNK	c-Jun N-terminal kinases
kDa	Kilodalton
KGF	Keratinocyte growth factor
K_M	Michaelis constant
mA	Milliamps
MAPK	Mitogen-activated protein kinases
mg	Milligram
mL	Millilitre
mm	Millimetres
mM	Millimolar

MMP	Matrix metalloproteases
mRNA	Messenger ribonucleic acid
NF-Kβ	Nuclear factor- Kβ
ng	Nanogram
nm	Nanometres
NaCl	Sodium chloride
NHS	National Health Service
NICE	National Institute for Health and Care Excellence
NPUAP	National Pressure Ulcers Advisory Panel
NSILA	Non-suppressible insulin-like activity
PAD	Peripheral arterial disease
PBS	Phosphate buffer saline
PDGF	Platelet-derived growth factor
PDI	Polydispersity index
PDK-1	Phosphoinositide-dependent protein kinase-1
PEG	Poly(ethylene glycol)
PET	Poly(ethylene terephthalate)
PI3K	Phosphoinositide 3-kinase
PIP_2	Phosphatidylinositol 4,5-bisphosphate
PKB	Protein kinase-B
PKC	Protein kinase-C
PLGA	Poly(D,L-lactide-co-glycolide)
PMMA	Poly(methyl methacrylate)
PVA	Poly(vinyl alcohol)
PVAc	Poly(vinyl acetate)

PVD	Peripheral vascular disease
PVP	Poly(N-vinylpyrrolidone)
rpm	Revolutions per minute
RTP	Room temperature and pressure
SD	Standard deviation
SDS-PAGE	Sodium dodecyl sulphate poly(acrylamide) gel electrophoresis
SEM	Standard error of the mean
sVEGFR-1	Soluble vascular endothelial growth factor receptor-1
TGF-β	Transforming growth factor-β
TIMP	Tissue inhibitors of metalloproteinases
TNF-α	Tumour necrosis factor-α
UV-Vis	Ultraviolet-visible light
V	Volts
VEGF	Vascular endothelial growth factor
VEGFR	Vascular endothelial growth factor receptor
V_{max}	Maximum enzyme velocity
VRAP	VEGFR-associated protein
v/v	Volume/volume
w/w	Mass/mass
WADA	World Anti-Doping Agency
µg	Microgram
µL	Microliter
µm	Micrometer
°C	Degrees Celsius

CONTENTS

Chapter 1

Chapter 1

1 Introduction

1.1 Wounds

By definition, a wound is the loss of integrity and continuity of the epithelial layer of the skin, which may also include damage to the structure and function of underlying tissue (Enoch & Leaper, 2008). Wounds can be classified clinically as either acute or chronic according to the period of time that it takes the wound to heal (Velnar *et al.*, 2009). An acute wound usually fully repairs within 5 to 10 days, and within a maximum of six months. Acute wounds can be accidental due to a traumatic event, such as a laceration or abrasion, but can also be deliberate, such as an incision made by a surgeon. A chronic wound is one which has not progressed through the normal phases of healing within the expected time frame. The healing process may be disrupted at one or more of the stages resulting in the chronic state. Patient comorbidities and medication can also complicate the wound healing process (Menke *et al.*, 2007). In 2008, it was reported that 200,000 people in the UK had a chronic wound, costing the NHS an estimated £2.3–3.1 billion per year (Posnett & Franks, 2008).

1.2 Normal wound healing

Normal wound healing involves a highly regulated, complex series of events involving multiple growth factors and cytokines that results in the damaged tissue returning fully to its normal anatomical structure and function (Enoch & Leaper, 2008). The wound healing process involves three main stages, inflammatory, proliferation and remodelling. Some authors document a fourth initial stage known

as haemostasis, which is an immediate response by the vascular tissue to stop the bleeding (Li *et al.*, 2007). The different phases have a degree of overlap between them; however, they are still well defined with specific cell types only being present during specific phases of the healing process (Enoch & Leaper, 2008).

1.2.1 Haemostasis

Haemostasis is an immediate response to injury of blood vessels, with the main aim being to prevent severe blood loss and protect vital organs. The two main processes that occur during haemostasis are the development of a fibrin clot and coagulation (Li *et al.*, 2007). Platelets are the first cells to appear after injury and are activated when exposed to adhesive proteins, such as collagen and fibronectin of the extracellular matrix. Aggregation of the platelets triggers Hageman factor XII enzyme, which in turn initiates the intrinsic coagulation pathway (Figure 1.1). This concludes with the conversion of prothrombin to the active serine protease thrombin (Li *et al.*, 2007).

Thrombin carries out the proteolytic cleavage of soluble fibrinogen to insoluble fibrin. The fibrin strands are then cross-linked by factor XIII resulting in formation of a clot through the direct binding of fibrin to the platelets (Li *et al.*, 2007). The damaged tissue, along with activated endothelial cells and monocytes, express a lipoprotein known as tissue factor, which triggers the extrinsic coagulation pathway, which can be seen in Figure 1.1 (Li *et al.*, 2007). The fibrin clot not only has an important role initially in the healing process but also throughout the different phases of the wound healing, even though its degradation by plasminogen begins briefly after the formation of the clot. The fibrin clot acts as a structural frame for the migration of several cells, such as keratinocytes, fibroblasts, leukocytes and

endothelial cells, as well as a reservoir for growth factors, such as fibroblast growth factor-2 (FGF-2), vascular endothelial growth factor (VEGF), insulin-like growth factor-1 (IGF-1) that promote regeneration of the wound (Baum & Arpey, 2005).

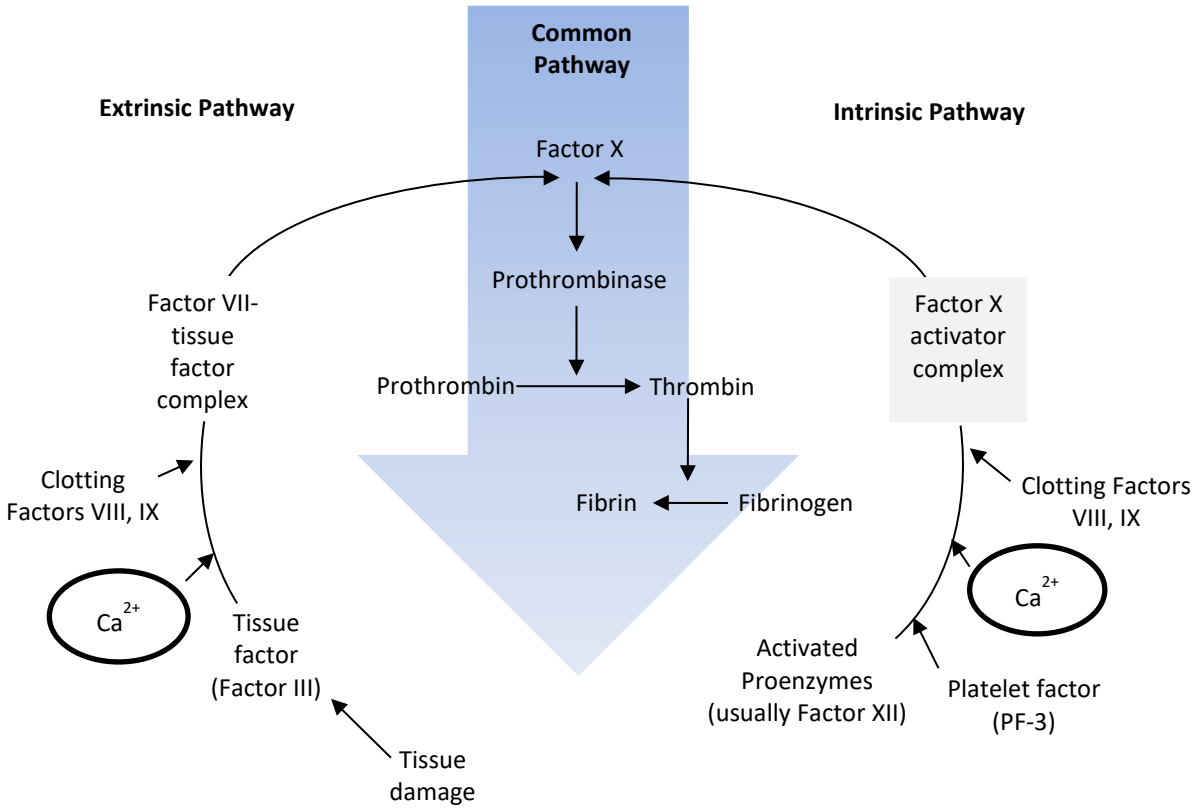

Figure 1.1 A schematic diagram showing the coagulation pathways of the haemostasis phase of wound healing.

1.2.2 Inflammatory Phase

The inflammatory phase follows on from haemostasis and can be characterised by oedema, erythema, heat and pain. It is divided into two sub-phases known as the early and late inflammatory phases (Hart 2002). The overall aim of inflammation is to mount an immune response in order to protect the body against foreign microorganisms. In the early phase, activation of the highly complex classical and alternative pathways of the complement cascade by IgG and IgM antibodies occurs at the onset of inflammation (Nesargikar *et al.*, 2012). Complement factors C3a and

C5a, as well as transforming growth factor-β (TGF-β) and components of the extracellular matrix, are chemo-attractants for circulating neutrophils. The neutrophils adhere to the endothelial cells and then infiltrate into the wound site by diapedesis, within 24-48 hours of injury (Baum & Arpey, 2005; Enoch & Leaper, 2008; Nesargikar *et al.*, 2012). Neutrophils clear the wound site of any bacteria, cell debris and foreign material through phagocytosis. The neutrophils then kill the bacteria using reactive oxygen species and proteolytic enzymes. After a few days, neutrophil activity begins to decrease and it is at this point, approximately 48-72 hours post injury, that the late phase commences (Velnar *et al.*, 2009). Monocytes, which transform into macrophages at the wound site, play a major role in the late phase. The same chemo-attractants as for neutrophils attract the macrophages along with additional growth factors, such as platelet-derived growth factor (PDGF), transforming growth factor-α (TGF-α), IGF-1 and VEGF (Werner & Grose, 2003).

Macrophages continue the removal of debris and apoptotic neutrophils by phagocytosis to allow the healing to progress into later stages of inflammation and onto the proliferation phase. Macrophages carry out further cleaning of the wound site via synthesis and secretion of enzymes known as matrix metalloproteinases (MMP), in particular MMP-1, 3, 9, 10 and 12 out of the 23 MMP known to be present in humans (Nagase *et al.*, 2006). MMP break down components of the extracellular matrix and are regulated by naturally occurring tissue inhibitors of metalloproteinases (TIMP) in order to prevent damage to surrounding healthy tissue. Macrophages also synthesize and secrete a serine proteinase urokinase plasminogen activator (uPA), which converts plasminogen to the active enzyme plasmin. Plasmin is crucial for the digestion of the fibrin clot formed in the initial haemostasis stage to allow for the deposition of granulation tissue as the wound begins to enter the

proliferation phase (Vassalli *et al.*, 1991). Macrophages also stimulate angiogenesis and promote re-epithelialisation through the secretion of several growth factors, such as FGF-2, TGF-β and IGF-1 (Baum & Arpey, 2005). These growth factors activate the recruitment of keratinocytes, fibroblast and endothelial cells and promote re-epithelialisation (Baum & Arpey, 2005).

1.2.3 Proliferation Phase

On the third day, post wounding the proliferation phase begins, overlapping with the late inflammatory stage. Macrophages are present in the wound for two or more weeks at the start of the proliferation phase. Fibroblasts are stimulated to migrate into the wound by factors, such as TGF-β and PDGF, which are released by platelets and other inflammatory cells (Velnar *et al.*, 2009). In the wound, fibroblast cells proliferate abundantly and produce fibronectin, hyaluronan, proteoglycans and collagen. These new proteins help to construct a new extracellular matrix, replacing the old matrix composed of fibrin. The new matrix provides an ideal scaffold to support cell migration and is a reservoir for cytokines, growth factors, and facilitates wound contraction (Li *et al.*, 2007). On completion of proliferation and secretion of the matrix proteins, fibroblast cells undergo a phenotype change to myofibroblasts. Myofibroblasts contain thick bundles of actin, which extend out in a phenomenon known as pseudopodia. These cytoplasmic projections attach specifically to fibronectin and collagen in the extracellular matrix. Once attached, the myofibroblasts begin to retract, causing wound closure by approximating the wound edges. (Velnar *et al.*, 2009). This process is also known as the granulation phase due to the presence of granulation tissue. Granulation tissue is soft, granular and pink in

appearance and characterised histologically by the presence of proliferating fibroblast and capillaries in the loose extracellular matrix (Enoch & Leaper, 2008).

Epithelialisation is controlled by keratinocyte growth factor (KGF) (Werner, 1998), fibroblast growth factor (FGF) (Werner, 1998) and epidermal growth factor (EGF) (Jorissen *et al.*, 2003). KGF is secreted predominately from fibroblast cells and is approximately 26–28 kDa in size. It is not fully understood how it initiates mitogenic activity in keratinocyte cells, but it is thought to be in a paracrine manner (Werner, 1998). EGF will be discussed in greater detail in section 1.4.2. However, upon binding to the EFG transmembrane receptor it causes activation of multiple interlinked pathways, such as Ras/ mitogen-activated protein kinases (MAPK), Src, janus tyrosine kinase-signal transducers and activators of transcription (JAK-STAT), phosphoionositide 3-kinase (PI3K), AKT (Jorissen *et al.*, 2003) In order for complete re-epithelialisation to occur bacterial control needs to have been accomplished, appropriate nutrition available and the wound environment moist. The aim of the re-epithelialisation phase is to restore a fully intact epidermis layer (Li *et al.*, 2007). Keratinocytes begin preparing for migration as early as twelve hours post wounding. Within each cell, there are numerous processes that occur, to prepare for migration, such as flattening and elongation, cytoplasmic projections, loss of cell to matrix contact and decreased cell-to-cell interaction (Li *et al.*, 2007).

Keratinocytes migrate over the granulation tissue, with the leading edge of migrating cells having their ability to proliferative temporarily inhibited. The leading edge of migrating cells leaves behind a close knit layer of proliferating keratinocytes (Baum & Arpey, 2005). The migrating cells use integrin surface receptors to bind to fibronectin in the newly formed ECM in the wound bed to steer the migration edge in the correct direction. MMP are responsible for dissociation of this integrin

fibronectin interaction to allow the edge to continue moving forward. Another source of keratinocytes is thought to be hair bulges that are near to the wound site. These keratinocyte stem cells are thought to migrate into the wound upon injury and contribute to the re-epithelialisation process (Baum & Arpey, 2005). Once the leading edges of the keratinocytes meet, their migration stops. This is known as contact inhibition. The cells then attach to the substratum and begin to develop and form the basement membrane, which separates the epidermis and the underlying dermis.

1.2.4 Remodeling Phase

This phase is characterised by the formation of scar tissue which is constantly being re-organised through degradation and re-synthesis of the extracellular matrix. The aim of the remodeling phase, also known as the maturation phase, is to try and regain normal tissue structure with the maximum tensile strength possible (de Oliveira Gonzalez *et al.*, 2016). Remodeling of the matrix continues up to 1 year or in certain cases longer after re-epithelisation has occurred (Witte & Barbul, 2005). When scar tissue first becomes evident, it is red-pink in colour due to the increased capillary network that was present to aid in the initial stages of the wound healing process. However, as time progresses, the scar begins to change in pigmentation as the capillaries begin to dissipate and there is an increase in collagen fibers (Sorg *et al.*, 2017). Collagen type III is degraded and replaced with newly synthesised collagen type I. Collagen type I becomes thicker and arranges in parallel to one and other forming a dense network (de Oliveira Gonzalez *et al.*, 2016) Another typical characteristic of scar tissue is the absences of sebaceous glands and hair follicles if the wound is deeper than the level of the hair bulbs in the dermis (Martin, 1997).

1.3 Chronic wound healing

A chronic wound can be defined as one that does not progress through the normal stages of wound healing in an efficient and timely manner. Guo and DiPietro (2010) state that it is well documented that most chronic wounds present as ulcers, which can be categorised into three main types; diabetic foot ulcers, venous leg ulcers and pressure ulcers. Table 1.1 shows the annual incidence and economic burden these chronic ulcers had on the NHS in a one year period alone. As well as being a huge financial burden on the health service, they often have a detrimental impact on the individual's quality of life. In the USA, chronic wounds pose a similar problem with 3–6 million people estimated to be affected by these wounds, of which 85 % are ≥ 65 years of age. This has led to an extortionate amount of expenditure on health care, estimated to be greater than $3 billion per year (Menke *et al.*, 2007).

Table 1.1Chronic wound treatment cost to the NHS (Posnett & Franks, 2008)

	Annual incidence	**Cost per patient**	**Annual NHS cost (2005-2006)**
Pressure ulcer	410,000	£4,300–6,400	£1.8–2.6 billion
Venous leg ulcer	108,600	£1,500–1,800	£168–198 million
Diabetic foot ulcer	57,000	£5,200	£300 million
Total	575,600	£4,000–5,400*	£2.3–3.1 billion*

*Values estimated averages

There are many factors, both local (characteristics of the wound itself) and systemic (overall health of the individual), that can affect the repair of a wound at one or more stages of the healing process (Guo & DiPietro, 2010). Systemic factors that can impair wound healing are as follows; age, co-morbidities, obesity, alcoholism,

smoking, poor diet, stress and medications, such as glucocorticoid steroids, non-steroidal anti-inflammatories and chemotherapy.

One problematic local factor is the presence of bacteria or bacterial biofilms, which are a common feature of most chronic wounds. It has been established that a level of $\geq 10^6$ micro-organisms per gram of tissue, regardless of what strain or type of bacteria are present, causes impaired healing of an open wound (Robson & Heggers, 1969; Robson, 1997). Once the bacterial load increases to the critical colonisation level, the body's host immune response is no longer able to fight the infection and the biofilm formation begins (Wysocki, 2002). These biofilms are colonies of bacteria surrounded by a protective layer made of poly(saccharides), which make the bacteria more resistant to antibiotics (Falanga, 2004). Biofilms usually cause erythema, swelling and produce a purulent malodorous exudate. These biofilms consist of a wide range of micro-organisms, such as *Pseudomonas aeruginosa*, *Staphylococcus aureus, Streptococci* and *Enterobacter* (Dowd *et al.*, 2008; Toy & Macera, 2011).

It is well known that for acute wounds to heal it is important that the wound remains moist in order to facilitate re-epithelisation. However, Falanga (2004) states that there is a distinct difference between the wound fluid of an acute and chronic wound. Samples of fluid taken from an acute wound caused an increase in proliferation *in vitro* of fibroblast, keratinocyte and endothelial cells, whereas fluid from chronic wounds caused inhibition of proliferation and angiogenesis (Bucalo, 1993; Drinkwater *et al.,* 2002). In chronic wound fluid, there is also higher than normal concentrations of MMP (Yager *et al.*, 1996) with no increase in TIMP to control the spike in MMP level. As mentioned previously, MMP play a vital role in the proliferation phase, but when they are present in excessive amounts, in particular

MMP 2 and 9, they begin to prevent wound healing by excessive degradation of vital extracellular matrix proteins, such as fibronectin, and prevent keratinocyte migration (Bullen *et al.*, 1995).

Other local factors that have been documented to prevent normal wound healing are impaired blood flow (Falanga, 2004), prolonged hypoxia (Falanga, 2004) and phenotypic changes to wound cells (Stephens *et al.*, 2003). These changes reduce the ability of cells to respond to growth factors and, therefore, proliferate. A phenomena known as fibrin cuff trapping, which will be discussed in section 1.3.2, is also thought to play a role in impairing normal wound healing (Stadelmann *et al.*, 1998).

1.3.1 Diabetic foot ulceration

It is estimated that the 4-10 % of patients diagnosed with diabetes mellitus will experience a foot ulcer at some point in their lifetime (Wu *et al.*, 2007). It is estimated that within the UK there are approximately 64,000 individuals at any one time with an active diabetic foot ulcer (Posnett & Franks, 2008), with 2,600 patients requiring lower limb amputation each year as a result of ulceration (Gordois *et al.*, 2003). As seen in Table 1.1, this is estimated to cost the NHS £300 million per year with this cost most certainly increasing every year.

Diabetes mellitus is a disease in which the body is unable to regulate its blood glucose levels sufficiently, causing hyperglycaemia. It is divided into two main types; Type 1 or Type 2. In patients suffering from Type 1 diabetes, hyperglycaemia is a result of their pancreatic islet cells producing no insulin to lower the blood glucose level. In Type 2 diabetes, hyperglycaemia is due to a combination of factors, such as insulin resistance and impaired insulin production, as well as life style and

genetic factors (Reiber *et al.*, 1998). Diabetic foot ulcers present as a complication in patients who have diabetes mellitus. The complex nature of diabetes results in the patient being at a higher risk of secondary conditions, such as neuropathy and peripheral vascular disease (PVD). These secondary conditions are what results in the formation of foot ulcers through a chain of events.

Neuropathy is the dysfunction of the peripheral nerves affecting the sensory and motor nerve fibers. Sensory neuropathy results in the patient having a diminished or complete loss of the perception of pain, heat and pressure (Reiber *et al.*, 1998). Therefore, the patient does not feel repetitive minor injury, or in some cases, major injury to their foot. Motor neuropathy affects the muscles in the foot causing them to weaken and experience partial paralysis. This causes changes in the balance of the intrinsic muscles within the foot, resulting in restricted podiatric movement when walking, leading to deformities such as, claw toe, hammer toe and Charcot foot (Reiber *et al.*, 1998; Jeffcoate & Harding, 2003). Another side effect of neuropathy is the skin on the feet becoming dry and brittle. As a result of the muscle deformities, the dry brittle skin becomes stretched, making it easier to puncture as it has reduced tensile strength (Shaw & Boulton, 1997). A combination of these neuropathic factors results in the formation of skin calluses, which if left untreated, become ulcerated.

PVD is when blood vessels begin to narrow and block, particularly in the lower extremities, reducing blood flow to that particular area of the body. PVD has an active role in causing ulceration, gangrene and impaired healing (Pecoraro *et al.*, 1990; Shaw & Boulton, 1997). The incidence of PVD in a diabetic patient is four times greater than a non-diabetic person, with the incidence increasing with duration of diabetes and the age of the patient (Pecoraro *et al.*, 1990). Pecoraro *et al*. (1990)

also documented that 62 % of non-healing foot ulcers are in patients who have PVD, of which, 46 % end up needing amputation. PVD causes arteriolar-venular shunting, leading to ischaemia at the site of ulceration. As a result of ischaemia, there is a reduced delivery of oxygen, nutrients, cytokines and growth factors, impairing wound healing (Jeffcoate & Harding, 2003).

A typical diabetic foot ulcer can be seen in Figure 1.2. A neuropathic ulcer will usually present on the underside of the foot, often at the metatarsal heads. An ulcer arising from PVD or ischaemia can, however, present anywhere on the foot or ankle. Diabetic foot ulcers were first classified using a grading system developed by Wagner, which only took into account the depth of the ulcer (Wagner, 1981). The Wagner classification was developed further with addition of a Wound Severity Scoring System. The scoring system takes into account factors such as, ulcer duration, pulses, oedema, neuropathy, ischaemia and infection. The scoring system also accounts for the presence or absence of necrotic tissue and granulation tissue. There are now many variations of this system, all of which give a more detailed description of the ulcer compared to Wagner's initial scoring system making choice of treatment easier for a multidiscipline clinical team (Table 1.2).

Table 1.2 Example of a diabetic foot ulcer grading system (Edmonds, 2006)

Grade	**Classification**	**Description**
1	Normal foot	No risk factors present
2	At risk foot	One or more risk factors present (neuropathy, ischaemia, deformity, callus, oedema).
3	Ulcerated foot	Neuropathic ulcer present on plantar surface and/or neuroischaemic ulcer on margins of foot.
4	Infected foot	Ulcer infected, cellulitis, lymphangitis, osteomyelitis.
5	Necrotic foot	Wet necrosis in neuropathic foot; dry necrosis in neuroischaemic foot-amputation likely.

Figure 1.2 A photograph taking of a typical neuropathic diabetic foot ulcer presenting on the underside of the foot close to the metatarsal head surround by callus skin (Jeffcoate & Harding, 2003).

Clinical studies show that early treatment with insulin and administration of vitamin A decreased the healing time and increased the strength of the healed wound (Laing, 1994). Laing (1994) also found in a study that on average it took two weeks longer for neuropathic ulcers in the plantar region of the foot to heal in the diabetic patient group compared to the non-diabetic group. However, the difference was not statistically significant. The best resolution to diabetic foot ulcers is to prevent occurrence, rather having to treat them. Screening of diabetic patients annually for risk factors and treating any early signs that can lead to ulceration can significantly reduce the burden a ulcer will have on the patient's life style as well has the economic cost of lengthy hospital stays and surgery needed for late stage ulcers.

1.3.2 Venous leg ulceration

Venous leg ulceration is estimated to cost the NHS in the UK £400 million per annum (Simon *et al.*, 2004) and account for 80% of all leg ulcers (Kolluri, 2014). Treatment of one individual ulcer alone costs the NHS approximately £1,298–£1,526 per year based on costings in 2001 (Iglesias *et al.*, 2010). The prevalence of chronic leg ulceration is approximately 0.1–0.3% (Nelzen *et al.*, 1994), with an estimated 1% of the UK population suffering from a leg ulcer at some point in their life time (Callam, 1992).

Venous leg ulcers are most commonly found in the area between the mid-calf to the ankle, known as the gaiter region. A typical venous ulcer will present as irregular in shape, generally shallow in depth and rarely extending to the muscle or bone. There may be red granulation tissue or a yellow coloured exudate present in the wound bed. Necrotic black tissue is rarely seen in venous ulcers (Etufugh & Phillips 2007). A typical venous ulcer can be seen in Figure 1.3.

Figure 1.3 A picture of a typical venous leg ulcer in the gaiter region. The ulcer has the typical characteristics of a venous leg ulcer shallow in depth, irregular in shape, with granulation tissue present around the perimeter of the ulcer (Grey *et al.*, 2006).

Blood flow within the lower leg is controlled by the venous system, which is made up of three types of veins; the superficial veins, perforator veins and deep veins (Etufugh & Phillips, 2007). These veins all contain venous valves, which project from the wall of the vein and prevent the backflow of blood. The calf muscle within the lower leg acts as a mechanical pump. On contraction of the muscle, there is a slight increase in pressure within the deep veins causing the values to shut, preventing retrograde blood flow and the blood is pumped to the heart. On relaxation of the calf muscle, the pressure drops and the valves re-open. This allows the de-oxygenated blood to drain from the superficial veins at the skin surface back into the deep veins situated in the calf muscle via the perforating veins (Figure 1.4) (Etufugh & Phillips 2007).

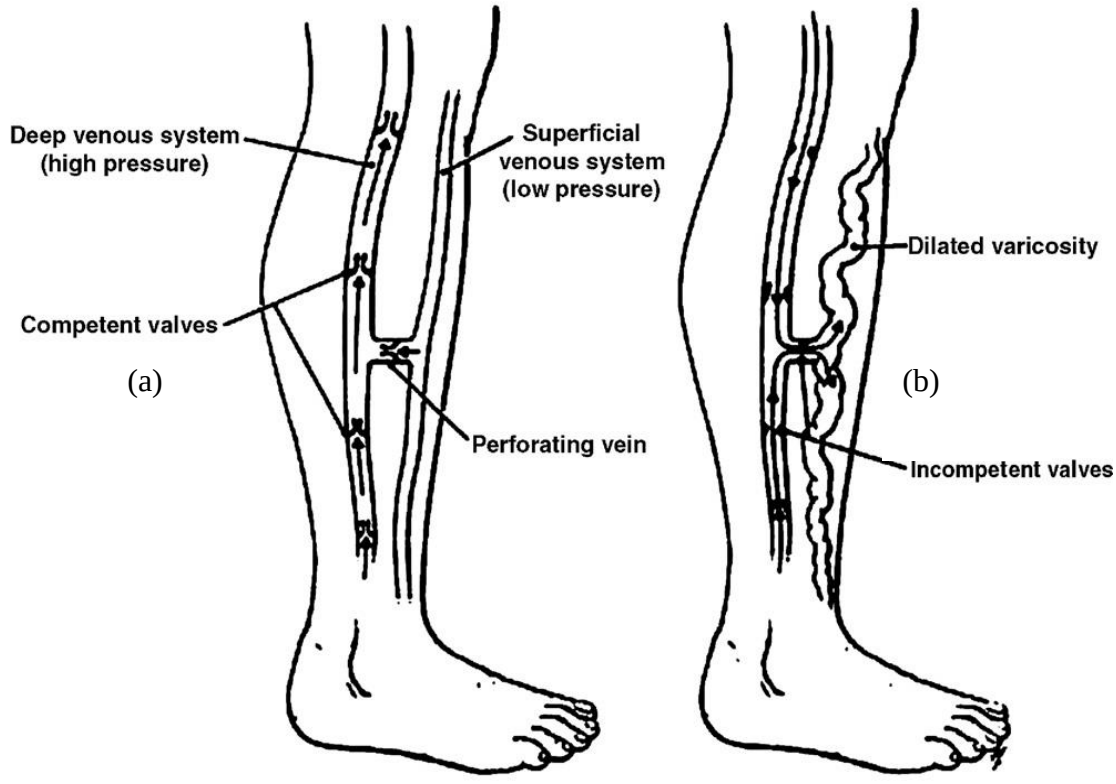

Figure 1.4 Schematic anatomy of the venous system of the lower leg. (a) Normal venous system function and (b) Venous insufficiency (Etufugh & Phillips 2007).

When this process does not occur as it should, it causes venous hypertension, which leads to a condition known as chronic venous insufficiency (CVI) or chronic venous disease (CVD) (Raffetto, 2009). CVI is the inability of the veins in the lower extremities to return blood towards the heart. The term CVI covers a range of pathological abnormalities, ranging from leg oedema, varicose veins, to the more serious venous leg ulcer. There are numerous risk factors for CVI, such as family history, advanced age, previous or current deep vein thrombosis (DVT), pregnancy, obesity, leg trauma and occupations that require prolonged periods of standing (Etufugh & Phillips 2007).

The exact pathophysiology that results in venous hypertension, leading to ulceration, is still unknown. However, over the past several decades, numerous theories have been proposed. Burnard *et al*. (1982) put forward the first theory, known as the fibrin cuff theory. The fibrin cuff theory proposes that raised venous pressure causes expansion of the endothelial pores, leading to molecules, such as fibrinogen, being able to pass from the capillary blood into the interstitial fluid. The fibrinogen forms an insoluble cuff of fibrin around the dermal capillaries. It was proposed that the fibrin cuff inhibited sufficient oxygen and nutrient diffusion from the blood capillaries into the interstitial fluid, resulting in cell death, tissue degradation and formation of the chronic venous ulcer (Burnand *et al.*, 1982). Another theory proposed is the inflammatory trap theory (Liu *et al.*, 2011). This is an extension to the fibrin cuff theory and stipulates that inflammatory cells, such as leukocytes, become trapped in the fibrin cuff (Coleridge Smith *et al.,* 1988). The trapped leukocytes then release free radicals and proteolytic enzymes, which cause further damage to the endothelial cells and capillaries. This causes an increase in their permeability to macromolecules, further exacerbating the fibrinogen depositing

and inflammatory state. This leads to a hypoxic environment, resulting in cell death and ulceration (Abbade & Lastoria, 2005). More recent studies have extended this theory by stating that there is an imbalance in both the wound bed and wound exudate of numerous key cytokines, growth factors and enzymes. The most frequently studied are neutrophil elastase, MMP, transforming growth factor-beta (TGF-β), tumour necrosis factor-alpha (TNF-α) and α2-macroglobulin (Abbade & Lastoria, 2005; Liu *et al.*, 2011).

1.3.3 Pressure ulceration

Despite having NICE clinical guidelines available for the treatment and management of pressure ulcers, as well as advanced medical devices and technology readily available, the occurrence of pressure ulcers is still increasing. Cox (2011) reported that from 1993 to 2006, there was an 80 % increase in the occurrence of pressure ulcers in hospitalised patients. It was also found that the prevalence rates (14–42 %) were highest in ICU patients, with 1 in 5 hospital patients estimated to have a pressure ulcer (Posnett & Franks, 2008; Cox, 2011). As seen in Table 1.1, approximately 410,000 people develop a pressure ulcer annually in the UK, costing the NHS an estimated £1.8–2.6 billion from 2005–2006.

Hippocrates in 400 BC was the first to document a pressure ulcer in his clinical lecture on bedsores saying "at times they erupt from under intact skin" (Black *et al.*, 2007). The European Pressure Ulcer Advisory Panel (EPUAP) defines a pressure ulcer as an area of localised damage to the skin and underlying tissue caused by pressure, friction or shear forces or a combination of these (Grey *et al.*, 2006). Pressure ulcers occur as a result of long-term repetitive compression of soft tissue, most commonly between an external surface and a boney prominence.

Approximately two thirds of pressure ulcers develop around the pelvis region, with the other third being primarily in on the lower limbs, in particular the heel. A typical pressure ulcer can be seen in Figure 1.5, with the elderly being the most susceptible age group to develop pressure ulcers, especially those over 70 years old (Grey *et al.*, 2006).

Figure 1.5 A picture of a typical pressure ulcer in the pelvic region cover by eschar, which can inhibit accurate grading of the ulcer (McSwiggan, 2011).

There is no exact understanding of what triggers the breakdown of soft tissue in response to the forces mentioned above. The following theories are thought to play a role in pressure related tissue degradation; impaired interstitial fluid flow (Reddy *et al.*, 1981) and lymphatic drainage (Miller & Seale, 1981), ischaemia of the surrounding area (Daniel *et al.*, 1981), sustained deformation of localised cells (Bouten *et al.*, 2003) and reperfusion injury (Peirce *et al.*, 2000). Grey *et al.* (2006) document that sustained high pressure on a specific area causes closure of blood and lymphatic vessels leading to localised tissue ischaemia. Once ischaemic conditions are established, necrosis of the multiple layers of skin, subcutaneous tissue and muscle begins, leading to the onset of ulceration.

It has been calculated that an external pressure of 50 mm Hg, if applied over a boney prominence, can cause an actual pressure of 200 mm Hg on that area of tissue (Grey *et al.,* 2006). Shear forces are the result of the movement of bone and subcutaneous tissue, but not the skin, which is held in a stationary position by frictional forces. Frictional forces can also result from poor fitting prosthetic limbs or shoes, for example. These frictional forces lead to epidermal blistering and increased erosion of the skin surface, which lead to ulcer formation. Grey *et al.* (2006) have reported that the effects of friction is five times more damaging on areas of high pressure if moisture is present. Moisture at the area of high pressure can result from perspiration, incontinence or excessive wound exudate. Moisture also causes skin maceration over a prolonged period of time, which further intensifies the effect of the aforementioned forces.

Over several decades, there has been numerous systems developed for grading pressure ulcers into different stages. The first one to be developed was by Guttmann in 1955 (Black *et al.*, 2007). But the first system using a numeric classification based on the pathology of the ulcer was developed by Shea (1975). In 1989, the National Pressure Ulcers Advisory Panel (NPUAP) developed a 4 stage grading system, which was used widely for the following 20 years, with regular updates and revisions taking place as more knowledge about the pathogenesis of pressure ulcers emerged with advances in medical technology (National Pressure Ulcer Advisory Panel, 1989; Black *et al.*, 2007). The European Pressure Ulcer Advisory Panel (EPUAP) also developed a 4 stage grading system similar to the NPUAP in 1998, which also undergoes regular reviews and updates. A summarised version of the EPUAP grading system can be seen in Table 1.3 (Grey *et al.*, 2006; Black *et al.*, 2007).

Table 1.3 European Pressure Ulcer Advisory Panel grading system

Grade	Description of ulcer
1	Non-blanching redness if intact skin, warmth, increase in firmness of the skin may also be used in people with dark coloured skin as an indicator.
2	Partial thickness skin loss involving epidermis or dermis or both. Ulcer presents on the skin surface as a blister or abrasion.
3	Full thickness skin loss with damage to or necrosis of the subcutaneous tissue.
4	Extensive damage, tissue necrosis evident, damage to muscle, bone or supporting structures with or without full thickness skin loss.

As with diabetic foot ulcers and venous leg ulcers, prevention of risk factors for pressure ulcers is key to reducing the long-term impact on the patient's life style and economic burden on the health system. NICE guidance for the prevention and management of pressure ulcers document the following as risk factors for pressure ulcers; acute illness, age, level of consciousness, limited mobility or immobility, sensory impairment, chronic or terminal diseases, malnutrition or dehydration and past history of pressure damage (National Institute for Health and Care Excellence, 2014).

1.3.4 Arterial ulceration

Arterial ulceration is a common complication in patients who have peripheral arterial disease (PAD). PAD is estimated to affect 8–12 million Americans, of which 20 % are ≥ 65 years of age (Weitz *et al.*, 1996). The prevalence of arterial ulcers are 0.12–1.8 % amongst the American population (Sieggreen & Kline, 2004). Amputation is highly probable (50–60 %) in arterial ulceration, with 10 % of those amputations being above the knee (Hafner *et al.*, 2000)

Arterial ulcers commonly present on, or around, the toes, over boney prominences, or on the heel of the foot. The ulcer has a characteristic punched out look giving the wound well defined edges (Figure 1.6a). The skin surrounding the wound is usually pale, thin, taut, shiny and cool to touch, provided there is no infection present (Grey *et al.*, 2006). There is usually no oedema present with an arterial ulcer compared to a venous ulcer, with wound exudate low or non-existent. In early stage ulceration, the wound has a low volume of slough present and a yellow-like film on the bed, as seen in Figure 1.6a. As ischaemic conditions increase, the tissue quickly becomes gangrenous, particularly if the ulcer is present on a toe, as seen in Figure 1.6b.

Figure 1.6 Photographs of typical arterial ulceration of the foot. a) Shows an arterial ulcer over the boney prominence at the base of the great toe. It can be seen to display the characteristic feature of an arterial ulcer, punched out look with well-defined edges and a yellow film present in the wound bed (Vascular Society of Great Britain and Ireland, 2017). b) Shows an arterial ulcer of the great toe in the later stage of ulceration where gangrene of the toes and foot as occurred (Grey *et al.*, 2006).

Early-stage chronic arterial peripheral disease in the lower extremities causes the patient to experience a cramping sensation in the calf muscle on walking, known as claudication. Claudication has also been reported in the thigh, buttock and foot of PAD patients (Sieggreen & Kline, 2004). The pain experienced by the patient will shift from claudication on walking, which is eased by resting, to pain when resting as the ulcer progresses. This pain, also called rest pain, is most common at night, often waking the individual from their sleep (Sieggreen & Kline, 2004). Rest pain can be relieved by either of the following methods; sleeping upright in a chair, hanging the affected leg down over the edge of the bed, or taking brief walks. Pain experienced with an arterial ulcer is said to be an intense burning sensation, whereas, pain with a venous ulcer is dull, unless excessive exudate or infection are present (Grey *et al.*, 2006).

Blood leaving the heart descends through the descending aorta into a complex network of arteries. Eventually the blood ends up in the anterior tibial artery (Figure 1.7) in the lower leg, which becomes the dorsalis pedis artery at the ankle (Martini & Nath, 2009). The dorsalis pedis artery divides into the medial and lateral pedis arteries, which supply the plantar surface of the foot with oxygenated blood. The medial and lateral pedis arteries form two loops called the dorsal and plantar arches (Martini & Nath, 2009), as seen in Figure 1.7. The dorsal and plantar arches have numerous smaller arteries branching out from them that supplies the furthest away portions of the foot and the toes with oxygenated blood.

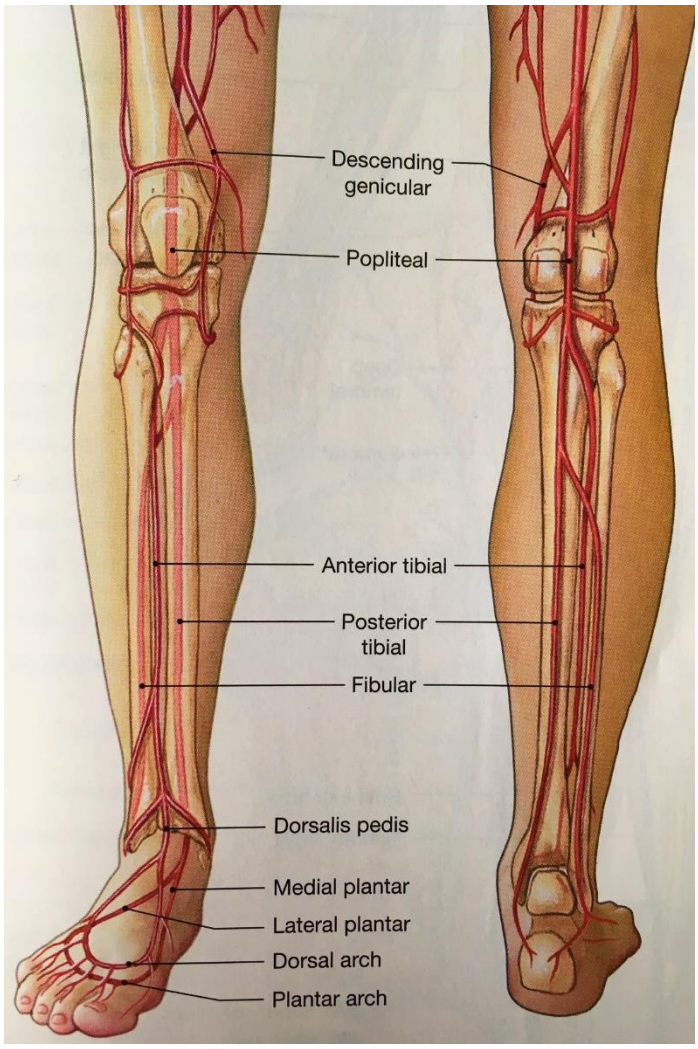

Figure 1.7 A schematic diagram showing the arterial network of the lower limb, in which oxygenated blood travels through (Martini & Nath, 2009).

Arterial ulcers develop as a result of poor arterial blood flow, causing ischaemic tissue, leading to necrotic tissue and ulceration. The most common cause or arterial ulceration is atherosclerosis of the medium and large arteries (Schroeder *et al.*, 2006). Atherosclerosis is the buildup of fatty material, known as atheroma, on the endothelial lining of the arteries (Falk, 2006). Atheroma causes the artery to narrow, therefore, naturally reducing the blood flow. When part of an atheroma plaque breaks away from the arterial wall, it travels downstream to a smaller artery, where it becomes lodged causing complete, or partial, occlusion of the vessel This can cause

a number of life threating events depending where the atheroma becomes lodged, such as a heart attack, stroke or PAD (British Heart Foundation, 2016).

A Doppler ultrasound can be used to determine the extent of the arterial disease. The Doppler ultrasound detects changes in arterial blood flow, with three distinct phases being seen on the trace in normal arterial function. The first phase above the baseline is the forward flow of the blood. The second phase below the baseline is the relaxation of the artery and some retrograde blood flow. The third phase is thought to be the aortic valve bulging during diastole (Sieggreen & Kline, 2004). In early onset PAD, the third phase starts to diminish and as the PAD progresses, the first phase wave becomes dampened and broadened (Sieggreen & Kline, 2004).

The ankle-brachial index (ABI), also known as the ankle-arm index, is another standard test to evaluate PAD. The ABI is defined as the ratio of the systolic blood pressure at the ankle to the systolic blood pressure at the brachial artery in the arm (Aboyans *et al.*, 2012). The ABI is measured using a Doppler ultrasound and blood pressure cuff (Aboyans *et al.*, 2012). The Doppler ultrasound is used in this scenario to determine when to stop inflating the cuff, once the signal disappears, and when to take the pressure reading, once the signal reappears on deflation of the cuff (Schroeder *et al.*, 2006; Aboyans *et al.*, 2012). A summary of the ABI and its descriptors can be seen in Table 1.4.

Table 1.4 Summary of the ankle-brachial index (Sieggreen & Kline, 2004)

Ankle-brachial index value	Classification
1.0–0.9	Normal, asymptomatic
0.71–0.89	Mild disease, claudication present
0.41–0.70	Moderate disease, claudication present
≤ 0.40	Severe disease, rest pain, ulceration

1.4 Growth factors

Growth factors, cytokines and low molecular weight compounds found in the serum play a vital role, instantly after injury and throughout the wound repair process. Immediately after injury, degranulation of α-granules in the platelet cells occurs. The α-granules are the main source of growth factors needed at the initial stage. The blood clot acts as a reservoir for growth factors needed in the latter stages of the wound healing process (Werner & Grose, 2003). Throughout the inflammatory phase, and into the proliferative phase of the healing process, various inflammatory cells, such as macrophages, neutrophils and eosinophils also secrete specific growth factors. These growth factors stimulate various skin cells, such as fibroblasts and keratinocytes.

The exact function and role of many endogenous growth factors is still not fully understood. However, over the last decade, with advances in experimental and clinical studies, some light has been shed on the role of endogenous growth factors in wound healing. Many of the growth factors are believed to have multifunctional roles, in the complex, highly orchestrated, cell signalling network. In this section, several of the main growth factors will be discussed in detail, in relation to wound healing and treatment of chronic wounds.

1.4.1 Platelet-derived growth factor (PDGF)

Platelet-derived growth factor (PDGF) is thought to have several functions in wound healing. PDGF causes chemotaxis of macrophages and neutrophils to the wound site. PDGF also upregulates the production of various components of the extracellular matrix, such as collagen, proteoglycans, fibronectin and hyaluronic acid (Pierce *et al.*, 1991; Heldin *et al.*, 2002). PDGF stimulates fibroblast proliferation, and triggers the phenotype change of fibroblasts to myofibroblasts at the end of the proliferation phase in the wound healing (Werner & Grose, 2003).

PDGF consists of a family of homodimer and heterodimer growth factors. The PDGFs comprise A and B disulfide bonded poly(peptide) chains. Each of the chains are approximately 100 amino acid residues in length (Heldin & Westermark, 1999). The A and B chains are synthesised as precursor molecules, which are then subject to proteolytic cleavage, leading to the formation of three isoforms, PDGF-AA, PDGF-BB or PDGF-AB. The main source of PDGF is from platelet α-granules (Ross *et al.*, 1974). However, numerous types of cells, such as fibroblasts, keratinocytes, macrophages and smooth muscle cells can also synthesise PDGF, in response to external stimuli (Heldin & Westermark, 1999). The majority of these cells can synthesise both chains, suggesting that isoform formation is random. Although these cells are able to produce both poly(peptide) chains, synthesis of each chain is independently controlled at transcriptional and posttranscriptional level (Dirks & Bloemers, 1996). Recently, two new homodimer isoforms of PDGF have been discovered PDGF-CC and DD. The C and D chains have the same motif consisting of eight cysteine amino acids as the A and B chains, but have an extra three residues within the motif (Li *et al.*, 2000; LaRochelle *et al.*, 2001). The mechanism of

activation for PDGF-CC and DD *in vivo* is still unclear, but both can be activated *in vitro* by addition of plasmin (Heldin *et al.*, 2002).

PDGF receptors are α and β transdermal membrane tyrosine kinase receptors, located across the cytoplasmic membrane of target cells. As the isoforms are dimeric, they bind two receptors at the same time causing dimerisation of the receptors (Heldin & Westermark, 1999). An example of one such PDGF isoform receptor binding combination can be seen in Figure 1.8. The receptor specificity for each PDGF isoform is summarised in Table 1.5.

Table 1.5 Summary of receptors specificity for PDGF isoforms

PDGF isoform	**Tyrosine kinase receptor**
AA	αα
AB	αα, αβ
BB	αα, αβ, ββ
CC	αα, αβ*
DD	ββ, αβ*

* Some authors document that PDGF- CC and DD can also induce αβ receptor complexes (Gilbertson *et al.*, 2001; LaRochelle *et al.*, 2001).

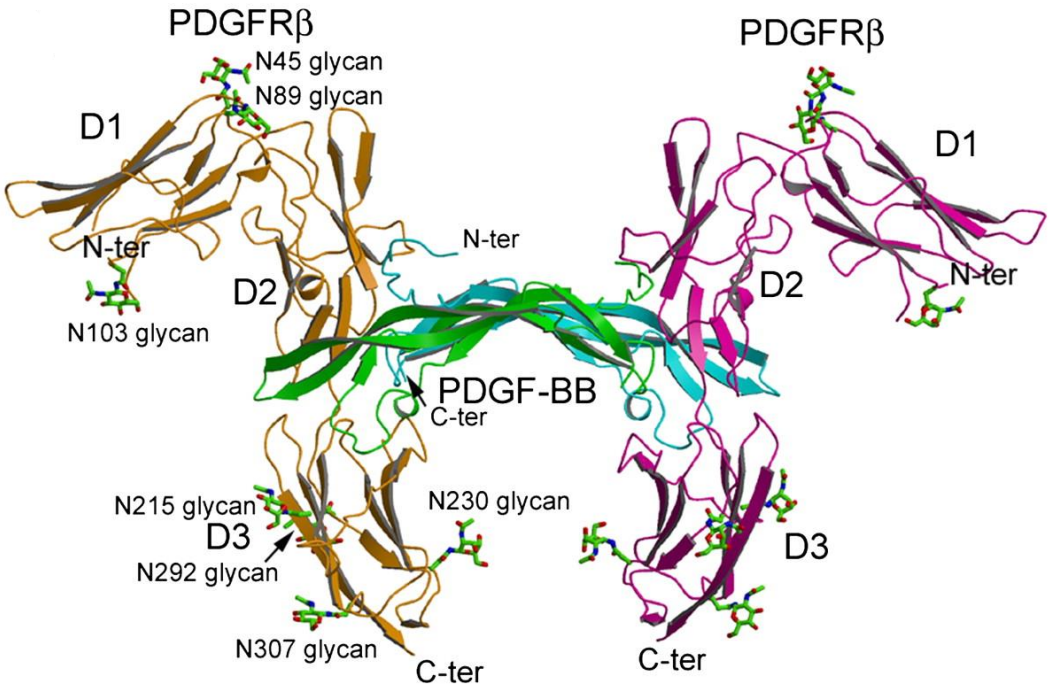

Figure 1.8 Shows the ribbon model complex of PDGF-BB binding to PDGFR-ββ, causing dimerisation. PDGF-BB is represented by the blue and green ribbons, one PDGFR-β represented by orange ribbons, and the other purple ribbons (Shim *et al.*, 2010).

On binding of PDGF to either receptor, it causes the transduction of mitogenic signals causing the cell to start cell division (mitosis). However, each receptor causes a different effect on the actin filaments of the cell (Eriksson *et al.*, 1992). Another difference is β-receptor activation, causing chemotaxis, whereas, α-receptor activation prevents chemotaxis of certain cells, such as smooth muscle and fibroblast cells (Heldin & Westermark, 1999).

Greenhalgh *et al.* (1990) delivered topically recombinant human platelet-derived growth factor (rhPDGF) (1 or 10 μg) in a 5 % poly(ethylene glycol) delivery vehicle, to full-thickness skin wounds, in genetically modified diabetic mice. They found that wounds treated with rhPDGF had a significantly greater rate of wound closure, at day 21, compared to the control (Greenhalgh *et al.*, 1990). Likewise, Sun *et al.* (2007) showed that addition of a short collagen-binding domain (CBD) to native human PDGF-BB isoform, increased the concentration of bioactive PDGF-BB

at the wound site. On testing the CBD-PDGF-BB system in a rabbit dermal ischemic ulcer model, they found that this form of topically delivered PDGF-BB promoted ulcer healing. On histological examination of the tissue, they documented increased re-epithelisation, formation of capillary lumens-and increased collagen deposition (Sun *et al.*, 2007).

Regranex® gel is a FDA approved gel containing 0.01 % becaplermin manufactured by Smith & Nephew. Regranex® is licensed for use in USA for the treatment of lower extremity diabetic neuropathic ulcers that extend into the subcutaneous tissue, or further, and have a sufficient blood supply (Rees *et al.*, 1999; Smith & Nephew, 2015). Becaplermin is a recombinant version of the naturally occurring homodimeric PDGF-BB isoform. Becaplermin is produced using recombinant DNA technology, by inserting the coding gene for the B chain into yeast (*Saccharomyces cerevisiae*) (Nagai & Embil, 2002). A phase two randomised, double-blind, placebo-controlled study using becalpermin gel to treat pressure ulcers was found to have positive results (Rees *et al.*, 1999). Rees *et al.* (1999) concluded that once daily application of becalpermin gel (100 or 300 μg g^{-1}) to chronic pressure ulcers, resulted in a significant increase in the number of completely healed, and ≥ 90 % healed chronic pressure ulcers, compared to the control gel. Interestingly, they found that the 300 μg g^{-1} gel did not show any significantly greater rate of healing than the 100 μg g^{-1} gel (Rees *et al.*, 1999).

1.4.2 Epidermal growth factor (EGF)

Epidermal growth factor (EGF) is another important growth factor contributing to the wound healing process. It has been documented that EGF is up regulated after acute injury causing accelerated re-epithelisation, through increased migration of the

keratinocytes (Barrientos *et al.*, 2008). EGF also promotes re-epithelisation through stimulation of angiogenesis, fibronectin synthesis, collagenase activity and fibroplasia (Hardwicke *et al.*, 2008).

EGF was first isolated in 1962 by Stanley Cohen, from a mouse submaxillary gland. This formed part of Cohen's Nobel Prize winning work in relation to growth factors (Cohen, 1962; Cohen, 1986). The EGFs are a family of proteins, all of which have mitogenic activity. The members of the family are EGF, transforming growth factor-α (TGF-α), heparin-binding EGF (HB-EGF), amphiregulin, epiregulin, betacellulin, epigen and neurglins 1–4 (Werner & Grose, 2003; Barrientos *et al.*, 2008). EGF itself is a 53 amino acid single-chain poly(peptide), which includes six cysteine residues, forming three disulfide bonds, as seen in Figure 1.9.

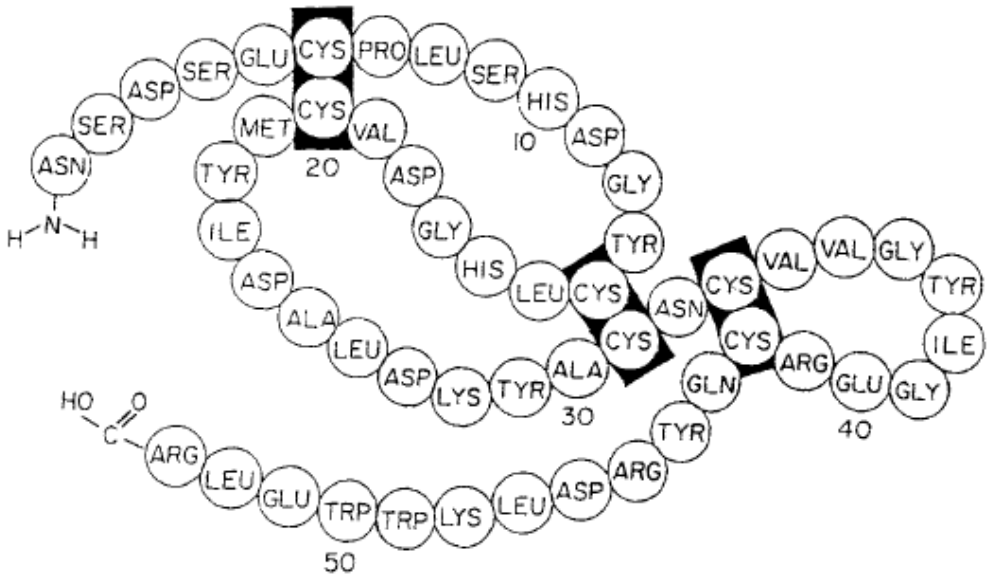

Figure 1.9 The primary 53 amino acid sequence of human EGF. The 6 cysteine amino acids can be seen highlighted, which form the 3 disulfide bonds, folding the primary chain (Schultz *et al.*, 1991).

EGF ligands are released from macrophage (Barrientos *et al.*, 2008), fibroblast and platelet cells (Shiraha *et al.*, 1999; Barrientos *et al.*, 2008), with their primary function being to initiate re-epithelisation. Keratinocytes surrounding the edge of the wound and hair follicle epithelial cells release TGF-α (Werner & Grose, 2003).

TGF-α causes increased keratinocyte proliferation and migration, via upregulation of keratin-6 and 16 production (Jiang *et al.*, 1993). Post-wounding HB-EGF is upregulated, with increased secretion from keratinocytes, promoting early stage re-epithelisation (Barrientos *et al.*, 2008). As with PDGF, there is more than one receptor for EGF ligands to bind to. The EGF ligands bind to each of the following receptors; EGFR, human epidermal growth factor receptor 2 (HER2), HER3 and HER4, with different degrees of affinity (Werner & Grose, 2003). These receptors are also referred to as ErbB1–4, and EGFR is also called HER1 (Werner & Grose, 2003).

EGFR is first synthesised as a precursor poly(peptide) with a total of 1210 amino acid residues (Jorissen *et al.*, 2003). The precursor poly(peptide) then undergoes proteolytic cleavage, yielding the active EGFR receptor, which has 1186 amino acid residues. The active EGFR is then inserted into the cell membrane, of which 622 amino acids make up the extracellular binding region for the EGF ligands (Ogiso *et al.*, 2002). Ogiso *et al.* (2002) documented that amino acids, tryosine13, isoleucine23, arginine41 and leucine47 are especially important for the binding of EGF to the receptor. Table 1.6 summarises the specificity of the EGF ligands for the four receptors.

Table 1.6 Summary of the EGF family ligands and their corresponding receptors

Receptor	**Ligand**
EGFR/HER1/ErB1	EGF, TGF-α, epigen, amphiregulin, HB-EGF, betacellulin, epigregulin
HER2/ErbB2	None
HER3/ErbB3	Epigregulin, neuregulin-1, neuregulin-2
HER4/ErbB4	Betacellulin, HB-EGF, epigregulin, neuregulin-3, neuregulin-4

All four receptors are present in the membrane of target cells as monomers, known as, transmembrane tyrosine kinase receptors. On binding of an appropriate ligand to a receptor, dimerisation occurs (Rubin & Yarden, 2001). Receptors can pair up with a receptor of the same type, forming a homodimer (e.g. HER3-HER3), or a receptor of a different type, forming a heterodimer (e.g. HER3-HER4). Dimerisation is thought to occur as a result of the complex formed between a ligand and two receptors being more stable than a ligand and one receptor (Rubin & Yarden, 2001). None of the ligands of the EGF family can bind directly to HER2, nor is there any known ligand to exist (Rubin & Yarden, 2001). However, HER2 can be activated when recruited as a second receptor in the dimerisation process, forming a heterodimer. Therefore, HER2 still plays a vital role in normal wound repair. It is well documented that overexpression of HER2 plays a causative part in tumorigenesis (Werner & Grose, 2003), in particular breast cancer (Rauser *et al.*, 2010; Mitri *et al.*, 2012); but also, non-small-cell lung cancer (Cappuzzo *et al.*, 2005), ovarian cancer (Moasser, 2007), and gastrointestinal tract cancers (Rubin & Yarden, 2001).

Upon binding of any ligand to the appropriate tyrosine kinase receptor, autophosphorylation occurs. This results in the simultaneous switching on of multiple cellular pathways. Binding of the EGF ligand is thought to activate the Ras proto-oncogene, Grb2 adaptor protein, Shc, PLCγ protein, MAPK, PI3-K, JAKs and STATs signal pathways (Jorissen *et al.*, 2003). This activation can be both direct and indirect, due to the complex interlinking between pathways (Jorissen *et al.*, 2003). Neuregulins bind to HER3 and HER4 causing mitogenic activity within the target cell through activation of the MAPK signaling pathway (Pinkas-Kramarski *et al.*, 1998). EGF promotes both migration and proliferation, but via different pathways.

Chen *et al.* (1994a) found that the PLCγ proteins activation of signaling pathways is necessary for cell motility, with cell movement halting on inhibition of PLCγ. They documented that activation of MAPK on its own was not sufficient to cause cell motility, but concluded that it plays a role in cell movement through regulating integrin adhesion (Chen *et al.*, 1994a; Chen *et al.*, 1994b).

Choi *et al.* (1994) produced biodegradable electro-spun nanofiber polymers, to which recombinant human EGF (rhEGF) was conjugated to, for the treatment of diabetic ulcers. The new delivery system was tested in diabetic mice, which had full-thickness dorsal wounds. It was found that the topically applied nanofiber mesh conjugated with rhEGF showed accelerated wound closure, compared to the control groups (Choi *et al.*, 2008). Choi *et al.* (2008) also demonstrated that human keratinocyte cells cultured on top of rhEGF nanofibers showed a significantly greater increase in gene expression of keratin-1 and loricrin, compared to the control groups. Keratin-1 and loricrin are both essential proteins needed for proliferation and differentiation of keratinocytes (Choi *et al.*, 2008).

A gelatin based wound dressing, loaded with either free EGF or microspheres loaded with EGF, was formulated by Ulubayram *et al*. (2001). Two dose of EGF (1 or 15 μg cm^{-2}) were loaded into the dressings and applied to full-thickness wounds on rabbits. They found that both the free EGF and microsphere loaded EGF, at 1 μg cm^{-2}, closed the wounds faster than the control groups. However, there was no difference, in the rate of wound closure, between the free and microsphere encapsulated EGF dressings. Interestingly, on increasing the concentration in the dressings to 15 μg/cm^2, the EFG-loaded microspheres exhibited faster wound closure than the free EGF and the control groups (Ulubayram *et al.*, 2001).

An Indian biotechnology company, Bharat Biotech, have developed and manufactured a topical gel containing rhEFG called Regen-D™ 150 for treatment of diabetic foot ulcers (Mohan, 2007). They also have a lower strength gel, Regen-D™ 60 for use in bed sores and burns (Bharat Biotech, 2015). Mohan documents that Regen-D™ 150 was found to increase the quantity of healthy granulation tissue present, promoting epithelisation and faster wound healing.

1.4.3 Transforming growth factor-β (TGF-β)

Transforming growth factor-β2 (TGF-β2) and TGF-β3 are both involved in the recruitment of fibroblast and inflammatory cells to the wound site, post injury. TGF-β2 and TGF-β3 play vital roles in angiogenesis and neovascularisation, respectively in wound healing (Roberts *et al.*, 1986; Pepper, 1997). TGF-β2 is also implicated in the laying down of type I and type II collagen in the extracellular matrix and scar formation. TGF-β3 is thought to be an important stop signal for differentiation in tissue (Tyrone *et al.*, 2000) and play a part in keratinocyte migration (Barrientos *et al.*, 2008). Unlike the TGF-β1 and 2 isoforms, TGF-β3 promotes collagen re-organisation and suppresses scar formation, indicating the healing process is coming to an end.

TGF-β is a family of proteins consisting of TGF-β1, TGF-β2, TGF-β3, bone morphogenic proteins (BMP), Mullerian inhibiting substance, nodals, inhibins and activins (Werner & Grose, 2003). TGF-β1 is made up of two identical 112 amino acid chains, which are linked by disulfide bonds (Massague, 1990). Each of the two chains are initially synthesised as precursor poly(peptides) (390 amino acid residues), which undergo proteolytic cleavage yielding the two chains to form the active dimeric ligand (Massague, 1990). TGF-β isoforms 1–3 are found in mammals, and

although they are structurally similar, 60–80 % homology, they have different biological functions (Penn *et al.*, 2012). TGF-β1–3 are secreted by several cells found in the wound site, such as platelets, macrophages, keratinocytes and fibroblasts (Barrientos *et al.*, 2008).

The three isoforms of TGF-β bind to two receptors simultaneously in the cell membrane, known as type I (TGF-βRI) and type II (TGFR-βII) (Werner & Grose, 2003). There is a third TGF-β receptor (TGF-βIII), which all three isoforms bind to with high affinity. However, the type III receptor is a non-signaling receptor, the main purpose of which is to present the TGF-β isoforms in the correct orientation to the type II receptor for binding (Roberts, 1998). Upon binding of a TGF-β ligand to the type II receptor, it becomes phosphorylated. The phosphorylated type II receptor attracts, binds and phosphorylates the type I receptor, forming a heterodimer complex. Once the receptor-ligand complex is formed, it results in the activation of the Smad intracellular signaling pathway (Penn *et al.*, 2012).

The Smad signal transduction begins through phosphorylation of the Smad-2 and Smad-3 receptors, which then bind to Smad-4 (Figure 1.10). On binding to Smad-4, they move across the nuclear membrane into the nucleus, where they cause up-regulation of specific genes (Werner & Grose, 2003; Mazzieri *et al.*, 2005). It has also been documented that TGF-β1 activates other intracellular signaling pathways, such as, MAPK, extracellular signal-regulated kinases (ERK) and c-Jun N-terminal kinases (JNK) pathways (Rolfe *et al.*, 2007).

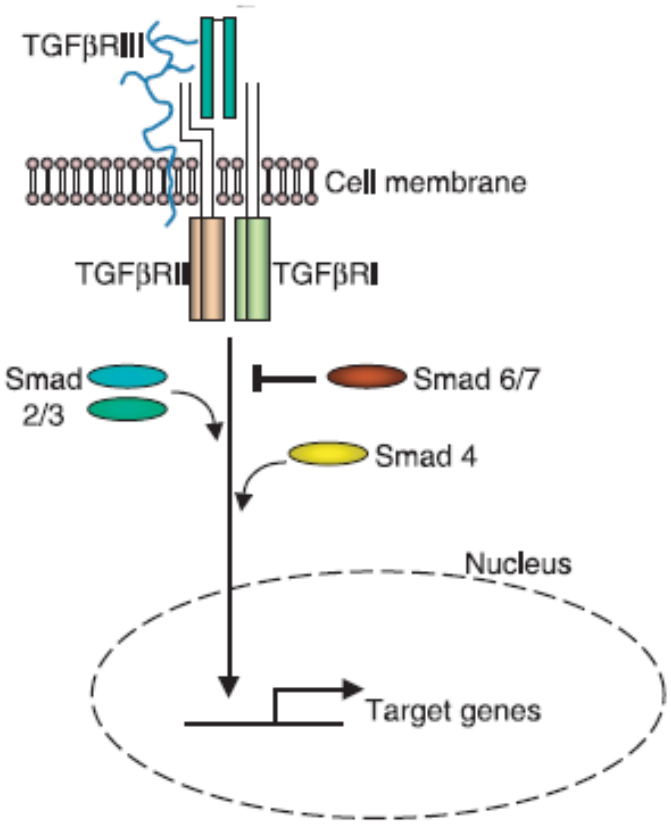

Figure 1.10 Schematic diagram depicting the activation of the Smad intracellular signaling pathway, activated by a TGF-β ligand. The TGF-β ligand can be seen being presented to the type II receptor in the correct orientation by the type III receptor, which then recruits the type I receptor. This forms the heterodimer ligand-receptor complex, activating the Smad pathway and upregulation of target genes (Werner & Grose, 2003).

Upon injury, TGF-β1 is secreted from platelets and acts as a chemo-attractant for fibroblasts, macrophages and neutrophils. This initial release of TGF-β1 is important for the initiation of the inflammatory phase. Once these inflammatory cells are *in situ* they begin to produce, and release, TGF-β1 further increasing the TGF-β1 levels within the wound (Barrientos *et al.*, 2008). It is also thought that TGF-β1 inhibits the production of superoxides by macrophages, thus preparing the wound for granulation tissue formation, by protecting surrounding healthy tissue (Mitra & Khar, 2004).

In vitro studies using TGF-β1 have shown an up-regulation of the genes required for the formation of several extracellular matrix components. These components are fibronectin, collagen (Goldberg *et al.*, 2007), tissue inhibitors of

metalloproteinases (TIMP) (Zeng *et al.*, 1996), MMP (White *et al.*, 2000) and fibronectin receptors (Barrientos *et al.*, 2008). Several studies and review articles (Barrientos *et al.*, 2008; Werner & Grose, 2003), however, have documented the effect of TGF-β1 in relation to keratinocyte re-epithelisation to be paradoxical. Some authors concluded that addition of TGF-β1, *in vivo* and *in vitro,* resulted in decreased keratinocyte proliferation (Coffey *et al.*, 1988; Sellheyer *et al.*, 1993; Amendt *et al.*, 1998). It was also demonstrated that Smad3-null mice had increased wound healing compared to the wild-type mice (Ashcroft *et al.*, 1999). This result further complements the conclusions drawn by the previous authors. Conversely, over expression of TGF-β1 was found to aid in the facilitation of the phenotypic change of the keratinocytes. In particular, in the later stages of healing, to a more proliferative type (Bottinger *et al.*, 1997). Also, addition of TGF-β1 to wounds on pigs was found to stimulate the expression of integrins needed for keratinocyte migration (Gailit *et al.*, 1994). Interestingly, prolonged overexpression of TGF-β1 is thought to play a role in fibrosis, leading to the formation of keloid scars (Rudolph & Vande Berg, 2005).

Werner & Grose (2003) document in their review that a significant amount of research has been conducted to try and understand why foetuses, in the early stages of gestation, do not scar. Again, there has been a lot of conflicting data published on this area, most likely due to the conflicting data on the role of TGF-β1 in wound healing. But one logical theory that is thought to play a part, is the reduction in the expression of TGF-β1 in the foetus, along with the reduced length of time the TGF-β1 is present in the wound site (Yates *et al.*, 2012). This is thought to result in reduced expression of extracellular matrix components, leading to reduced scarring. However, this is not thought to be the sole factor contributing to reduce scarring in a

foetus, as there are many differences in the wound healing process between a foetus and an adult. Some of these other different factors documented by Yates *et al.* (2012) are, no acute inflammatory phase, reduced secretions of PDGF and EGF.

TGF-β2, purified from bovine bone, was used topically to treat venous ulceration (Robson *et al.*, 1995). The treatment regime was three times per day for up to 6 weeks, using a lyophilised collagen vehicle as the delivery system. On clinical evaluation, it was concluded that the quantity and quality of the granulation tissue was healthier, in the treated group compared to the control group (Robson *et al.*, 1995). Results from the two trials both showed an increase in the rate of wound closure. However, only in one trial was the difference between the control group and treated group significant.

1.4.4 Vascular endothelial growth factor (VEGF)

Vascular endothelial growth factor (VEGF) has an important role in the inflammatory phase of the wound healing process. At the inflammatory stage VEGF facilitates wound repair by increasing the vascular permeability at the site of injury, which provides the necessary access for inflammatory cells and growth factors. VEGF is also though to play a part in angiogenesis, lymphangiogenesis and re-epithelisation at the wound site (Bauters *et al.*, 1994; Takeshita *et al.*, 1994; Bauters *et al.*, 1995; Walder *et al.*, 1996).

VEGF was first discovered in the 1980s, by Harold Dvorak and Napeleone Ferrara. VEGF is also referred to as vascular permeability factor (VPF), due to its ability to induce vascular leakage (Claesson-Welsh, 2016). VEGF is essential for vascular development and angiogenesis. The VEGF family consists of five structurally similar mammalian poly(peptides); VEGF-A, VEGF-B, VEGF-C,

VEGF-D and placenta growth factor (PlGF). There are other members of the VEGF family, such as a sheep parapoxvirus VEGF-E (Lyttle *et al.*, 1994) and a poly(peptide) derived from snake venom, known as VEGF-F (Koch & Claesson-Welsh, 2012). The mammalian factor VEGF-A is further subdivided into several isoforms, identified by the number of amino acids in their sequences. The four isoforms are VEGF-A_{121}, VEGF-A_{165}, VEGF-A_{189} and VEGF-A_{206}. These isoforms are produced due to alternative splicing of the eight exons in the messenger ribonucleic acid (mRNA) sequence, which encodes the VEGF poly(peptide) (Cross *et al.*, 2003). In humans, the most prevalent isoform is VEGF-A_{165}, which does not contain exons 6a and 6b, as seen in Figure 1.11.

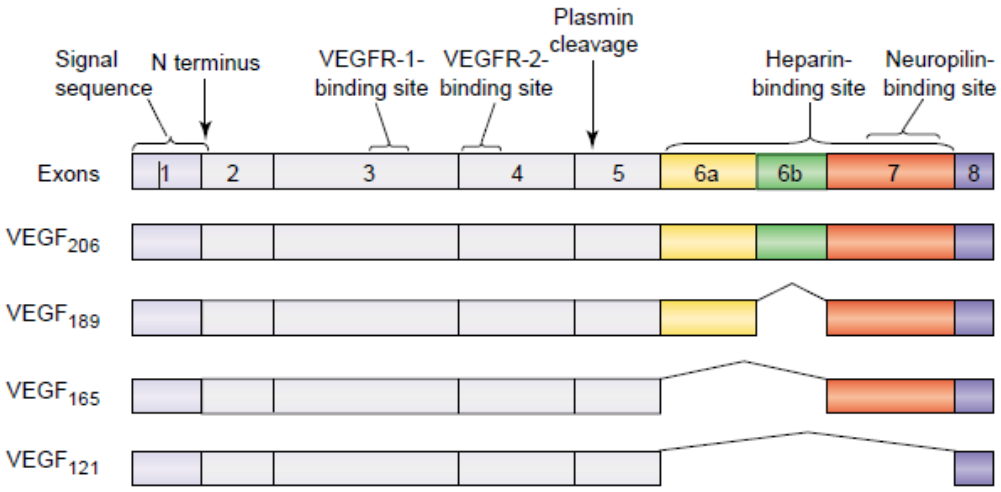

Figure 1.11 Schematic diagram showing the mRNA exon splicing variations for VEGF-A. Each of the four isoforms vary in the total number of amino acids in the poly(peptide). VEGF-A_{165} is the most common isoform found in humans (Cross *et al.*, 2003).

VEGF-A_{121} is an acidic poly(peptide), which does not contain exons 6 and 7, as seen in Figure 1.11. As a result of the exclusion of exons 6 and 7 VEGF-A_{121} does not have the ability to bind to heparin (Ferrara *et al.*, 2003). VEGF-A_{165} also has exon 6 missing, but still can bind to heparin. This would suggest that heparin binding is more dependent on exon 7, rather than exon 6. It is thought that the absence of the

heparin binding domain results in a significant decrease in mitogenic activity of the VEGF-A_{121} isoform (Keyt *et al.*, 1996). Native VEGF is a 45 kDa homodimeric glycoprotein, to which VEGF-A_{165} is functionally similar to (Ferrara & Henzel, 1989). VEGF-A_{189} and VEGF-A_{206} are strongly basic, do contain exons 6 and 7 and, therefore, can bind to heparin (Figure 1.11). VEGF-A_{189} and VEGF-A_{206} are isolated mainly to the EMC, being released on proteolytic degradation of the EMC components (Ferrara *et al.*, 2003).

There are several factors responsible for the regulation of VEGF gene expression. Major growth factors, such as EGF, TGF-β, TGF-α, FGF, IGF, PDGF, keratinocyte growth factor and cytokines interleukin-1α (IL-1α) and IL-6, upregulate the mRNA expression for VEGF (Ferrara *et al.*, 2003). In a hypoxic environment, such as a wound site, hypoxia-inducible factor is released by *in situ* cells. Hypoxia-inducible factor binds to a VEGF-A promoter, stimulating the production and secretion of VEGF-A (Ferrara *et al.*, 2003). Therefore, there is a concentration gradient of both oxygen and VEGF-A present between normal and hypoxic tissue. In a hypoxic micro-environment, the oxygen tension is low and the VEGF-A concentration is high, with the opposite occurring in normal tissue. The VEGF-A stimulates angiogenesis, reinstates tissue perfusion and increases the oxygen tension in the micro-environment (Barrientos *et al.*, 2008). However, a minimum amount of VEGF-A must remain in the micro-environment to prevent apoptosis of the endothelial cells (Neufeld *et al.*, 1999; Matsumoto & Claesson-Welsh, 2001). Barrientos *et al.* (2008) document that in acute wounds the expression of VEGF-A by endothelial cells, fibroblasts, monocytes, keratinocytes and myocytes is intensified in response to the hypoxic conditions.

VEGF-B is found to be expressed in abundance in embryotic heart tissue in early stage gestation. In adults, it is expressed to certain degree in nearly all tissue, but expression is found to be more pronounced in the spinal cord, brown fat and heart tissue. The VEGF-C isoform has also been detected in several embryonic and adult tissues (Matsumoto & Claesson-Welsh, 2001). VEGF-C mRNA is strongly expressed in areas of tissue where lymphatic vessels are produced, playing a fundamental role in lymphangiogenesis (Matsumoto & Claesson-Welsh, 2001).

The five VEGF ligands and the four VEGF-A isoforms bind to three, homodimeric, tyrosine kinase transmembrane receptors, denoted as VEGFR-1, VEGFR-2 and VEGFR-3 (Claesson-Welsh, 2016). There is a fourth receptor known as soluble VEGFR-1 (sVEGFR-1). The sVEGFR-1 is not dimeric and has no transmembrane or intracellular domains. The sVEGFR-1 is believed to play a negative regulatory role, whereby, it binds with strong affinity free VEGF-A, preventing it from binding to the functional VEGFRs (Cross *et al.*, 2003). VEGF also interacts with neuropilin membrane co-receptors (Ferrara *et al.*, 2003). Neuropilin-1 is thought to present VEGF-A_{165} to the VEGFR-2 in such a way that it enhances the signal transduction upon activation of VEGFR-2 (Soker *et al.*, 1998).

VEGFR-1, also denoted as Flt-1, is a 180 kDa receptor found to be expressed on the surface of vascular endothelial cells, macrophages, monocytes and haematopoietic stem cells (Cross *et al.*, 2003). VEGFR-1 binds to VEGF-A, VEGF-B and PIGF ligands, with high affinity. VEGFR-1 structure is made up of an extracellular domain consisting of seven immunoglobulin-like domains, a transmembrane region and an intracellular tyrosine kinase sequence, which contains a kinase-insert domain (Ferrara *et al.*, 2003). Cross *et al.* (2003) document that

VEGFR-1 binds VEGFA with an affinity of K_d 10 pM, but only gives a weak twofold increase in kinase activity.

VEGFR-2, also denoted as Flk-1 or KDR, is a 200–230 kDa receptor found to be expressed in lymphatic and vascular endothelial cells. VEGFR-2 has a strong affinity for VEGF-A, VEGF-C, VEGF-D and VEGF-E ligands (Cross *et al.*, 2003). VEGF-A is thought to bind to the second and third immunoglobulin-like domains in the extracellular part of VEGFR-2. In particular, amino acids Arg(82), Lys(84) and His(86) in these immunoglobulin-like domains are thought to facilitate the binding of the ligand (Neufeld *et al.*, 1999). VEGF-A has a lower affinity for VEGFR-2 (K_d 75-125 pM) compared to VEGFR-1, even though both receptors are structurally similar. (Cross *et al*., 2003).

VEGFR-3 is a 195 kDa receptor also known as Flt-4, with an affinity for VEGF-C and VEGF-D. VEGFR-3 undergoes cleavage during synthesis, in the fifth extracellular immunoglobulin-like domain (Pajusola *et al.*, 1994). VEGFR-3 is mainly expressed on lymphatic endothelial cells, which, when activated, initiates migration, proliferation and survival of the lymphatic cells (Cross *et al*., 2003). A summary of specific VEGF ligand-receptor binding, and the cells, which primarily express the receptors, can be seen in Figure 1.12.

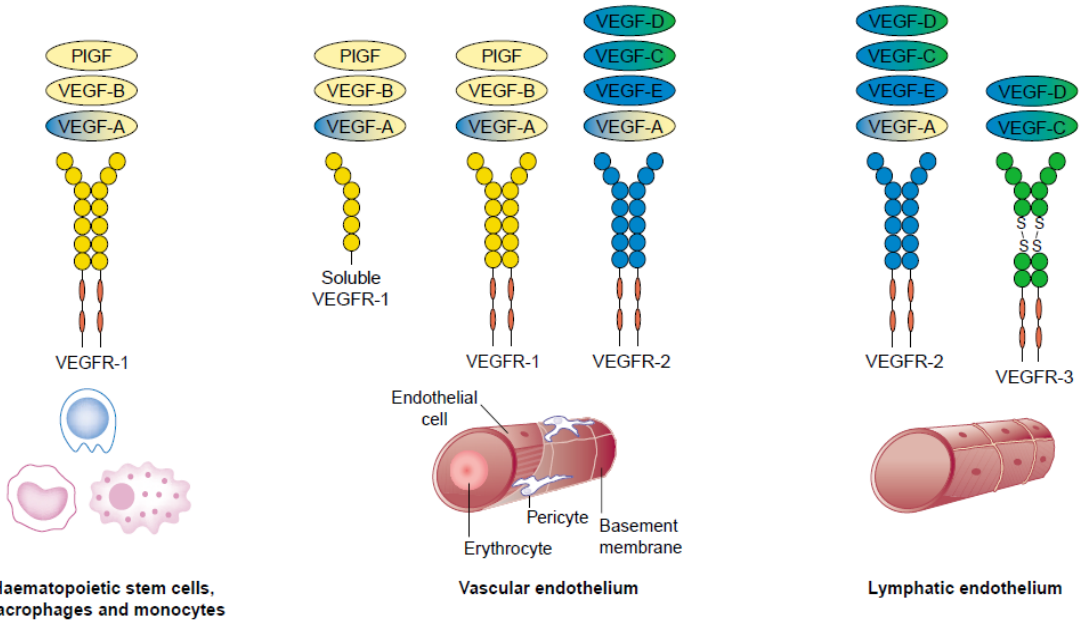

Figure 1.12 Schematic diagram showing VEGF ligands and their corresponding receptors. VEGFR-1 is yellow and its corresponding ligands are also yellow. VEGFR-2 is blue with its corresponding ligands shaded blue. VEGFR-3 is green with its corresponding ligands shaded green. VEGF ligands which contain two colours, indicates that they bind to more than one ligand. It can also be seen which types of cells or tissues expresses specific ligands (Cross *et al*., 2003).

Upon binding of a VEGF ligand to a receptor, several of the tyrosine residues within the intracellular domains undergo autophosphorylation. Three intracellular proteins, VEGFR-associated protein (VRAP), Sck and PLC-γ, bind to the activated tyrosine residues through their Src homology-2 (SH2) domain. This causes activation of the membrane bound phosphatidylinositol 4,5-bisphosphate (PIP_2), which through a series of event leads to the activation of protein kinase-C (PKC) transduction protein (Ferrara *et al.*, 2003; Claesson-Welsh, 2016). PKC activates several other downstream signal transducers, Raf, MEK, ERK, with the end result being cell proliferation (Figure 1.13). PI3K and P38MAPK signal transduction pathways are activated directly by autophosphorylation of the intracellular domains of the VEGFR, leading to cell migration (Koch & Claesson-Welsh, 2012), as seen in Figure 1.13. Other signal transducers and pathways are activated indirectly as a result of VEGFR activation, such as Rac, Akt/protein kinase-B (PKB) and Ras

(Cross *et al.*, 2003). Numerous downstream signal transduction molecules are activated in a cascade of events leading to cellular functions, such as, endothelial permeability, proliferation and migration.

It is documented that activation of the Akt/PKB pathway, activates an enzyme called endothelial nitric oxide synthase (eNOS) (Fulton *et al.*, 1999). This enzyme generates nitric oxide, which causes an increase in vascular permeability (Dimmeler *et al.*, 1999).

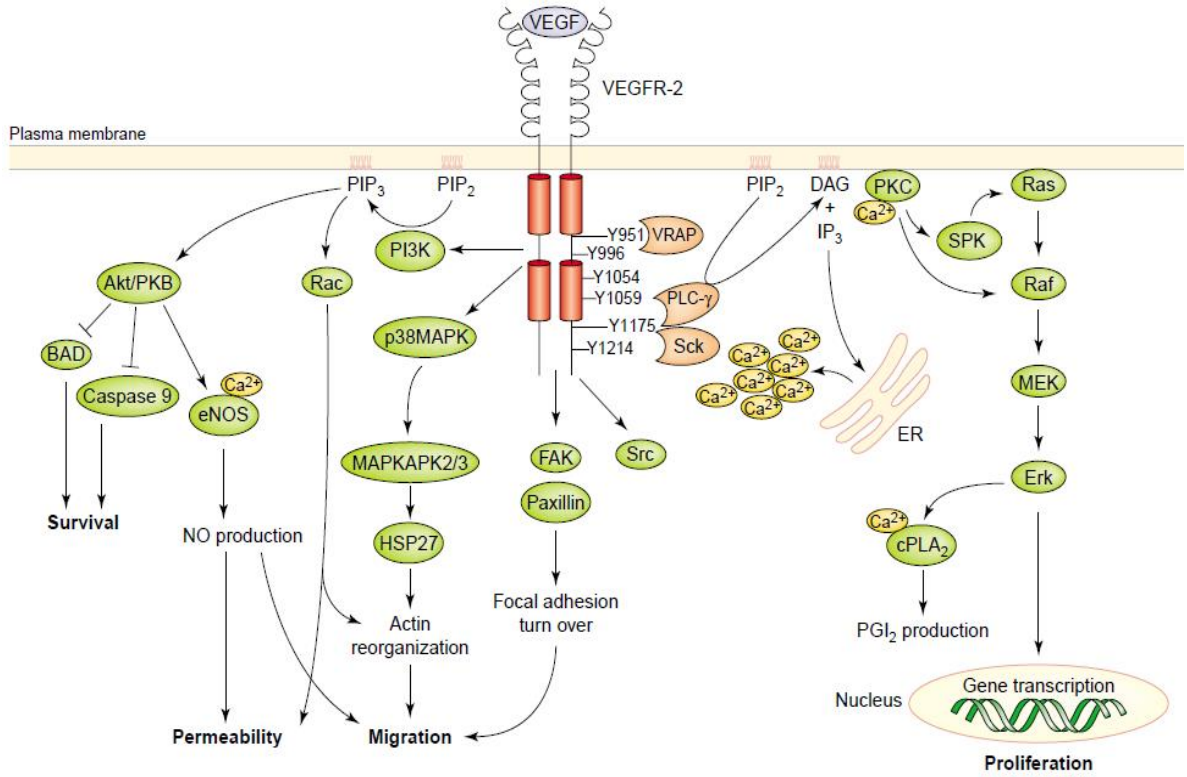

Figure 1.13 A schematic diagram representing the intracellular signal transduction, which takes place upon binding of a VEGF ligand to VEGFR-2. Upon binding to the VEGFR-2 numerous tyrosine residue undergo autophosphorylation, leading to activation of several intracellular proteins and signal transduction cascades, resulting in vascular permeability, migrations and proliferation (Cross *et al.*, 2003).

Several studies treating ischemic wounds in hind legs of rabbits with VEGF-A have been carried out (Bauters *et al.*, 1994; Takeshita *et al.*, 1994; Bauters *et al.*, 1995; Walder *et al.*, 1996). In these studies, VEGF-A was delivered either intramuscularly or intravenously, with various dosing regimens (3 mg kg^{-1} of VEGF

only or in combination with heparin). As a result of these studies, it was found that administration of VEGF-A increased and restored angiogenesis, and initiated re-epithelisation (Bauters *et al.*, 1994; Takeshita *et al.*, 1994; Bauters *et al.*, 1995; Walder *et al.*, 1996). Galiano *et al*. (2004) topically treated full-thickness dorsal wounds in diabetic mice with 20 μg of $rhVEGF_{165,}$ on alternate days, for a total of five doses. Results showed that the wounds treated with $rhVEGF_{165}$ demonstrated decreased wound closure time (12 days), compared to the control group (25 days) (Galiano *et al.*, 2004). Saaristo *et al*. (2006) administered, via injection, an adenoviral vector encoding human VEGF-C to full-thickness dorsal wounds in diabetic mice. They found that there was an up-regulation in VEGF-C expression, leading to a noted increase in lymphangiogenesis and angiogenesis. This resulted in significant, accelerated wound healing, compared to the control group (Saaristo *et al.*, 2006).

1.4.5 Fibroblast growth factor (FGF)

In adults fibroblast growth factors (FGFs) have been identified to play a role in wound healing, internal tissue repair and control of the nervous system. FGF-2, FGF-7 and FGF-10 are thought to be the most influential members of the FGF family with regards to wound healing (Barrientos *et al.*, 2008). FGF-7 is also known as keratinocyte growth factor-1 (KGF-1) and FGF-10 as keratinocyte growth factor-2 (KGF-2).

The family of FGFs consists of 22 growth factors in total. These 22 FGFs range in size from 17–34 kDa (Ornitz & Itoh, 2001). Each growth factor consists of a section of 120 amino acid that shows up to 65 % homology. FGFs control several cellular functions during embryo development, such as cell migration, proliferation

and differentiation. FGF has also been implicated in the development and progression of tumour angiogenesis (Eswarakumar *et al.*, 2005). As with all the previously discussed growth factors, FGFs also bind to transmembrane tyrosine kinase receptors. There are four FGF receptors, denoted FGFR-1–4, consisting of an intracellular cytoplasmic domain, a single transmembrane domain and an extracellular ligand-binding domain. The extracellular domain, consists of three immunoglobulin-like domains, D1–D3 (Schlessinger, 2000). Within the extracellular domain there is a linker known as the acid box. The acid box is a short sequence of acidic residues linking the D1 and D2 domains. The D2 domain contains a positive charged region for the binding of heparin (Schlessinger *et al.*, 2000). FGFR-1–3 undergo exon splicing, in a similar manner as the previously mentioned VEGF ligands. The splicing occurs in the D3 domain of the extracellular component in FGFR-1–3, but not FGFR-4 (Werner & Grose, 2003). Eswarakumar *et al*. (2005) have documented in their review that exon 7 encodes the N-terminal half (denoted as a) of the D3 domain of FGFR-2 while exons 8 and 9, which can be alternatively spliced, encode the C-terminal half of D3. Exons 8 and 9 are denoted as b and c, respectively. A summary of the FGFR isoforms and their known specific ligand binding can be seen in Table 1.7, modified from (Eswarakumar *et al.*, 2005).

Table 1.7 FGFR isoforms specific ligand binding (Eswarakumar *et al.*, 2005)

FGFR isoform	**FGF ligand specificity**
1b	1, 2, 3, 10
1c	1, 2, 4, 5, 6
2b	1, 3, 7, 10, 22
2c	1, 2, 4, 6, 9, 17, 18
3b	1, 9
3c	1, 2, 4, 8, 9, 17, 18
4	1, 2, 4, 6, 8, 9, 16, 17, 18, 19

FGFs also bind to heparin and heparan sulphate proteoglycans (HSPG), but with a lower affinity, compared to the FGFRs. Heparin and heparan sulphate are found on the cell surface and also in the extracellular matrix. They do not themselves transmit a signal within the cell, but play a vital role in the regulation and bind to the FGFRs. Heparan sulphate is synthesised and distributed by a wide range of tissues and organs, binding to core proteins forming the heparan sulphate proteoglycans (Nugent & Iozzo, 2000), whereas, heparin is only synthesised by mast cells found in connective tissue and involved in the inflammatory response. Binding of FGFs to these molecules, stabilises FGFs through protection from heat denaturation, acid denaturation and proteolytic cleavage (Nugent & Iozzo, 2000). Binding of one of these molecules to the FGFR, along with an appropriate ligand, leads to the formation of a FGF-FGFR-HSPG or heparin dimer (ratio 2:2:2) complex (Zhang *et al.*, 2006), as seen in Figure 1.14. Therefore, heparin and HSPGs are a necessity for stable binding of FGF to the receptor and subsequent activation.

Figure 1.14. Shows the ribbon diagram of the FGF-2-FGFR-1-heparin dimeric complex. The extracellular binding domains D2 and D3 of FGFR-1 are in green and blue, FGF-2 is yellow and heparin red (Eswarakumar *et al.*, 2005).

As seen in Table 1.7, FGF-1 binds to all the FGFR isoforms, whereas FGF-7 binds only to FGFR-2b. The FGFR isoforms not only exhibit different ligand binding, but also specific expression by certain cell types (Zhang *et al.*, 2006). Epithelial cells are thought to express only the FGFR-2b isoform (Orrurtreger *et al.*, 1993), with mesenchymal cells expressing only the FGFR-2c isoform (Ornitz & Itoh, 2001; Eswarakumar *et al.*, 2005). It is this specific expression of these receptors by different cell types that allows the directional communication, between the two different tissue layers, during development (Ornitz & Itoh, 2001). For example, FGFR-2b (expressed in the epithelial layer) is activated by FGF-7 and FGF-10, which are synthesised and secreted from the mesenchymal layer (Igarashi *et al.*, 1998), whereas FGFR (expressed in the mesenchymal layer) is activated by FGF-8 synthesised and secreted by the epithelial layer (MacArthur *et al.*, 1995). Therefore, none of the FGFs activates the receptors found in the layer, which they are produced in, but in different tissue layer. This facilitates the communication between the different tissue layers.

Once an appropriate ligand-receptor complex has formed, the tyrosine residues present in the intracellular domains undergo autophosphorylation. This then follows a similar process as discussed previously for the other growth factors. FGF are thought to activate several intracellular signal pathways. On activation of the receptor, the FRS2α and FRS2β docking proteins undergo phosphorylation. This leads to the recruitments of Grb2 and Sos protein complexes (Kouhara *et al.*, 1997). As a result of the recruitment of these proteins, the Ras, Raf and MAPK pathways are activated, in a downstream signaling cascade (Kouhara *et al.*, 1997). Grb2, once recruited, causes phosphorylation of Gab1 adaptor protein, which consequently leads

to the downstream recruitment of PI3K and activation of the Akt anti-apoptotic pathway (Eswarakumar *et al.*, 2005).

In chronic wounds, a number of growth factors, including FGF-2, are found to exist in the wound at a reduced concentration in comparison to a normal acute wound (Robson, 1997). This led to a significant amount of research being carried out, using exogenous FGF as a potential treatment for chronic wounds. A randomised, blinded, placebo-controlled clinical trial was conducted using a recombinant version of basic fibroblast growth factor, which is another name for FGF-2, to treat chronic pressure ulcers (Robson *et al.*, 1992). Patients received a placebo treatment or recombinant human FGF-2 (rhFGF-2), at three different concentrations (100, 500 or 1000 μg mL^{-1}). This was done in accordance with a dosing schedule, dependent on the tier of the study, for up to 22 days (Robson *et al.*, 1992). Robson *et al*. (2008), found from their study that when all the subgroups were combined, that those treated with rhFGF-2 showed a significant decrease ($p<0.05$) in pressure ulcer volume, in comparison to the placebo treated group. This was further reinforced when histological sections taken from treated patients showed an increase in fibroblast numbers and capillaries, compared to sections taken from the placebo group (Robson *et al.*, 1992). Similarly, in a randomised double-blind, parallel-group, placebo controlled, multicenter (15) study, repifermin was used to treat chronic venous ulcers, in 94 patients (Robson *et al.*, 2001). Repifermin is a shortened recombinant form of FGF-10, which shares 57 % homology with FGF-7.(Robson *et al.*, 2001). Patients received either placebo or repifermin twice weekly for 12 weeks, along with compression therapy. Repifermin (20 or 60 μg cm^{-2}) and the placebo were delivered topically via a spray held at 2–3 inches from the wound. Robson *et al*. (2001) concluded from this study that repifermin showed accelerated

wound healing, with significantly more patients accomplishing 75 % wound closure, compared to the placebo group. Interestingly, they noted that the repifermin showed a greater effect in a subgroup of patients whose wounds were ≤ 18 months old and ≤ 15 cm^2.

1.4.6 Insulin-like growth factor (IGF)

Due to IGF-1's ability to cause an increase in cell migration, proliferation and, therefore, tissue growth, research has been conducted to determine the effects of exogenous IGF-1 to promote and initiate wound healing (Tsuboi *et al.*, 1995; Koshizuka *et al.*, 1997; Nagano *et al.*, 2003; Emmerson *et al.*, 2012; Nunes Achar *et al.*, 2014). The insulin-like growth factor family consists of 3 peptide ligands (IGF-1, IGF-2 and insulin), six binding proteins (IGFBP-1–6) and two receptors (IGF-1R and IGF-2R). IGF was first discovered by Salmon and Daughday in 1957, who initially called IGF sulphation factor. This was due to its ability to incorporate sulphate into cartilage tissue (Salmon & Daughaday W., 1957). In 1963, it was discovered that sulphation factor was similar to proinsulin; however, the biological actions of sulphation factor could not be inhibited by anti-insulin antibodies. As a result of this finding, sulphation factor was given the term non-suppressible insulin-like activity (NSILA) factor (Frosech *et al.*, 1963). In the early 1970s, the terms sulphation factor and NSILA were replaced by somatomedin, due to its function as the mediator of effects of somatotropin, more commonly known as growth hormone (GH) (Jones & Clemmons, 1995). Rinderknecht and Humbel, in 1976, isolated two active molecules from human serum, which upon sequencing were found to share approximately 50 % homology with proinsulin. These two active molecules were thought to be the sulphation factor initially discovered by Salmon and Daughday and

further worked on by Frosech *et al*. (1963). The first molecule was named insulin-like growth factor-1 (IGF-1), due to the similarity of its amino acid sequence to that of proinsulin (Rinderknecht & Humbel, 1976). The second molecule was named insulin-like growth factor-2 (IGF-2), due its structure being similar to IGF-1, but not identical (Rinderknecht & Humbel, 1976). IGF-1 is still referred to as somatomedin C and IGF-2 as somatomedin A.

IGF-1 is a 7.6 kDa poly(peptide) consisting of 70 amino acids, with an A and B chain linked by disulphide bonds, in a similar manner as insulin (Laron, 2001). GH secreted from the anterior pituitary gland stimulates the synthesis of IGF-1 in most tissues. However, the liver is the major source of IGF-1 circulating in the bloodstream (Dercole *et al.*, 1984). The main function of IGF-1 is to control the differentiation and, therefore, growth of body tissue. Interestingly, this physiological function of increasing growth of body tissue, in particular, the increase in muscle protein synthesis and glycogen storage, has led to its misuse and abuse by bodybuilders (Guha *et al.*, 2013). Guha *et al*. (2013) have documented that its use is openly discussed on amateur bodybuilding internet forums. Although to date, there has been no confirmed cases in professional sport, there is no test currently in place to detect IGF-1 misuse (Guha *et al.*, 2013). The performance-enhancing benefits, such as increased strength, muscle size, energy, endurance, bone density and benefits to the immune system, make it very appealing for illicit use by athletes (Guha *et al.*, 2013). This has led to IGF-1 being added to the World Anti-Doping Agency's Prohibited Substances List (WADA, 2017).

A large portion (approx. 80 %) of circulating IGF-1 is bound with high affinity to the 46–53 kDa IGFBP-3. In addition to the binary complex of IGF-1 and IGFBP-3, a 88 kDa molecule, known as an acid labile subunit (ALS), binds to the

already existing complex, forming a ternary complex (Laron, 2001). ALS is a glycoprotein, also synthesised by the liver and regulated by GH, which prevents the passage of the ternary complex through the capillary endothelia layer to activate receptors. The formation of the ternary complex serves to extend the half-life of IGF-1, by protecting it from proteolytic degradation and controls the IGF-1 IGF-1R interaction (Laviola *et al.*, 2007). It is estimated that the half-life of circulating unbound IGF-1 is only a few minutes (Rosenfeld *et al.*, 1999). Whereas, the formation of the binary complex of IGFBP and IGF-1, increases the half-life to 30 minutes, which increases to 12 to 15 hours on formation of the ternary complex (Rosenfeld *et al.*, 1999). IGFBP-3 is thought to be mainly regulated by GH and to a lesser extent by IGF-1 (Kanety *et al.*, 1993; Laron, 2001). As IGFBPs and IGFRs both bind IGF ligands, it can be said there is localised competition between IGFBP and IGFR for the ligands. This provides evidence that IGFBPs also play an inhibition/regulatory role on IGF signaling.

Both IGF-1 and IGF-2 bind with high affinity to two cell surface tyrosine kinase transmembrane receptors. The IGF-1R binding domain has similar homology to the insulin receptors binding domain and can, therefore, bind insulin, but with a much lower affinity (Laviola *et al.*, 2007). The IGF-1R can also bind IGF-2, but with a 100-fold lower affinity than IGF-1 (Laviola *et al.*, 2007). The IGF-2R binds IGF-2 with the highest affinity and IGF-1 with a much lower affinity, but, it cannot bind insulin (Laviola *et al.*, 2007). At higher than normal concentrations, IGF-1 can bind to the insulin receptor with a low affinity of 1–5 % compared to the affinity of insulin (Guler *et al.*, 1987).

IGF-1R consists of an extracellular α-subunit (706 amino acids) and a transmembrane β-subunit (620 amino acids) (Jones & Clemmons, 1995). The two

subunits are linked via disulphide bonds, resulting in the formation of one half of the receptor. This half receptor binds to another identical half receptor through disulphide binding between the α-subunits to give the complete hetero-tetrameric receptor (Jones & Clemmons, 1995; Laviola *et al.*, 2007). On binding of an appropriate ligand to the IGF-1R, it is thought to activate several intracellular signaling pathways. IGF-1R has been documented to prevent programmed cell death (apoptosis) via the activation of the Akt pathway (Vincent & Feldman, 2002). PI3K is activated by binding to insulin receptor substrate-1 (IRS-1) via its SH2 domain. This results in an increase in PIP3 activity, which directly, and indirectly (via activation of phosphoinositide-dependent protein kinase-1 (PDK-1)) activates the Akt/PKB pathway (Figure 1.15). The Akt/PKB causes a downstream signaling cascade, which results in the increase levels of anti-apoptotic factors, such as nuclear factor-Kβ (NF-Kβ), Bcl2 and BclX, as seen in Figure 1.15 (Vincent & Feldman, 2002).

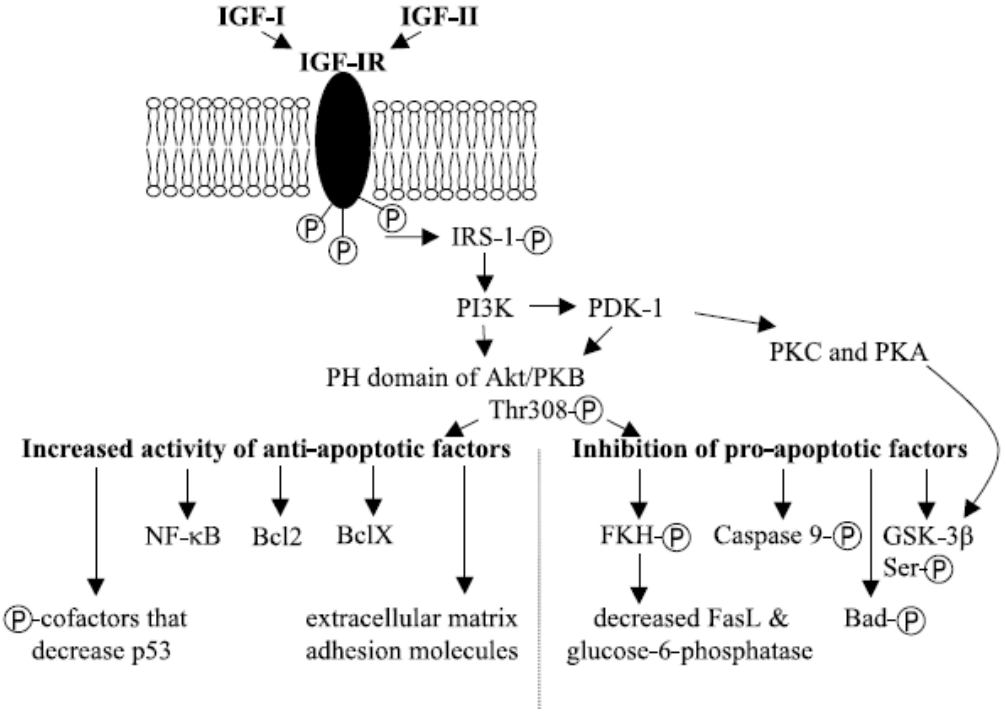

Figure 1.15 A schematic diagram showing how the activation of the IGF-1R, prevents apoptosis via activation of the Akt/PKB signaling pathway (Vincent & Feldman, 2002).

Other pathways, which are activated by IGF-1R are the Ras/Raf/MAPK and ERK pathways. Once the IGF-1R is activated by autophosphorylation, the Shc protein is activated at the tyrosine residues on the intracellular domain of the receptor (Vincent & Feldman, 2002). The activated Shc binds to Grb2 leading to the upregulation of the Ras G-protein and upregulation of the Raf and ERK. This pathway has been linked to cell migration and differentiation (Vincent & Feldman, 2002).

There are two commercially available recombinant preparations of IGF-1 for clinical use. The first is Increlex™ (mecasermin) manufactured by Ipsen Biopharmaceuticals (New Jersey, USA) and the other is iPLEX™ (mescasermin rinfabate) manufactured by Insmed (Virginia, USA) (Rosenbloom, 2009). The drug iPLEX™ is a combination of equimolar quantities of rhIGF-1 and rhIGFBP-3 (Williams *et al.*, 2008). The advantage of having a combination product is that the binding protein is readily available to form the binary and then ternary complex, therefore, prolonging its half-life and maintain an adequate concentration of rhIGF-1 in circulation. Increlex™ is indicated for treatment of growth failure in children, aged 2-17 years, with severe primary IGF-1 deficiency (BNF, 2017). The dosing regime is initially 40 μg kg^{-1} twice daily for one week, increasing in 40 μg kg^{-1} steps to a maximum dose of 120 μg kg^{-1} twice daily. Increlex™ is given by subcutaneous injection and is to be discontinued after one year if no response is evident (BNF, 2017). However, iPLEX™ is no longer available for growth therapy treatment (Rosenbloom, 2009).

Creams containing 1 % and 3 % IGF-1 were applied topically to wounds in diabetic and non-diabetic rats, to evaluate the effect on wound healing (Nunes Achar *et al.*, 2014). As a result of this study, Nunes Acher *et al*. (2014) found that both

creams increased the rate of re-epithelisation in both, diabetic and non-diabetic rats, compared to the control groups. There was also a significant increase in the expression of myofibroblast cells in the diabetic rats treated with the 3 % cream, compared to untreated diabetic rats. Nunes Acher *et al*. (2014) also noted that there was an increased expression of myofibroblasts in the non-diabetic treated groups, compared to the diabetic treated groups. This led to the suggestion that there may be a decrease in IGF receptor expression in diabetic animals (Nunes Achar *et al.*, 2014). They concluded from the study that topically applied 1 and 3 % IGF-1 creams to wounds increased the re-epithelisation rate by increased myofibroblast expression in rats (Nunes Achar *et al.*, 2014). Likewise, Provenzano *et al*. (2007) concluded that systemic administration of IGF-1, via subcutaneous injection, resulted in increased healing of ligament wounds in the hind legs of rats, compared to the control group and GH administered group. It was found that in the ambulatory groups that IGF-1, although not achieving full repair, after three weeks, did improve the tissue strength by approximately 60 % in comparison to the control group (Provenzano *et al.*, 2007). This was an interesting finding that suggests IGF-1 could be used to increase tissue strength in the healing of limbs that are disused due to patient immobilisation.

Emmerson *et al*. (2012) showed that the re-epithelisation by IGF-1 is mediated through binding to the IGF-1R, while certain anti-inflammatory effects were mediated through cross talk between the IGF-1R and estrogen receptor-α (ERα) in mice. This was demonstrated using ERα null mice, which showed reduced healing and increased inflammation, on administration of IGF-1, compared to the non-ovariectomised, ERα positive mice.

1.5 Hydrogels

Due to advances in molecular biology several growth factor based drugs have been widely studied for the treatment of chronic wounds, as discussed in the previous section. Hydrogels offer an efficient and effective way to topically administer a sustained release of these growth factors to the wound site, promoting and enhancing wound repair.

By definition, hydrogels are cross-linked 3D polymer networks, which have the ability to absorb and retain large volumes of water. It has been documented that some hydrogels can absorb up to 20 times their own weight in water or biological fluid (Kim *et al.*, 1992). Hydrogels can be formulated by several methods, which are split into two main categories, chemical and physical cross-linking. However, in some cases more than one of these cross-linking methods is used. As a result of the wide range of formulation methods available, using many different polymers, hydrogels can be produced with the exact physical and chemical properties needed for their intended use. This has led to the application of hydrogels in a vast range of disciplines, such as, the food industry (Shewan & Stokes, 2013), pharmaceutical industry (Peppas *et al.*, 2000), oil industry (Abidin *et al.*, 2012) and art industry (Carretti *et al.*, 2009).

1.5.1 Chemical cross-linking

Chemically cross-linked hydrogels display greater mechanical strength in comparison to physically crossed-linked hydrogels. As a result they are more resistant to degradation and complete dissolution in an aqueous environment (Hennink & van Nostrum, 2012). However, if the hydrogel needs to be biodegradable over a period of time, labile bonds can be added to the network to

facilitate this process. Labile bonds can be in the cross-links themselves or on the backbone of the polymer. They can be broken by various methods *in situ*, such as chemically or enzymatically, but the most common is by hydrolysis (Hennink & van Nostrum, 2012). Chemical cross-linking involves the formation of covalent bonds and includes chemical process, such as free radical polymerisation (Matyjaszewski *et al*., 1998), chemical reactions of complementary groups (Draye *et al*., 1998), high energy irradiation (Jabbari & Nozari, 2000), UV polymerisation (Ward & Peppas, 2001), or by enzymes (Sperinde & Griffith, 2000).

1.5.2 Physical cross-linking

The main interest behind physically cross-linked hydrogels are that it avoids the use of cross-linking agents and initiators. These compounds usually have to be extracted from the chemically cross-linked hydrogel before they can be used in a biological system. This is because they are often toxic substances that can cause harm and kill living organisms and have negative effects on the active components loaded into the hydrogel network (Hennink & van Nostrum, 2012). Physical cross-linking utilises non-covalent interactions, such as, ionic interactions (Hossain *et al*., 2001), stereo-complexation (de Jong *et al*., 2001), crystallisation (Peppas & Scott, 1992) and hydrogen bonding (Bell & Peppas, 1996).

1.5.3 Poly(vinyl alcohol)

Several synthetic polymers, such as poly(methyl methacrylate), (PMMA) poly(N-vinylpyrrolidone) (PVP), poly(ethylene glycol) (PEG) and poly(vinyl alcohol) (PVA) have been used by the pharmaceutical industry to manufacture hydrogels for drug delivery systems. PVA is synthetic polymer that is odourless, white to cream in

colour, and used for a wide range of applications. One of its most common and well known uses is as an adhesive. Other uses are in the textile industry as sizing and coating agent (Reddy *et al.*, 2014), a thickening agent in latex paint, in the manufacturing of paper, in gypsum based cements, in the food industry (DeMerlis & Schoneker, 2003) and pharmaceutical industry (Kadajji & Betageri, 2011). PVA is soluble in hydrophilic solvents, such as water, ethylene glycol and dimethyl sulfoxide (DMSO) (Kadajji & Betageri, 2011). A fully hydrolysed monomer of PVA has the molecular formula of $CH_2CH(OH)$, as seen in Figure 1.16. However, the vinyl alcohol monomer cannot exist as a stable form and, therefore, PVA polymers are synthesised through a two-step process (Hassan & Peppas, 2000). First, the vinyl acetate, which does exit in a stable monomer, undergoes free radical polymerisation giving poly(vinyl acetate) (PVAc). PVAc is then hydrolysed to yield PVA (Hassan & Peppas, 2000). The hydrolysis of PVAc never reaches completion, yielding PVA with different degrees of hydrolysis and acetate groups. Therefore, PVA actually exists as a co-polymer of PVAc and PVA. Different grades of PVA are available commercially with a range of degrees of hydrolysis (80–99 %) (Sigma-Aldrich, 2017).

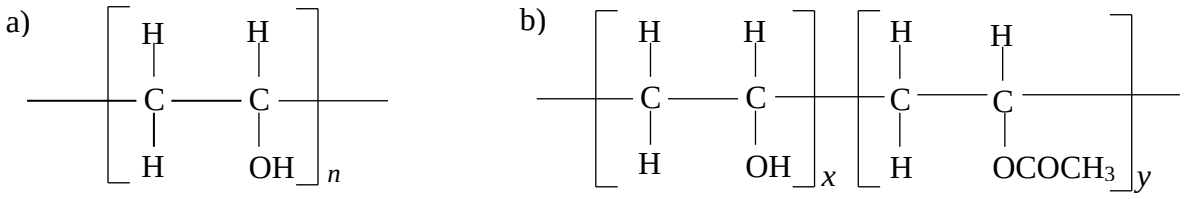

Figure 1.16 Skeletal formula of a) fully hydrolysed PVA, and b) a representation of partial hydrolysis of the PVA_c poly(vinyl alcohol-co-vinyl acetate).

Briscoe *et al*. (2000) express the degree of hydrolysis as a percentage using Equation 1.1, where *x* and y represent the molar fractions of the hydroxyl and acetate groups, respectively.

$$\text{Degree of hydrolysis} = \frac{x}{x+y} \text{ x } 100\ \% \qquad \text{Equation 1.1}$$

Both the degree of hydrolysis and amount of acetate groups present affect the solubility and crystallisation of the PVA variant (Kadajji & Betageri, 2011). Another factor, which is influenced by the degree of hydrolysis, and is thought to play a part in the solubility of PVA, is the presence of intra- and inter-chain hydrogen bonding, between the hydroxyl groups (Briscoe *et al.*, 2000). Therefore, it is expected that both the hydroxyl–solvent hydrogen bonding and the intra- and inter-chain hydrogen bonding play a part in determining the viscosity of a polymer solution, as a direct result of effecting the solubility. It can be seen in Figure 1.17, the degree of hydrolysis increases as solubility of the PVA decreases. It can also be seen that on increasing the temperature from 20 °C to 40 °C, the solubility of highly hydrolysed PVA increases.

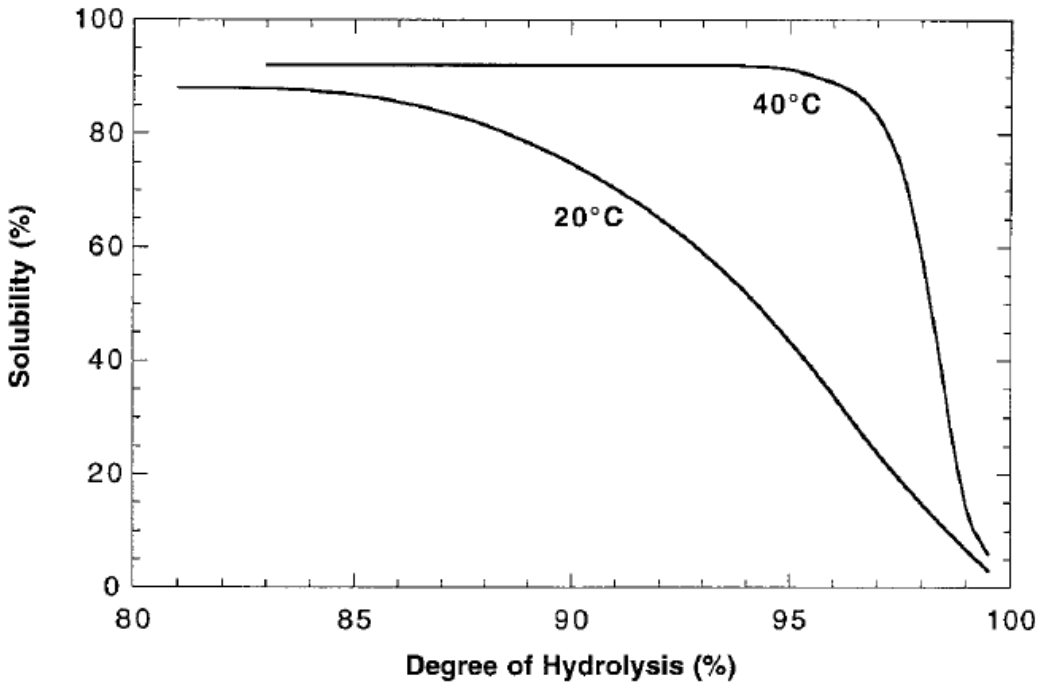

Figure 1.17 shows a solubility curve for PVA of average molecular weight 77,000 g mol^{-1} and varying degrees hydrolysis, at two different dissolution temperatures (20 °C and 40 °C) (Hassan & Peppas, 2000).

As mentioned previously, PVA is synthesised by free radical polymerisation of PVA_c followed by hydrolysis. This process results in the production of PVA of different molecular weights. Hassan & Peppas (2000) document that a polydispersity index (PDI) value of 2.0–2.5 is common in most commercial grade PVA and incidences of a PDI of 5 are not uncommon. The molecular weight of the PVA effects both its physical and chemical properties, such as adhesion, diffusivity, crystallisation and mechanical strength (Hassan & Peppas, 2000). As with degree of hydrolysis, similarly, there are many different grades of PVA available commercially, with varying ranges of molecular weight. For example, molecular weight ranges can fall between, 31,000–186,000 g mol^{-1} (Sigma-Aldrich, 2017). El-Kader *et al*. (2002) found from their study, that as the molecular weight of the PVA was increased (5000, 17,000, 72,000 and 125,000 gm mol^{-1}), the mechanical properties of PVA films, such as Young's modulus and the tensile strength at the break decreased. This resulted in the PVA films becoming more flexible, with an increase in PVA molecular weight (El-Kader *et al.*, 2002).

1.5.4 Sodium tetraborate decahydrate (borate)

Sodium tetraborate decahydrate (borate) is one substance that can be used to cross-link polymer chains to form a hydrogel network. Borate is of particular interest for cross-linking PVA hydrogels, due to its relatively low toxicity. In comparison, vanadate cross-linked polymers exhibit high toxicity towards living tissue, and, therefore, are not favourable for drug delivery (Loughlin *et al.*, 2008).

Boron is a naturally occurring solid state element, with an atomic number of 5 and relative atomic mass of 10.81 g mol^{-1}. Boron is present in large deposits throughout the world as mineral salts, such as sodium metaborate and borax. The

average soil concentration is 10–20 ppm and in boron mineral rich soil, it can be as high as 100 ppm (Woods, 1994). Large deposits have been exploited in Turkey, as early as 1865, closely followed by several deposits in California and Nevada in the USA. Borates have many uses, such as manufacturing of glass, fiberglass insulation, enamels, glazes, detergents, bleaches, alloys metals, agriculture and gold mining (Woods, 1994).

Sodium tetraborate decahydrate dissociates in water to yield equimolar quantities of borate ions and boric acid (Lin *et al*., 2003), as summarised in Equation 1.2. Borate anions can exist in different structural forms as the boron atom can coordinate in the trigonal or tetrahedral forms (Goel *et al*., 2013).

$$Na_2B_4O_7{:}10H_2O \longrightarrow 2B(OH)_3 + 2B(OH)_4^- + 2Na^+ \qquad \text{Equation 1.2}$$

1.5.5 Poly(vinyl alcohol) borate hydrogels

PVA hydrogels have gained interest within the pharmaceutical industry as drug delivery systems. This is because PVA hydrogels are biocompatible, non-toxic, non-carcinogenic and inexpensive to manufacture, on a large scale (Han *et al.*, 2014). In particular, PVA-borate hydrogels have shown to exhibit the required viscoelastic properties necessary, for topical drug delivery to wounds (McCarron *et al.*, 2011). PVA-borate is the preferred polymer-ion complex as it is the most biocompatible (Loughlin *et al.*, 2008). PVA can complex with other metal ions and charged secondary diazo dyes, such as Congo Red, cupric and vanadate ions (Loughlin *et al.*, 2008). However, polymer-vanadate complexes exhibit high toxicity towards living tissue, and, therefore, are not favourable for drug delivery (Loughlin *et al.*, 2008). The PVA-borate hydrogel network is the result of two different types of cross-

linking. First, there is complexation between the hydroxyl groups of the PVA polymer and the $B(OH)_4^-$ anion. Second, there is thought to be a certain degree of intra and inter chain cross-linking. This cross-linking is thought to be a combination of both polymer chain entanglement, as well as intra- and inter-chain hydrogen bonding, of the hydroxyl groups of the PVA (Briscoe *et al.*, 2000).

The complexation process between PVA and borate has been studied using ^{13}C and ^{11}B nuclear magnetic resonance (NMR) (Dawber & Green, 1986; Sinton, 1987; Bowcher & Dawber, 1989). It has been eluded that the complexation is a two-step process, whereby a mono-diol complex is initially produced, resulting in a poly(electrolyte), as seen in Figure 1.18a. As a result of the poly(electrolyte) formation there is electrostatic repulsion between the similar charged mono-diol complexes. This repulsion causes expansion of the polymer chains, leading to a sterically viable environment for the second step to proceed. The second reaction results in the formation of the di-diol complex, as seen in Figure 1.18b. Once an adequate amount of di-diol complexes have been formed the network forms a gel-like system (Loughlin *et al.*, 2008). As seen in Equation 1.2, the dissociation of sodium tetraborate decahydrate yields Na^+ cations. These Na^+ cations are though to also play a role in the overall shape of the polymer chains by exerting a shielding effect on the charged complexes (Lin *et al.*, 2005). Lin *et al*. (2005) state that the overall shape of the polymer chains in the hydrogel is due to a balance between the excluded volume of the polymer, electrostatic repulsion and the shielding effect of the Na^+ cations.

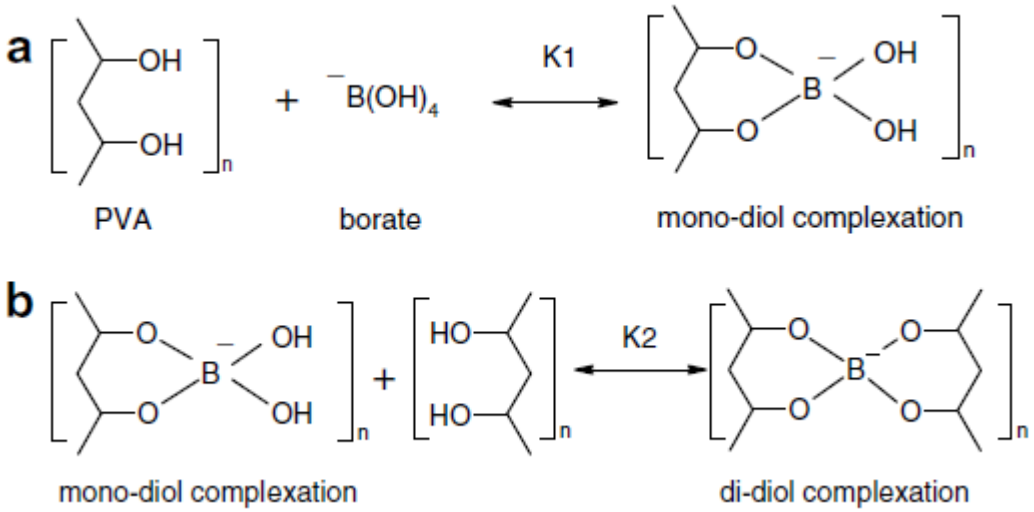

Figure 1.18 Shows the two-step complexation reaction between PVA and borate anions to form a hydrogel network. (a) Shows the first step of the reaction resulting in the formation of the mono-diol complex. (b) shows the second step of the reaction between the mono-diol complex and PVA, leading to the formation of the di-diol complex and thus the hydrogel network (Loughlin *et al.*, 2008).

The PVA-borate cross-link is reversible in nature, giving the PVA-borate hydrogels unique, self-healing and viscoelastic flow properties. These viscoelastic properties are advantageous for topical drug delivery in wound management and repair. The viscoelastic properties allow the PVA-borate hydrogel to flow into the wound crevasse, providing maximum wound-hydrogel contact, for drug delivery. However, the cross-linking present provides enough cohesive integrity to allow for complete intact removal from the wound. Another advantageous property of PVA hydrogels, which the PVA-borate hydrogels also possesses, is the ability to absorb excessive wound exudate, due to their ability to swell (Kim *et al.*, 2003; Holloway *et al.*, 2011). Chemically cross-linked gels possess good elasticity and cohesive integrity to remain intact *in situ* and be removed intact (Murphy *et al.*, 2012). However, they lack the sufficient fluid-like nature to flow into the wound itself. This results in a reduced gel-wound contact area, and therefore, reduced drug delivery. In contrast, physically cross-linked gels display good flow properties, but often lack the cohesive integrity

to be removed completely intact, needing to be physically washed and clean from the wound (Murphy *et al.*, 2012).

The reversible nature of the PVA-borate cross-link was studied using light scattering techniques by Lin *et al.* (2005). They observed that the cross-links had finite life-time (t_{life}), with the length of the observation determining the type of response. During short observations (high frequency) (Figure 1.19a) the cross-links do not have time to dissociate and, therefore, the system behaves like an elastic solid ($t < t_{life}$ and G' > G"). G" in rheological terms represents the loss modulus, or liquid-like response of the network system. While, G' represents the storage modulus, or elastic/solid-like response of the network system. During a long observation (low frequency) (Figure 1.19b) the cross-links have adequate time to dissociate and the system behaves overall like a viscous liquid ($t > t_{life}$ and G" > G') (Lin *et al.*, 2005; Murphy *et al.*, 2012).

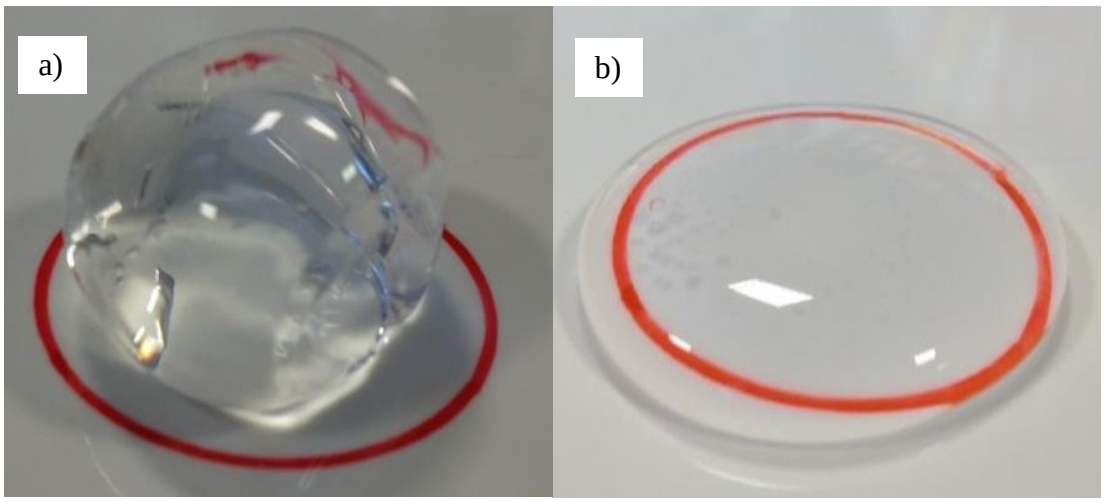

Figure 1.19 Photographs of samples of PVA-borate hydrogel (PVA 6 % w/w borate 2.0 % w/w) exhibiting its viscoelastic properties. a) The hydrogel sample was subject to high frequency, short observations by manually rolling it into a ball between two flat surfaces before being placed inside the red circle. This demonstrates the elastic solid-like response of the hydrogel system (G' > G"). b) On leaving the hydrogel sample to rest it experiences a low frequency, long observations. Thus the cross-linking has time to dissociate and the gel system flows like a viscous liquid down, out over the red circle. Demonstrating the liquid-like response (G" > G').

Chapter 2

Chapter 2

2 Formulation and characterisation of PVA-borate hydrogels

2.1 Introduction

Oscillating rheometry has been used to study several novel drug delivery formulations, including cross linked polymer semi-solids (Jones, 1999; Woolfson *et al.,* 2000; Jones *et al.,* 2001). In this study, oscillating rheometry was used to characterise physically the viscoelastic properties of the PVA-borate hydrogels. The word rheology is derived from two Greek words, *rheos* meaning stream current (e.g. flowing) and *logos* meaning study of. However, the modern day scientific definition of rheology can be defined as the study of flow and deformation of a material. It is important to ascertain accurately the rheological (mechanical) properties of pharmaceutical preparations, as these rheological properties allow for optimisation and quality control (Jones, 1999).

Hooke's Law defines the rheological behaviour of an ideal elastic solid. The law states that the applied stress to a sample is directly proportional to the strain of the sample, provided the specific elastic limit for the material is not exceeded. The resulting proportionality constant is known as Young's Modulus (E) (Equation 2.1).

$$\text{Youngs Modulus (E)} = \frac{\text{Stress } (\sigma)}{\text{Strain } (\gamma)} \qquad \text{Equation 2.1}$$

This elastic solid-like behaviour can be illustrated using a spring with an applied loaded, as seen in Figure 2.1. On applying a load (stress) to the spring, it is extended (strain) instantaneously, and is independent of time. Therefore, according to Hooke's Law it can be said that the load applied to the spring is directly

proportional to the spring's extension (Jones *et al.*, 2012). Once the load has been removed the spring returns instantaneously to its original length, by using the stored elastic energy from the extension process.

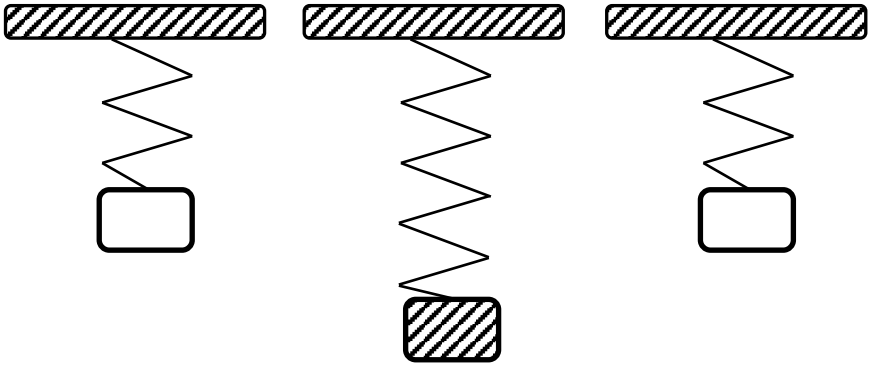

Figure 2.1 A schematic diagram representing Hooke's Law. It can be seen that on applying a load to the spring extension occurs. The elastic limit has not been exceed and on removal of the load the spring returns to its original length. The white box represents no load and the dashed box represents a load.

Newton proposed that for ideal liquids the applied stress is directly proportional to the rate of deformation (shear rate), with the proportionality constant known as viscosity (Equation 2.2) (Jones, 1999). Therefore, the viscosity of a Newtonian liquid is not dependent on the rate shear and will remain constant throughout a range of shear rates (Figure 2.2).

$$\text{Newtonian viscosity } (\eta) = \frac{\text{Stress } (\sigma)}{\text{Shear rate } (\gamma)} \qquad \text{Equation 2.2}$$

When liquids deviate from the ideal (Newtonian) behaviour, the relationship between the stress and shear rate is no longer directly proportional. These liquids are known as non-Newtonian liquids or fluids, which can either exhibit shear-thinning (pseudoplastic) or shear thickening (dilatant) behaviour, as seen in Figure 2.2.

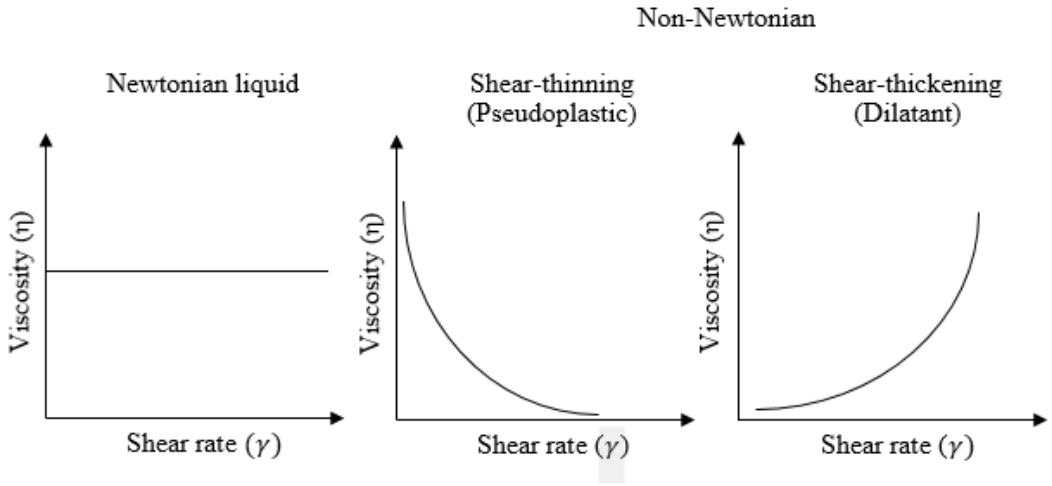

Figure 2.2 Typical schematic rheograms showing Newtonian and non-Newtonian flow behaviour, in relation to change in viscosity, when subject to an increasing shear rate.

Polymeric materials that are used for the production of biomedical and pharmaceutical products display viscoelastic properties. Viscoelastic materials exhibit both solid and liquid properties. The elastic component behaves in accordance with Hooke's law, while the viscous component behaves in accordance with Newton's law.

Materials can be further characterised by phase angle (δ) as a viscoelastic solid or viscoelastic liquid. An ideal liquid has a phase angle of 90° because the input strain and measured sinusoidal stress signal are one quarter of a cycle out of phase. Whereas, an ideal elastic material has a phase angle of zero as the input strain and output stress are in phase, as seen in Figure 2.3. A viscoelastic material will exhibit a phase angle between 0° and 90° with 45° being the boundary between the elastic solid-like and viscous liquid-like behaviour. If the elastic solid-like component is dominant over the viscous liquid-like component, the phase angle will be < 45° and the material will act like an elastic solid. But, if the viscous liquid-like component is dominant over the elastic solid-like component, the phase angle will be > 45° and the material will act like a viscous liquid.

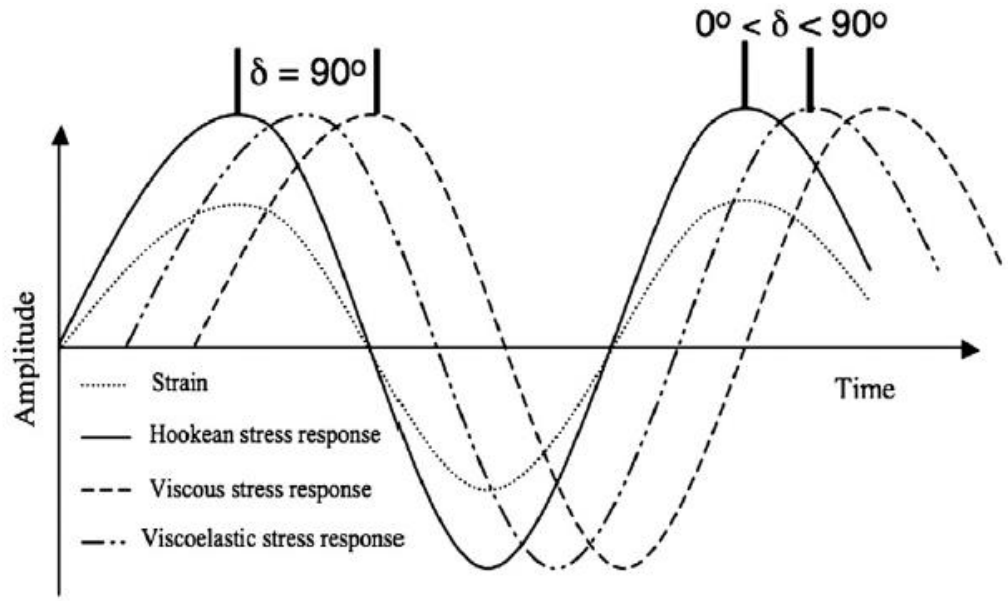

Figure 2.3 Schematic diagram showing the stress response of an ideal liquid, ideal solid and viscoelastic material on application of an input sinusoidal strain (Jones *et al.*, 2012).

Viscoelastic liquid behaviour can be illustrated using Maxwell's model. Maxwell's model consists of a spring and dashpot connected in series, in which both can be deflected independently (Mezger, 2014). Before loading, both the spring and dashpot show no deformation (Figure 2.4a). On loading with a constant force the spring deforms instantly, until it reaches a constant deflection, which is directly proportional to the loading force (Mezger, 2014), as seen in Figure 2.4b. After a short period of time, while the constant loading force is still being applied to the system, the piston of the dashpot beings to deform continuously. Both components of the system are now displaying deformation, as seen in Figure 2.4c. On removal of the loading force the spring instantly recoils, fully, to its original shape and length. However, the piston of the dashpot remains unchanged, demonstrating that viscoelastic liquid materials can remain partially deformed after a loading cycle is complete, as seen in Figure 2.4d (Mezger, 2014). This is because the reformation of the original shape is never totally complete, even after a prolonged period of rest, as these materials usually change shape to completely fill the space they occupy

(Mezger, 2014). Therefore, these types of materials essentially behave like a liquid, hence why they are called viscoelastic liquids or Maxwell fluids (Mezger, 2014).

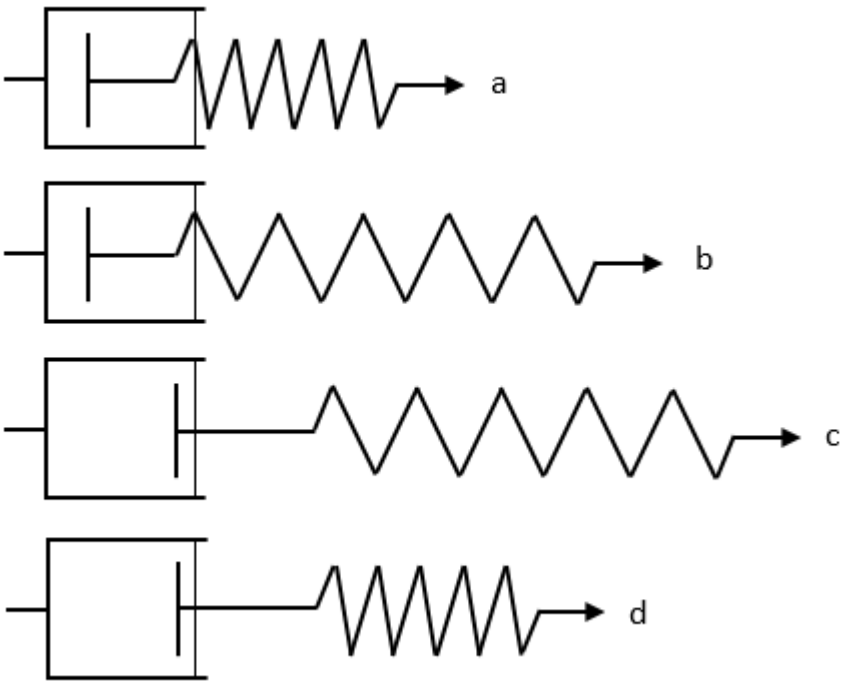

Figure 2.4 Schematic diagram representing the deformation of a viscoelastic liquid using Maxwell's model. a) No loading force applied. b) The spring representing the elastic component is deformed on application of a constant loading force. c) The piston of the dashpot has now been deformed after a short period of time, as the loading force is still being applied. d) The loading force has now been removed and the spring has recoiled. But the piston remains unchanged indicating partial irreversible deformation.

Viscoelastic solid behaviour can be illustrated using the Kelvin and Voigt's model. In a similar manner to the Maxwell model, the Kelvin and Voigt model uses a spring and dashpot to represent the elastic and viscous components, respectively. In this model, however, the spring and dashpot are connected in parallel by a rigid frame (Mezger, 2014). In Figure 2.5a both components exhibit no deformation. On application of a constant loading force, both the spring and the piston of the dashpot are deformed simultaneously, to the same extent (Mezger, 2014), as seen in Figure 2.5b. As the two components are rigidly connected, the spring cannot deform

instantaneously, due to the dashpot slowing the deformation process. Upon removal of the loading force, the spring begins to recoil in a non-instantaneous, time-dependent manner. This again is because the dashpot slows down the reformation process in a similar manner to the deformation process. However, due to the rigid connection between the two components, they both return to their original position and there is no partial permanent deformation (Mezger, 2014), as seen in Figure 2.4c.

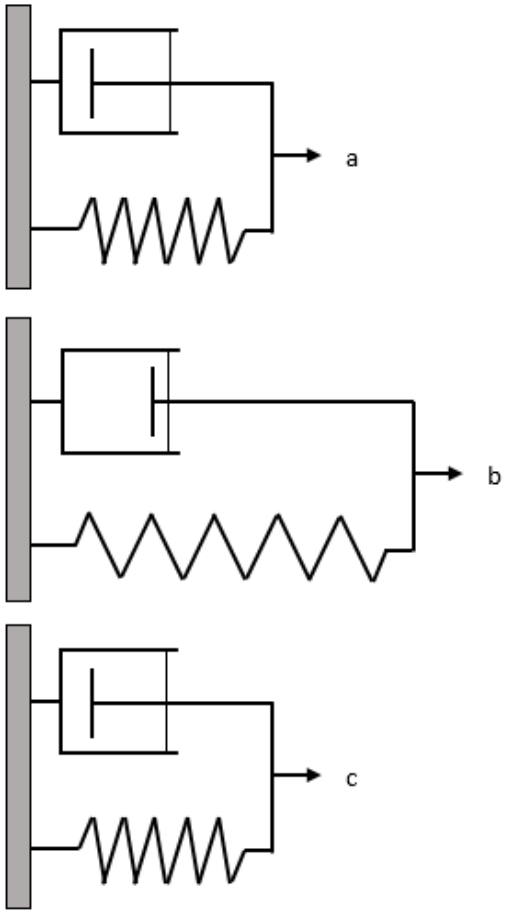

Figure 2.5 Schematic diagram representing the deformation of a viscoelastic solid using Kelvin and Voigt's model. a) No loading force applied. b) On application of a constant loading force the spring and piston of the dashpot are both deformed simultaneously, to the same extent and in a time-dependant manner. c) The piston and spring reform completely in a time-dependent manner with no permanent deformation of the system.

PVA-borate hydrogels have shown to exhibit the required viscoelastic properties necessary for topical drug delivery to wounds (McCarron *et al.*, 2011). The liquid-like behaviour of the PVA-borate hydrogels allows the hydrogel to flow

into the wound, completely filling the wound cavity. This provides maximum surface area for drug delivery from the PVA-borate hydrogel to the wound. However, the solid-like behaviour that occurs over short time periods allows the hydrogel to be removed completely intact from the wound cavity. This makes the PVA-borate hydrogel an ideal candidate for an advanced topical drug delivery system for wound management and repair.

2.2 Aims and objectives

The aim of work in this chapter is to formulate a range of PVA-borate hydrogels and characterise physically their viscoelastic properties.

Objectives;

- formulate a range of hydrogels of varying PVA and borate concentration,
- characterise the viscoelastic properties of the PVA-borate hydrogels using oscillatory rheometry,
- determine the swelling ability of the PVA-borate hydrogels,
- evaluate the effect of temperature on the viscoelastic properties of the hydrogels,
- evaluate the effect of varying concentrations of PVA and borate on the pH of the hydrogel formulation,
- determine the hydrogel stability over 24 months using oscillating rheometry.

2.3 Materials

Chemicals and reagents

Poly(vinyl alcohol) (PVA) (M_w = 31–50 kDa, 98–99 % hydrolysed), sodium tetraborate decahydrate (ACS reagent ≥ 99.5 %) and dialysis tubing cellulose membrane (Mw cut off 14 kDa, average flat width 43 mm) were purchased from Sigma-Aldrich Ltd. (Gillingham, Dorset, UK).

All reagents were of appropriate laboratory standard and used without further purification.

Deionised water (R ≥ 18 MΩ cm) was obtained from a Purelab Ultra, purification system, Egla (Marlow, UK)

Apparatus

Kinexus Pro rheometer, Malvern instruments (Malvern, Worcestershire, UK).

2.4 Methods

2.4.1 Formulation of PVA-borate hydrogels

A PVA stock solution (24 % w/w) was prepared by placing PVA (120 g) into a 500 mL Duran® bottle at 25 °C. Deionised water was added to bring the total weight to 500 g. The sealed bottle containing the PVA and deionised water was placed in a pre-heated water bath at 80 °C, swirling periodically until complete dissolution occurred. The Duran® bottle was then reweighed and adjusted to the required weight with deionised water. A borax stock solution (5 % w/w) was prepared by placing sodium tetrahydroxyborate decahydrate (10 g) into a 250 mL Duran® bottle at 25 °C. Deionised water was added to bring the total weight to 200 g. The sealed bottle was

then placed on a heated magnetic stirring mantle (50 °C, 30 rpm) until complete dissolution had occurred.

A range of PVA-borate semi-solid hydrogels were prepared by mixing various weights of PVA stock solution (24 % w/w), borax stock solution (5% w/w) and deionised water, to give hydrogels of final concentrations of PVA (6.0, 8.0, 10.0, 12.0 % w/w) and borax (1.0, 1.5, 2.0, 2.5 % w/w). A homogenous fluid-like gel was formed upon heating to 80 °C for approximately three hours, with periodic stirring. Hydrogels were weighed before and after heating and any weight loss was replenished with deionised water to achieve the desired total weight. The fluid-like gel was then transferred to poly(propylene) storage containers and left for 48 hours at room temperature and pressure (RTP) to allow complete gelation to occur before characterisation took place. Final formulations were clear and homogenous in appearance with no air bubbles present.

2.4.2 Physical characterisation of viscoelastic properties

Analysis of the viscoelastic properties was carried out using a Kinexus Pro rheometer (Malvern Instruments Ltd., Worcestershire, UK) on all hydrogel formulations. All tests were carried out at 25 °C ± 0.2 °C, using 20 mm diameter stainless steel parallel plate geometry and a working gap of 1-2 mm (Figure 2.6a). The linear viscoelastic region (LVR) of the PVA-borate hydrogel was determined by an amplitude sweep (0.01–100 % strain at a frequency of 1.0 Hz). All tests, thereafter, were performed within the LVR. Three replicates were performed for each formulation (n=3). A sample of the hydrogel was loaded onto the lower plate (Figure 2.6b.) as per the rSpace© software on screen instructions.

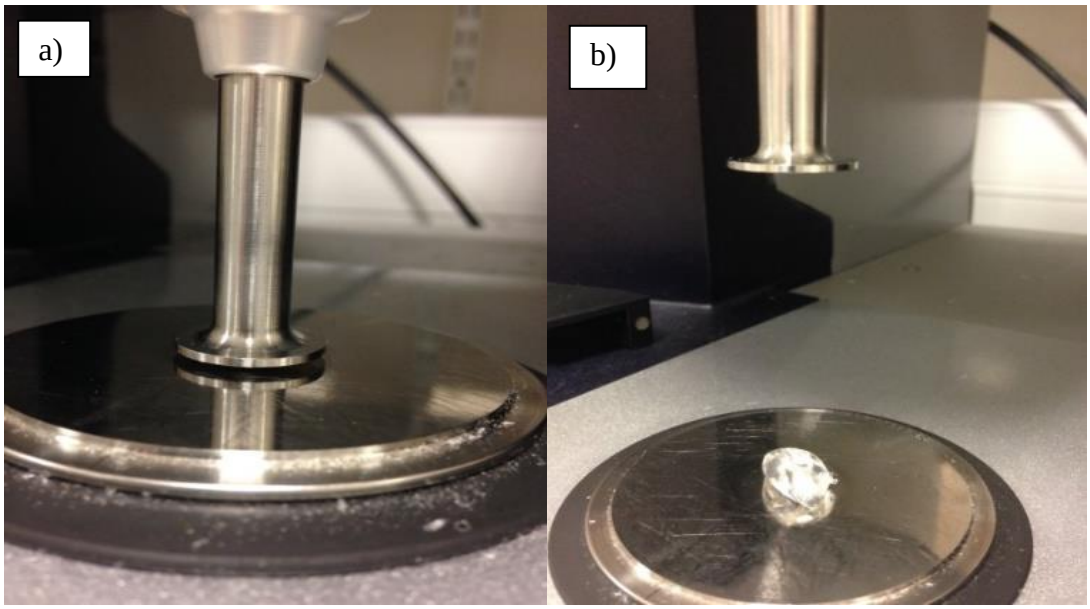

Figure 2.6 Shows photographs of the parallel plate geometry (20 mm) on the Kinexus Pro rheometer. a) Shows the 1 mm working gap width b) Shows a small sample of hydrogel loaded onto lower plate prior to compression by top plate.

A strain (1.0 %) controlled frequency sweep (0.1–10 Hz) was carried out, from which the crossover modulus (G_c) and relaxation time (t_r) were determined. The relaxation time was calculated from the crossover angular frequency using Equation 2.3 (Woolfson *et al.*, 2000), where t_r = relaxation time (s), ω = angular frequency (rad s^{-1}) and ν = frequency (Hz).

$$2\pi\nu = \omega \qquad t_r = \frac{1}{2\pi\nu} = \frac{1}{\omega} \qquad \text{Equation 2.3}$$

The cross model for oscillation data (Equation 2.4) was applied to the frequency sweep using the rSpace© software producing a plot of complex viscosity against angular frequency (ω). From the cross model, zero shear viscosity (η_0) and the correlation coefficient were derived.

$$\eta^* = \eta_\infty + (\eta_0 - \eta_\infty) / (1+(k\omega)^n) \qquad \text{Equation 2.4}$$

In Equation 2.4 η^* = complex viscosity (Pas), η_∞ = infinite viscosity (Pas), η_0 = Zero shear viscosity (Pas), ω = angular frequency (rad s^{-1}), k is inversely proportional to the onset of shear thinning and n is the shear thinning index.

2.4.3 Working gap width test

To obtain accurate reproducible crossover modulus readings for the more rigid formulations, the working gap width of the parallel plate geometries was increased from 1.0 mm to 1.5 mm and 2.0 mm. To ascertain if changing the working gap width altered the magnitude of the crossover value and, therefore, skew the data, four hydrogel formulations were selected (PVA 8 % w/w borate 1.0, 1.5, 2.0, 2.5 % w/w) and a frequency sweep was ran on each, as detailed in section 2.4.2, at each of the three working gap widths. Statistical analysis was used to determine any significant changes in the crossover modulus of each formulation by applying two-way analysis of the variance (ANOVA) to the data.

2.4.4 Yield stress analysis

Yield stress (σ) was determined by stress growth carried out using a Kinexus Pro rheometer (Malvern Instruments Ltd., Worcestershire, UK) on all hydrogel formulations. Shear rate was kept constant (0.01 s^{-1}) and stress build up was monitored over a 5 minute period with a sampling interval of 1 second. Peak stress was analysed and recorded by the rSpace © software. All tests were carried out at 25 °C ± 0.2 °C, using 20 mm diameter stainless steel parallel plate geometry and a working gap of 1 mm. Three replicates were performed for each formulation (n=3).

2.4.5 Adhesive analysis

Adhesiveness of each hydrogel formulation was determined from the normal force profile as a function of time as the gap between the top and bottom parallel plate increased. This was carried out using a Kinexus Pro rheometer (Malvern Instruments Ltd., Worcestershire, UK). The top plate was submerged 2 mm into each sample (10.00 g) in a poly(propylene) container (Sarstedt diameter 43 mm depth 55 mm) with a contact time of 30 s before the pull-away test was triggered, as seen in Figure 2.7. Pull-away speed was 10.33 mm s^{-1} as used by Murphy *et al*. (2012). The rSpace© software carried out peak normal force analysis which provided the pull away force (N). Three replicates were performed for each formulation (n=3).

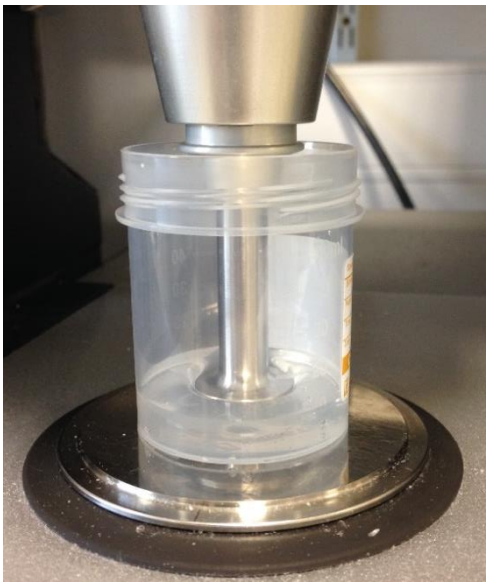

Figure 2.7. Photograph showing the 20 mm upper plate submerged into a PVA borate hydrogel sample (10.00 g) prior to the triggering of the pull-away test, at room temperature.

2.4.6 Temperature sweep

The effect temperature had on complex viscosity of several PVA borate hydrogels was determined using a Kinexus Pro rheometer (Malvern Instruments Ltd., Worcestershire, UK). A single frequency (2.0 Hz) shear strain (1.0%) controlled

temperature ramp was run on each hydrogel sample. Samples were equilibrated to 25 ± 0.2 °C before starting the temperature ramp. The temperature ramp range was 25–80 °C with the temperature increasing at a constant rate of 5 °C min^{-1} and a sampling interval of 2 seconds. All tests were carried using 20 mm diameter stainless steel parallel plate geometry and a working gap of 1–2 mm.

2.4.7 pH study

The pH of each hydrogel formulation was measured using a Sensorex® spear tip pH probe for measuring the pH of semi-solid materials. The probe was submerged into each hydrogel and the pH recorded once the reading remained constant for 10 s. Three replicates were performed for each formulation (n=3).

2.4.8 Hydrogel swelling study

The ability of each hydrogel formulation to swell was measured using a fluid uptake study. A sample of hydrogel (10.00 g) was placed into cellulose membrane dialysis tubing with a 14 kDa molecular weight cut off. The tubing was tied tightly at each end ensuring there were no air spaces between the tubing and the gel. The tubing containing the hydrogel sample was weighed before being placed in beaker containing 100 mL phosphate buffer saline (pH 6.8) at 37 °C. The hydrogel was removed at 30 minute intervals over a total time of 180 minutes. The surface of the dialysis membrane was patted dry with tissue paper to remove any surface liquid and weighed before being placed back into the beaker. The swelling ratio was calculated as a percentage using Equation 2.5 (Kim *et al*., 2003), where w_s = weight of swollen sample and w_d = weight of initial dry sample.

$$\% \text{ Swelling ratio} = \frac{(Ws - Wd)}{Wd} \times 100 \qquad \text{Equation 2.5}$$

2.4.9 Hydrogel formulation stability study

Stability of hydrogel formulations was monitored over 2 years by measuring the crossover modulus at 9, 12, 18 and 24 months. Three replicates were performed for each formulation (n=3). Statistical analysis was used to determine any significant changes in the crossover modulus of each formulation by applying two-way analysis of the variance (ANOVA) to the data.

2.5 Results

A range of PVA-borate formulations were found to have sufficient complexation to produce hydrogels for topical drug delivery. The concentrations of PVA and borate used to produce sixteen formulations were 6.0, 8.0, 10.0, 12.0 % w/w and 1.0, 1.5, 2.0, 2.5 % w/w, respectively. Each hydrogel formulation was clear and homogenous in appearance, once complete gelation had occurred, as seen in Figure 2.8. The viscoelastic properties of each formulation were characterised physically using oscillating rheometry, as stated in section 2.4.

Figure 2.8 Picture of a sample of a PVA (6.0 % w/w)–borate (2.0 % w/w) hydrogel at room temperature, manufactured as described in section 2.4.1.

A typical plot of $G`$ $G``$ and phase angle (δ) against frequency from a frequency sweep test of a PVA-borate hydrogel can be seen in Figure 2.9. As seen in

Figure 2.9, the crossover point is the frequency at which the loss modulus (G'') and the storage modulus (G') crossover each other. The corresponding shear force at this frequency is then documented as the crossover modulus value, which is unique to each formulation. The crossover modulus allows for precise reproducibility of any formulation. At low frequencies (long time scales) the PVA-borate hydrogel has a liquid-like behaviour as the viscous component G'' is dominant over the elastic component G' and the phase angle is greater than 45°. At the point where the two components cross the hydrogel ceases to behave like a liquid and begins to behave like a solid. Now the solid component G' is dominant over the liquid component G'' at higher frequencies (short time scales) and the phase angle is less than 45°, therefore, the hydrogel now has solid like behaviour.

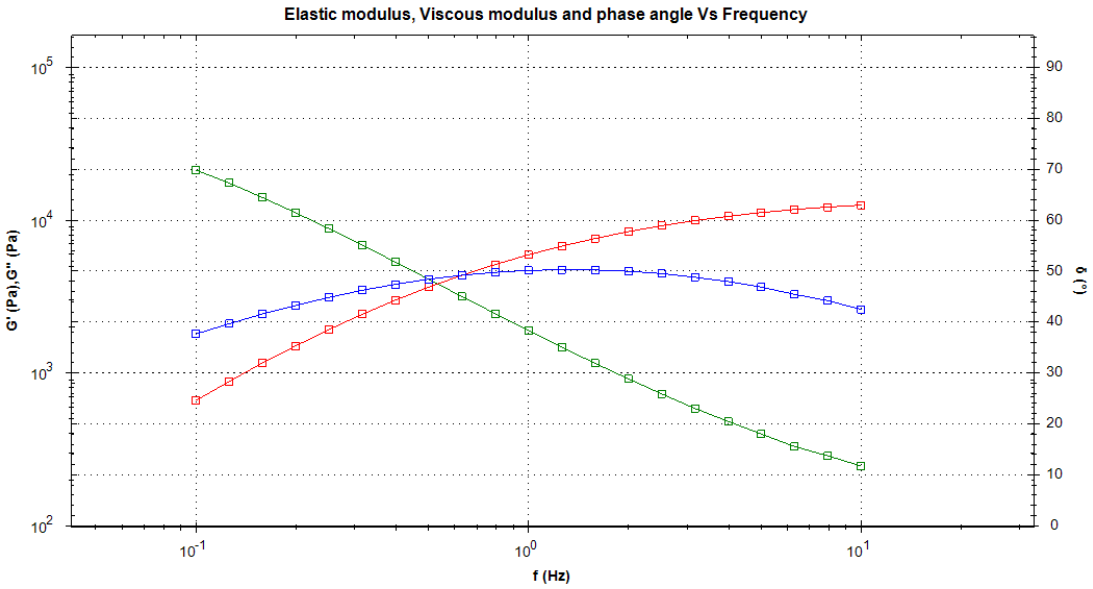

Figure 2.9 A typical PVA-borate hydrogel plot of *G`* *G``* and phase angle (δ) against frequency, produced from a strain controlled frequency sweep (1.0–10 Hz) at 25 °C ± 0.2 °C. The green line represents the phase angle (δ), the red line represents the elastic solid-like component of the hydrogel and the blue line the viscous liquid-like component.

Figure 2.10 shows the results from strain controlled frequency sweeps with crossover point analysis carried out on each of the sixteen hydrogel formulations. It can been seen from Figure 2.10 that increasing the PVA concentration from 6 to 12

% w/w increased the crossover modulus. Increasing the borate concentration also caused the crossover modulus to increase. A more pronounced increase in crossover modulus was seen when increasing the borate concentration from 1.0 to 2.5 % w/w for PVA concentrations 8.0, 10.0 and 12.0 % w/w. However, the 6.0 % w/w PVA concentration only showed a marginal increase in crossover modulus on increasing the borate concentration. It was observed that when increasing the PVA concentration from 10.0 to 12.0 % w/w, whilst keeping the borate concentration constant at 2.0 and 2.5 % w/w, the increase in crossover modulus was more pronounced than when increasing the PVA concentration from 6.0 % through to 10.0 % w/w, for the same borate concentrations. The largest crossover modulus was 25037 ± 2625 Pa for PVA 12.0 % w/w borate 2.5 % w/w hydrogel and the lowest crossover modulus was 3678 ± 374 Pa for the PVA 6.0 % w/w borate 1.0 % w/w gel.

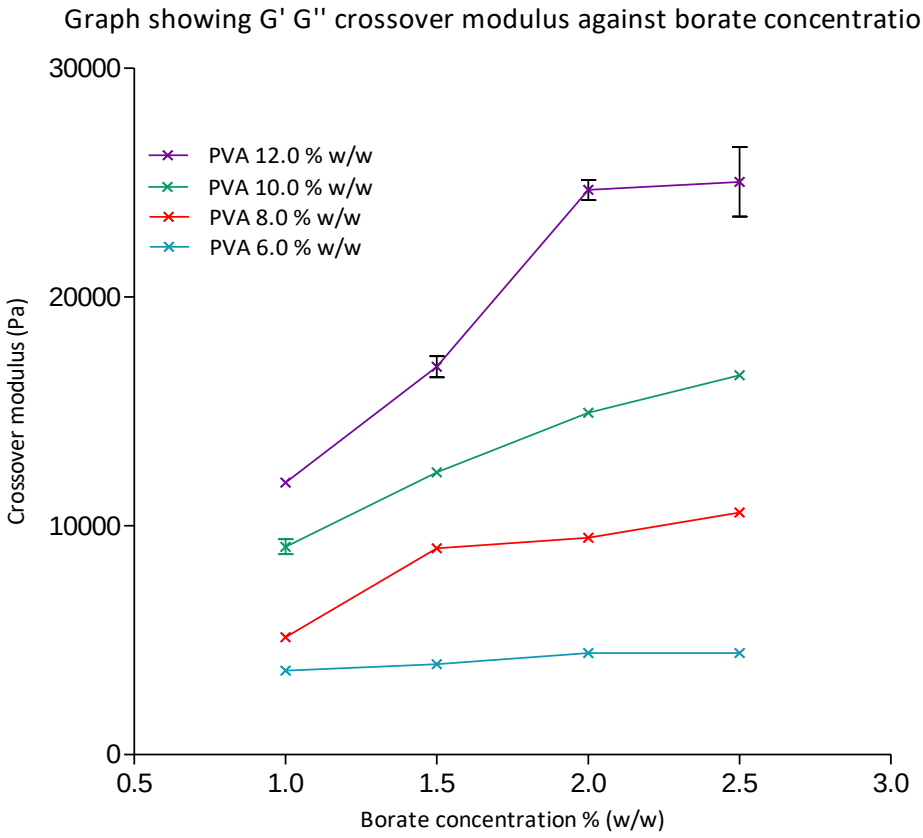

Figure 2.10 Crossover modulus plotted against borate concentration. Data was from a strain (1.0 %) controlled frequency sweep (0.1–10 Hz). Data shown as mean ± standard deviation (n=3). All measurements carried out at 25°C ± 0.2°C.

To obtain crossover values for formulations PVA 12.0 % w/w borate 2.0 % w/w and PVA 12.0 % w/w borate 2.5 % w/w, the working gap width of the parallel plate geometry had to be increased from 1.0 mm to 1.5 mm and 2.0 mm, respectively. The experimental study in section 2.4.3 was designed and carried out to determine if increasing the working gap width had any significant effect on the magnitude of the crossover modulus. It can be seen from Figure 2.11 that there is only a small variance in the crossover modulus for each of the hydrogels tested on increasing the working gap width. Two-way ANOVA statistical analysis on the data set further confirmed that there was no significant difference between the three crossover modulus values for each of the hydrogels.

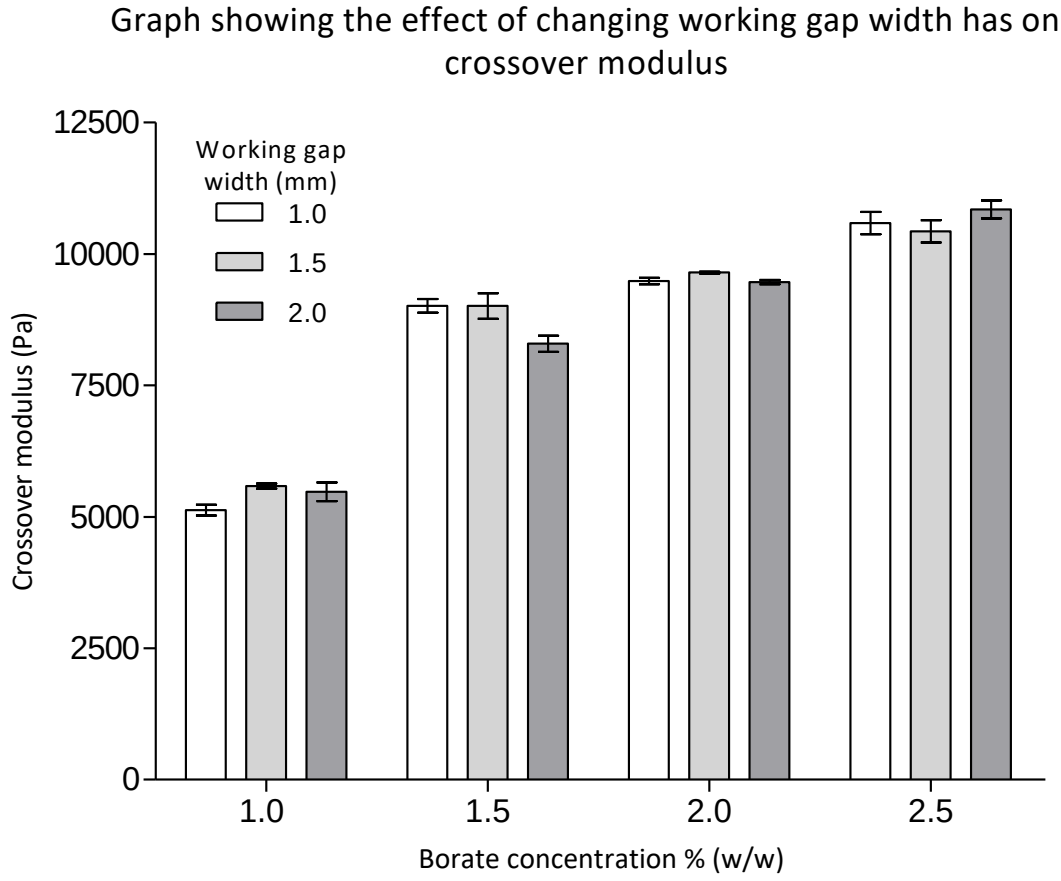

Figure 2.11 Graph showing the effect of changing working gap width on crossover modulus values of PVA 8.0 % w/w borate 1.0, 1.5, 2.0, 2.5 % w/w hydrogels. Data shown as mean ± standard deviation (n=3). All measurements carried out at 25°C ± 0.2°C. $p < 0.05$ (*), $p < 0.01$ (**), $p < 0.001$ (***).

Relaxation time was determined for each formulation and plotted against PVA concentration, as seen Figure 2.12. For formulations containing 2.0 and 2.5 % w/w borate, it was observed that the relaxation time increased with an increase in PVA concentration. The hydrogel formulation containing PVA 12.0 % w/w borate 2.5 % w/w took the longest time, 0.369 ± 0.019 s, to recover from the applied strain with formulation PVA 12.0 % w/w borate 1.0 % w/w taking the shortest time (0.106 ± 0.002 s) to recover. Another trend identified was the decrease in relaxation time for hydrogels containing 1.0 % w/w borate with an increase in PVA concentration from 6.0 to 12.0 % w/w. The formulation PVA 6.0 % w/w borate 1.0 % w/w exhibited a relaxation time of 0.191 ± 0.004 s, which decreased to 0.106 ± 0.002 s on increasing the PVA concentration to 12.0 % w/w. This trend was the opposite of that observed for the other three borate concentrations. Hydrogels containing 1.5 % w/w borate showed little change in relaxation time on increasing the PVA concentration, when compared to the other borate concentrations. Increasing the borate concentration increased the relaxation time for all the PVA concentrations. The smallest increase in relaxation time overall on increasing the borate concentration was observed in hydrogels containing PVA 6.0 % w/w. It could, therefore, be stated that the borate concentration has a greater effect on relaxation time than PVA concentration. However, changes in either or both result in altered relaxation times.

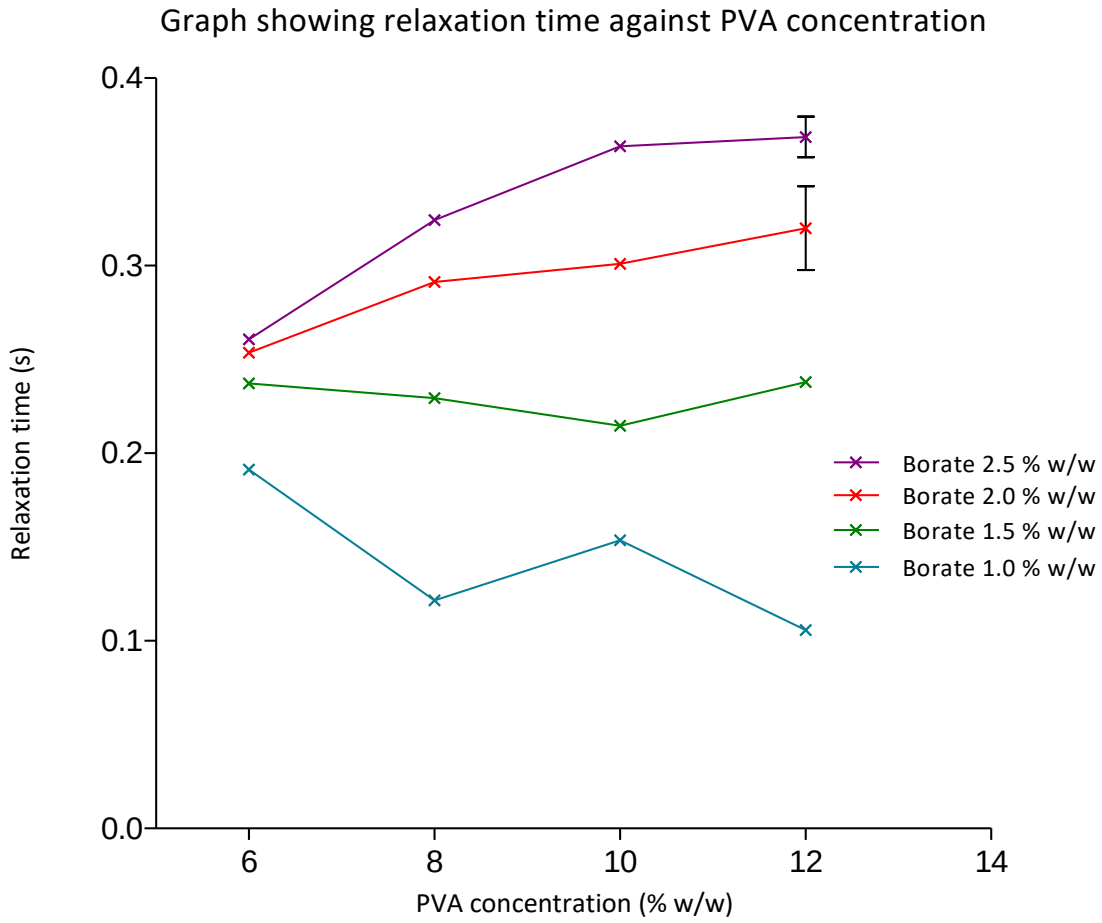

Figure 2.12 Relaxation time calculated from the crossover modulus data using Equation 2.3, plotted against PVA concentration. Data shown as mean ± standard deviation (n=3).

The zero shear viscosity was determined for each formulation by applying the cross model to the frequency sweep data. The cross model takes into account the whole flow curve produced, which includes the zero shear viscosity region, power law region and infinite shear viscosity region. The zero shear viscosity value is determined at the point where the viscosity plateaus, as the shear rate decreases and approaches zero. Therefore, it represents the viscosity of a material at rest and is useful to predict stability of pharmaceutical preparations. Figure 2.13 shows the zero shear viscosities for each of the hydrogel formulations. It can be stated that as PVA and borate are increased, the zero shear viscosity of the hydrogel also increases. One exception to this statement was seen for the PVA 8.0 % w/w borate 2.5 % w/w

hydrogel formulation. On increasing the borate concentration of a hydrogel containing 8.0 % w/w PVA from 2.0 to 2.5 % w/w, the zero shear viscosity decreased from 18077 ± 819 to 13493 ± 178 Pas. The increase in zero shear viscosity on increasing the borate concentration was minimal for hydrogels containing 6.0 % w/w PVA, compared to PVA 12.0 % w/w hydrogels, which displayed an increase in zero shear viscosity on increasing the borate concentration from 1.0 % w/w (3109 ± 148 Pas) to 2.5 % w/w (55150 ± 418 Pas), as seen in Figure 2.13.

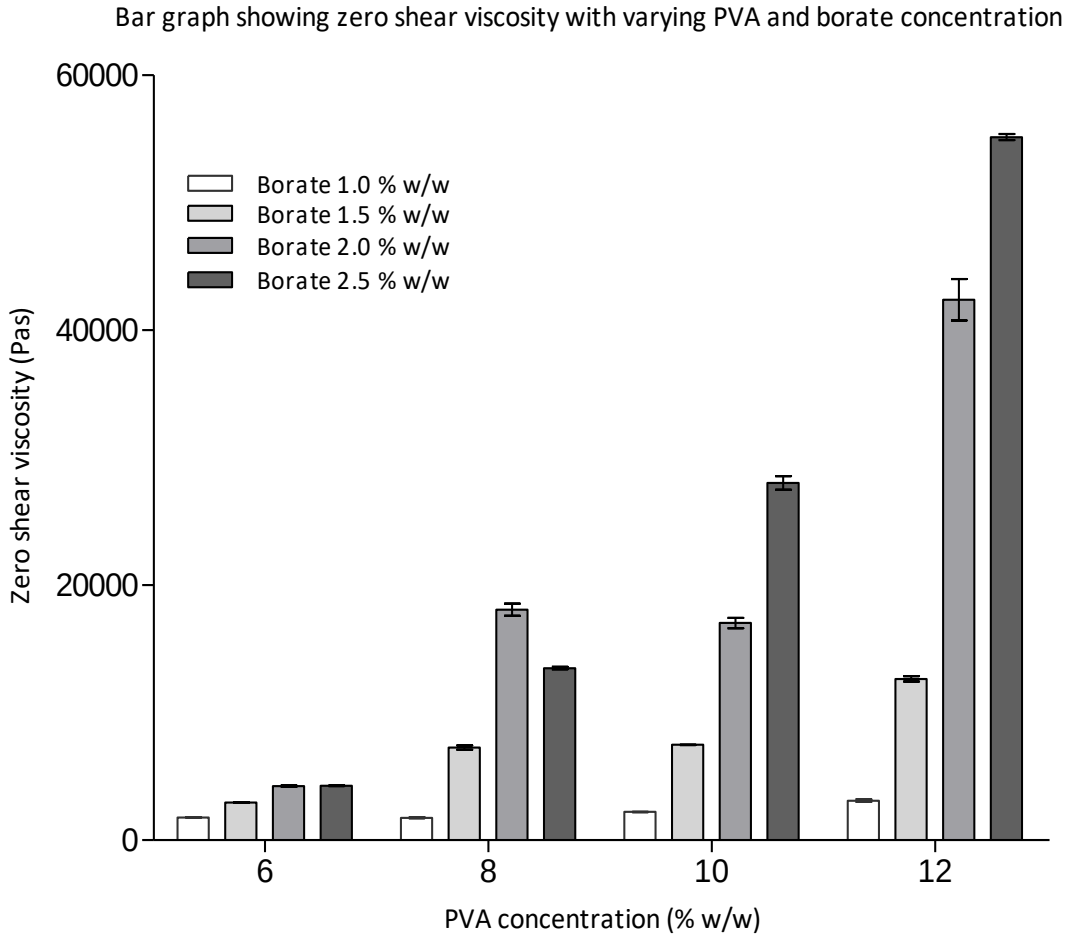

Figure 2.13 Zero shear viscosity calculated using cross model (Equation 2.4) fitted to crossover modulus data plotted against PVA concentration. Data shown as mean ± standard deviation (n=3).

Yield stress analysis determines the stress required to reach the yield point. The yield point is the point up until which any deformation if elastic is non-permanent, and on removal of the stress the material will return back to its original shape. After the yield point any further deformation is permanent, and the material will not return to its original shape. The trends seen in Figure 2.14 are similar to those seen in Figure 2.10 for the crossover analysis. As PVA and borate concentrations were increased, so did the shear stress required to reach the yield point. Hydrogels containing 6.0 % w/w PVA showed a minimal increase in shear stress with increasing borate concentration. The largest increase was observed for the PVA 12.0 % w/w hydrogels when the borate concentration was increased from 2.0 to 2.5 % w/w giving a pronounced increase in shear stress from 288.5 ±24.2 Pa to 771.9 ± 52.0 Pa.

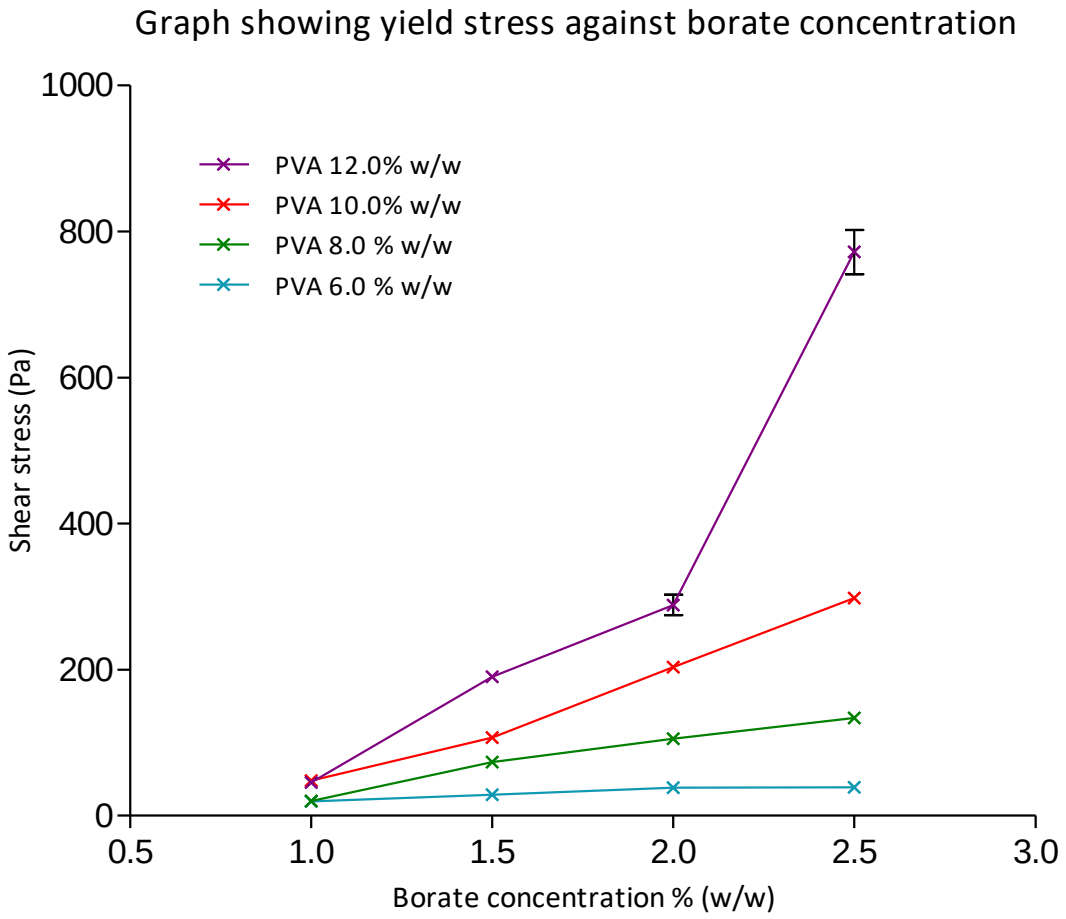

Figure 2.14 Graph showing the effect varying PVA and borate concentrations had on yield point stress represented as shear stress (Pa) in the graph. Data shown as mean ± standard deviation (n=3).

A tackiness test was designed to run on the rheometer using a normal force pull-away sequence. The test was designed to mimic the sequence of events and parameters that a texture analyzer uses to determine adhesive properties. It was found that increasing both the PVA concentration and the borate concentration caused an increase in tackiness of the hydrogels. The hydrogel formulation containing PVA 12.0 % w/w borate 2.5 % w/w was the tackiest, requiring a normal force of 9.60 ± 0.30 N to pull the submerged top parallel plate out of 10 g of hydrogel after a contact time of 30 sec. The formulation PVA 6.0 % w/w borate 1.0 % w/w was the least tacky requiring a normal force of 2.23 ± 0.25 N to pull the submerged top plate out of the hydrogel. Increasing the borate concentration from

1.0 to 1.5 % w/w, while keeping the PVA concentration constant at 6.0 % w/w had no effect on tackiness of the formulations, as seen in Figure 2.15. A similar trend was seen when increasing the borate concentration from 1.5 % to 2.0 % w/w, while keeping the PVA concentration constant at 8.0 % w/w, resulting in 4.04 ± 0.37 N and 4.09 ± 0.76 N normal forces, respectively.

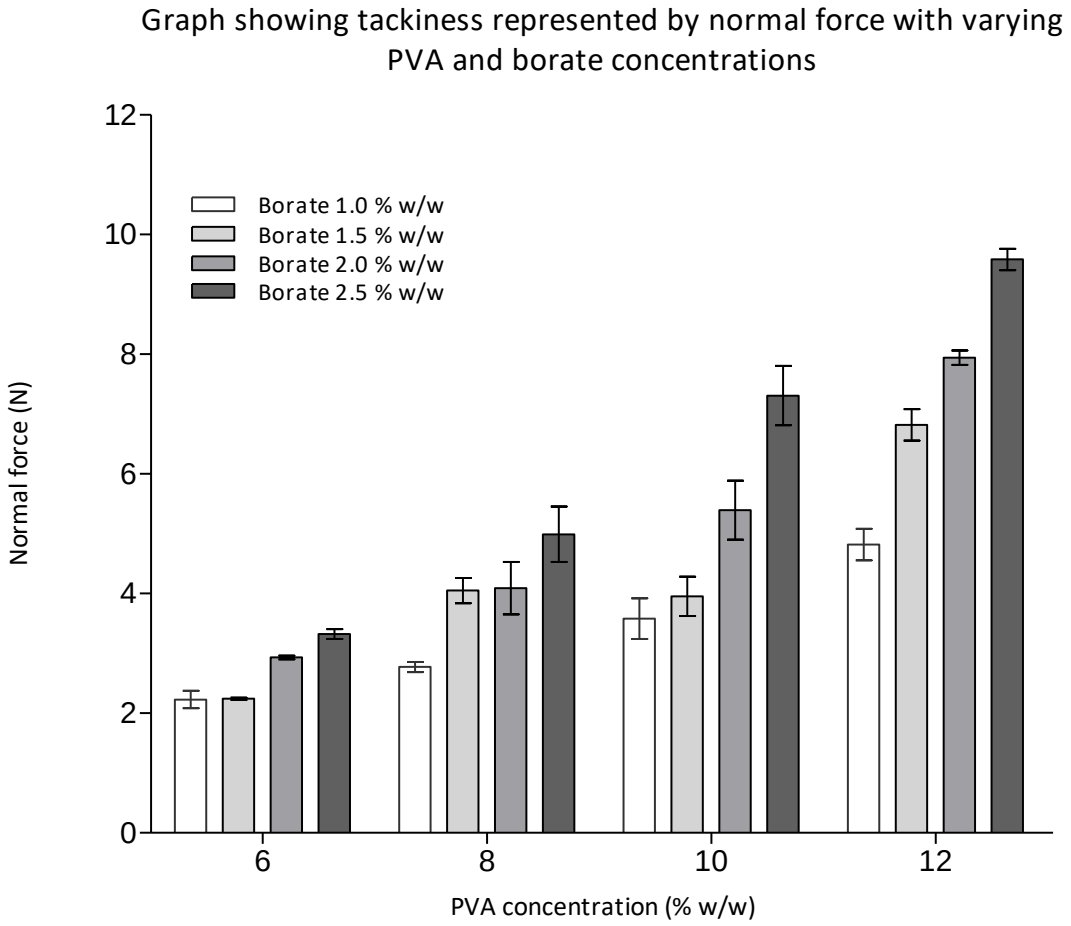

Figure 2.15 . Tackiness represented as normal force plotted against PVA concentration. Contact time of 30 s and pull-away speed was 10.33 mm s^{-1}. Data shown as mean ± standard deviation (n=3). All measurements carried out at 25°C ± 0.2°C.

Temperature sweeps were carried out on each formulation to determine how an increase in temperature affected the viscosity of the hydrogels. Figure 2.16 shows the effect of temperature increase on the viscosity of hydrogels of a constant PVA concentration (8.0 % w/w), but varying borate concentration. It can be seen from Figures 2.16 and 2.17 that as the temperature is increased from 25 to 80 °C the

viscosity of all the hydrogels decreases until the gel system is completely fluid like. It was expected that all four formulations on reaching 80 °C would be of similar viscosity. This is because during the formulation process, as detailed in section 2.4.1, the gels are heated to 80 °C for several hours to allow for complete fluidisation and homogeneity. Figure 2.17 shows the same temperature sweep as Figure 2.16 but with a constant borate concentration (2.0 % w/w) and varying the PVA concentration. The same trend was observed as in Figure 2.17 with the viscosity of all the hydrogels of varying PVA concentration decreasing with increasing temperature.

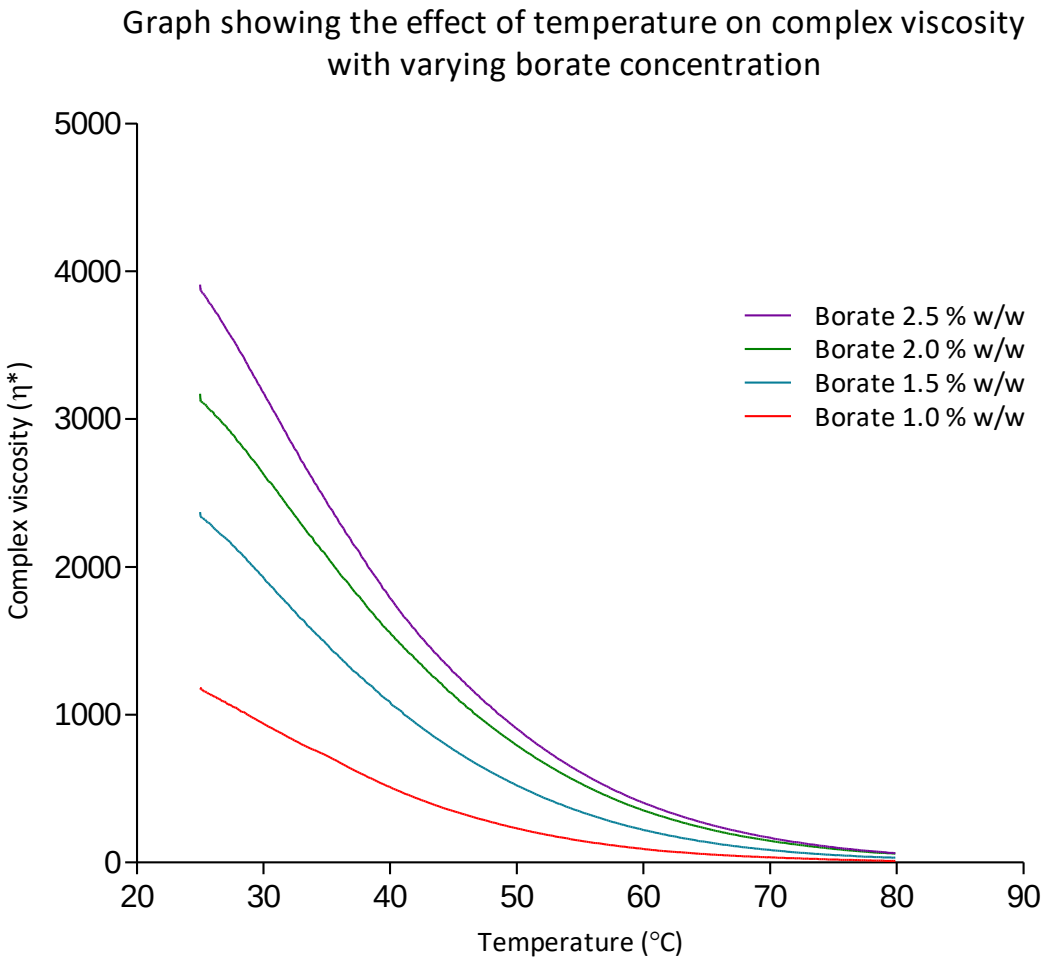

Figure 2.16 Graph showing temperature sweep (25–80 °C) plotted against complex viscosity for four PVA borate hydrogels with varying borate concentration (1.0, 1.5, 2.0, 2.5 % w/w) and a constant PVA concentration of (8.0 % w/w).

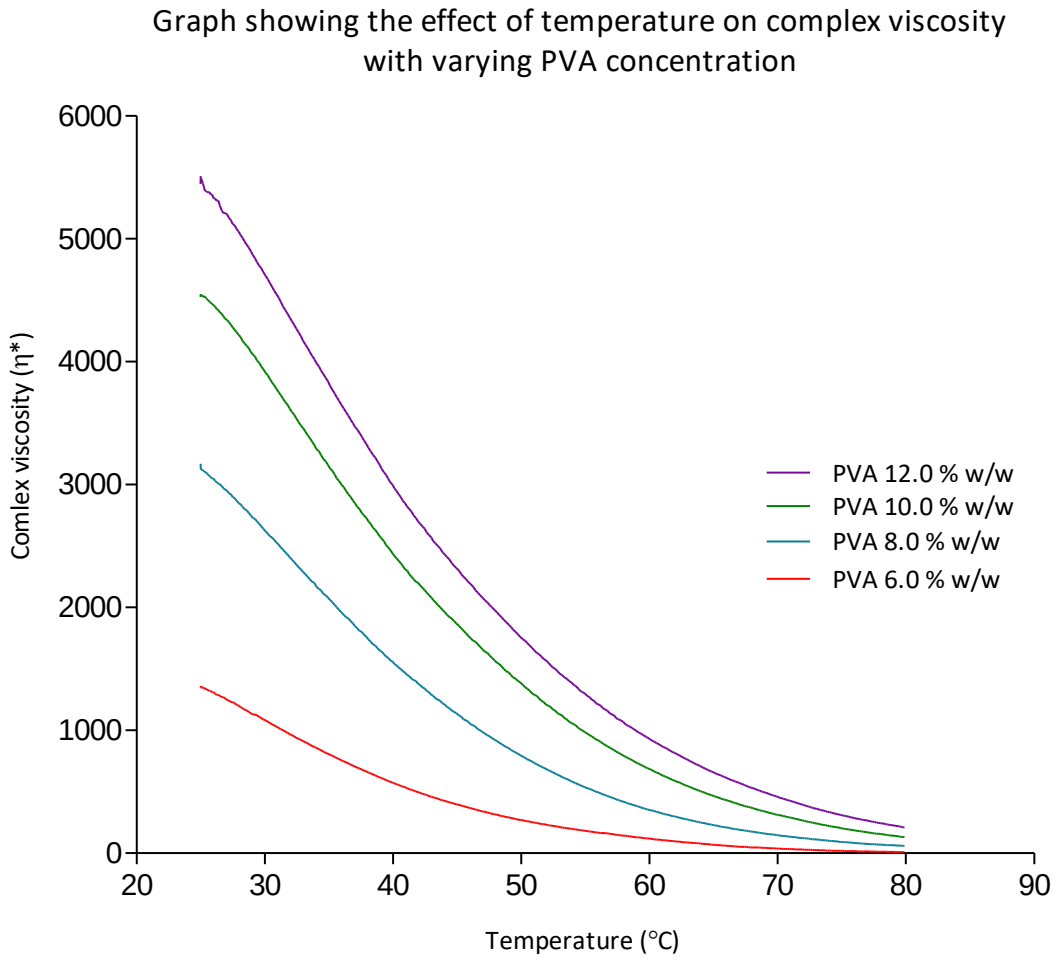

Figure 2.17 Graph showing temperature sweep (25–80 °C) plotted against complex viscosity for four PVA–borate hydrogels with varying PVA concentration (6.0, 8.0, 10.0, 12.0 % w/w) and a constant borate concentration of (2.0 % w/w).

The pH was recorded for each of the sixteen formulations using a pH probe for semi-solid materials. It was found that all the formulations fell within the pH range of 7.3–8.3. Therefore, it can be concluded that hydrogels are neutral in pH with three formulations being slightly basic. The basic formulations occur when high concentrations of borate are incorporated with low concentrations of PVA. It can be seen from Figure 2.18 that the higher the borate concentration was in the formulation, regardless of the PVA concentration, the higher the pH was. As a result of this finding it can be stated that the concentration of borate in the formulation has a greater effect on the pH than the PVA concentration. However, it was also observed that the lower the PVA concentration was within the formulation the higher

the pH of the hydrogel. The PVA 6.0 % w/w borate 2.5 % w/w hydrogel was found to have the highest pH of 8.3, with the PVA 12.0 % w/w borate 1.0 % w/w hydrogel having the lowest pH of 7.3.

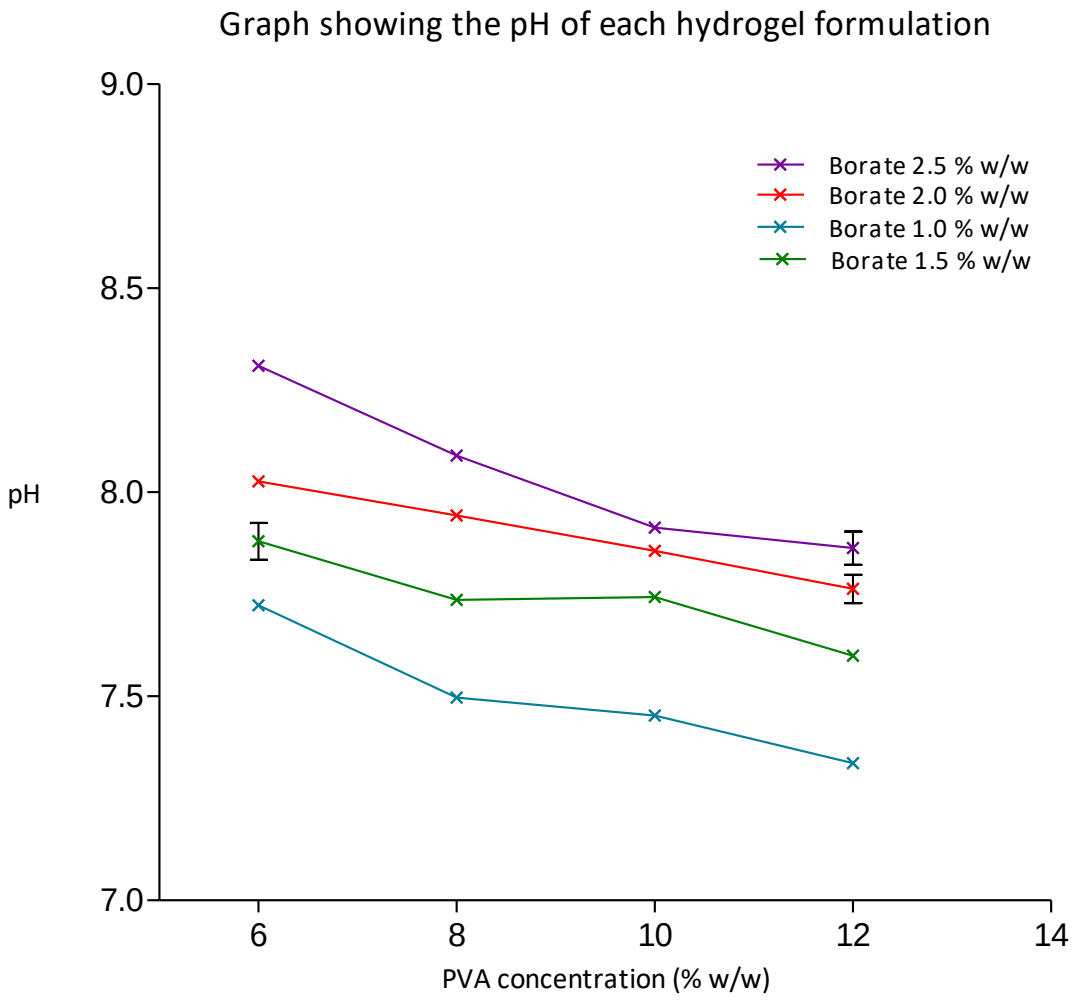

Figure 2.18 pH of sixteen formulations of PVA-borate hydrogels with varying concentrations of PVA and borate. Data shown as mean ± standard deviation (n=3).

It is important to understand the ability of the formulations to absorb fluid as part of their development because some wounds can have heavy exudate present. Swelling studies were conducted on all the formulations using a dialysis tubing-based method, as described in section 2.4.8. The percentage swelling was then calculated using Equation 2.5 and plotted against time. Figure 2.19 shows that from 90 to 120 minutes formulations containing the lowest borate concentration (1.0 %

w/w) had the greatest percentage swelling compared to the other three borate concentrations at these time points. At the 30-minute time point, the 2.0 % w/w borate concentration showed the most swelling, whilst the 1.5 % w/w concentration showed the least. At the 60-minute time point, the 2.5 % w/w borate concentration had the greatest swelling compared to the 1.5 % w/w borate concentration, which again showed the lowest percentage swelling. It was found that the highest concentration of PVA (12.0 % w/w) exhibited the greatest swelling at all time points (30–180 minutes) when the borate concentration was kept constant at 1.5 % w/w, as seen in Figure 2.20. At 150 and 180 minutes, all four concentrations followed the same trend of increased PVA concentration causing increased swelling. However, the 10.0 % w/w PVA-borate 1.5 % w/w hydrogels consistently gave the lowest percentage swelling from 30 to 120, as seen in Figure 2.20. The formulation that had swollen the least after 180 minutes was PVA 6.0 % w/w borate 1.5 % w/w hydrogel with 7.53 ± 0.09 % increase in mass. The PVA 12.0 % w/w borate 1.5 % w/w had swollen the most after 180 minutes with an increase in mass of 8.90 ± 0.09 %, followed by the PVA 10.0 % w/w borate 1.5 % w/w formulation with a 8.28 ± 0.10 %, increase in mass from time zero.

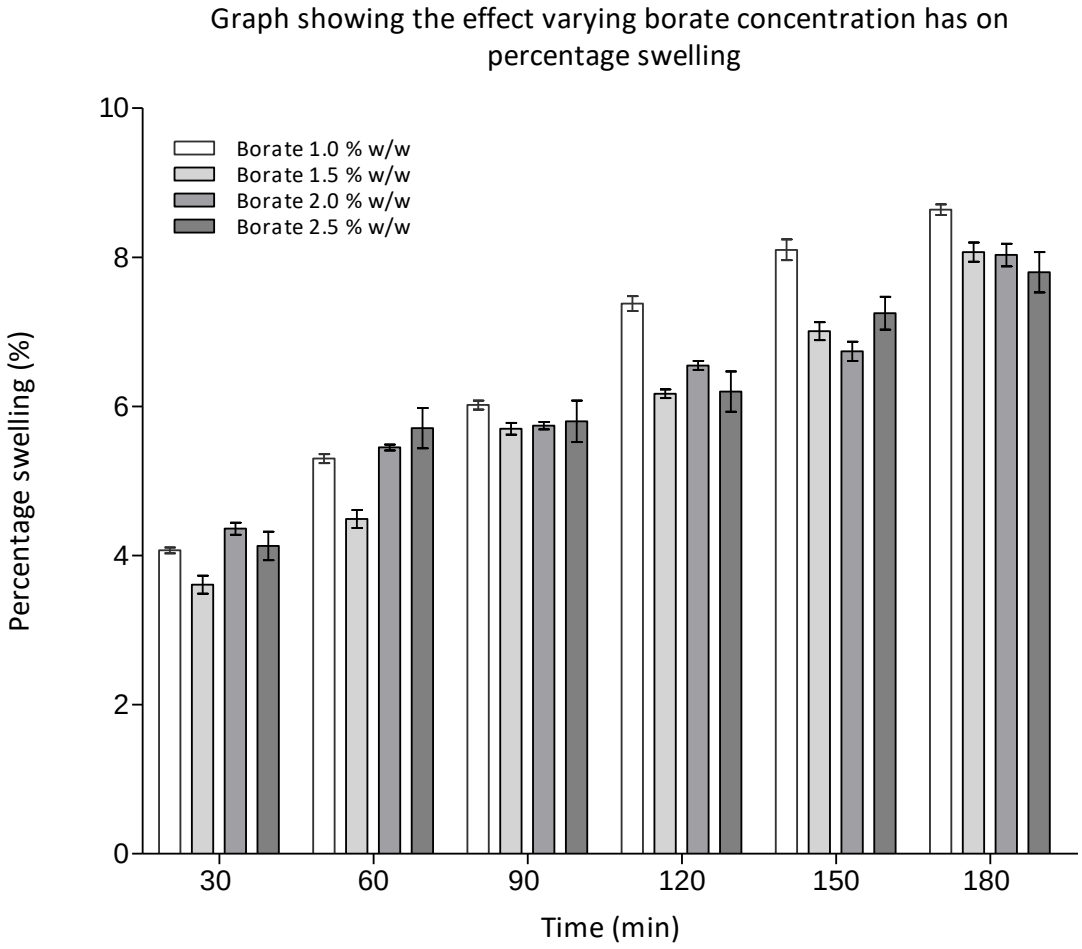

Figure 2.19 Percentage swelling of PVA-borate hydrogels varying borate concentration and keeping PVA concentration constant at 8.0 % w/w. A sample (10.00 g) of hydrogel contained within cellulose dialysis tubing was placed in 100 mL of phosphate buffer saline (pH 6.8) at 37 °C. Data shown as mean ± standard deviation (n=3).

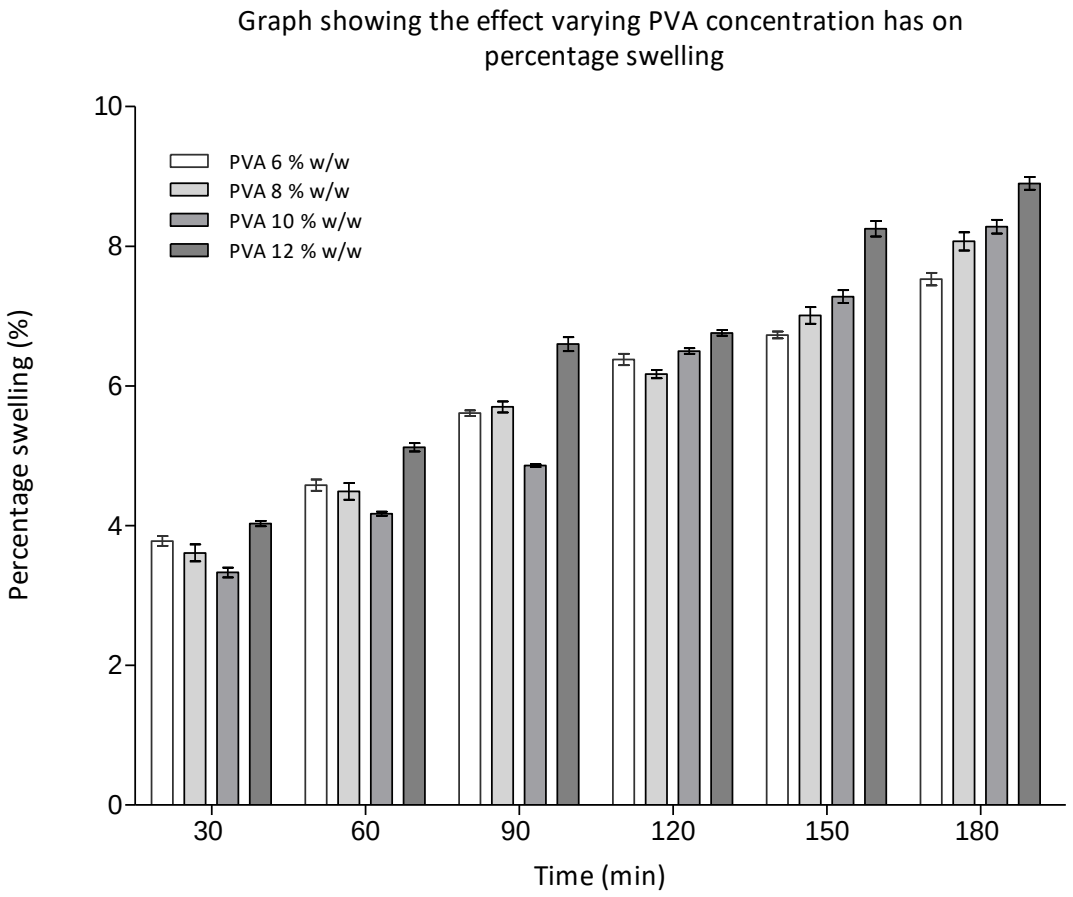

Figure 2.20 Percentage swelling of PVA-borate hydrogels varying PVA concentration and keeping borate concentration constant at 1.5 % w/w. A sample (10.00 g) of hydrogel contained within cellulose dialysis tubing was placed in 100 mL of phosphate buffer saline (pH 6.8) at 37 °C. Data shown as mean ± standard deviation (n=3).

The stability of fourteen of the sixteen formulations was monitored over 24 months, using the crossover modulus to determine any changes in viscoelastic properties. The PVA 6.0 % w/w borate 2.5 % w/w and PVA 8.0 % w/w borate 1.0 % w/w hydrogels showed no statistically significant changes in the crossover modulus over the 24 months, as seen in Figure 2.21 and Table 2.1. Therefore, this would suggest they are the most stable formulations and have a shelf-life of 18–24 months. The PVA 6.0 % w/w borate 2.0 % w/w formulation was stable for 12 months with a significant change in viscoelastic properties at 18 and 24 months. The PVA 8.0 % w/w borate 2.0 % w/w and PVA 10.0 % w/w borate 1.0 % w/w formulations exhibited poor stability, both showing a highly significant change in viscoelastic

properties after 9 months. Formulations containing PVA 10.0 % w/w borate 1.0 and 2.0 % w/w, and PVA 12.0 % w/w borate 1.0 and 2.0 % w/w all exhibited significant changes in viscoelastic properties after 18 months.

Table 2.1 Two-way ANOVA statistics for stability data seen in Figure 2.21

Formulation PVA /borate (% w/w)	**0 month V 9 month**	**0 month V 12 month**	**0 month V 18 month**	**0 month V 24 month**
6.0/1.0	-	-	-	*
6.0/1.5	-	***	***	***
6.0/2.0	-	-	***	***
6.0/2.5	-	-	-	-
8.0/1.0	-	-	-	-
8.0/1.5	-	-	-	***
8.0/2.0	***	***	***	***
8.0/2.5	-	-	-	*
10.0/1.0	***	***	***	-
10.0/1.5	-	**	***	**
10.0/2.0	-	***	***	-
10.0/2.5	-	-	-	***
12.0/1.0	-	*	**	-
12.0/1.5	-	**	***	-

Key: - P> 0.05 (no significance), * p<0.05, ** p< 0.01, *** p< 0.001.

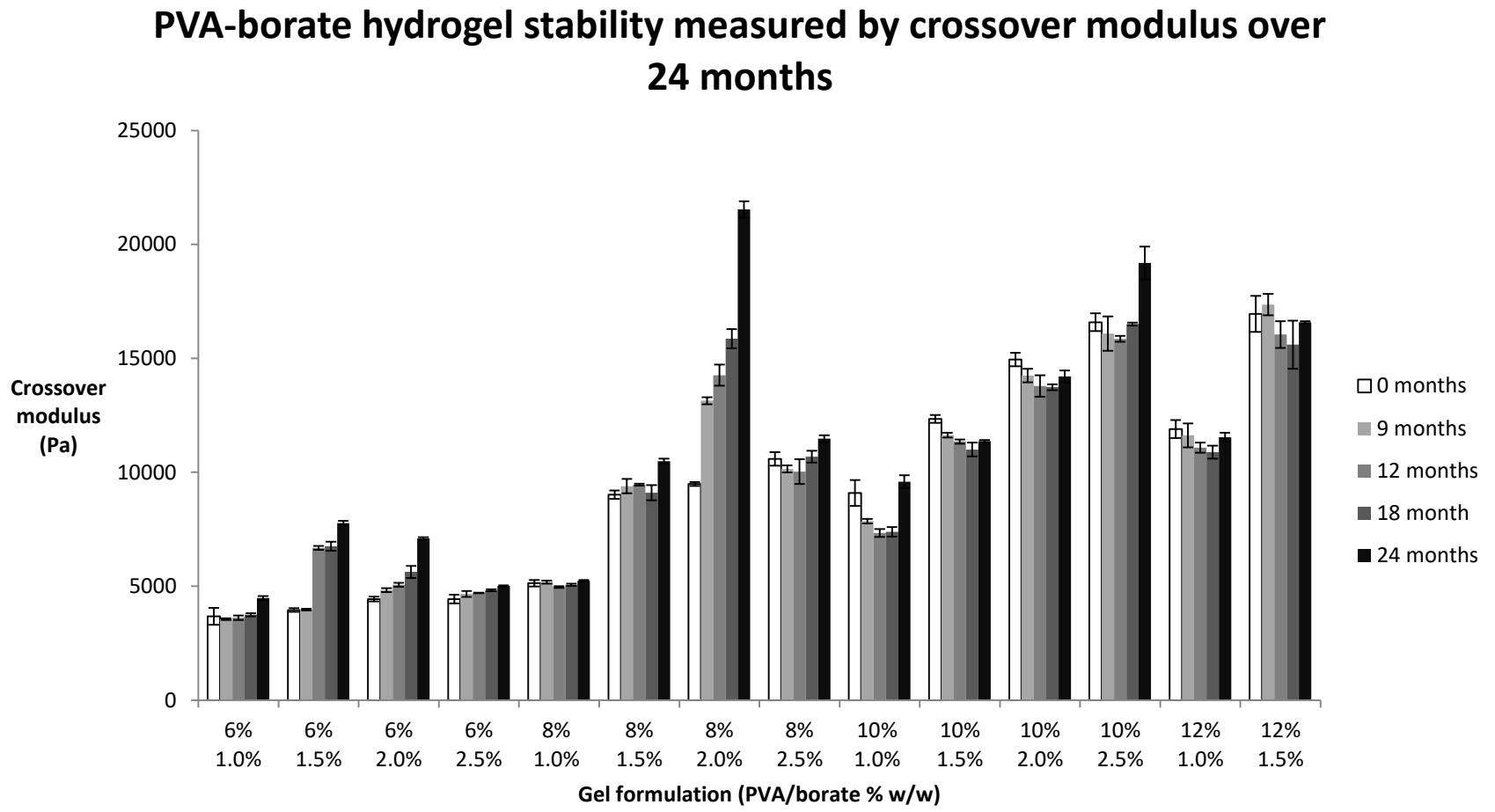

Figure 2.21 A graph showing the stability of fourteen of the hydrogel formulations over 24 months. Crossover modulus was used to monitor changes in hydrogels viscoelastic properties. Data shown as mean ± standard deviation (n=3). All measurements carried out at 25°C ± 0.2°C.

2.6 Discussion

PVA-borate hydrogels are of particular interest as a topical drug delivery system for wound management and repair, due to their novel viscoelastic properties. In this chapter, sixteen PVA-borate hydrogel formulations of varying PVA and borate concentration were manufactured and characterised physically using oscillating rheometry.

The unique viscoelastic properties of PVA-borate hydrogels used in this work are due to the response of the cross-link interaction between the PVA and borate to an applied force, for a specific duration of time. On rheological characterisation of the hydrogel formulations, it was found that at high frequencies (short time periods) the hydrogels exhibited elastic solid-like behaviour, due to the elastic component dominating the liquid viscous-like component ($G' > G''$). At high frequencies or high shear rates, the cross-links between the PVA polymer chains and the borate molecules do not have sufficient time to dissociate ($t < t_{life}$), therefore, the system behaves like an elastic solid (Loughlin *et al*., 2008). When the PVA-borate system demonstrates this elastic solid-like behaviour, the gel is comparable in nature to the chemically cross-linked PVA-glutaraldehyde hydrogel, which has an infinite lifetime (t_{life}), showing no flow-like behaviour (Lin *et al*., 2005). The solid-like behaviour displayed at high frequencies allows the hydrogel to be handled and manipulated into the shape of the wound prior to application. It also allows for complete intact removal of the gel as one mass of material, post treatment, without any further trauma to the wound site (Loughlin *et al*., 2008; Murphy *et al*., 2012). The low bio-adhesiveness of the hydrogel also partly contributes to the reduced trauma at the wound site. In comparison, it was found from the rheological analysis that at low frequencies (long time periods) the hydrogels exhibit viscous liquid-like behaviour,

as the viscous component dominates over the elastic solid-like component (G" > G'). This is because at low frequencies the cross-links have sufficient time to dissociate ($t > t_{life}$), relax and reorientation, allowing the gel system to flow like a viscous liquid (Lin *et al*., 2005). This liquid-like behaviour is advantageous for a topical delivery system for wound treatment as it allows the hydrogel to flow into the wound, filling the cavity entirely. This facilitates maximum contact between the wound surface and the hydrogel surface, maximising drug delivery.

The concentrations of both the PVA and borate present in the formulation were found to have an effect on the viscoelastic properties of the PVA-borate hydrogels. Therefore, the viscoelastic properties of the hydrogel could be controlled by altering the quantity of PVA or borate present in the formulation, to achieve an optimum formulation. On increasing the concentration of the PVA, or borate, or both in the formulation the rheological parameters measured, such as crossover modulus, yield stress, zero shear viscosity and relaxation time also increased. The increase in these rheological parameters is thought to occur as a result of increased cross-linking between the PVA polymer chains and borate ions, but also an increase in hydrogen bonding of the hydroxyl groups of the polymer chains (Koike *et al*., 1995; Lin *et al*., 2005; Murphy *et al*., 2012). An increase in cross-linking leads to a denser gel network, which increases the viscosity of the gel, giving a larger elastic response at low frequencies (Murphy *et al*., 2012). On increasing both the PVA and borate concentrations within the hydrogel formulation, the crossover modulus increased. The crossover modulus is the frequency at which the elastic and liquid shear moduli are equal and, therefore, indicates the transition of the gel system behaving like a viscous liquid to an elastic solid, with increasing frequency. Murphy *et al*., (2012) identified similar trends, stating that an increase in both the PVA and

borate concentration caused an increase in both the storage (elastic) and loss (liquid) moduli, hence also the crossover modulus. The relaxation time for the hydrogel formulations containing borate 1.0 % w/w and PVA 6.0, 8.0, 10.0 and 12.0 % w/w did not increase on increasing PVA concentration, but instead decreased. This could be the result of an insufficient amount of borate being present in the formulation to participate in further cross-linking on addition of increasing PVA. Therefore, these non-cross-linked PVA polymer chains can relax and re-orientate much faster on removal of the applied stress, than those involved in cross-linking with borate (Lin *et al*., 2003). Murphy *et al*. (2012) also observed a similar trend with regards to the crossover frequency. They suggested that by increasing the PVA concentration, whilst the borate concentration remains low, encourages the formation of the mono-diol complex rather than the di-diol complex. The formation of mono-diol poly(electrolyte) complex causes the polymer chains to expand due to the electrostatic repulsion. This results in reduced polymer-polymer interactions, which is not sufficiently counteracted by PVA-borate interactions due to the low concentration of borate present. This causes a reduced elastic solid-like response by the hydrogel and the overall gel system having a greater viscous liquid-like response.

Determination of crossover moduli for hydrogel formulations containing PVA 12.0 % w/w, with 2.0 % and 2.5 % borate was not achievable using a 1.0 mm working gap width. This problem was not encountered during determination on, the first fourteen formulations. The traces displayed by the rheometer were showing a dog leg effect, indicating that a phenomena known as wall slip was occurring (Malvern Instruments, 2015). Wall slip is the slipping of the material between the two parallel plates, which have smooth surfaces, due to a loss of friction. The recommended method to overcome this, according to the manufacturer's application

note on wall slip, is to use roughened of serrated plates (Malvern Instruments, 2015). However, this was not an available option during this work. One disadvantage of using roughened or serrated plates is the interaction between the plate surface and the material has to be taken into consideration when interpreting data. The working gap width is the distance between the two geometries of the rheometer. It was thought that if the force applied to the hard solid-like hydrogel sample was reduced by a small amount it may be possible to overcome the wall slip, but maintain enough friction to achieve a crossover modulus value. On increasing the working gap width to 1.5 mm for the PVA 12.0 %, borate 2.0 % w/w and 2.0 mm for the PVA 12.0 % w/w borate 2.5 % w/w it was possible to obtain crossover values for these two formulations. Therefore, the experiment, as detailed in section 2.4.3, was then carried out to confirm that changing the working gap width had no statistically significant effect in the magnitude of the crossover modulus value and that they could be compared to the other fourteen values measured using the commonly used, standard 1.0 mm working gap width.

The tackiness study carried out using the rheometer was performed as detailed in section 2.4.5. The results obtained show that as both the borate and PVA concentration increased the tackiness of the formulation also increased. When the borate concentration is kept constant and the PVA concentration is increased, it would be expected that the formulation would become tackier in nature. This is because there is a higher ratio of PVA to borate present resulting in less cross-linking. As a result of less cross-linking, a higher quantity of the PVA polymers are present in a viscous fluid-like formulation and it is known that solutions of PVA have adhesives properties (Park *et al.*, 2011; Cakir *et al.*, 2011). Therefore, it is presumed that formulations with high PVA concentrations and low borate

concentrations will naturally be tackier. Murphy *et al*. (2012) found that on increasing the borate concentration the adhesiveness of the PVA-borate formulation decreased, which is the opposite of the trend seen in this study. A decrease in adhesive properties with an increase in borate concentration is what would be expected, due to an increase in cross-linking of the PVA polymers with the borate ions, resulting in fewer non-cross-linked PVA polymers contributing to the adhesiveness of the formulation. Murphy *et al*. (2012) used a texture analyser in adhesive mode, an instrument purpose made for measuring adhesion, unlike the rheometer. The rheometer measures normal force, which is the force required to pull the submerged top plate out of the hydrogel. The expectation is that the tackier the formulation the larger the force required to pull the top plate out. This is a method suggested and recommended by Malvern Instruments who manufacturer the rheometer and, therefore, was deemed a suitable way to measure tackiness and adhesiveness of the hydrogel formulations. The texture analyser measures the force required to pull the top plate off the surface of the hydrogel (McCarron *et al*., 2011). Whereas, the rheometer measures the force required to pull a submerged probe or plate out of the hydrogel formulation. It is this difference in the way the two instruments operate, which could have led to the difference in results. As PVA and borate are increased in the formulation the resultant hydrogels becomes physically more rigid and solid-like, due to increased cross-linking density. Therefore, the submerged plate of the rheometer will require a larger force to pull the plate out of the gel as the formulations increase in rigidity. This is due to the hydrogel flowing over the outer edge of upper plate, as seen in Figure 2.22. Therefore, not only must the adhesive force be overcome, but the structure of the gel matrix must also be disrupted. This may explain the results obtained from this experiment and perhaps

the results are more indicative of a combination of rigidity and tackiness of the formulation.

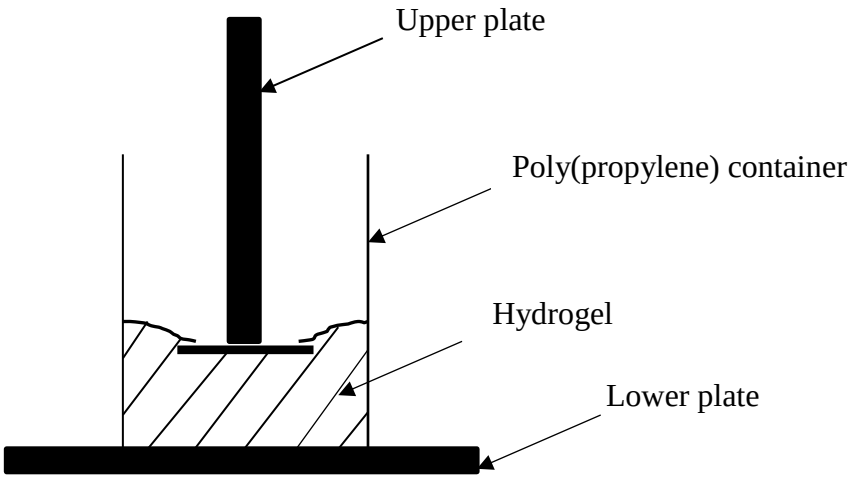

Figure 2.22 Schematic diagram showing the upper plate of the rheometer submerged in a pot containing 10 g of PVA-borate hydrogel. It can be seen that the hydrogel begins to flow over the edge of the upper plate as it is pushed against the gel surface with a constant force, before the pull-away test is triggered after 30 s contact time. This shows that not only does the adhesive force of the gel have to be overcome when the upper plate is pulled out, but also the structure of the gel has to be disrupted.

It is important to assess the effect temperature has on the PVA-borate hydrogel as the temperature of wounds can vary, affecting the viscoelastic properties and the release of the drug from the hydrogel (Dini *et al*., 2015). Temperature had a profound effect on the viscosity of all the hydrogels tested. It was found that on increasing the temperature from 20 °C to 80 °C that the complex viscosity decreased for all hydrogel formulations. The PVA-borate cross-link are thermos-reversible in nature and upon heating above a threshold temperature the cross-links dissociate and the gel behaves like a viscous liquid. Once the temperature drops below the threshold temperature the gel cross-linking network reforms. As the temperature of the PVA-borate hydrogel is increased, the di-diol complex formed and the hydrogen bonding between polymer chains begin to dissociate (Lin *et al*., 2003). Lin *et al*. (2003) found that the PVA-borate hydrogel only behaves like a weak gel below 40 °C.

Therefore, as body temperature is 37 °C and the temperature range of wound beds are between 33–38 °C (Dini *et al*., 2015), the PVA-borate gel network will stay intact when applied to a wound. Loughlin *et al*. (2008) found a similar effect occurring with the PVA-borate hydrogel on heating and that it also effected the release of lidocaine from the hydrogel, due to an increase in free borate ions concentration as a result of the di-diol complex dissociation.

The pH of the majority of the sixteen formulations were found to be neutral, with those that were not neutral being weakly basic. The weakly basic hydrogel formulations were those that contained a high borate concentration and low PVA concentration. This can be explained by the presence of excess free borate ions in the aqueous environment of the hydrogel, which are not participating in cross-linking interactions (Guan & Zhang, 2013). These free borate ions are then driving the pH of the hydrogel up from neutral to basic. Loughlin *et al*. (2008) found that on adding D-mannitol to the PVA-borate formulation it acted as a scavenger molecule, binding up the free borate ions. The binding up of these free borate ion caused a decrease in pH of the hydrogel system, confirming that the free borate ions caused the increase in pH. On increasing the PVA concentration of the hydrogel formulations containing high concentrations of borate (2.0 and 2.5 % w/w), in this study, caused the pH of the hydrogels to return to neutral. It can be assumed that increasing the PVA concentration resulted in the excess free borate ions being used in cross-linking interactions and, therefore, were not available to drive up the pH of aqueous environment within the hydrogel.

By definition, hydrogels are 3D cross-linked structures, which can retain and accommodate large volumes of water (Hoffman, 2002). This advantageous property of hydrogels makes them attractive for treatment of chronic wounds as they have the

ability to absorb excess exudate from the wound site, or donate water to the wound site. Their ability to donate water to necrotic tissue allows it to soften and be removed in process known as autolytic debridement (Trudgian, 2000). A study revealed that a typical pressure ulcer produced on average 6 mL day^{-1} of wound exudate, with other chronic wounds, such as diabetic foot ulcers producing on average 25–40 mLs day^{-1} (Iizaka *et al.*, 2011). Smith & Nephew (2009) in their clinical guidelines stated that the typical chronic wound can produce 20–50 mLs day^{-1}. Iizaka *et al.* (2011) estimated, using their model that a 20 cm^2 pressure ulcer classified with light exudate, would produce approximately 2.7 mL day^{-1} of exudate. Therefore, it can be predicted according to the swelling data that a sample (10.00 g) of PVA-borate hydrogel would be able to manage exudate in a wound classed with light exudate and not a heavy exudate wound, such as a diabetic ulcer. Hydrogels can also be applied to viable tissue throughout the wound healing to promote the warm moist environment required for keratinocyte proliferation and tissue regeneration (Trudgian, 2000; Gantwerker & Hom, 2012). Therefore, it is important to investigate the swelling characteristic of the PVA-borate hydrogel formulations to ascertain their ability to absorb and retain fluid. The swelling kinetics of several chemically cross-linked hydrogels have been studied extensively, such as PVA-N-isopropylacrylamide, PVA-diallyldimethylammonium chloride, PVA-methacrylic acid (Kim *et al.*, 2003), poly(ethylene glycol)-poly(methyl vinyl ether-co-maleic acid) (Singh *et al.*, 2009) and poly(acrylamide-co-methyl methacrylate)-NN'-methyl-ene bis acrylamide (Begam *et al.*, 2002). As dry hydrogels begin to absorb water for the first time, the water molecules hydrate the most hydrophilic groups within the matrix first, known as primary bound water. As the matrix begins to swell, there is exposure of hydrophobic groups, which interact with the water entering the matrix

and is known as secondary bound water. The primary and secondary bound water together are called the total bound water (Hoffman, 2002). Additional water is then absorbed into the hydrogel matrix by osmosis as the water soluble polymers aim for infinite dilution. However, this is counteracted by chemical and physical cross-links. This extra water, which is thought to fill voids and pores between the cross-linked network chains is known as bulk or free water (Hoffman, 2002). If the cross-links are labile to dissolution in aqueous solution then as the network continues to swell the hydrogel will begin to breakdown and dissolve. The PVA-borate hydrogels are labile to complete dissolution when submerged in an aqueous solution. Therefore, samples of the hydrogels were enclosed in cellulose dialysis tubing membrane to complete the swelling studies for this chapter. The dialysis membrane allowed for diffusion of the water into the hydrogel while, maintaining the structural integrity of the hydrogel. However, one limitation of this was after a prolonged period of time certain formulations did begin to disintegrate, despite having the dialysis tubing in place. As the PVA-borate hydrogel disintegrates, free PVA and boron species are released. Therefore, there is potential for the absorption of the hydrogel excipients on topical application to an open wound. In this project the extent of the release of free PVA and boron species was not investigated. However, Murphy *et al.* (2012) did detect and quantify the cumulative release of free PVA and boron species, measured as boric acid, in an *in vitro* release study, over a period of two hours. It was found that as the concentration of borate in the formulation increased, so did the release of boron species from the formulation, in a non-linear fashion (Murphy *et al.*, 2012). However, as the borate concentration is increased within the formulation the degree of cross-linking increases, which is thought to constrict the network and reduce the diffusion of both free PVA and boron species (Murphy *et al.*, 2012).

Murphy *et al.* (2012) also suggest that above a borate concentration of 0.025 M (approximately 1.0 %) poly(borate) species form. Poly(borate) species are though to display slower diffusion of free boron species, such as boric acid. It was found that on increasing the PVA concentration within the formulation there was no clear trend shown on the release of boric acid. This is thought to be because excess boron species are available from the boric acid-tetrahydroxyborate equilibrium to participate in di-diol cross-linking, assuming the concentration of cross-linking is small in comparison to the concentration boric acid (Murphy *et al.*, 2012). In this study the concentration of borate within the chosen optimum formulation was 2.0 % w/w, therefore, it can be assumed that poly(borate) species are formed, reducing the release of free boron species. Murphy *et al*. (2012) found that PVA with a high degree of hydrolysis (28–99 %) exhibited a lower release of boron species and free PVA, compared to PVA of a similar molecular weight but lower degree of hydrolysis (26–88 %). Higher degrees of hydrolysed PVA will result in denser network formation, through increased di-diol cross-linking, reducing PVA diffusivity. In this study the PVA used was 98–99 % hydrolysed and, therefore, the release of free boron species can be assumed to be minimal. McCarron *et al*. (2011) observed no adverse reactions, caused by application of a sample (4.0 g) of PVA-borate hydrogel loaded with lidocaine anesthetic for 30 minutes to lacerations.

It was found that on increasing the PVA concentration within the hydrogel formulation the percentage swelling increased. In comparison, as the borate concentration within the formulation was increased the percentage swelling decreased. A similar trend has been reported for PVA-poly(vinylpyrrolidone) (PVP) hydrogels, produced by freeze-thaw cycling (Holloway *et al*., 2011). On increasing the concentration of PVA in the formulation, while the concentration of PVP

remained constant the percentage swelling increased. The PVA-borate hydrogel can be compared in relation to the swelling ability of the chemically cross-linked PVA-glutaraldehyde hydrogel (Varshosaz & Koopaie, 2002). Varshosaz & Koopaie, (2002) reported that on increasing the concentration of glutaraldehyde, while keeping the PVA concentration constant within the hydrogel film formulation the percentage swelling decreased. A similar trend seen when increasing the cross-linker (borate) for the PVA-borate hydrogels in this chapter. In both hydrogels the increase in the cross-linking agent, borate and glutaraldehyde, results in an increased cross-linking density within the hydrogel network, resulting in decreased network expansion and reduced uptake of fluid and swelling.

The stability of 14 of the sixteen hydrogel formulations where monitored over 24 months by detecting changes in the crossover modulus value, for each formulation. Several of the PVA-borate formulations showed statistically significant changes in the crossover modulus over 24 months, indicating instability. The exact reason for this instability in certain formulations is unknown. Further work involving repetition of this study and further analysis is needed to try and determine possible causes for this. One possible explanation for the change in crossover modulus may be due to a shift in the PVA-borate cross-link equilibrium or boric acid-tetrahydroxyborate equilibrium. Murphy *et al*. (2012) reported that release of boron species from the hydrogel as boric acid may occur over a prolonged period of time. Therefore, based on this information, there may be diffusion of free boron species as boric acid over time through the aqueous environment within the hydrogel. This may lead to pockets throughout the hydrogel having varying degrees of cross-linking density, resulting in varying crossover moduli.

2.7 Conclusion

The viscoelastic properties of the sixteen PVA-borate hydrogels formulated were investigated using oscillating rheometry. It was concluded from the rheological characterisation of the hydrogels that the viscoelastic properties could be modified by varying the PVA and borate concentrations. The hydrogel formulation, PVA 6.0 % w/w borate 2.0 % w/w was deemed to be the optimum formulation. The optimum formulation was deemed to be a hydrogel that displayed the correct balance between elastic cohesiveness and liquid-like flow, while showing low adhesive properties. The optimum gel when physically manipulated must retain its shape for several seconds before flowing at an acceptable speed, for ease of application to the wound site. These properties were determined and quantified using oscillating rheometry.

The PVA-borate hydrogels demonstrate the ability to uptake and carry small volumes (10.00g approximately 1–2 mL) of deionised water, making them advantageous for wound management and potentially suitable for application to exuding wounds. The work completed in this chapter, along with the results obtained, suggest that the PVA-borate hydrogels are a potentially suitable topical delivery system for wound management and repair.

Chapter 3

Chapter 3

3 Formulation, characterisation, *in vitro* release and stability study of protein-loaded PVA-borate hydrogels.

3.1 Introduction

The use of pharmaceutically active peptides and proteins has increased significantly since the introduction of the first therapeutic recombinant protein, human insulin, over 30 years ago (Vermonden *et al.*, 2012). Delivery of therapeutic proteins and peptides can be problematic due to their fragile 3D structures and poor stability. Oral administration presents a significant challenge, as the proteins are highly susceptible to proteolytic degradation by gastrointestinal enzymes and chemical degradation due to the acidic environment of the stomach, resulting in the loss of biological activity (Li *et al*., 1998). Another problem with oral administration is the large molecular weight and hydrophilic nature of many therapeutic proteins. Several of the recombinant poly(peptide) growth factors, such as VEGF, FGF and IGF-1, used in wound healing are typically 5–50 kDa (Ferrara & Henzel, 1989; Ornitz & Itoh, 2001; Laron, 2001). The high molecular weight and hydrophilic nature contributes to poor transdermal and biological membrane absorption, resulting in reduced bioavailability (Vermonden *et al*., 2012). Therefore, the main route of administration currently is parentally, however, parental administration also has drawbacks. One significant drawback is the need for frequent injections due to the short half-life of many proteins and peptides. Growth factors involved in wound healing act locally as they possess short diffusional distances across the extracellular matrix because they degrade within a short period of time. Platelet-derived growth factor, basic fibroblast growth factor and vascular endothelial growth factor after intravenous administration

have half-lives of 2, 3 and 30 minutes, respectively (Edelman *et al.*, 1993; Lee, 2000; Eppler *et al.*, 2002). The high frequency of injections required to maintain a plasma protein-drug concentration within a defined therapeutic window will lead to reduced patient compliance and concordance (Li *et al.*, 1998). Therefore, there is a need for an alternative controlled release delivery system, which is capable of enhancing the pharmacodynamics and pharmacokinetic properties of the therapeutic protein or peptide being delivered.

Polymeric hydrogels have been studied extensively as delivery systems for proteins and growth factors (Mellott *et al.*, 2001; Murthy *et al.*, 2002; Censi *et al.*, 2012). Proteins can be loaded into hydrogel matrices in numerous ways, such as (i) being physically entrapped, (ii) being adsorbed to the matrix by interactions or (iii) participating in the formation of the gel structure through covalent or non-covalent binding (Vermonden *et al.*, 2012). By choosing specific hydrogel excipients and a particular method of incorporation, site-specific sustained release can be achieved, while maintaining protein stability and biological activity. An important objective of pharmaceutical development is achieving a zero-order sustained release of the therapeutic drug (Huang *et al.*, 2002). Zero-order kinetics occurs when the rate of drug release, decomposition or dissolution is independent of the concentration of reactants, leading to a constant rate of release, decomposition or dissolution (Aulton, 2007). However, achieving zero-order sustained release kinetics for a complex delivery system is not an easy task as many factors influence the release of the loaded drug.

The mechanism by which proteins are released from hydrogels is governed by both the protein and polymer network characteristics (Censi *et al.*, 2012). A general assumption is, if the pores between the polymers are larger than the hydrodynamic

radius of the protein, diffusion occurs. The rate of diffusion is dependent on the size of the protein and the free-volume water content of the hydrogel (Amsden, 1998). However, if the hydrodynamic radius of the protein is larger than the hydrogel pores, generally, swelling and erosion or degradation are required for protein release (Censi *et al.*, 2012). Increasing the cross-linking density, decreasing the water content within the hydrogel or increasing the size of the protein all result in decreased drug release. Equation 3.1, derived by Ritger and Peppas (1987), is applied widely to release data to determine the mechanism of drug release (Censi *et al.*, 2012). M_t is the amount of drug released at time *t*, M_∞ is the total amount of drug present in the hydrogel, *k* is the release rate constant and *n* is the release coefficient used to determine the mechanism of release (Ritger & Peppas, 1987). A summary of the release coefficient values and the corresponding mechanism of drug release can be seen in Table 3.1.

$$\frac{M_t}{M_\infty} = kt^n \qquad \text{Equation 3.1}$$

Table 3.1 Summary of drug release mechanisms

Release coefficient value *n*	**Mechanism of drug release**
0.5	Fickian diffusion
$0.5 < n < 1.0$	Anomalous transport (non-Fickian diffusion)
1.0	Case II transport
$n > 1.0$	Super Case II transport

Fickian diffusion (case I transport), and case II transport can both be defined by a single parameter, unlike anomalous transport, which is a combination of parameters.

Case I and II transport are delivery systems controlled solely by diffusion and polymer relaxation, respectively (Ritger & Peppas, 1987). However, anomalous non-Fickian diffusion is governed by both diffusion and relaxation (Ritger & Peppas, 1987). Censi *et al.* (2012) suggest that case II transport and anomalous diffusion can be a result of erosion rather than polymer relaxation depending on the specific polymers used in the hydrogel formulation. In some scenarios, the release coefficient value can exceed 1.0, indicating super case II transport, which is controlled by erosion (Holowka & Bhatia, 2014). Deviations in the release mechanisms mentioned above can occur when the hydrogel is subject to specific external stimuli, such as temperature, pH, presence of certain molecules, presence of a magnetic or electric field.

The isoelectric point of proteins has implications on both the loading and release of proteins from hydrogels due to electrostatic interactions (Jensen *et al.*, 2002; Koetting & Peppas, 2014). Therefore, in this chapter model payloads with different isoelectric points will be selected in order to determine the effect the isoelectric point has on the loading to, and release from the PVA-borate hydrogel. The isoelectric point is the pH at which a particular molecule carries no overall net charge (Righetti, 2004). If the pH of the environment in which the molecule is situated deviates in either direction from the isoelectric point then the molecule will obtain either a positive of negative overall net charge (Denniston *et al.*, 2008). If the pH of the environment is lower than the isoelectric point the molecule will have a positive net charge. Alternatively, if the pH of the environment is higher than the isoelectric point the molecule will be negatively charged.

PVA-borate hydrogels have been extensively studied as potential drug delivery systems for wound management. One drug that has been delivered topically

using the PVA-borate hydrogel is lidocaine anaesthetic, prior to the suturing of lacerations, in an emergency department setting (Loughlin *et al.*, 2008; Jenkins *et al.*, 2014). The PVA-borate hydrogel also demonstrated efficient and effective delivery of two photosensitiser drugs, methylene blue and meso-tetra (N-methyl-4-pyridyl) porphine tetra tosylate, for photodynamic antimicrobial chemotherapy, of heavily infected wounds (Donnelly *et al.*, 2009).

An important question to be answered in this chapter was to decide if a PVA-borate hydrogel was capable of providing a sustained release of three model proteins. These model payloads would have different isoelectric points and different molecular weights. The proteins used were bovine serum albumin (BSA), haemoglobin (Hb) and trypsin. The release and stability of the three model peptides was confirmed first. It was important to do this before, carrying out further experimental work with considerably more expensive therapeutic payloads, such as insulin-like growth factor-1.

3.2 Aims and objectives

The aim of work in this chapter is to formulate, characterise and complete *in vitro* release studies for several PVA-borate hydrogels (PVA 6.0 % w/w borate 2.0 % w/w) loaded with bovine serum albumin (BSA), haemoglobin (Hb) and trypsin.

Objectives;

- formulate PVA-borate hydrogels loaded with varying concentrations BSA, Hb and trypsin,
- determine a suitable non-destructive method for loading proteins and peptides into the PVA-borate hydrogels,
- characterise the viscoelastic properties of the protein-loaded PVA-borate hydrogels using oscillatory rheometry,
- determine a suitable compatible receiver phase for the release studies,
- complete *in vitro* release studies of the three model proteins from the hydrogel using Franz diffusion cells,
- detect and quantify the protein released from the hydrogels using a bicinchoninic acid (BCA) assay and UV-Vis spectroscopy,
- determine any degradation of the released proteins from the hydrogel using sodium dodecyl sulphate poly(acrylamide) gel electrophoresis (SDS-PAGE).

3.3 Materials

Chemicals and reagents

Poly(vinyl alcohol) (PVA) (Mw = 31–50 kDa, 98–99 % hydrolysed), sodium tetraborate decahydrate (ACS reagent ≥ 99.5 %), D-mannitol (ACS reagent), sodium chloride (BioXtra ≥ 99.5 %), potassium chloride (BioXtra ≥ 99.5 %), di-Sodium hydrogen phosphate, potassium di-hydrogen phosphate, haemoglobin from bovine blood, trypsin from porcine pancreas (BioReagent 1000-2000 BAEE units/mg solid), bovine serum albumin (lyophilised powder ≥ 96 %), Victoria Pure Blue dye and Transwell® tissue culture inserts (Poly(carbonate) membrane, pore size 8.0 µm) were purchased from Sigma-Aldrich Ltd. (Gillingham, Dorset, UK).

A Pierce™ BCA Protein assay kit was purchased from Medical Supply Company. (Dublin, Ireland). Phosphate-buffered saline tablets (Dulbecco A tablets) Oxoid were purchased from ThermoFisher scientific (Hampshire, UK).

NuPage® Bis-Tris gel 4–12 % (1.0 mm x 10 well) Novex®, NuPage® MOPS SDS running buffer (20x) Novex®, SeeBlue® Plus2 Prestained standard Novex® were purchased from Life Technologies Ltd. (Paisley, UK).

Coomassie brilliant blue R-250 staining solution, Bio-rad laboratories Inc. (Hertfordshire, UK).

All reagents were of appropriate laboratory standard and used without further purification.

Apparatus

Kinexus Pro rheometer, Malvern instruments (Malvern, Worcestershire, UK).

Varian Cary 50 Scan UV-Vis spectrophotometer supplied by Manson Technology. (Dublin, Ireland); used with a 10 mm quartz cuvette.

FLUOstar® Omega microplate reader, BMG LABTECH Ltd. (Ortenburg, Germany). Franz diffusion cells, Perme-Gear diffusion cells & systems. (USA) and Techne TE 10D Tempette® water bath & pump, Bibby scientific Ltd. Staffordshire. (UK)

3.4 Methods

3.4.1 Peptide and protein loading method development

Samples (4.00 g) of PVA 6 .0% w/w borate 2.0 % w/w hydrogel were weighed, placed in small glass jars and allowed to sit for 24 hours, until evenly distributed within the jar. Victoria Pure Blue dye solution (500 μL) was then added to each hydrogel sample by two different processes. One sample was injected into the centre of the hydrogel sample and another was placed on the surface of the hydrogel, prior to being mixed into the hydrogel sample mechanically using a stainless steel spatula. Each hydrogel sample was left for 72 hours at room temperature. Photographs were taken at 3, 24 and 72 hours as a visual record of monitoring the diffusion of the dye throughout the gel. After 72 hours, UV-Vis spectrometry was used to determine the homogeneity of the dye throughout the hydrogel. Four samples (0.50 g) from each hydrogel and dissolved in 5 mL of deionised water in a glass beaker on a magnetic stirring mantle at room temperature. Once fully dissolved, the absorbance of each solution was read at 619 nm, the average absorbance was calculated and Student's t-test statistical analysis was carried out on the data.

3.4.2 Formulation of BSA, haemoglobin (Hb) and trypsin-loaded hydrogels

An optimum hydrogel formulation of 6.0 % w/w PVA and 2.0 % w/w borate was selected from rheological studies in Chapter Two to be loaded with various quantities of bovine serum albumin (BSA), haemoglobin (Hb) and trypsin (0.05, 0.10, 0.20, %

w/w). A sample (25 g) of this formulation was prepared by mixing 6.25 g of PVA stock solution (24 % w/w) and 10.00 g of borax stock solution (5.0 % w/w). A homogenous fluid-like gel was formed upon heating to 80 °C for approximately three hours, with periodic stirring. Hydrogels were weighed and any weight loss was replenished with deionised water. The gels were then transferred to poly(propylene) storage containers and left for 48 hours at room temperature and pressure (RTP) to allow complete gelation. To a desired quantity of hydrogel, the appropriate volume of protein stock solution (5 mg mL^{-1}) was added to the hydrogel and mixed in using a stainless steel spatula. The hydrogels were then stored in the fridge (2–8 °C) until used.

3.4.3 Viscoelastic analysis of hydrogels loaded with peptides

Viscoelastic analysis of the hydrogels, loaded with various concentrations of bovine serum albumin, haemoglobin (Hb), trypsin and D-mannitol, was carried out using a Kinexus Pro rheometer (Malvern Instruments Ltd., Worcestershire, UK) as described previously in sections 2.4.2. Briefly, a strain (1.0 %) controlled frequency sweep (0.1–10 Hz) was completed from which, the crossover modulus (G_c) was determined. All tests were carried out at 25 °C ± 0.2 °C, using 20 mm diameter stainless steel parallel plate geometry and a working gap of 1 mm. Three replicates were performed for each formulation (n=3). Student's t-test statistical analysis was carried out on the data.

3.4.4 Optimisation of *in vitro* receiver phase, study I

Samples (2.00 g) of hydrogel (PVA 6.0 % w/w, borate 2.0% w/w) containing no protein were weighed and placed in 12-well hanging cell culture inserts (membrane PET pore size 8.0 µm). The inserts were suspended in glass jars containing 25 mL of receiver phase (PBS or deionised water). Cling film was placed over the top of the jars to prevent evaporation. The experiment was run for 24 hours at room temperature, on magnetic stirring mantle at 100 rpm. After 24 hours, the gels were removed from the inserts, reweighed and photographed to document any observations indicative of the formulation becoming de-stabilised.

3.4.5 Optimisation of in vitro receiver phase - study II

The experiment described in section 3.4.4 was repeated with the components of the PBS solution separated out and each made as a receiver phase solution, as seen in Table 3.2. PBS and deionised water were used as positive and negative controls, respectively. A photograph of each hydrogel sample was taken after 24 hours to document any visual observations indicative of the formulation becoming de-stabilised.

Table 3.2 Composition of receiver phases used in section 3.4.5

Chemical name	Concentration (mM)
Sodium chloride	137
Sodium chloride	154
Potassium chloride	2
di-sodium hydrogen phosphate	8
Potassium di-hydrogen phosphate	1
PBS	–
Deionised water	–

3.4.5.1 Optimisation of *in vitro* receiver phase, study III

The experiment described in section 3.4.4 was repeated again, with the receiver phase kept constant (sodium chloride solution 154 mM). A range of PVA borate hydrogels (PVA 6.0 % w/w) borate (2.0 % w/w) were formulated as described in section 2.4.1 with the addition of varying concentrations of D-mannitol (0.5, 1.0, 1.5, 2.0 % w/w), which were added to the borate solution in the formulation process. After 24 hours, photographs were taking to document any observations indicative of the formulation becoming unstable.

3.4.6 *In vitro* release studies

Protein release studies were carried out using Franz diffusion cells (Perme-Gear cells & Systems, USA) and a Techne TE 10D Tempette® water bath & Pump (Bibby scientific Ltd. Staffordshire, UK), as seen in Figure 3.1. All release studies were carried out at 37 °C using poly(carbonate) membranes cut to size (pore size 8.0 µm, Sigma Aldrich). A sample (1.00 g) of protein-loaded hydrogel (PVA 6.0 % w/w, borate 2.0 % w/w) was placed in each of the donor chambers at time zero. Samples (0.5 mL) were withdrawn at specified time intervals (0–8 hours) and replaced with 0.5 mL of fresh receiver phase. A blank PVA-borate hydrogel of the same formulation was ran as a control.

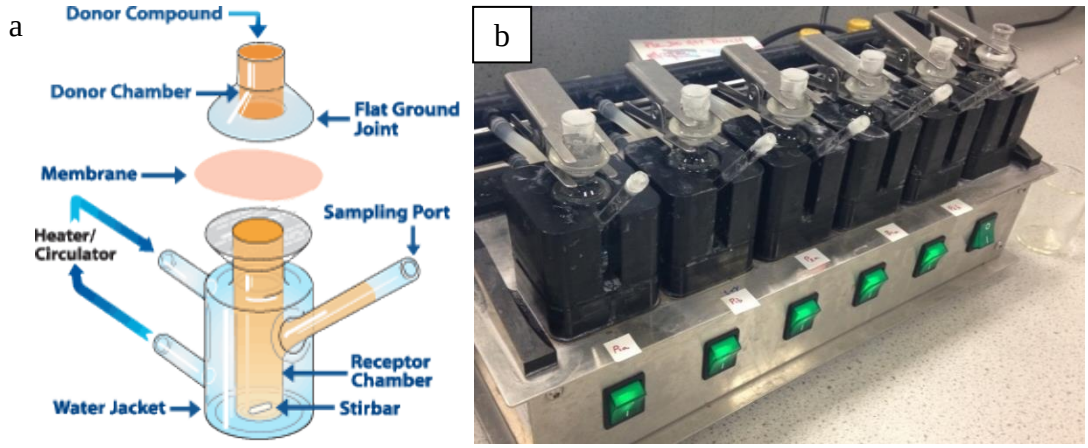

Figure 3.1 a) Shows a schematic diagram of a single Franz diffusion cell setup. b) A photograph of the actual Franz diffusion cell apparatus used in the laboratory for all the *in vitro* release studies. Parafilm can be seen placed over the end of the sampling port and the top of the donor chamber to prevent any evaporation.

3.4.7 Detection and quantification of BSA, Hb and trypsin

Samples were analysed for the presence of BSA and trypsin, and quantified, using a bicinchoninic acid (BCA) assay. A calibration plot was produced using nine dilutions (20–2000 μg mL^{-1}) from a stock solution (2 mg mL^{-1}) of each protein. Samples (25 μL) of each dilution and samples from the *in vitro* release study were pipetted into a 96-well plate. To each of these wells, 200 μL of BCA assay working reagent was added to obtain a sample to working reagent ratio of 1:8. The 96-well plate was then placed on an orbital shaking incubator at 37 °C at 100 rpm for 30 minutes. The plate was then removed and allowed to cool to room temperature prior to the absorbance of each well being measured at 562 nm using a FLUOstar® Omega microplate reader, (BMG LABTECH Ltd. Ortenburg, Germany).

Samples were analysed for the presence of haemoglobin using UV-Vis spectrometry. Haemoglobin was found to have a λ_{max} of 405 nm. A calibration plot was produced using nine dilutions (0.00–0.16 mg mL^{-1}) from a 0.50 mg mL^{-1} stock solution of haemoglobin. A quartz cuvette with a path length of 10 mm was used

and rinsed with deionised water between each sample. Three replicates were performed for each calibration plot dilution and each time point sample (n=3).

3.4.8 Sodium dodecyl sulphate poly(acrylamide) gel electrophoresis

Sodium dodecyl sulphate gel electrophoresis (SDS-PAGE) was carried out using an XCell SureLock™ Mini-Cell electrophoresis system (Invitrogen, Life Technologies Ltd, Paisley, UK). Samples (20 µl) from the *in vitro* release study and protein standards dissolved in deionised water, were prepared under reducing conditions in laemmli buffer and loaded onto a Bis-Tris NuPAGE® 4–12 % resolving gel. Electrophoresis was run using NuPAGE® MOPS SDS running buffer (x1), in constant voltage mode (200 V) and a varied current of 100–125 mA and 60–80 mA during stacking and running, respectively. After the electrophoresis had finished, the gel was removed from the cassette and placed in coomassie brilliant blue R-250 stain for 60 minutes on an orbital shaker (45 rpm), at room temperature. The coomassie blue stain was removed and the gel was rinsed twice with deionised water for 5 minutes each time. The gel was then placed in de-staining solution, consisting of methanol, acetic acid and deionised water at the ratio of 50:10:40 % v/v for 30 minutes on an orbital shaker (45 rpm) for 30 minutes, at room temperature. After 30 minutes, the de-staining solution was diluted to methanol 12.5 %, acetic acid 2.5 % using deionised water. The gel was then left overnight on the orbital shaker at room temperature, after which it was imaged.

3.5 Results

The experiment as stated in section 3.4.1 was completed to determine how long it would take a substance to reach a state of homogeneity throughout a completely

gelled hydrogel network. After 72 hours, it was found that injecting Victoria blue dye into the centre of the gel was ineffective at achieving homogeneity of the dye throughout the gel. However, in comparison, the gel that had the dye physically and mechanically mixed in using a stainless steel spatula had achieved a homogenous mix of dye throughout the gel, within the same time period, as seen in Figure 3.2.

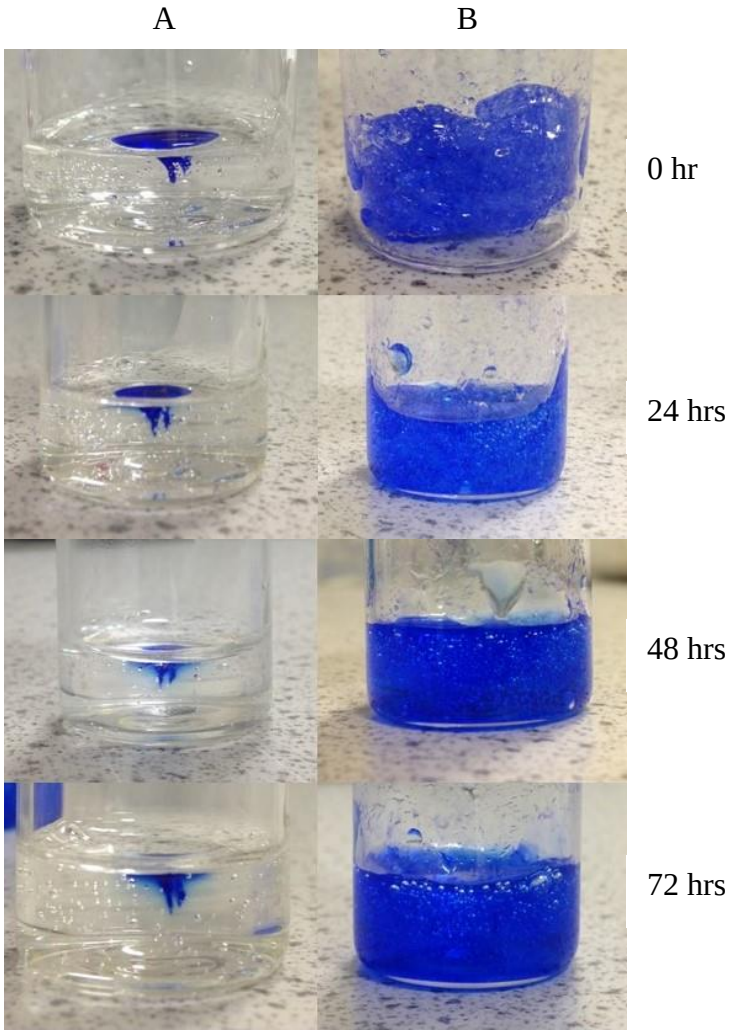

Figure 3.2 Photographs showing the diffusion of Victoria blue dye through two hydrogel samples (PVA 6.0 % w/w borate 2.0 % w/w) over a 72-hour period at room temperature. A) dye injected into hydrogel and B) dye mixed in physically using a spatula.

On further investigation using UV-Vis spectrometry, it was quantitatively confirmed that there was a homogenous mix of dye throughout hydrogel sample B (Figure 3.2). This finding was further confirmed as the Student's t-test analysis

deemed that there was no significant difference in the absorbance values between the four samples taken from hydrogel B, as seen in Table 3.3. It was concluded that this would be a suitable non-destructible method to use to achieve homogenous loading of proteins and peptides into the PVA-borate hydrogels.

Table 3.3 Absorbance values for four random samples of hydrogel containing Victoria blue dye dissolve in deionised water. $\lambda = 619$ nm, n=3.

Sample number	**Absorbance (a.u.) (Mean ± SD)**	**Student's t-test (P value)**
1	0.3027 ± 0.0028	–
2	0.3023 ± 0.0017	0.8421
3	0.3015 ± 0.0002	0.5001
4	0.3030 ± 0.0007	0.8659
Blank gel (no dye)	0.0028 ± 0.0004	<0.0001

P value > 0.05 = no significant difference, p < 0.001 = highly significant difference

Upon addition of BSA and trypsin into the hydrogel formulation, the gels remained clear and homogenous in appearance with no air bubbles present. However, the haemoglobin hydrogels were a translucent brown colour once fully re-congealed. To aid protein stability hydrogels where stored in the fridge (2–8 °C).

Each protein-loaded hydrogel was subject to an oscillating rheometry frequency sweep test. This was to determine what effect the concentration and molecular weight of the protein had on the viscoelastic properties of the hydrogel. It can be seen from Figure 3.3 that upon incorporation of all three concentrations of BSA (0.05, 0.10 and 0.20 % w/w) into the hydrogel, there was a decrease in the crossover modulus compared to the blank hydrogel, containing no BSA. The 0.10 % w/w BSA concentration showed a significant ($p < 0.05$) difference from the blank

hydrogel. However, the 0.05 and 0.20 % w/w crossover modulus showed no significant change from the blank hydrogel ($p>0.05$). The 0.05 % w/w had the lowest crossover modulus (2571 ± 426 Pa) of the three BSA concentrations followed by the 0.10 % w/w (2638 ± 175 Pa) in comparison to the blank hydrogel, which had a crossover modulus of 3384 ± 425 Pa.

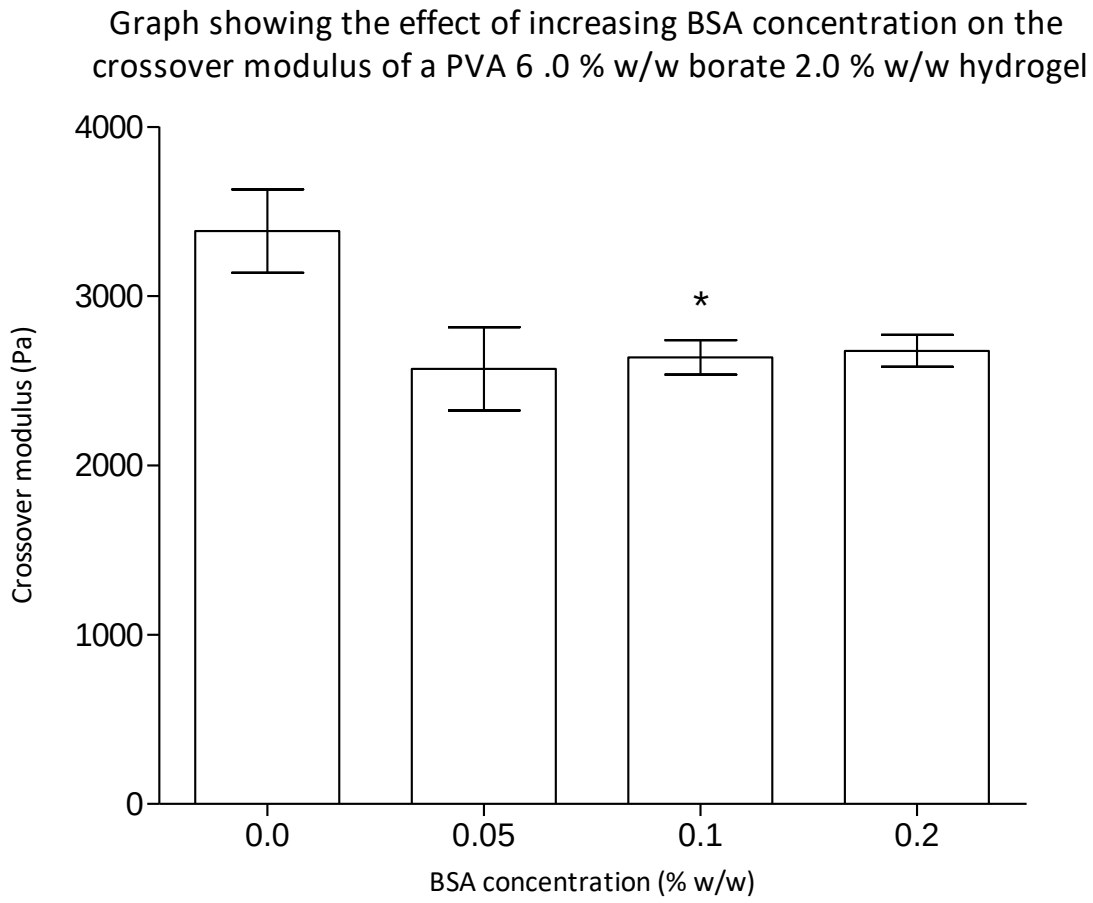

Figure 3.3 Graph showing the effect of incorporating three concentrations of BSA into a PVA (6.0 % w/w) borate (2.0 % w/w) hydrogel has on the crossover modulus, compared to a blank hydrogel, of the same formulation. Data shown as the mean ± standard deviation (n=3). All measurements carried out at 25°C ± 0.2°C. $p < 0.05$ (*), $p < 0.01$ (**), $p < 0.001$ (***).

On incorporating three concentrations of trypsin (0.05, 0.10 and 0.20 % w/w) into the hydrogel all three concentrations caused a decreases in the crossover modulus, compared to the blank hydrogel. The 0.05 % concentration showed the largest reduction in crossover modulus in comparison to the blank hydrogel, from 3100 ± 70 Pa to 2517 ± 62 Pa, respectively. A similar overall general trend can be seen for

trypsin and BSA in Figure 3.4 and Figure 3.3, respectively. It can be seen from Figure 3.4 that as the concentration of trypsin increased the reduction of the crossover modulus became less significant. Trypsin 0.20 % w/w showed the least significant reduction ($p<0.05$) of the three concentrations, when compared to the 0.05 ($p<0.001$) and 0.10 % w/w gels ($p<0.01$).

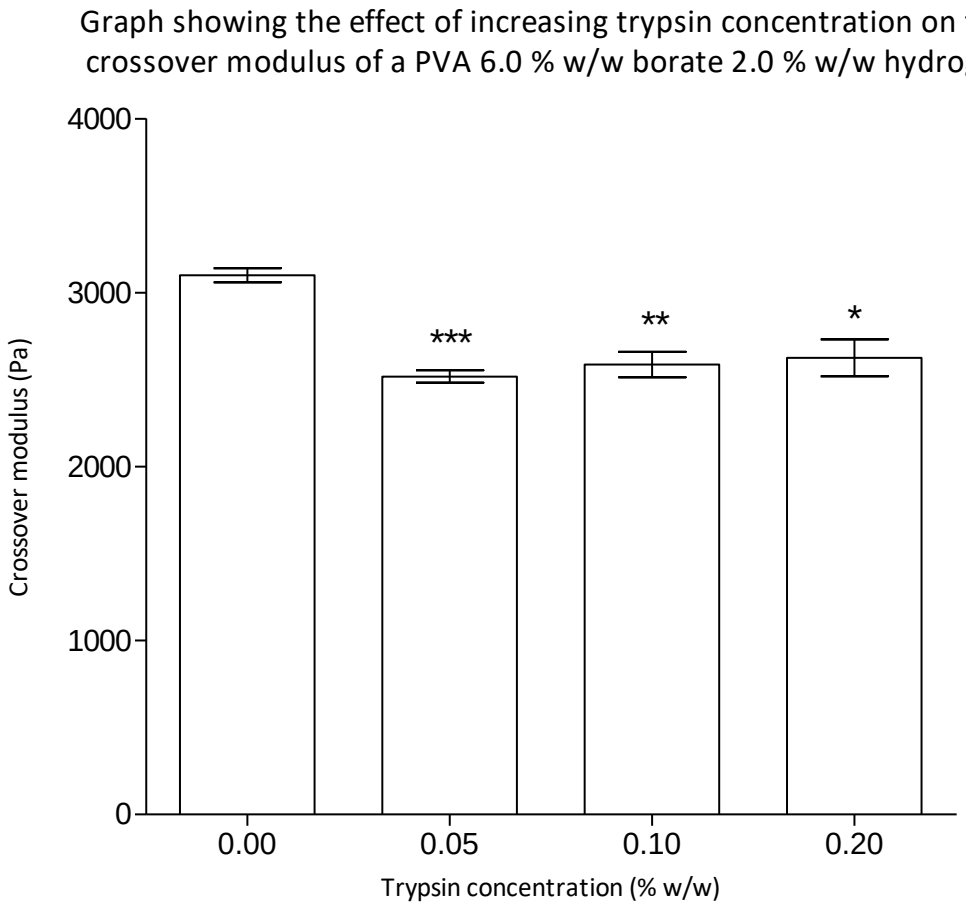

Figure 3.4 Graph showing the effect of incorporating three concentrations of trypsin into a PVA (6 % w/w) borate (2.0 %) w/w hydrogel has on the crossover modulus, compared to a blank hydrogel, of the same formulation. Data shown as the mean ± standard deviation (n=3). All measurements carried out at 25°C ± 0.2°C. $p < 0.05$ (*), $p < 0.01$ (**), $p < 0.001$ (***).

Conversely, haemoglobin had the opposite effect on the crossover modulus compared to BSA and trypsin. Upon addition of 0.05 % w/w haemoglobin the crossover modulus for the blank hydrogel increased from 2990 ± 49 Pa to 3431 ± 354 Pa. However, on statistical analysis of the data this increase was not statistically significant ($p = 0.0995$). Increasing the haemoglobin concentration further to 0.10 %

w/w caused the crossover modulus to increase to 3569 ± 150 Pa, which was a statistically significant ($p < 0.01$), when compared to the blank hydrogel. The 0.20 % w/w haemoglobin concentration gave the largest crossover modulus (3871 ± 6 Pa), which was a highly significant ($p < 0.001$) increase from the crossover modulus of the blank hydrogel. Therefore, as the concentration of haemoglobin in the hydrogel increased, the crossover modulus also increased, as seen in Figure 3.5. All three concentrations caused an increase in the crossover modulus compared to the blank gel, but only the 0.10 and 0.20 % w/w hydrogels were statistically significant.

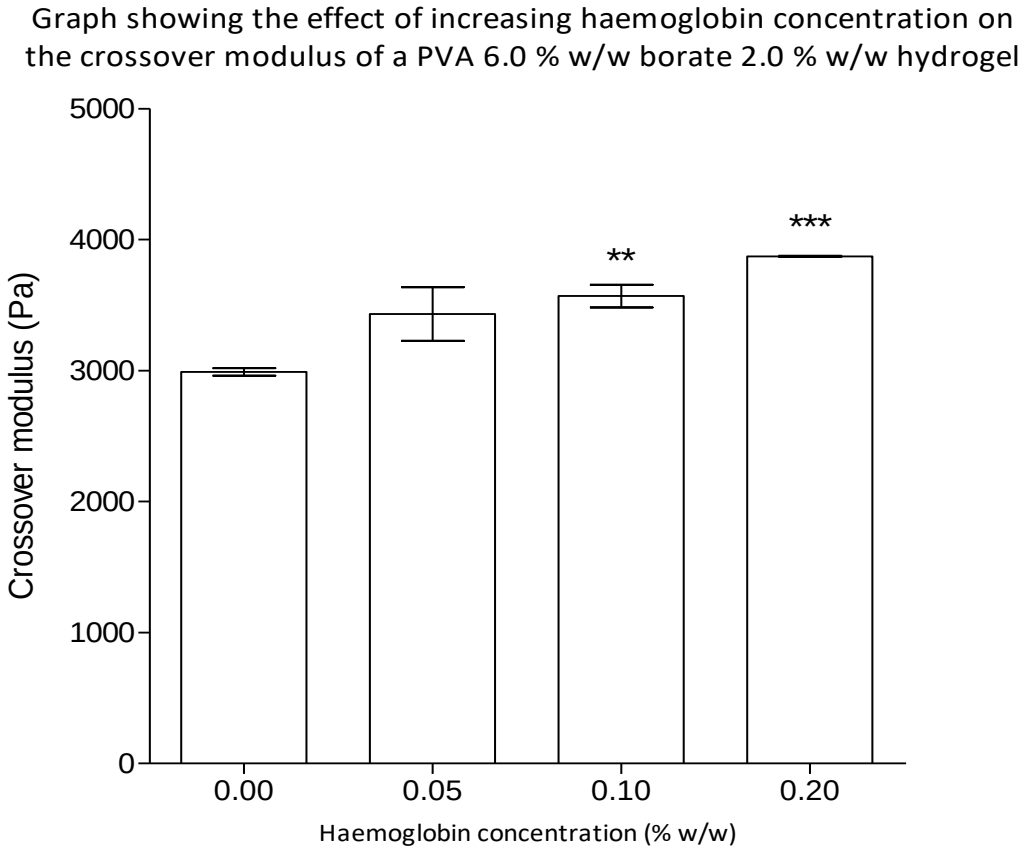

Figure 3.5 Graph showing the effect of incorporating three concentrations of haemoglobin into a PVA (6.0 % w/w) borate (2.0 % w/w) hydrogel has on the crossover modulus, compared to a blank hydrogel, of the same formulation. Data shown as the mean ± standard deviation (n=3). All measurements carried out at 25°C ± 0.2°C. $p < 0.05$ (*), $p < 0.01$ (**), $p < 0.001$ (***).

Before commencing release studies using the Franz diffusion cell apparatus, a short investigation was conducted to determine an appropriate receiver phase. After 24

hours in contact with the two receiver phases, deionised water and phosphate buffer saline (PBS), the hydrogel samples that were in contact with PBS receiver phase showed formation of a hard, white, dense layer, as seen in Figure 3.6. In comparison, the hydrogel samples that were in contact with deionised water showed no formation of this dense white layer.

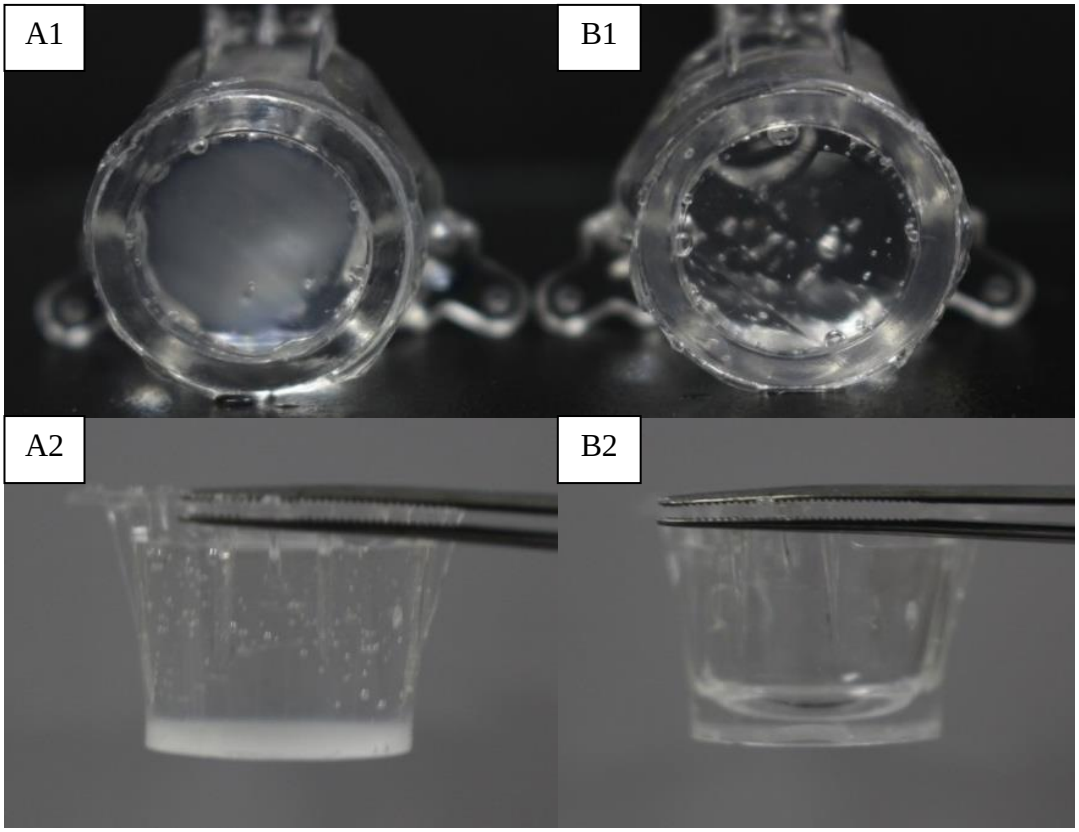

Figure 3.6 A representative photograph of two samples (2.00 g) of PVA (6.0 % w/w) borate (2.0 % w/w) hydrogel in 12-well hanging cell culture inserts after 24 hours in contact with two different receiver phases, at room temperature. A1 and A2 show a sample that was in contact with a PBS receiver phase. B1 and B2 show a sample that was in contact with a deionised water receiver phase. Both samples had pictures taken side-on (A2 and B2) and from the bottom of the insert (A1 and B1).

After 24 hours, each sample was reweighed. It was found that the hydrogel samples that were in contact with the PBS receiver phase had lost an average weight of 0.18 ± 0.06 g. In comparison, the hydrogel samples that were exposed to the deionised water had lost 1.62 ± 0.07 g. As seen in Table 3.4, the deionised water had caused an average percentage loss of 81.00 % compared to only 9.00 % for the PBS receiver

phase. This would suggest that the white layer that forms in the gel when in contact with PBS is less permeable than the normal hydrogel matrix. A visual representation of weight loss of the samples exposed to deionised water and PBS can be seen in the Figure 3.7.

Table 3.4. Average weight loss of hydrogel samples exposed to two different receiver phases

Weight Mean ± SD (g)	**PBS**	**Deionised water**
Initial	2.00 ± 0.00	2.00 ± 0.00
Final	1.82 ± 0.06	0.33 ± 0.07
Weight Loss	0.18 ± 0.06	1.62 ± 0.07
Percentage weight loss (%)	9.00	81.00

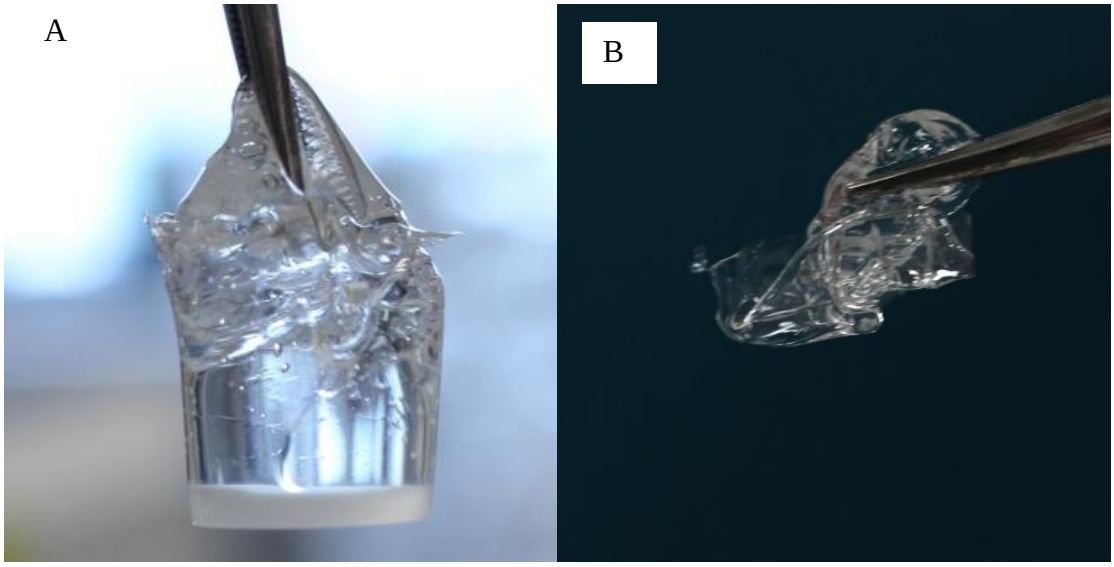

Figure 3.7 Representative photographs showing hydrogel samples removed from the 12-well hanging culture insert after 24 hours in contact with two different receiver phases, at room temperature. Photograph A is the hydrogel sample exposed to PBS in which the white layer can be seen at the bottom of the hydrogel. Photograph B is the hydrogel sample exposed to deionised water and the extent of reduction in the mass of the sample can be clearly seen in comparison to the sample in photo A.

To determine if it was a specific component of the PBS buffer that was causing the formation of the white layer, the single components that make up a PBS tablet were

made in separate solutions. Samples of hydrogel were then exposed each of solution, as detailed in section 3.4.5. It can be seen from Figure 3.8 that a 154 mM (sodium chloride) NaCl solution caused the formation of the dense white layer, more so than the PBS. It can also be noted that the 137 mM NaCl concentration did not cause the formation of the white layer. This suggests that the white layer formation may be dependent on the concentration of NaCl. On further investigation it was found that both the concentration and volume of the salt solution played a crucial role in the formation of the white layer. All the other components of the PBS tablet did not cause the white layer to form, as seen in Figure 3.8.

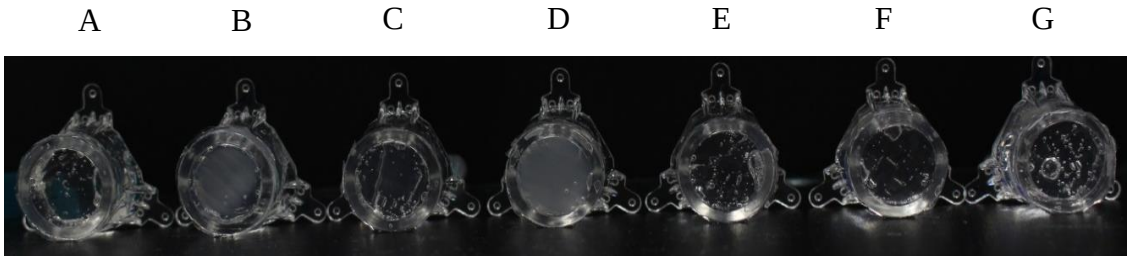

Figure 3.8 A representative photograph showing several hydrogel samples that have been in contact with several different receiver solutions for 24 hours at room temperature. A) deionised water, B) PBS, C) NaCl 137 mM, D) NaCl 154 mM, E) KCl 2 mM, F) Na_2HPO_4 8 mM, G) KH_2PO_4 1 mM.

Loughlin *et al.* (2008) found that upon addition of D-mannitol to the hydrogel formulation it prevented the precipitation of lidocaine hydrochloride from the PVA-borate hydrogel system. They also saw that upon precipitation of the lidocaine, the hydrogel became dense, rigid and white, similar to what the findings are when the hydrogel was in contact with the PBS and NaCl. Therefore, the experiment outlined in section 3.4.5.1 was carried out to identify if the de-mixing caused by the salts could be counteracted by addition of D-mannitol to the formulation. Four concentrations of D-mannitol were incorporated into the formulation of a PVA 6.0 % w/w borate 2.0 % w/w hydrogel. The changes in viscoelastic properties of the hydrogels on the addition of the D-mannitol were determined using oscillatory

rheometry. On adding 0.5 % w/w D-mannitol to the hydrogel, the crossover modulus decreased from 6411 ± 59 Pa to 4951 ± 106 Pa, which is a statistically significant difference, as seen in Figure 3.9. On increasing the concentration of D-mannitol further until a maximum concentration of 2.0 % w/w the crossover modulus continued to decrease to a minimum value of 1487 ± 32 Pa.

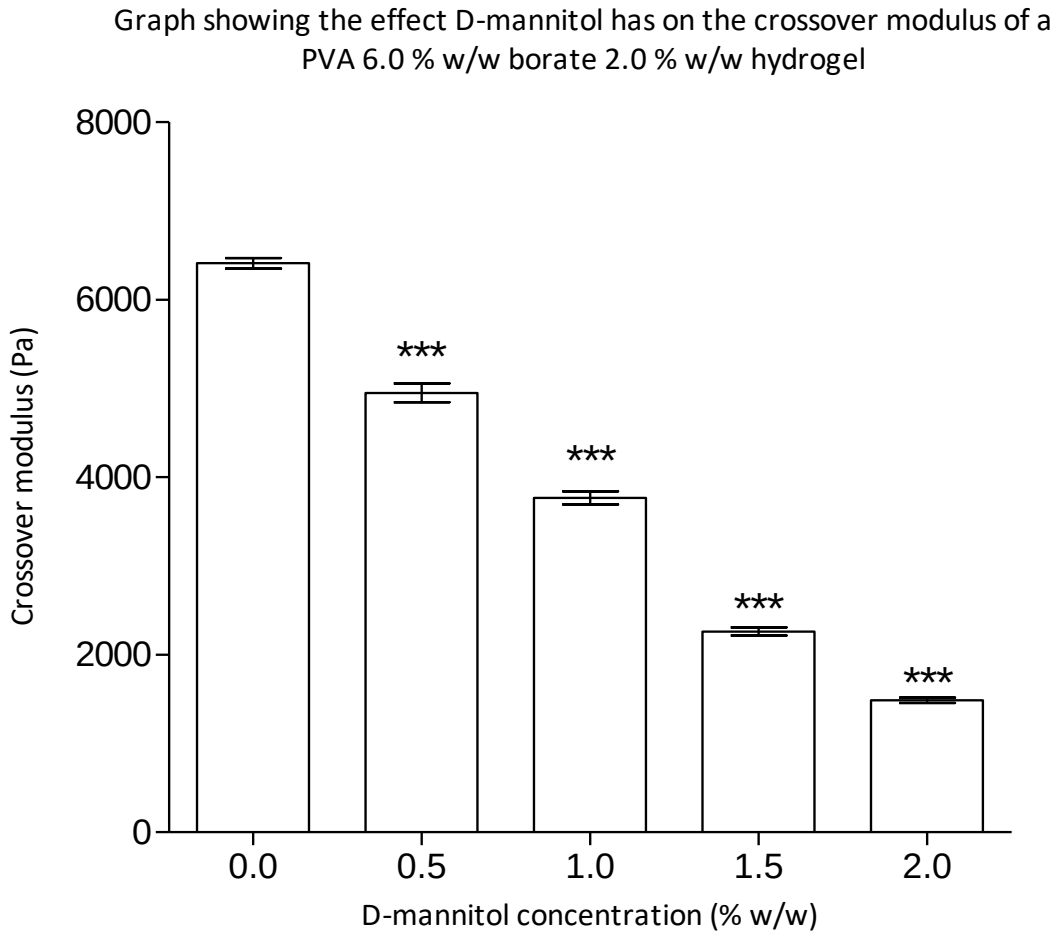

Figure 3.9 Graph showing the effect several concentrations of D-mannitol has on the crossover modulus of a PVA 6.0 % w/w borate 2.0% w/w hydrogel. Data shown as the mean ± standard deviation (n=3). All measurements carried out at 25°C ± 0.2°C. $p < 0.05$ (*), $p < 0.01$ (**), $p < 0.001$ (***).

Addition of D-mannitol to the hydrogel formulation also caused a decrease in the yield stress. D-mannitol 0.5 % w/w caused a statistically significant decrease ($p<0.001$) to 25.03 ± 0.11 Pa from 38.27 ± 0.2 Pa, recorded for the hydrogel

containing no D-mannitol. On increasing the concentration of D-mannitol the yield stress continued to decrease, as seen in Figure 3.10. This is the same trend that was observed for the crossover modulus. The 2.0 % w/w D-mannitol formulation had the lowest yield stress of 1.76 ± 0.45 Pa. It can be seen from Figure 3.11 that addition of D-mannitol prevented the formation of the white de-mixed layer in the hydrogel at all concentrations.

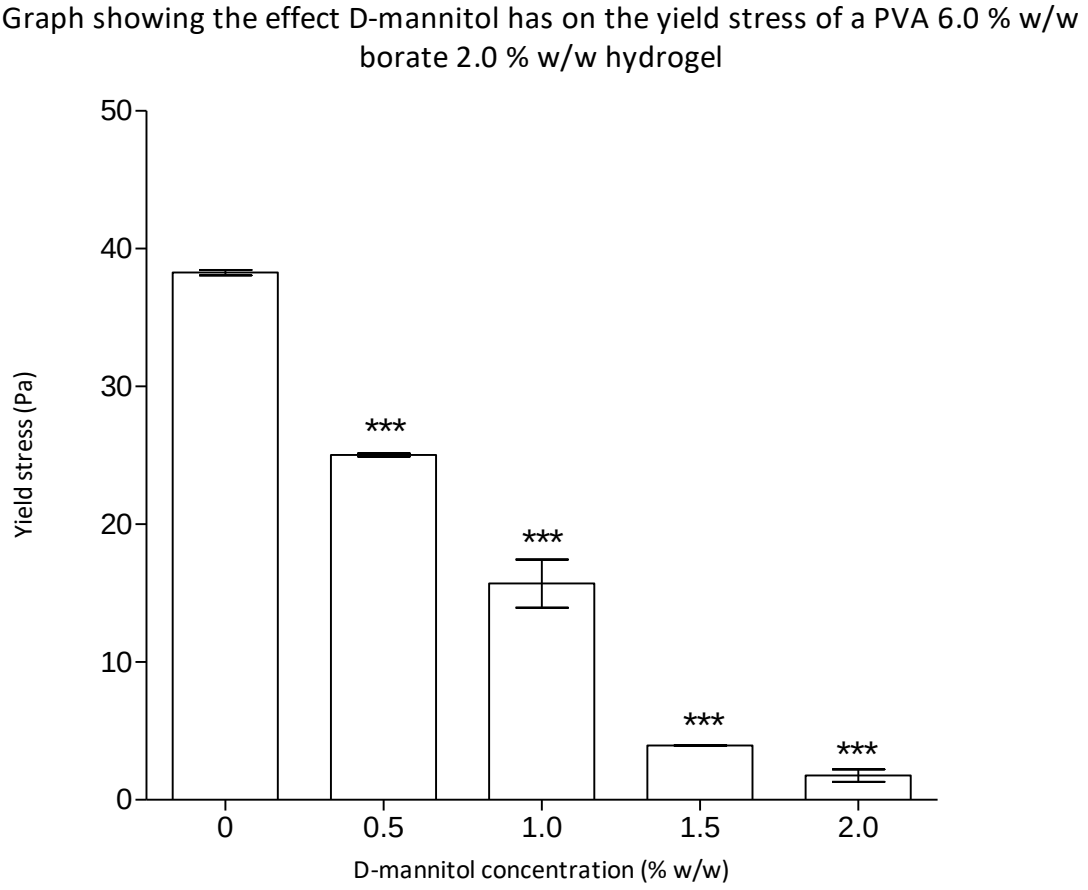

Figure 3.10 Graph showing the effect several concentrations of D-mannitol has on the yield stress of a PVA 6.0 % w/w borate 2.0% w/w hydrogel. Data shown as the mean ± standard deviation (n=3). All measurements carried out at 25°C ± 0.2°C. $p < 0.05$ (*), $p < 0.01$ (**), $p < 0.001$ (***).

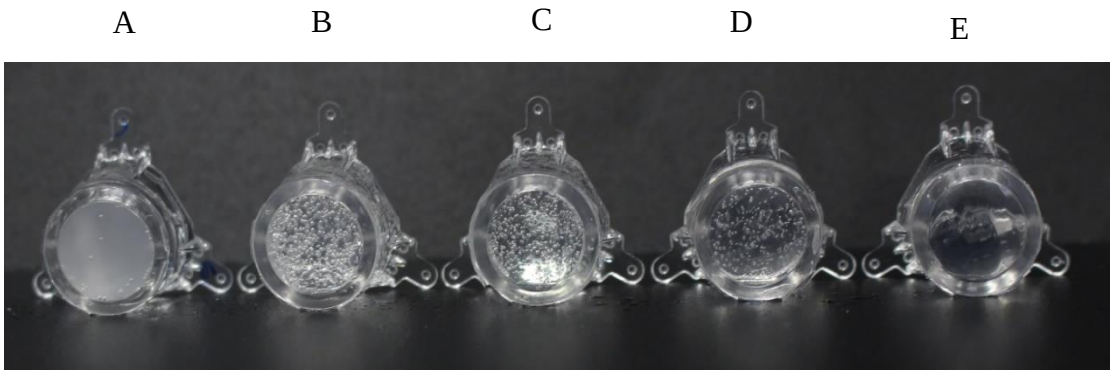

Figure 3.11 A representative photograph showing how D-mannitol incorporated into a PVA (6.0 % w/w) borate (2.0 % w/w) hydrogel prevented the formation of a white layer when in contact with PBS solution for 24 hours at room temperature. D-mannitol concentrations A) 0.0, B) 0.5, C) 1.0, D) 1.5 and E) 2.0 % w/w.

To observe how the dense white layer formation affected the release of proteins from the hydrogel, a release experiment was carried out using PBS and deionised water receiver phases. It was found that after 8 hours, there was 51 % less BSA released from the hydrogel, which was in contact with the PBS, compared to the hydrogel in contact with the deionised water. After 8 hours, 47.03 ± 2.33 % of the BSA was released from the hydrogel into the PBS receiver phase. In comparison, 98.75 ± 2.58 % of the loaded BSA was released from the hydrogel into the deionised water receiver phase, as seen in Figure 3.12.

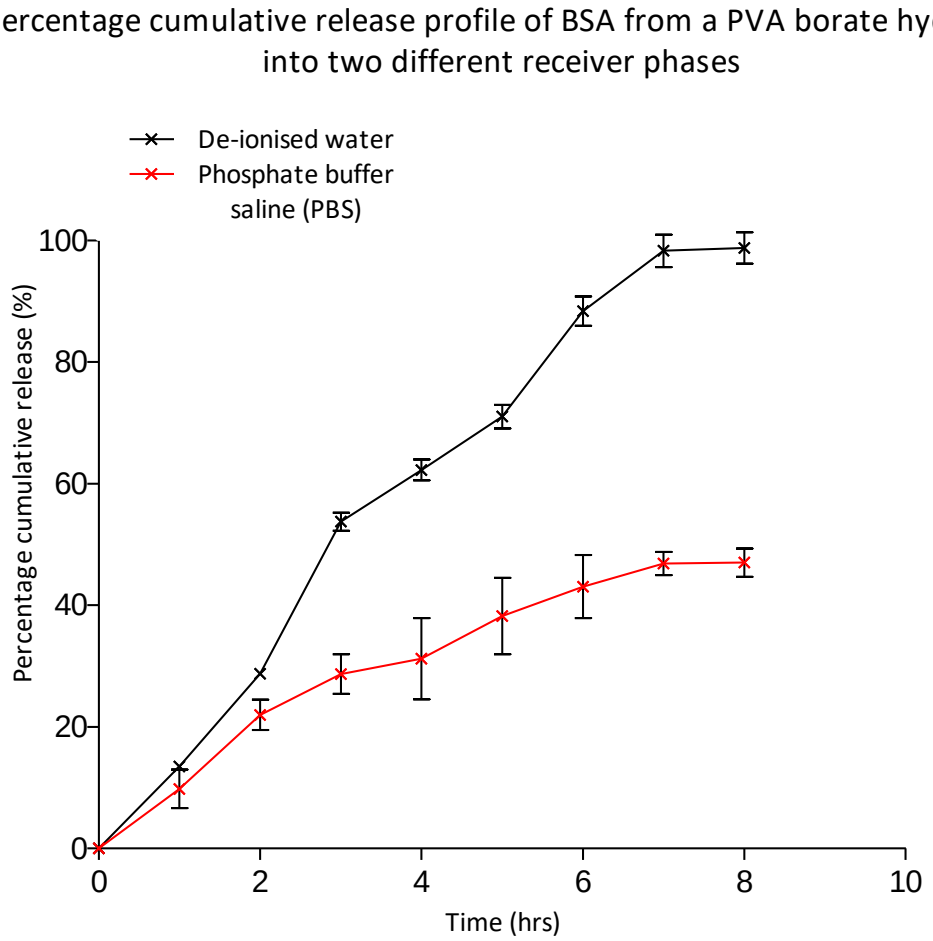

Figure 3.12 A percentage cumulative release profiles for BSA-loaded PVA (6.0 % w/w) borate (2.0 % w/w) hydrogel over 8 hours into two different receiver phases, PBS and deionized water. Release studies were carried out at 37 °C, using poly(carbonate) membranes with a pore size 8.0 µm on Franz diffusion cells. Data shown as the mean ± SD (n=3).

Protein release studies were carried out using a Franz diffusion cell apparatus. Deionised water was used as the receiver phase to avoid any complications with de-mixing even though it was found to be inhibited by addition of D-mannitol.

Figure 3.13 shows a typical BCA assay calibration plot that was used to determine the BSA concentration in each sample taken from the receiver phase. A calibration plot was performed on each micro-plate of samples to account for day–to-day and plate-to-plate optical variability. As the r^2 value is 0.99 it can be said that the data are correlated and confidence can be had in calculated values using the line equation.

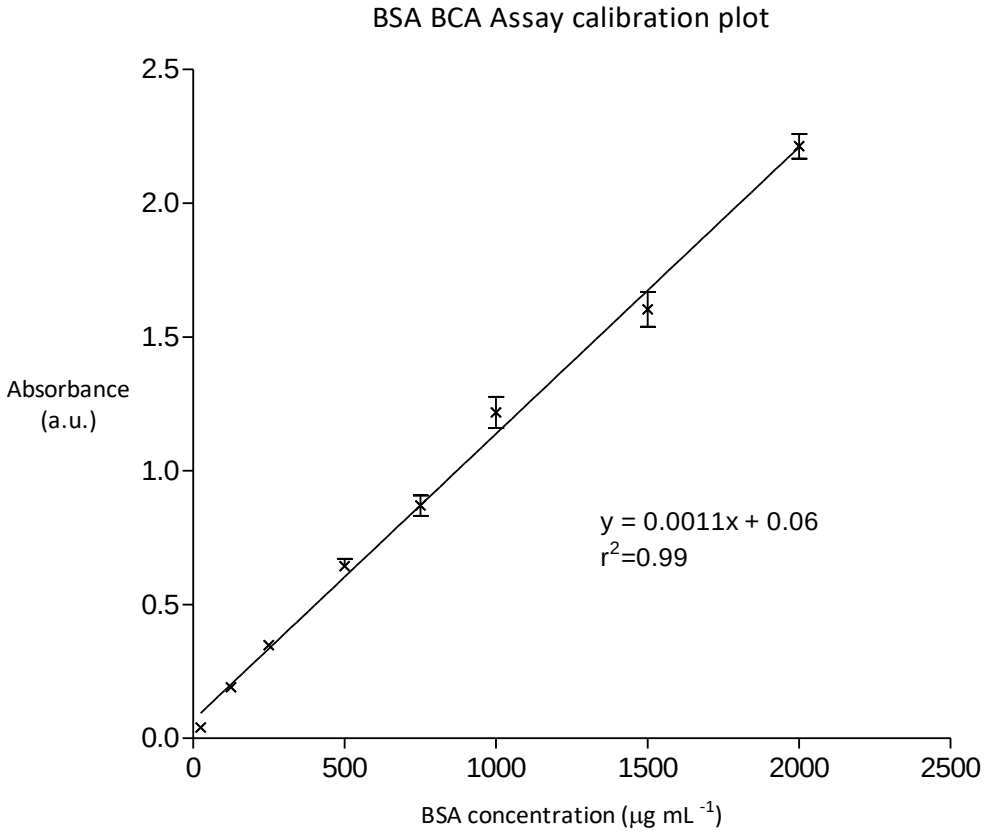

Figure 3.13 BCA assay calibration plot produced using several dilutions of a BSA stock solution 2 mg mL^{-1}. BSA standard dilutions concentration range 20–2000 μg mL^{-1}. The λ = 562 nm and data are shown as the mean ± standard deviation (n=3).

Figure 3.14 shows three concentration of BSA released from a hydrogel (PVA 6.0 % w/w borate 2.0 % w/w), over an 8-hour period. It can be seen that the 0.10 % w/w concentration gave the highest percentage cumulative release at all time points over the 8 hours, compared to the 0.20 and 0.05 % w/w hydrogels. The 0.05 % w/w concentration gave the lowest release up until 5 hours, with hour 8 giving a higher percentage cumulative release (52.22 ± 2.02 %) than that of the 0.10 % w/w BSA concentration. The 0.10 % w/w loaded hydrogel had released 58.34 ± 1.17 % after 8 hours. At hour 6, the 0.05 and 0.10 % w/w had similar percentage cumulative release values of 45.98 ± 2.72 % and 45.82 ± 2.87 %, respectively. Likewise at hour 7, the 0.05 and 0.10 % BSA hydrogels again had the same percentage cumulative release values of 49.52 ± 3.88 % and 49.81 ± 2.96 %, respectively. The BSA 0.20 %

w/w loaded hydrogel released the least amount of BSA (50.24 ± 2.60 %) at 8 hours compared to the two lower concentrations. One general trend displayed by all three BSA-loaded hydrogel release profiles was, as time increased the quantity of BSA released increased. All three release profiles began to plateau at approximately 6 hours.

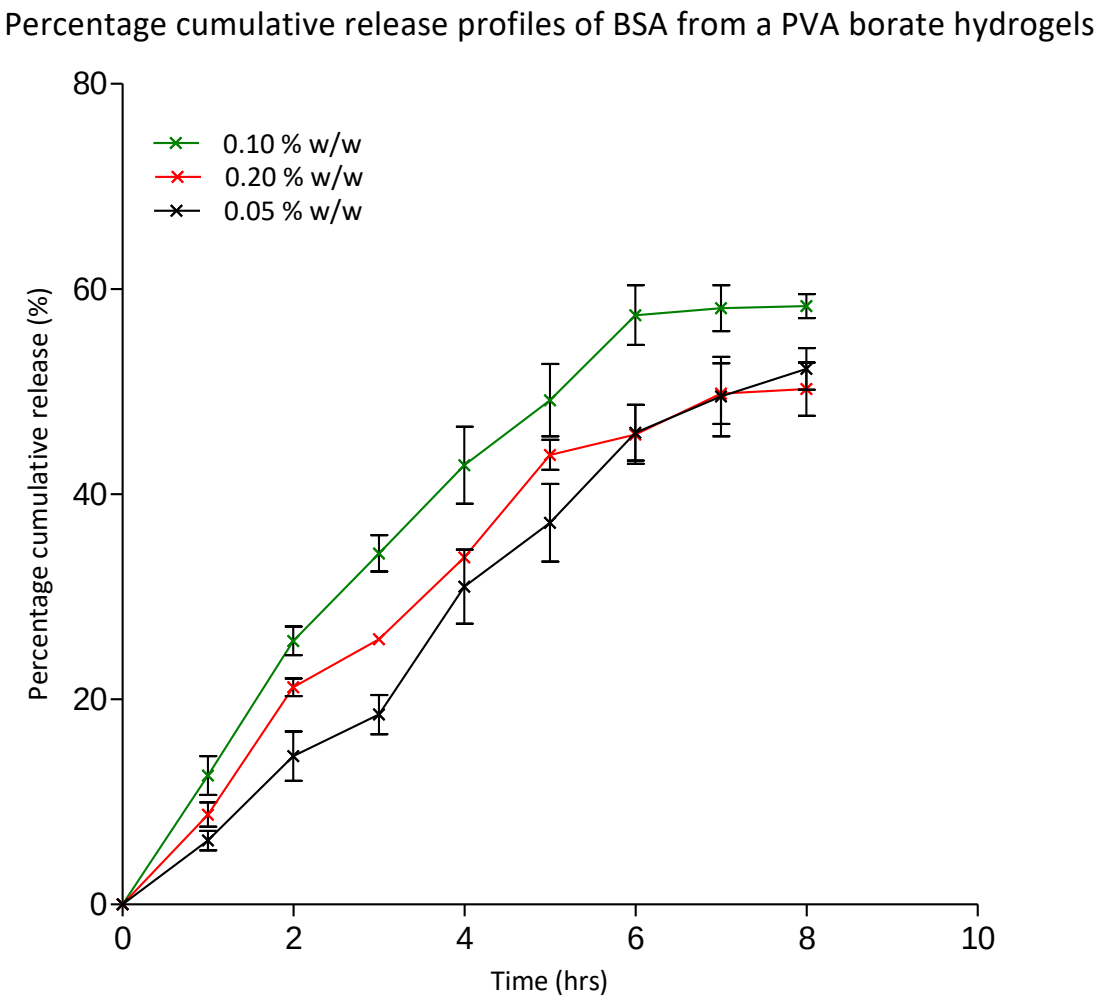

Figure 3.14 Percentage cumulative release profiles for three BSA-loaded PVA (6.0 % w/w) borate (2.0 % w/w) hydrogels of varying BSA concentration, over 8 hours. Release studies were carried out at 37 °C using poly(carbonate) membranes with a pore size 8.0 µm, on Franz diffusion cells. The data are shown as the mean ± standard deviation (n=3).

A haemoglobin calibration plot was produced using nine dilutions (0.00–0.16 mg mL^{-1}) of a 0.50 mg mL^{-1} stock solution dissolved in deionised water, as seen in Figure 3.15. Each dilution was then analysed using UV-Vis spectrometry at a λ max

of 405 nm. A calibration plot was carried out on each plate of samples to account for day–to-day and plate-to-plate optical variability. As seen in Figure 3.15, the r^2 value is 0.99. Therefore, it can be said that the data are correlated and confidence can be had in calculated values using the line equation.

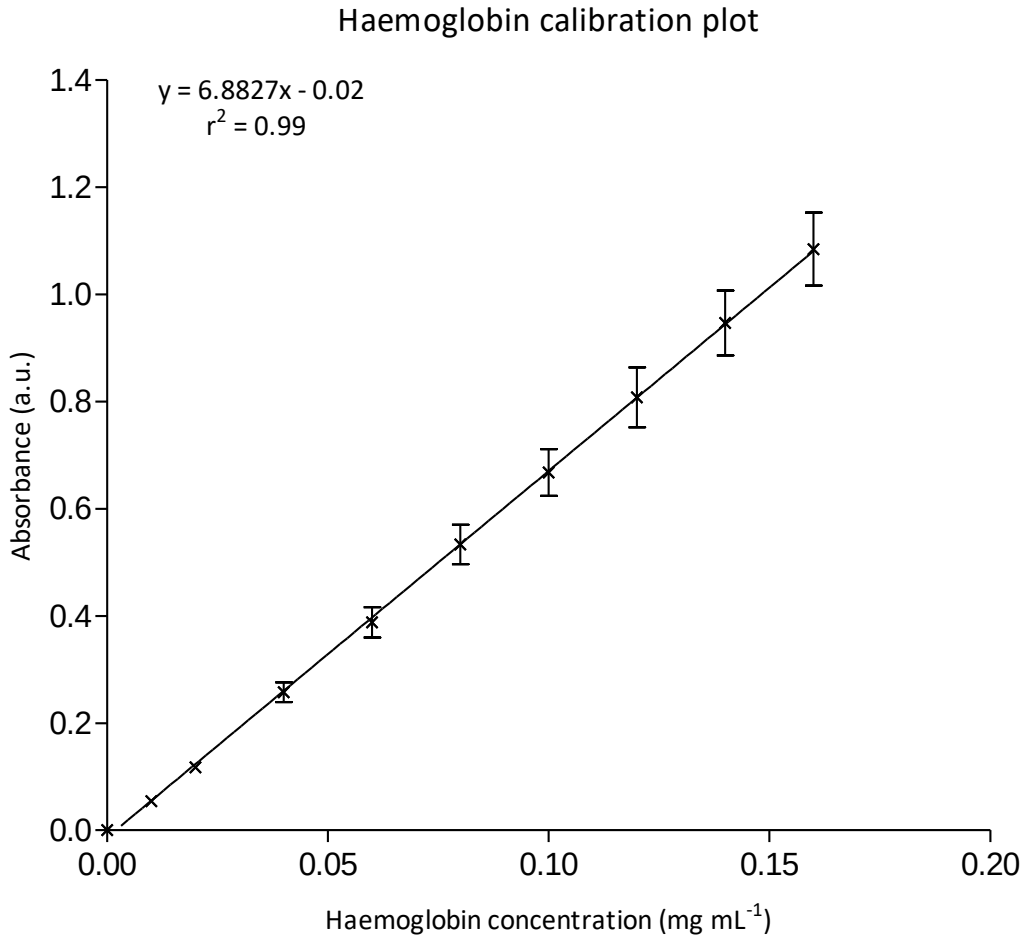

Figure 3.15 A UV-Vis haemoglobin calibration plot produced using nine dilutions of a bovine haemoglobin stock solution (0.50 mg mL^{-1}). The nine standard dilutions were within the concentration range 0.00–0.16 mg mL^{-1}. The λ = 405 nm and the data are shown as the mean ± standard deviation (n=3).

Figure 3.16 shows three percentage cumulative release profiles for hydrogels of the same formulation (PVA 6.0 % w/w borate 2.0 % w/w) loaded with varying concentrations of haemoglobin. The 0.10 % w/w concentration of haemoglobin had the highest percentage release at all time points, except for the first time point (1 hour). The 0.10 % w/w haemoglobin hydrogel yielded the largest overall percentage

cumulative release (50.62 ± 1.52 %) at 8 hours, compared to the other two higher concentrations of haemoglobin. At 1 hour, the 0.05 % w/w haemoglobin gel gave the highest percentage release of 16.27 ± 0.61 %, but, at 8 hours it had released the least amount of haemoglobin (34.10 ± 3.02 %), in comparison to the other two concentrations. From zero to four hours, the 0.20 % w/w hydrogel gave the lowest percentage release of haemoglobin. However, from 4 to 8 hours it gave a higher percentage release of haemoglobin than the 0.05 % w/w loaded gel. Interestingly, as observed in Figure 3.14, for BSA the middle concentration (0.10 % w/w) gave the highest percentage release. A general trend that is displayed by the three release profiles is as time increases the percentage of haemoglobin released also increases. Only the 0.05 and 0.20 % w/w profiles show signs of plateauing at approximately 6 and 7 hours, receptively. However, as seen Figure 3.16, it is feasible that the 0.10 % w/w release profile would plateau at approximately 60 % release had the experiment been permitted to run for a longer duration.

Figure 3.16 Percentage cumulative release profiles for three haemoglobin-loaded PVA (6.0 % w/w) borate (2.0 % w/w) hydrogels of varying haemoglobin concentration, over 8 hours. Release studies were carried out at 37 °C using poly(carbonate) membranes with a pore size 8.0 µm, on Franz diffusion cells. The data are shown as the mean ± standard deviation (n=3).

A typical BCA assay calibration plot for trypsin can be seen in Figure 3.17. The line equation of this plot was used to determine the trypsin concentration in each sample from the release study. A calibration plot was carried out on each plate of samples to account for day–to-day and plate-to-plate optical variability. As the r^2 value is 0.99, therefore, it can be said that the data are correlated and confidence can be had in calculated values using the line equation.

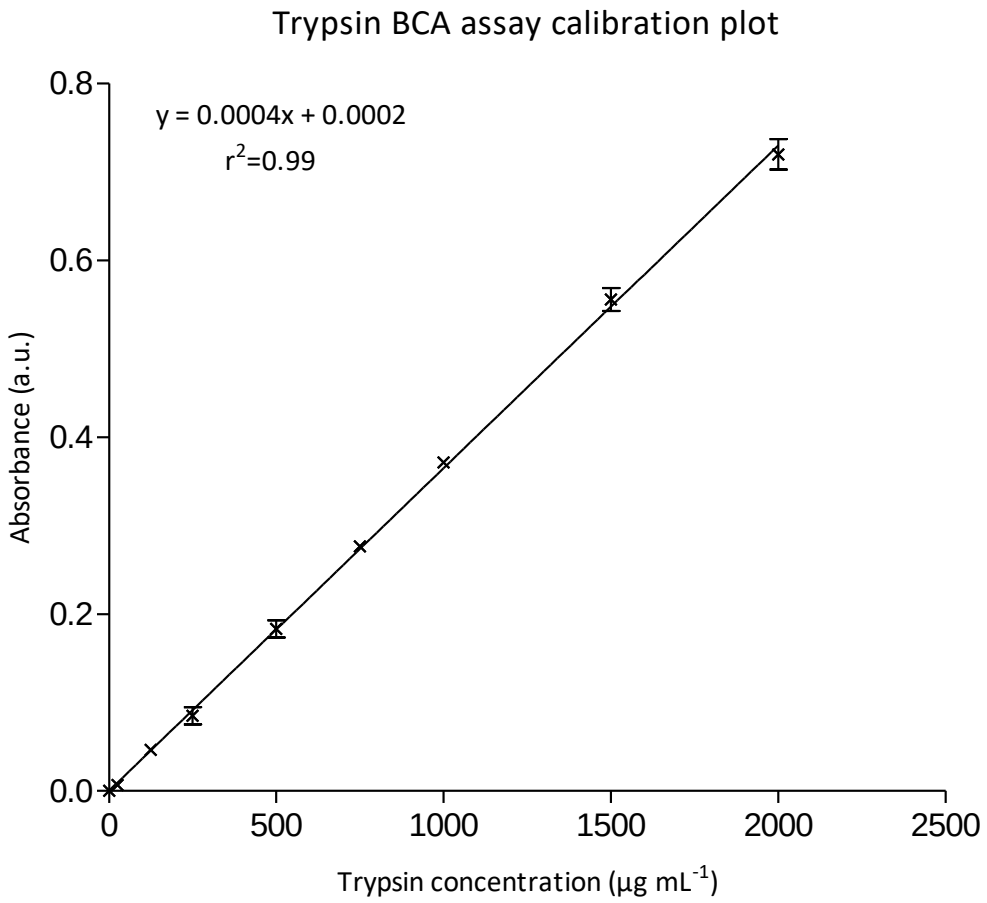

Figure 3.17 BCA assay calibration curve produced using several dilutions of a trypsin stock solution 2 mg mL^{-1}. The standard dilutions concentration range 20–2000 µg mL^{-1}. The λ = 562 nm and the data are shown as mean ± standard deviation (n=3).

One observation from comparing the trypsin calibration plot to the haemoglobin and BSA calibration plots, is that the absorbance values for the trypsin standards are lower than those for BSA and haemoglobin of the same concentration. This would suggest that the BCA assay may be less sensitive towards trypsin compared to BSA and haemoglobin.

The percentage cumulative release profiles for the three concentrations of trypsin-loaded into the PVA-borate hydrogels can be seen in Figures 3.18, 3.19 and 3.20. The hydrogel loaded with 0.05 % w/w trypsin gave the lowest percentage cumulative release (31.24 ± 11.92 %) at 8 hours, as seen in Figure 3.18. The 0.05 % w/w loaded hydrogel released no detectable quantities of trypsin until the fourth

hour. The release profile in general is erratic with large deviations in the mean values obtain for the 4 to 8 hour time points.

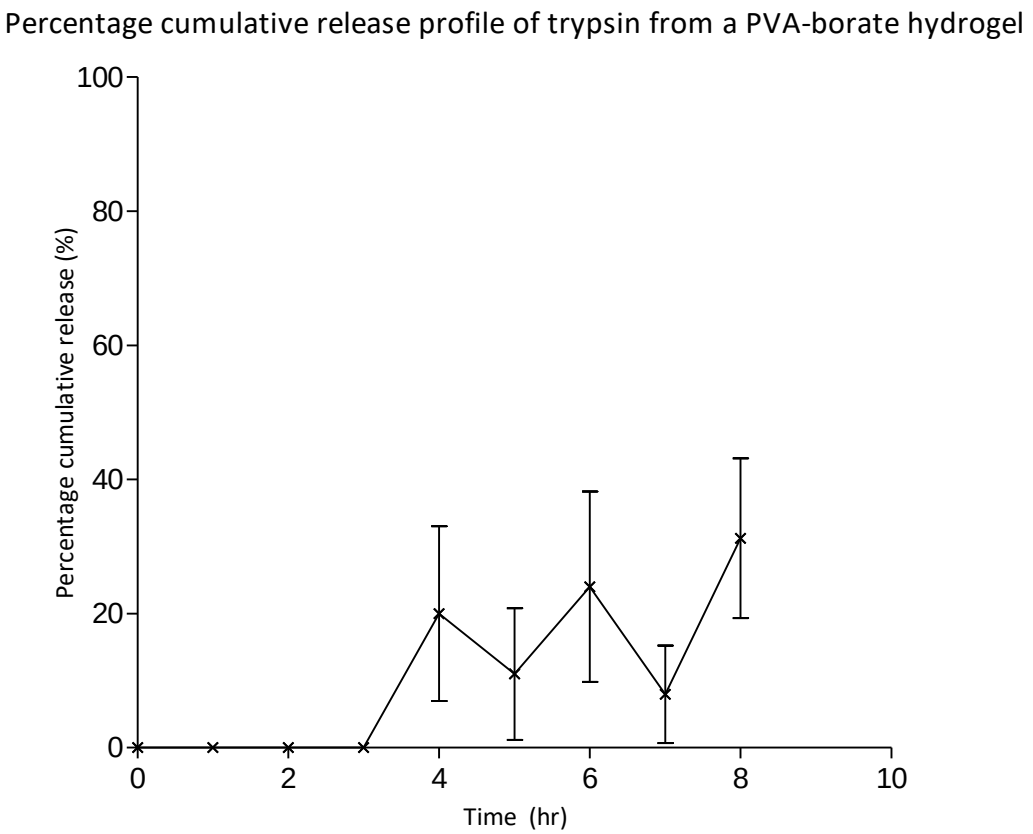

Figure 3.18 Percentage cumulative release profile for a PVA (6.0 % w/w) borate (2.0 % w/w) hydrogel loaded with 0.05 % w/w trypsin. Release studies were carried out at 37 °C for 8 hours using poly(carbonate) membranes with a pore size 8.0 µm, on Franz diffusion cells. The data shown as the mean ± standard deviation (n=3).

The release profile for the 0.10 % w/w trypsin-loaded hydrogel can be seen in Figure 3.19. The maximum percentage cumulative release was found to be 51.14 ± 16.73 % at 8 hours. Similar to the 0.05 % w/w loaded hydrogel the 0.10 % w/w trypsin-loaded gel did not release any detectable quantities of trypsin until the fourth hour, at which point it had released 24.60 ± 3.15 %. Again, this hydrogel showed erratic release of trypsin with large deviations in the mean values obtained for time points 5 to 8.

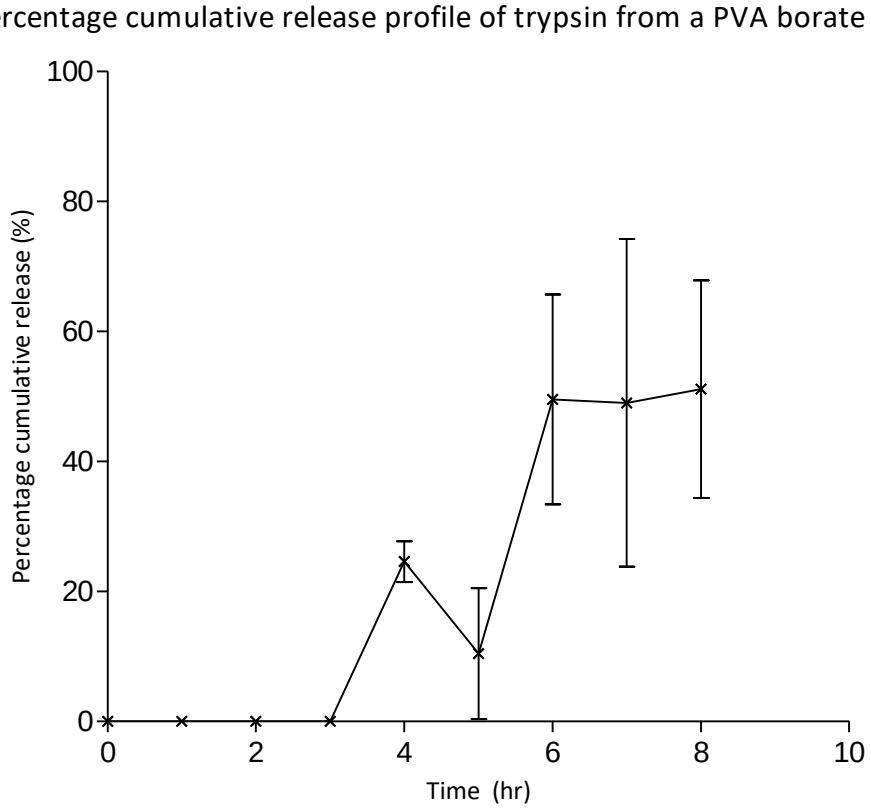

Figure 3.19 Percentage cumulative release profile for a PVA (6.0 % w/w) borate (2.0 % w/w) hydrogel loaded with 0.10 % w/w trypsin. Release studies were carried out at 37 °C for 8 hours using poly(carbonate) membranes with a pore size 8.0 µm, on Franz diffusion cells. The data shown as the mean ± standard deviation (n=3).

The 0.20 % w/w trypsin-loaded hydrogel gave the highest percentage cumulative release of trypsin at 8 hours (80.32 ± 18.37 %), as seen in Figure 3.20. The 0.20 % w/w trypsin gel gave a more typical release profile shape, similar to the BSA and haemoglobin. However, the standard deviation of the mean values were again large in comparison to those for BSA and haemoglobin. Unlike the 0.05 and 0.10 % w/w trypsin-loaded hydrogels, the 0.20 % w/w hydrogel did release detectable quantities of trypsin before the fourth hour. But, there was still no instant release seen, as the first detectable quantity of trypsin was at hour 2, as seen in Figure 3.20.

The 0.05 and 0.10 % w/w trypsin-loaded hydrogels did not show release profiles indicative of sustained release, in comparison to the release profiles for haemoglobin and BSA, as seen in Figures 3.14 and 3.16, respectively. Also all the

mean percentage cumulative release values for all three trypsin concentrations showed large variation in the mean values, compared to the BSA and haemoglobin mean values.

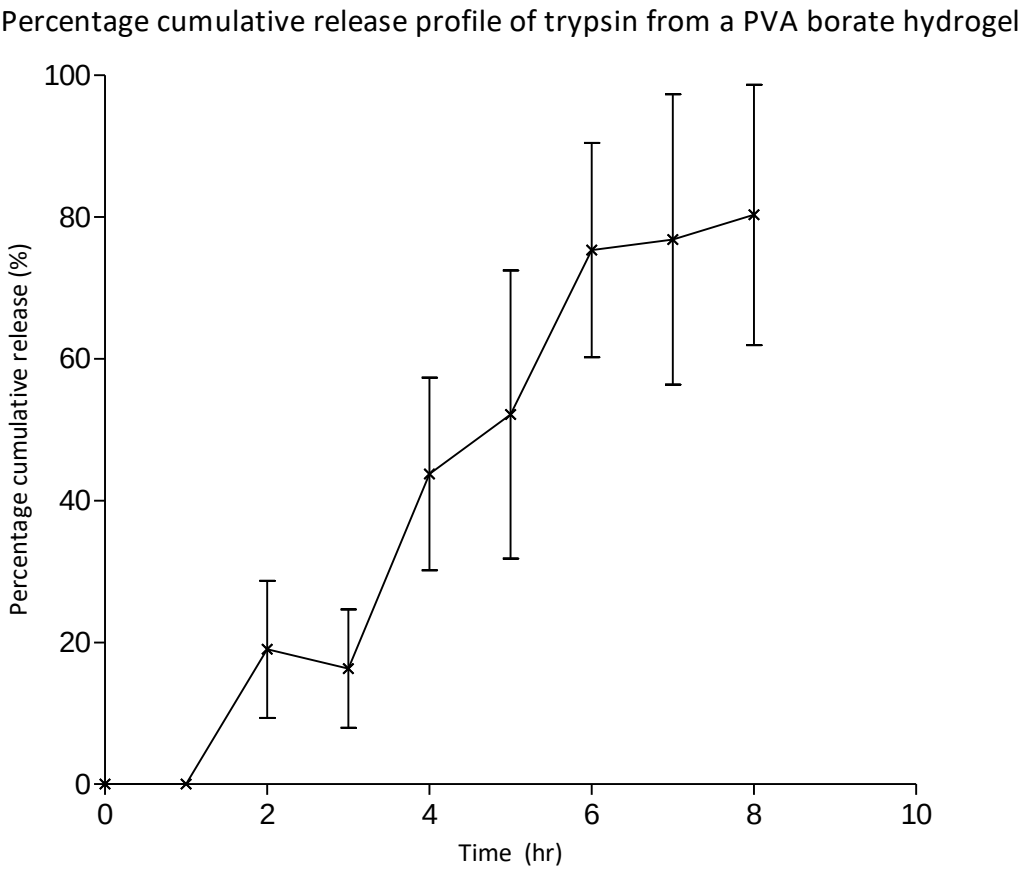

Figure 3.20 Percentage cumulative release profile for a PVA (6.0 % w/w) borate (2.0 % w/w) hydrogel loaded with 0.20 % w/w trypsin. Release studies were carried out at 37 °C for 8 hours using poly(carbonate) membranes with a pore size 8.0 µm, on Franz diffusion cells. The data shown as the mean ± standard deviation (n=3).

Figure 3.21 shows the resultant SDS-PAGE gel for the molecular weight checks on the released haemoglobin, BSA and trypsin, compared to a standard of each protein. It can be seen from lanes 3 and 4 that the BSA released from the hydrogel was not subject to any degradation when compared to the standard BSA sample. The BSA was also in proximity to the 62 kDa molecular marker, which in the SeeBlue® Plus2 Prestained standard Novex® solution is BSA. The haemoglobin did show degradation, however, it was degraded prior to being added to the hydrogel, as seen

in lane 6 of Figure 3.21. Haemoglobin has a molecular weight of approximately 64 kDa, however, it can be seen from lanes 6 that the haemoglobin had been degraded prior to being loaded into the hydrogel. In lane 7, it can be seen that the hydrogel released haemoglobin without any sign of further degradation. Lanes 9 and 10 show the trypsin standard and trypsin sample from the release study, respectively. It can be seen that the trypsin released from the hydrogel was not subject to any further degradation upon release, than what had already occurred prior to incorporation within the hydrogel. But, similarly to the haemoglobin it can be seen from lane 9 that the trypsin standard had degraded prior to being added to the hydrogel. The trypsin is in the proximity to the 14 kDa molecular marker and trypsin has a molecular weight of 23.3 kDa.

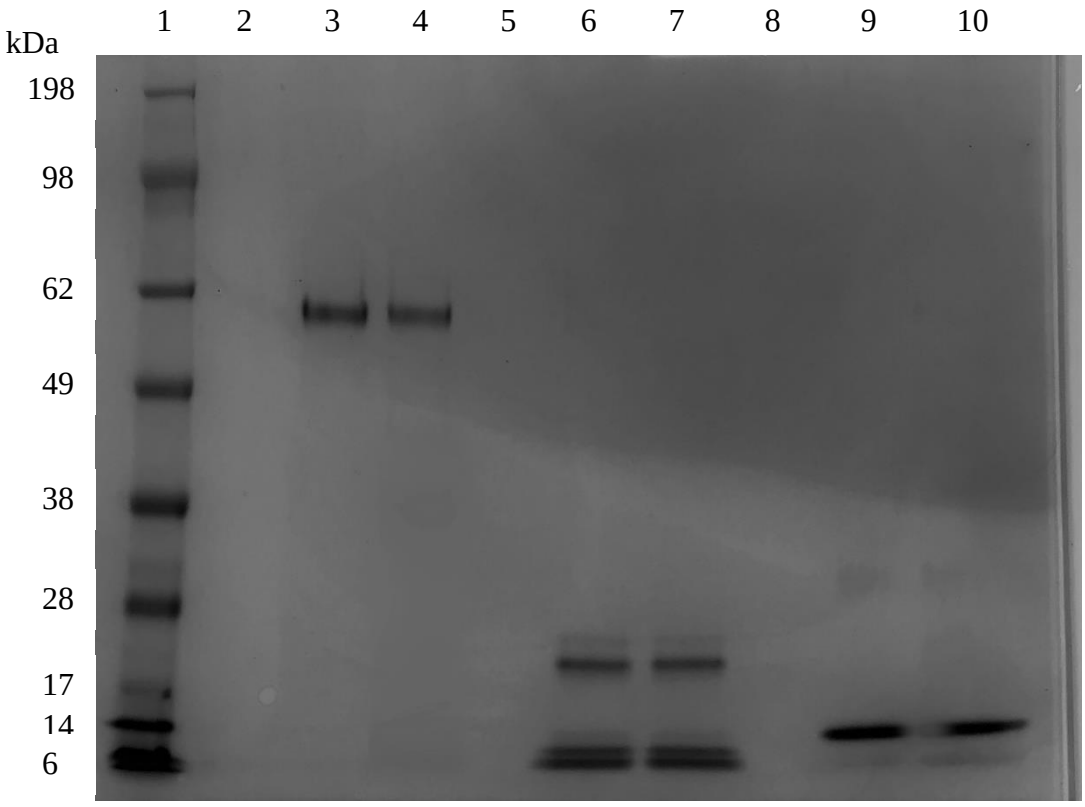

Figure 3.21 Image of the SDS-PAGE NuPAGE® Bis–Tris 4-12 % resolving gel (1.0 mm x 10 well), stained with coomassie blue for the three proteins released from a hydrogel (PVA 6.0 %w/w Borate 2.0 % w/w) and their standards. Lane 1 molecular markers, lane 3 BSA standard, lane 4 BSA sample, lane 6 Hb standard, lane 7 Hb sample, lane 9 trypsin standard, lane 10 trypsin sample. Lanes 2, 5 and 8 were intentionally left blank.

3.6 Discussion

PVA-borate hydrogels have been extensively studied as potential drug delivery systems for wound management. However, delivering a protein or peptide for wound management and repair using the PVA-borate hydrogel is a novel application. Therefore, no published literature is available to indicate if the PVA-borate hydrogel system is capable of delivering a therapeutic protein or peptide, which is still intact and biologically active. With this in mind, it was deemed not financially viable to commence the work using the intended insulin-like growth factor-1 (IGF-1), but, instead use three model proteins first. Therefore, in this chapter, a PVA 6.0 % w/w borate 2.0 % w/w hydrogel was used to deliver three model proteins of varying isoelectric points and molecular weights, summarised in Table 3.5, to determine the percentage release and stability.

Table 3.5 Summary of model proteins properties

Protein	**Molecular weight (kDa)**	**Isoelectric point**	**Net charge in hydrogel**
Bovine serum albumin	66.0	4.2–5.4	Negative
Bovine haemoglobin	64.5	6.8	Negative
Trypsin	23.3	10.1–10.5	Positive

Lidocaine hydrochloride (Loughlin *et al.*, 2008), methylene blue and meso-tetra (N-methyl-4-pyridyl) porphine tetra tosylate (Donnelly *et al.*, 2009) were all previously incorporated into the PVA-borate hydrogel system using a similar formulation process to that used in section 2.4.1 of this thesis. However, these drugs remained stable on heating to 80 °C during the manufacturing process and it is known that proteins and peptides undergo degradation upon heating. To prevent

denaturation of plasma proteins during a cardiopulmonary bypass the maximum temperature of the heat exchanger is maintained between 40–42 °C (Vazquez & Larson, 2013). It was found that on increasing the temperature of the heat exchanger to between 43–45 °C degradation of the plasma proteins had begun, detected using SDS-PAGE (Vazquez & Larson, 2013). Therefore, a new method for incorporating proteins and peptides into the PVA-borate hydrogel needed to be ascertained. Gehrke *et al*. (1998) formulated dextran-divinylsulfone cross-linked hydrogels for delivery of proteins. They loaded both model proteins, ovalbumin and α-amylase, by soaking samples of the hydrogel in excess buffer solutions containing the dissolved proteins (Gehrke *et al.*, 1998). They concluded that the loading process involved both adsorption and absorption, known collectively as sorption. Similarly, Jensen *et al*. (2001) loaded four model peptides into chondroitin 4-sulphate hydrogels using the same equilibrium swelling technique to avoid heating the proteins to 60 °C during the formulation process. However, Jensen *et al*. (2001) found that the three positively charged model proteins were concentrated in the gel system, but, the negatively charged bovine serum albumin (BSA) was not. They concluded that the positively charged proteins were involved in ionic interactions with the negative charged polymer backbone in the hydrogel, thus giving higher loading concentrations. In comparison, the repulsion between the negatively charged BSA and the negative charges of the polymers, hindered the loading. They suggest that BSA was loaded passively, by diffusing in the water phase of the gel, thus giving a lower loaded concentration in comparison to the other two proteins.

It was decided for the purpose of this work that the most cost effective way to incorporate the model proteins was to add the desired volume of protein solution to the desired quantity of pre-made hydrogel and mix it in by hand, using a stainless

steel spatula, at room temperature. On physically cutting up the hydrogel with the spatula, it created a larger surface area for uptake of the protein solution. The hydrogel then self-healed upon resting at room temperature, providing a hydrogel with a homogenous mix of protein throughout its matrix. One advantage of carrying out the loading process using this method was it kept protein wastage to a minimum, which will be extremely important in later work when loading the expensive bioactive growth factor. Second, using the swelling equilibrium method showed poor uptake of opposite charged proteins, which required up to two weeks to achieve an acceptable amount of protein in the hydrogel (Jensen *et al.*, 2002). Whereas, the process used in this thesis resulted in loaded hydrogels ready to use within 12–24 hours. Appel *et al.* (2012) found that mixing solutions of BSA and lysozyme into preformed modified PVA hydroxyethyl cellulose hydrogel resulted in homogenously loaded gels.

BSA has been widely used as a model protein for novel delivery system release studies due to its high stability (Shalaby *et al.*, 1993; Mellott *et al.*, 2001; Khoury *et al.*, 2003; Balasubramanian *et al.*, 2010). On loading three concentrations of BSA into the PVA-borate hydrogel, crossover moduli analysis was carried out using oscillating rheology. This was used to determine if addition of the BSA had caused any changes in the viscoelastic properties of the hydrogel. BSA was found to decrease the crossover modulus of the hydrogel in comparison to a hydrogel of the same formulation containing no BSA. BSA when solubilised in deionised water and incorporated into the PVA-borate hydrogel system has an overall negative charge, due to having an isoelectric point in the range of 4.2–5.4 (Shalaby *et al.*, 1993; Jensen *et al.*, 2002; Khoury *et al.*, 2003). Jensen *et al.* (2002) observed what was thought to be repulsion between the negatively charged BSA and the negative

charged regions on the polymers, which hindered the loading. A similar electrostatic repulsion may be occurring in the PVA-borate hydrogel. Loughlin *et al*. (2008) state that the mono-diol complex formed during the first step, in the two step cross-linking reaction between the PVA and borate is a negatively charged poly(electrolyte). Therefore, it may be possible that not all of the polymers fully cross-link forming the di-diol complex, leading to some negatively charged regions on the polymeric backbone. Negatively charged regions could also result temporarily from the reversible nature of the PVA-borate cross-link. If this were the case, then there is the possibility of repulsion between the BSA and the negatively charged regions on the polymers, similar to what Jensen *et al*. (2002) observed. As a result, the cross-linking density may be reduced as the negatively charged BSA would push the PVA poly(electrolytes) further apart, reducing the cross-linking density and polymer entanglement. Hence, reducing the hydrogel viscosity and crossover modulus. Lin *et al*. (2005) also stated that the Na^+ cation produced from the dissociation of sodium tetraborate decahydrate plays a part in the overall shape of the polymer chains and cross-linking process due to a shielding effect on the poly(electrolyte). The shielding effect reduces the repulsion between the poly(electrolytes), increasing the cross-linking and polymer entanglement by causing the polymer chains to re-orientate to reside closer together and interact. Therefore, another possible explanation for the reduction in the crossover modulus on addition of BSA may be due to the negatively charged BSA interacting with the Na^+ cation, reducing its ability to provide the necessary shielding effect. As a result, the repulsion between the polymers is increased, reducing cross-linking, resulting in a hydrogel with weak viscoelastic properties.

On adding trypsin to the hydrogel, the crossover modulus decreased in comparison to the blank hydrogel formulation. This is similar to the trend seen for the BSA and indicates that the hydrogel viscosity and viscoelastic properties have been reduced. Trypsin has an isoelectric point between 10.0–10.5 (Tietze, 1953; Walsh, 1970), therefore, as the PVA 6.0 % w/w borate 2.0 % w/w hydrogel is pH 8.0 the trypsin will have an overall positive charge when in the hydrogel. The trypsin is the opposite charge to the BSA when loaded in the hydrogel, yet, also causes a decrease in crossover modulus. Therefore, the proposed theory of what is occurring due to electrostatic repulsion between the BSA and negative regions of the polymers cannot be the cause of the decrease in crossover modulus caused by trypsin. One possible reason for the reduced crossover modulus could be explained by a different interaction. The positively charged trypsin molecules may interact with the negatively charged borate anion, resulting in decreased cross-linking with the PVA. If this is the case, decreased cross-linking will cause a reduction in the crossover modulus and, therefore, a low viscosity gel with a weak elastic response at low frequencies (Murphy *et al.*, 2012).

Incorporation of haemoglobin into the hydrogel caused an increase in the crossover modulus value, despite being negatively charged in the hydrogel environment. The increase in crossover modulus indicates that the haemoglobin is causing an increase in the cross-linking density of the hydrogel matrix. The exact mechanism of how it is causing this increase in the crossover modulus within the PVA-borate hydrogel is uncertain. However, Patton *et al*. (2006) demonstrated that it was possible to cross-link bovine haemoglobin to a poly(acrylamide) hydrogel matrix. It was concluded that the haemoglobin-poly(acrylamide) cross-link was the result of a covalent attachment between specific amino acids in the large tetrameric

haemoglobin structure and the poly(electrolytes) (Patton & Palmer, 2006). Therefore, the bovine haemoglobin in this study may also be partaking in a cross-link reaction with the PVA polymer. If this is the case, it would result in a hydrogel matrix with an increased cross-linking density, thus explaining the increase in the crossover modulus.

Prior to commencing the release studies, an appropriate receiver phase was selected. The first choice was phosphate buffer saline as it is commonly used in biological research due to the osmolarity and ion concentration being similar to that of human blood. However, on running a trial release experiment it was observed that a white, opaque, dense looking layer formed at the surface of the hydrogel, which was in contact with the PBS receiver phase. On further investigation, it was found that the PBS was the cause of this white layer forming and that both the concentration and volume of the salt solution played a crucial role in the formation of the white layer. A similar occurrence was seen by Loughlin *et al*. (2008) on addition of lidocaine hydrochloride to the PVA-borate hydrogel. On addition of high concentrations of the lidocaine hydrochloride (≥ 3.0 % w/w), they documented an ionic induced gel network collapse and drug precipitation. The network collapse, or de-mixing, is caused by an increase in the free ion concentration within the hydrogel. On increasing the free ion concentration within the formulation, the repulsion between the poly(electrolyte) network decreases due to an increased shielding effect by the exogenous free ions. This alteration in the sensitive balance between the repulsive force and shielding effect leads to over shielding, increasing in the PVA-borate cross-linking density to an extent that causes phase separation and de-mixing (Pezron *et al*., 1988a; Loughlin *et al*., 2008). When the hydrogel comes in contact with the PBS solution, it begins to absorb the PBS due to its ability to uptake fluid

and swell. As the PBS is absorbed it reaches a threshold free ion concentration within the hydrogel causing the ionic induced de-mixing and increased cross-linking density. Loughlin *et al*. (2008) reported that the de-mixing only occurred when the lidocaine hydrochloride concentration within the hydrogel was ≥ 3.0 % w/w. Likewise, in the experiment completed in this chapter, it was found that the formation of the de-mixed, dense white layer only formed when the total salt concentration was ≥ 154 mM.

Loughlin *et al.* (2008) found that by adding D-mannitol to the PVA-borate-lidocaine formulation, the de-mixing caused by the high concentrations of lidocaine hydrochloride no longer occurred. D-mannitol is a polyol sugar, which acts as a scavenger molecule for the free borate ions within the formulation. Complexation between two different poly-functionalised alcohol sugars, D-mannitol and D-sorbitol, with borate was studied using matrix-assisted laser desorption/ionization Fourier-transform mass spectrometry (Penn *et al.*, 1997). Penn *et al*. (1997) found that both polyol sugars form monoester and diesters with the borate ions, with the diester formation more energetically favourable. Similarly, Pezron *et al.* (1988b) found that addition of D-mannitol also prevented the de-mixing of a galactomannan-borate cross-linked formulation in the presence of a 1 M NaCl solution. Galactomannans are polyhydroxy compounds similar to PVA (Pezron *et al*., 1988b). In a similar manner, it was found in the study completed in this chapter, that addition of D-mannitol prevented the formation of the white de-mixed layer when a hydrogel sample came in contact with the PBS receiver phase. This is due to the D-mannitol complexing with the free borate ions, therefore, preventing them from causing an increase in cross-linking density.

It was found that on addition of D-mannitol to the PVA 6.0 % w/w borate 2.0 % w/w formulation, the viscoelastic properties of the hydrogel changed. These changes were observed by changes in the crossover modulus and yield stress analysis. As the concentration of D-mannitol increased both the crossover modulus and the yield stress values decreased. As the D-mannitol binds with the free borate ions, they are no longer available to partake in the cross-linking reaction, thus, reducing the cross-linking density of the hydrogel. As a result of reduced cross-linking, the hydrogel has a low viscosity and becomes more fluid like. D-mannitol has a greater affinity for the borate ions than the PVA polymer. Consequently, the D-mannitol competes with the PVA polymer for the borate ions and can remove borate from the PVA-borate interaction, also causing the hydrogel system to fluidise (Loughlin. *et al*., 2008). D-mannitol can also sequester the borate bound to the PVA, which results in the diol complex not forming, resulting in a more fluid-like hydrogel system. Both Loughlin *et al.* (2008) and Pezron *et al*. (1988b) found that on adding D-mannitol to their borate cross-linked polymers, their formulations became more fluid-like. Despite showing that the de-mixing can be prevented by the incorporation of D-mannitol into the PVA-borate formulation, it was decided that deionised water would be used as the receiver phase. The reason for this was to avoid adding another variable component to the hydrogel formulation, which was found to affect the viscoelastic properties and had the potential to interact with the loaded proteins.

Release studies were carried out on Franz diffusion cell apparatus at 37 °C to mimic body temperature. Protein release from polymeric hydrogels is governed by the characteristics of both the hydrogel matrix and protein itself. Both the BSA and haemoglobin-loaded hydrogels gave sustained release profiles over 8 hours, for all three concentrations. As previously discussed, BSA caused a reduction in the

crossover modulus, leading to a more fluid-like hydrogel network. The reduction in hydrogel viscosity provides greater relaxation of the polymers, which allows greater swelling on contact with the receiver phase. The combination of these effects and the repulsion between the protein and the polymer could explain why the 0.10 % w/w BSA-loaded hydrogel gave the highest release (58.34 ± 1.17 %) of all the protein-loaded gels studied. Mellot *et al*. (2001) demonstrated a sustained released of BSA from cross-linked poly(ethylene glycol) diacrylate hydrogels, which they believed to be relaxation-controlled diffusive release.

Haemoglobin, although negatively charged in the hydrogel environment, caused an increase in the crossover modulus. The higher cross-over modulus is indicative of increased cross-linking, which reduces polymer relaxation and, therefore, reduces the swelling ability of the gel. The reduction in polymer relaxation and swelling means that the pores within the polymer network are not as large, sterically hindering the release of the larger haemoglobin molecule (64.5 kDa) out of the gel network. This may be the reason why the 0.10 % w/w haemoglobin loaded hydrogel achieved a lower cumulative percentage release of 50.62 ± 1.52 %, in comparison to the 0.10 % w/w BSA loaded gel. Similarly, Khoury *et al*. (2003) found that by increasing the cross-linking density of multi-polymer cross-linked hydrogels, there was a sharp decline in the release of loaded proteins.

The 0.05 % and 0.10 % w/w trypsin-loaded hydrogels gave poor and erratic release of trypsin, with the mean values having large standard deviations. Yet, the 0.20 % w/w gel gave a release profile indicative of sustained release, however, the mean values also had large standard deviations. As mentioned previously, the trypsin is positively charged in the PVA-borate hydrogel environment and could possibly be interacting with the borate anion. There may also be interactions

between specific amino acid residues and specific regions of the polymer backbone. If opposite charge attraction or interaction are occurring, then this may explain why no trypsin release was detected for the first 4 hours from the 0.05 % and 0.10 % w/w hydrogels. Also, with the concentration of trypsin loaded into these two hydrogels being low, all the trypsin may be involved in electrostatic or other bonding interactions. This would then suggest that the initial diffusive-burst release from the water-filled pores of the hydrogel is not taking place. Both Loughlin *et al*. (2008) and Haung & Brazel (2001) suggest that the initial burst release is brought about by migration of the loaded drug to the surface, leading to high surface concentrations. However, Khoury *et al*. (2003) stated that if the protein loaded in the hydrogel is of the opposite charge to the hydrogel itself, then the protein will be immobile in the hydrogel. They demonstrated this theory by a diffusive study using lysozyme, which was positively charged, in a negatively charged poly(acrylic) acid hydrogel displayed no diffusion through the hydrogel matrix. In comparison, BSA, which was negatively charged in the hydrogel, did diffuse through the gel. Therefore, a combination of low trypsin concentration and low diffusivity could be responsible for the low erratic release of trypsin from these gels. Once the concentration of trypsin in the hydrogel is increased (0.20 % w/w), there is excess trypsin available, which may not be irreversibly bound or hindered by electrostatic interaction. Therefore, this trypsin can freely diffuse through the hydrogel and be released immediately on contact with the receiver phase, as seen in other PVA hydrogel systems (Huang & Brazel, 2001; Loughlin *et al.*, 2008) and with the BSA and haemoglobin in this study. It was found in Chapter Two that prolonged exposure of the PVA-borate hydrogels to an aqueous solution caused it to swell until it reached appoint were the hydrogel matrix began to erode and disintegrate. This could

explain the release of trypsin seen after four hours from the 0.05 % and 0.10 % gels, with the initial release up to hour four observed for the 0.20 % w/w trypsin hydrogel being by diffusion only. This suggests that the mechanism of protein release from the PVA-borate hydrogels is anomalous (non-Fickian) transport, as it is a combination of both diffusion, polymer relaxation, erosion and degradation. Likewise, Loughlin *et al.* (2008) found that the PVA-borate hydrogels released lidocaine in an anomalous (non-Fickian) manner. Preliminary work completed by Winder (2013), demonstrated that the PVA-borate hydrogels released sodium fusidate, mupirocin calcium and poly(hexamethylene) biguanide hydrochloride by the anomalous (non-Fickian) mechanism. Polymeric hydrogel microspheres made from poly(acrylamide) grafted with guar gum and cross-linked with glutaraldehyde displayed Fickian release initially, but, on swelling displayed non-Fickian release, concluding that the drug released mechanism was anomalous (non-Fickian) (Soppirnath & Aminabhavi, 2002).

Sodium dodecyl sulphate poly(acrylamide) gel electrophoresis (SDS-PAGE) was used to check the molecular weight of the protein molecules released from the hydrogel, in comparison to standard samples of each protein and a protein molecular weight marker ladder. It was found that none of three proteins undergone any degradation while within the PVA-borate of hydrogel matrix or upon release from the gel. SDS-PAGE is a common standard technique for protein sizing, which is still widely used despite advances in protein analysing technologies (Goetz *et al.*, 2004). SDS is an anionic detergent, which gives the protein to be sized an overall negative charge. As the protein samples in question all have the same overall charge the proteins are separated solely by size when an electric field is applied across the poly(acrylamide) gel (Goetz *et al.*, 2004). The higher the molecular weight of the

protein the slower it migrates down the gel, with lower molecular weight proteins traveling much faster, resulting in size separation. BSA released from the PVA-borate hydrogel showed similar structural integrity to the BSA encapsulated and released from poly(D,L-lactide-co-glycolide) (PLGA) microspheres (Igartua *et al.*, 1998). Using SDS-PAGE, Igartua *et al*. (1998) determined that BSA remained structurally intact during encapsulation and upon release from the PLGA microspheres.

3.7 Conclusion

The work completed in this chapter has shown that the PVA-borate hydrogel is capable of delivering a sustained release of all three concentrations of BSA and haemoglobin over 8 hours at 37 °C. The hydrogel also displayed partial release of trypsin from 0.05% and 0.10 % w/w loaded hydrogels, after 4 hours and release from a 0.20 % w/w trypsin-loaded gel over 8 hours at 37 °C. However, the uncharacteristic release profiles for trypsin accompanied with large standard deviations of the mean values, may indicate certain limitations to the gels potential to provide a sustained release of specific proteins. It has found that addition of all three concentrations of each of the different model proteins caused changes in the viscoelastic properties of the hydrogel. On analysis of the released proteins using SDS-PAGE it was concluded that all three proteins were released from the hydrogel without degradation. To conclude, results from this study indicate that the most suitable protein payloads for incorporation into the PVA-borate hydrogel are those which will have a net negative charge when incorporated into the hydrogel matrix. The negatively charged proteins were released in sustained manner from the hydrogel system, unlike the positively charged trypsin. The results also indicate that

the high molecular weight proteins are released in a sustained manner. Therefore, it would be presumed that if the hydrogel can release large bulky high molecular weight proteins then it could also release lower molecular weight proteins.

Chapter 4

Chapter 4

4 Formulation, characterisation, *in vitro* release, stability and enzymatic activity study of a pepsin-loaded, PVA-borate hydrogel.

4.1 Introduction

In the previous chapter, it was determined that the PVA-borate hydrogel was capable of providing a sustained release of incorporated proteins, without any degradation of the protein structure. In this chapter, another protein, the enzyme pepsin, was chosen to undergo the same testing as detailed in the previous chapter with the addition of enzymatic studies. The important question to be answered in this chapter was to determine if the PVA-borate could deliver an enzyme, which still retained its enzymatic activity.

Enzymes are proteins, which work as catalysts for biochemical reactions. Catalysts for any chemical reaction, whether biological or non-biological, increase the rate of reaction by lowering the activation energy. This allows reactions to take place in a timely manner under less extreme conditions, such as physiological conditions. Enzymes do not change the equilibrium constant of the reaction, only the rate at which equilibrium is reached (Denniston *et al.*, 2008). Therefore, the energy difference between the products and reactants remains the same and only the activation energy (E_a) is reduced, as seen in Figure.4.1.

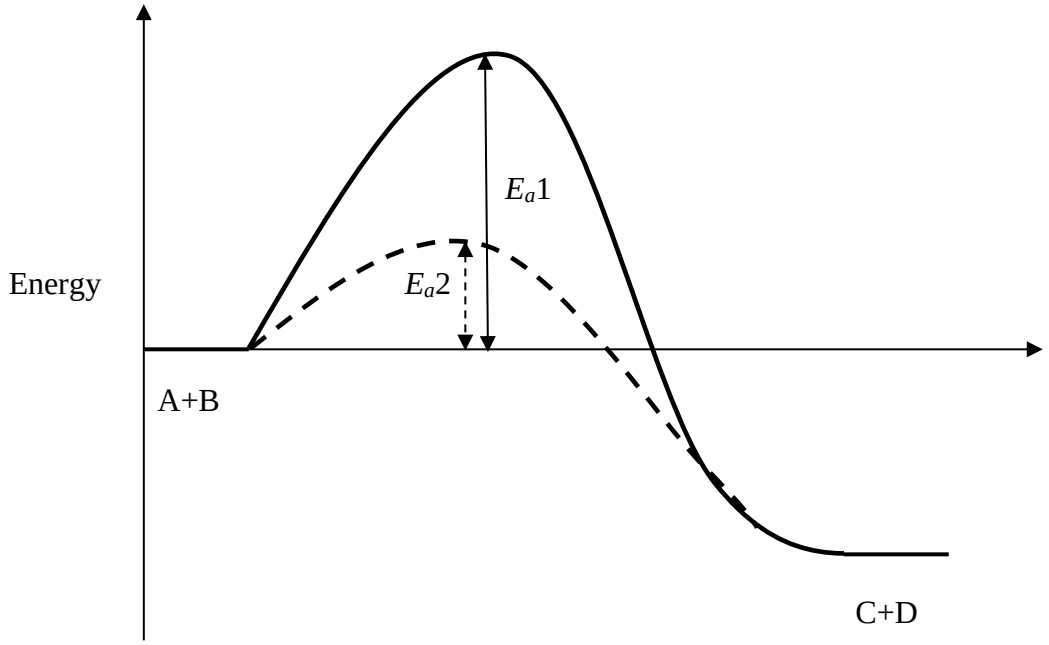

Figure 4.1 Schematic diagram showing how the addition of a catalyst, such as an enzyme lowers the activation energy (E_a) of the reaction. A+B represent the reactants and C+D the products. E_a1 represents the non-catalysed and E_a2 represents the catalysed reaction.

For a non-catalysed biochemical reaction, the rate of reaction is directly proportional to the substrate concentration, as seen in Figure 4.2a. However, for an enzyme-catalysed reaction, the rate of reaction is only directly proportional to the substrate concentration initially (Figure 4.2b). As the substrate concentration increases further, the rate of reaction begins to slow down and is no longer directly proportional to the substrate concentration. At a specific substrate concentration, the reaction reaches its maximum velocity (V_{max}), as seen in Figure 4.2b. At V_{max}, all the enzymes active sites are occupied and any further increase in the substrate concentration will have no effect on the rate of reaction (Denniston *et al.*, 2008).

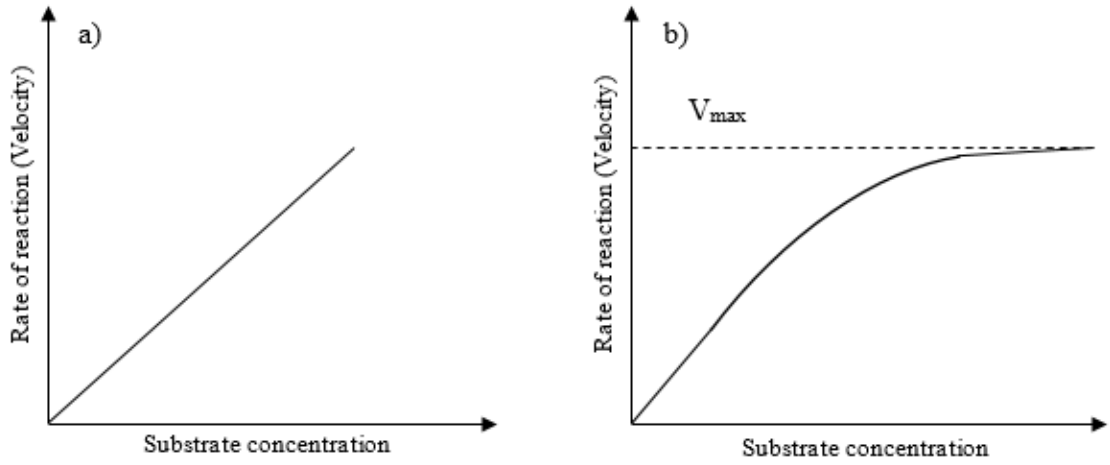

Figure 4.2 Schematic plots of the rate of reaction against substrate concentration for, a) a non-catalysed reaction, were the substrate concentration is directly proportional to the rate of reaction and b) an enzyme-catalysed reaction were the rate of reaction reaches a maximum velocity (V_{max}) when all the available enzymes' active sites are occupied.

The active site of an enzyme is the region of the molecule that binds the substrate molecules and gives enzymes their high specificity. Within the active site of an enzyme, there are specific functional groups, which bind the substrate molecule and other groups, which take no part in the binding process and are involved in the catalytic process (Voet *et al.*, 1999). The shape of the active site is thought to be complementary to the shape of the substrate molecule, increasing enzyme specificity. Emil Fischer in 1894, introduced the lock-and-key model for enzyme-substrate binding (Steed *et al.*, 2012). Fischer concluded that the substrate molecule simply clicked into the active site of the enzyme in a similar way to which a key fits a specific lock precisely. Building on Emil's theory, Daniel Koshland Jr. proposed that the active site of the enzyme was not completely rigid, like a lock receiving a key, but instead, flexible (Koshland, 1994). Koshland proposed that the active site was approximately similar in shape to the substrate and on binding of the substrate the active site orientates itself around the substrate providing the perfect, precise fit. Koshland named this the induced-fit model. Enzymes display different degrees of

specificity and can be classed according to their substrate specificity (Denniston *et al.*, 2008), as summarised in Table 4.1. However, enzymes are more commonly classified and named according to the type of chemical reaction they catalyse, as summarised in Table 4.2.

Table 4.1 Classification of enzymes according to specificity

Classification	**Degree of specificity**
Absolute	Catalyses only one specific substrate
Group	Catalyses molecules with the same functional groups
Linkage	Catalyses molecules with specific bonds
Stereochemical	Catalyses only one of the enantiomers

Table 4.2 Classification of enzymes according to type of chemical reaction (Voet *et al.*, 1999)

Classification	**Type of chemical reaction**
Oxidoreductases	Oxidation, reduction reaction
Transferases	Transfer of functional group
Hydrolases	Hydrolysis reaction
Lyases	Group elimination to form double bond
Isomerases	Isomerisation
Ligases	Bond formation coupled with ATP hydrolysis

Once the enzyme has bound the substrate in its active site forming the enzyme-substrate complex, which is a reversible reaction, the complex enters the transition state. During the transition state, the enzyme begins to change the substrate, which now has characteristics of both the original substrate and the new product (Denniston

et al., 2008). The transition state is where the rate of reaction can be increased. Examples of how the enzymes may do this are by applying stress to a bond, thus promoting its breakage or they can bring two reactants together in the correct orientation for the reaction to occur (Denniston *et al.*, 2008). The resultant complex formed from the transition state is the enzyme-product complex. The enzyme then releases the product or products and continues to bind another molecule of the substrate and commence the process over again. The classic enzyme mechanism is summarised in Equation 4.1, where E represents the enzyme, S the substrate, ES the enzyme-substrate complex, P the resultant product and K_{1-3} are the rate constants for the particular parts of the catalytic reaction. The enzyme throughout this whole process remains unchanged in composition (Voet *et al.*, 1999).

$$E + S \underset{k_2}{\overset{k_1}{\rightleftharpoons}} ES \xrightarrow{k_3} E + P$$

Equation 4.1

Environmental factors, such as pH and temperature, also affect the activity of enzymes. Certain enzymes are designed to function within a narrow pH range. For example, pepsin and trypsin are both proteolytic enzymes with similar mechanisms of action. Yet, pepsin is found in the stomach and has an optimum pH of 2 (Piper & Fenton, 1965), whereas, trypsin is found in the small intestine and has an optimum pH of 7.5 (Cheison *et al.*, 2011). Denniston *et al.* (2008) state that when the pH deviates from the optimum pH for that particular enzyme the degree of ionisation of the functional groups within the active site changes. This results in reduced ability of the substrate to bind to the active site. The further the pH deviates from the optimum the greater the decrease in biological activity until eventually the enzyme is

denatured. Similarly, enzyme reactions have an optimum temperature at which the rate of reaction is at the maximum velocity. All the enzymes present in the human body naturally have an optimum temperature of 37 °C. Although enzymes are stable at temperatures lower than 37 °C, hence, they are stored in refrigerators and freezers when not being used in clinical or experimental work. As the temperature increases towards 37 °C, the rate of reaction increases. Increasing the temperature until the optimum temperature is reached causes an increase in the number of viable collisions between the enzymes and molecules of substrate, therefore, increasing the rate of the reaction (Laidler & Peterman, 1979). Above the optimal temperature, thermal inactivation of the enzyme occurs as a result of increased vibrational energy of the bonds, which eventually leads to complete disruption of the bonds and other interactions causing the enzyme structure to breakdown, deforming the active site rendering it inactive (Laidler & Peterman, 1979).

In recent years, enzymes have been studied widely as possible therapeutic drugs for several diseases (Vellard, 2003). The majority of these disease are rare genetic diseases resulting in the loss of vital enzyme synthesis or function. These diseases are treated with enzymes, as summarised in Table 4.3. These therapeutic enzymes are delivered orally and intravenously, with the exception of Pulmozyme®, which is administered by inhalation (Quan *et al.*, 2001; Vellard, 2003).

Table 4.3 Summary of therapeutic enzymes for genetic diseases

Trade name	**Generic name**	**Indication**
Adagen® (Alconcel *et al.*, 2011)	Pegademase bovine	Adenosine deaminase-severe combined immunodeficiency (ADA-SCID)
Pulmozyme® (Quan *et al.*, 2001)	Dornase-α	Cystic fibrosis (CF)
Cerezyme® (Weinreb *et al.*, 2007)	Imiglucerase	Type I, II and III Gaucher's disease
Ceredase® (Friedman *et al.*, 1993)	Alglucerase	Type I Gaucher's disease
Sucraid (Puntis & Zamvar, 2015)	Sacrosidase	Congenital sucrose-isomaltase deficiency
Replagal™ (Tsuboi & Yamamoto, 2012)	α-Galactosidase A	Fabry's disease, long-term treatment
Oncasper® (Alconcel *et al.*, 2011)	Pegaspargase	Acute lymphocytic leukaemia
Fabrazyme® (Tsuboi & Yamamoto, 2012)	Agalsidase-β	Fabry's disease
Aldurazyme® (Pastores, 2008)	Laronidase	Mucopolysaccharidosis-I (MPS-I) disease
Elitek® (Jeha *et al.*, 2005)	Rasburicase	Hyperuricemia malignancy-associated or chemotherapy-induced
Creon® (Kuhn *et al.*, 2010)	Pancreatin	Cystic fibrosis, chronic pancreatitis, pancreatectomy and gastrectomy
Nutrizym 22® (Shah *et al.*, 1993)	Pancreatin	Cystic fibrosis, chronic pancreatitis, pancreatectomy and gastrectomy
Vimizin™ (Sanford & Lo, 2014)	Elosulfase alfa	Marquio A syndrome (MPS-IVA)
Naglazyme® (Koseoglu *et al.*, 2009)	Galsulfase	Mucopolysaccharidosis-VI (MPS-VI) disease
Brineura™ (Markham, 2017)	Cerliponase alfa	Neuronal ceroid lipofuscinosis type 2 (CLN2) disease

Several other enzymes have shown potential therapeutic use when delivered topically to burn wounds. The proteolytic enzyme vibriolysin, which originates from the marine microorganism *Vibrio proteolyticus*, has shown to be effective against debridement of denatured proteins in burn patients (Durham *et al.*, 1993). The treatment was successfully put through a Phase Ib clinical trial by BioMarin under

the brand name Vibrilase™, but progress has stalled since this trial. Another enzyme delivered topically to partial-thickness burn wounds in children for debridement with promising results was clostridiopeptidase, a collagenase (Rutter *et al.*, 2000). A topical gel base dressing called Debrase® containing a proteolytic enzyme bromelain extracted from the stem of a pineapple plant is indicated for burn wound debridement (Klasen, 2000; Vellard, 2003). The dressing has shown to be effective at debridement of necrotic eschar for partial to full-thickness burns, promoting re-epithelisation (Singer *et al.*, 2011). Therefore, although pepsin used in this chapter has no recognised use as a topically delivered therapeutic drug, at present, the results from this chapter and the overall project may highlight that the PVA-borate hydrogel has a potential use for delivering topically other types of enzymes for the management and repair of chronic wounds.

4.2 Aims and objectives

The aim of the work in this chapter was to formulate, characterise and complete *in vitro* release studies for pepsin-loaded PVA-borate hydrogels (PVA 6.0 % w/w borate 2.0 % w/w), and determine if the enzymatic activity of pepsin could be maintained upon release from the hydrogel.

Objectives;

- determine pepsin enzyme kinetics,
- formulate PVA-borate hydrogels loaded with varying concentrations of pepsin,
- characterise the viscoelastic properties of the pepsin-loaded PVA-borate hydrogels using oscillatory rheometry,
- complete *in vitro* release studies for the pepsin-loaded hydrogels using Franz diffusion cells,
- detect and quantify pepsin released from the hydrogels using a bicinchoninic acid (BCA) assay and UV-Vis spectroscopy,
- check degradation of the released pepsin from the hydrogel using sodium dodecyl sulphate poly(acrylamide) gel electrophoresis (SDS-PAGE),
- determine if the released pepsin has retained its enzymatic activity.

4.3 Materials

Chemicals and reagents

Poly(vinyl alcohol) (PVA) (M_w = 31–50 kDa, 98–99 % hydrolysed), sodium tetraborate decahydrate (ACS reagent ≥ 99.5 %), pepsin from porcine gastric mucosa (lyophilised powder 3,200–4,500 units/mg protein), haemoglobin from bovine blood,

trichloroacetic acid (ACS reagent ≥ 99.5 %), buffer solution, phosphate buffer solution, borax buffer solution and Transwell® tissue culture inserts (Poly(carbonate) membrane, pore size 8.0 µm) were purchased from Sigma-Aldrich Ltd. (Gillingham, Dorset, UK).

NuPage® Bis-Tris gel 4–12 % (1.0 mm x 10 well) Novex®, NuPage® MOPS SDS running buffer (20x) Novex®, SeeBlue® Plus2 Prestained standard Novex® were purchased from Life Technologies Ltd. (Paisley, UK).

Coomassie brilliant blue R-250 staining solution, Bio-rad laboratories Inc. (Hertfordshire, UK).

Pierce™ BCA Protein assay kit, Medical Supply Company. (Dublin, Ireland).

All reagents were of appropriate laboratory standard and used without further purification.

Apparatus

Kinexus Pro rheometer, Malvern instruments (Malvern, Worcestershire, UK).

XCell SureLock™ Mini-Cell electrophoresis system, Invitrogen, Life Technologies Ltd. (Paisley, UK).

Varian Cary 50 Scan UV-Vis spectrophotometer supplied by Manson Technology. (Dublin, Ireland); with a 10 mm quartz cuvette.

FLUOstar® Omega microplate reader, BMG LABTECH Ltd. (Ortenburg, Germany).

Franz diffusion cells, Perme-Gear diffusion cells & systems. (USA) and Techne TE 10D Tempette® water bath & pump, Bibby scientific Ltd. Staffordshire. (UK)

4.4 Methods

4.4.1 Determination of pepsin enzyme kinetics

Twelve test tubes were placed in a water bath at 37 °C. To each test tube, 0.5 mL of filtered bovine haemoglobin (0.25 % w/v, pH 2.0 ± 0.5) was added and allowed to reach 37 °C. To each test tube, 0.5 mL of pepsin (20 µg mL^{-1}) was added and a stop watch started. The reaction in each test tube was stopped at defined times (1, 2, 3, 4, 5, 10, 20, 30, 40, 50, 60 and 70 minutes) by addition of 5 % w/v trichloroacetic acid (5 mL) for 5 minutes. The solution was then filtered (0.45 µm) to remove any non-acid soluble material. Acid-soluble peptides were detected using UV-Vis spectrometry at a wavelength of 280 nm. A quartz cuvette with a path length of 10 mm was used and rinsed with deionised water between each sample. Three replicates were performed for each filtrate (n=3).

This method was repeated a further seven times varying the concentration of bovine haemoglobin (0.375, 0.450, 0.500, 0.625, 0.750, 1.000, 1.250 % w/v). For each concentration of haemoglobin, an absorbance against time graph was plotted from which the enzyme activity was calculated, using Equation 4.2, where $d(A_{280})$ is the change in product and $d(t)$ is the change in time. GraphPad Prism® software was used to plot the initial velocities against the corresponding haemoglobin concentrations to produce a Michaelis-Menten curve and Lineweaver-Burk plot.

$$\text{Unit mg}^{-1}\text{ min}^{-1} = \frac{(d(A_{280}) - A_{280}\text{ blank}) \text{ x } 1000}{(d(t) \text{ x mg of enzyme in reaction})} \qquad \text{Equation 4.2}$$

From the Michaelis-Menten plot, the Michaelis-Menten constant K_M and V_{max} can be determined using Equation 4.3. V_o is initial velocity of the reaction, V_{max} is the

maximum rate of the reaction, K_M is the Michaelis-Menten constant and [S] is the substrate concentration.

$$V_0 = \frac{V_{max}[S]}{K_M + [S]} \qquad \text{Equation 4.3}$$

4.4.2 Formulation of pepsin-loaded PVA-borate hydrogels

An optimum hydrogel formulation of 6.0 % w/w PVA and 2.0 % w/w borate was selected from previous studies to be loaded with various quantities of pepsin (0.05, 0.10, 0.20 % w/w). A sample (25 g) of this formulation was prepared by mixing 6.25 g of PVA stock solution (24 % w/w) and 10.00 g of borax stock solution (5% w/w). A homogenous fluid-like gel was formed upon heating to 80 °C for approximately three hours, with periodic stirring. Hydrogels were weighed and any lost weight was replenished with deionised water. The gels were then transferred to poly(propylene) storage containers and left for 48 hours at room temperature and pressure (RTP) to allow for complete gelation. To a desired quantity of hydrogel the appropriate volume of a pepsin stock solution (5 mg mL^{-1}) was added and mixed in using a stainless steel spatula. The hydrogels were stored in the fridge (2–8 °C) until used. Final formulations were clear and homogenous in appearance with no air bubbles present.

4.4.3 Viscoelastic analysis

Analysis of the viscoelastic properties was carried out using a Kinexus Pro rheometer (Malvern Instruments Ltd., Worcestershire, UK) on all hydrogel formulations, as described previously in sections 2.4.2. Briefly, a strain (1.0 %) controlled frequency sweep (0.1–10 Hz) was completed from which, the crossover modulus (G_c) was

determined. All tests were carried out at 25 °C ± 0.2 °C, using 20 mm diameter stainless steel parallel plate geometry and a working gap of 1 mm. Three replicates were performed for each formulation (n=3). Student's t-test statistical analysis was carried out on the data.

4.4.4 *In vitro* release study

Pepsin release studies were carried out using Franz diffusion cells (Perme Gear cells & Systems, USA) and a Techne TE 10D Tempette® water bath & Pump (Bibby scientific Ltd. Staffordshire, UK). All release studies were carried out at 37 °C using poly(carbonate) membranes cut to size (pore size 8.0 μm, Sigma Aldrich). A sample (1.00 g) of pepsin-loaded hydrogel (PVA 6.0 %w/w, borate 2.0 % w/w, pepsin 0.20 % w/v) was placed in each donor chamber at time zero. Samples (0.5 mL) were withdrawn at specific time intervals (0, 1, 2, 3, 4, 5, 6, 7 and 8 hours) and replaced with 0.5 mL fresh receiver phase. A blank PVA-borate hydrogel of the same formulation was ran as a control.

4.4.5 Detection and quantification of pepsin released from PVA-borate hydrogels.

Samples were analysed for the presence of pepsin and quantified using a bicinchoninic acid (BCA) assay, as previously described in section 3.4.7. A calibration plot was produced using nine dilutions (20–2000 μg mL^{-1}) from a stock solution (2 mg mL^{-1}) of pepsin. Samples (25 μL) of each dilution and samples from the *in vitro* release study were pipetted into a 96-well plate. To each of these wells, 200 μL of BCA assay working reagent was added. The 96-well plate was then placed on an orbital shaking incubator at 37 °C at 100 rpm for 30 minutes. The plate

was then removed and allowed to cool to room temperature prior to the absorbance of each well being measured at 562 nm using a FLUOstar® Omega microplate reader, (BMG LABTECH Ltd. Ortenburg, Germany).

4.4.6 Sodium dodecyl sulfate poly(acrylamide) gel electrophoresis

Sodium dodecyl sulphate gel electrophoresis (SDS-PAGE) was carried out using an XCell SureLock™ Mini-Cell electrophoresis system (Invitrogen, Life Technologies Ltd, Paisley, UK), as described previously in section 3.4.8. Briefly, samples (20 µl) from the *in vitro* release study and protein standards dissolved in deionised water, were prepared under reducing conditions and loaded onto a Bis-Tris NuPAGE 4–12 % resolving gel. Electrophoresis was run using NuPAGE MOPS SDS running buffer (x1), in constant voltage mode of 200 V and a varied current of 100–125 mA and 60-80 mA during stacking and running, respectively. The gel was stained with coomassie brilliant blue R-250 stain for 60 minutes on an orbital shaker (45 rpm), at room temperature. The coomassie blue stain was removed and the gel was rinsed twice with deionised water for 5 minutes each time. The gel was then de-stained with a solution of methanol, acetic acid and deionised water at the ratio of 50:10:40 % v/v on an orbital shaker (45 rpm) for 30 minutes, at room temperature. After 30 minutes, the de-staining solution was diluted to methanol 12.5 %, acetic acid 2.5 %, using deionised water. The gel was then left overnight on the orbital shaker at room temperature, after which it was imaged.

4.4.7 pH related enzyme activity of pepsin

Bovine haemoglobin was dissolved in several solutions (0.01 M HCl, phosphate buffer, borax buffer, buffer solution pH 4 and 6) to achieve five haemoglobin 1 %

w/w solutions, of varying pH (2.0, 4.0, 6.0, 7.0, 9.0). A volume (5 mL) of each solution of haemoglobin was placed into separate test tubes in a preheated water bath (37 °C). To each of the five test tubes, 0.5 mL of a pepsin solution (30 μg mL^{-1}) was added and a countdown timer, set for 10 minutes, was started. After this time had elapsed, 5 mL of TCA (5 % w/w) was added to each test tube and incubated for a further 5 minutes before being filtered through a 0.45 μm sterile filter to remove any non-acid soluble material. The absorbance of the filtrate was measured using a UV-Vis spectrophotometer at 280 nm. The enzymatic activity of the pepsin in each solution was calculated using Equation 4.4.

$$\text{Unit mg}^{-1}\text{ min}^{-1} = \frac{(A_{280}\ \text{filtrate} - A_{280}\ \text{blank}) \times 1000}{(10\ \text{mintues} \times \text{mg of enzyme in reaction})} \qquad \text{Equation 4.4}$$

4.4.8 Altering the overall pH of the PVA-borate hydrogel

A volume (1 mL) of different concentrations of hydrochloric acid (2.000, 1.000, 0.500, 0.250, 0.125 M) were added to 4.0 g samples of hydrogels (PVA 6.0 % w/w borate 2.0 % w/w) and left for 48 hours. After 48 hours the pH of each gel was measured in triplicate (n=3) and visually inspected for any colour change or de-mixing.

4.5 Results

Eight graphs showing the absorbance of each of the filtered samples containing acid-soluble hydrolysed haemoglobin plotted against time can be seen in Figure 4.3a and 4.3b. It can be seen that increasing the concentration of haemoglobin caused an increase in the time it took for the graph to plateau.

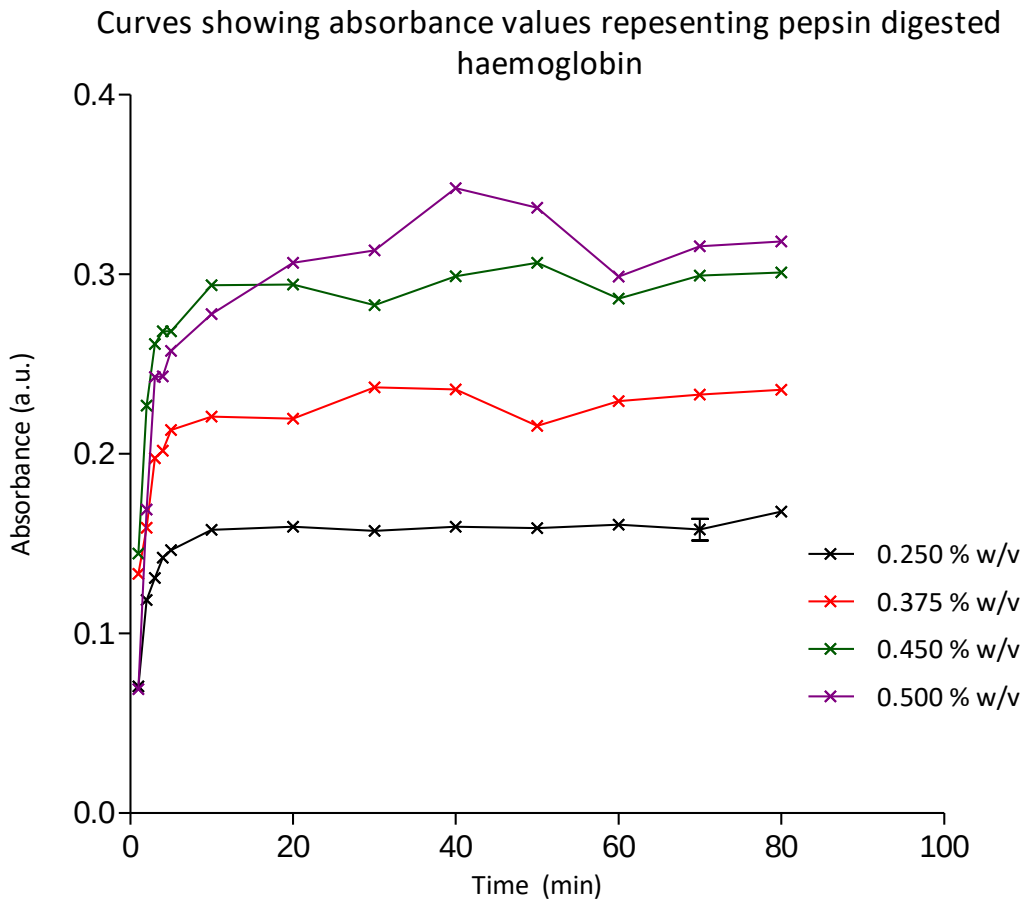

Figure 4.3a Curves showing absorbance plotted against time for hydrolysed acid-soluble bovine haemoglobin digest, measured using UV-Vis spectroscopy, λ = 280 nm. Haemoglobin concentration varied (0.250, 0.375, 0.450 and 0.500 % w/v), while pepsin concentration remained constant at 20 μg mL^{-1}. All experiments were carried out at 37 °C and haemoglobin solution were pH 2.0 ± 0.5. Data shown as the mean value ± standard deviation (n=3).

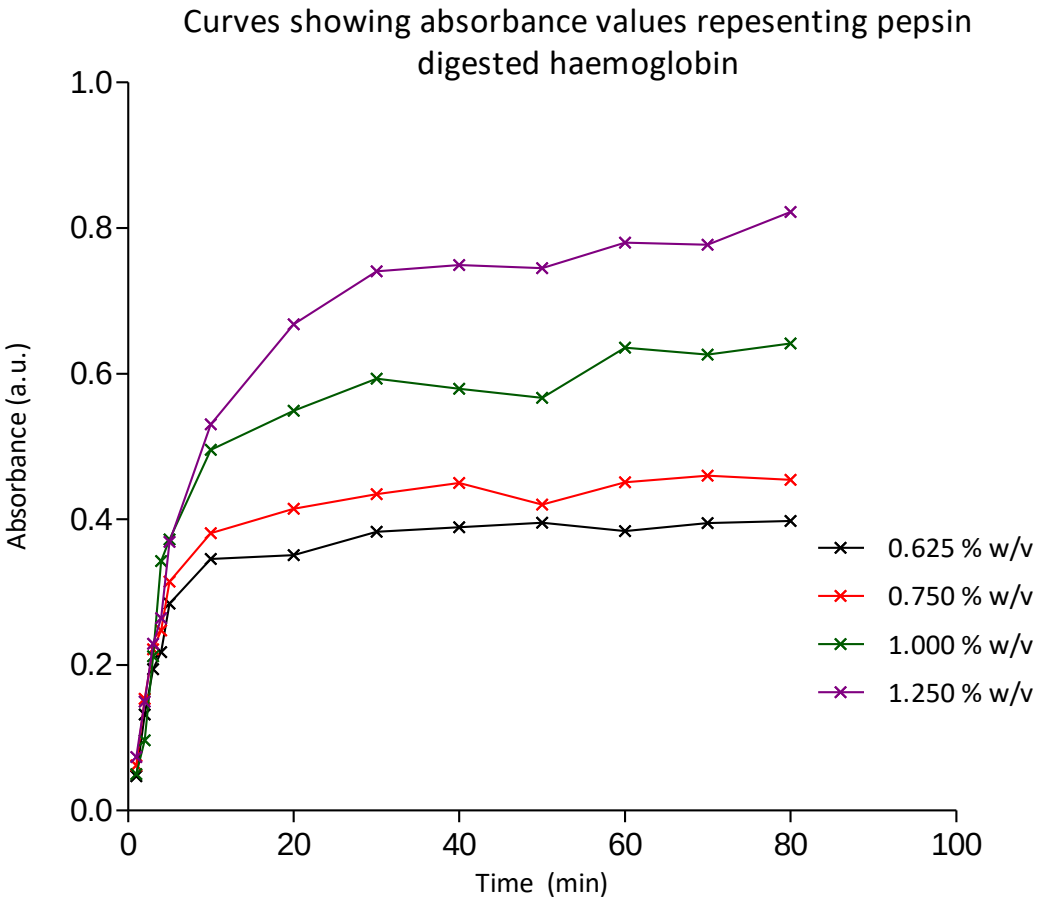

Figure 4.3b Curves showing absorbance plotted against time for hydrolysed acid-soluble bovine haemoglobin digest, measured using UV-Vis spectroscopy, λ = 280 nm. Haemoglobin concentration varied (0.625, 0.750, 1.000 and 1.250 % w/v), while pepsin concentration remained constant at 20 μg mL^{-1}. All experiments were carried out at 37 °C and haemoglobin solution were pH 2.0 ± 0.5. Data shown as the mean value ± standard deviation (n=3).

The initial velocities values calculated from graphs in Figure 4.3a and 4.3b, using Equation 4.2, were plotted against the corresponding haemoglobin concentrations to produce the Michaelis-Menten plot, which displays pepsin's enzymatic kinetics, as seen in Figure 4.4.

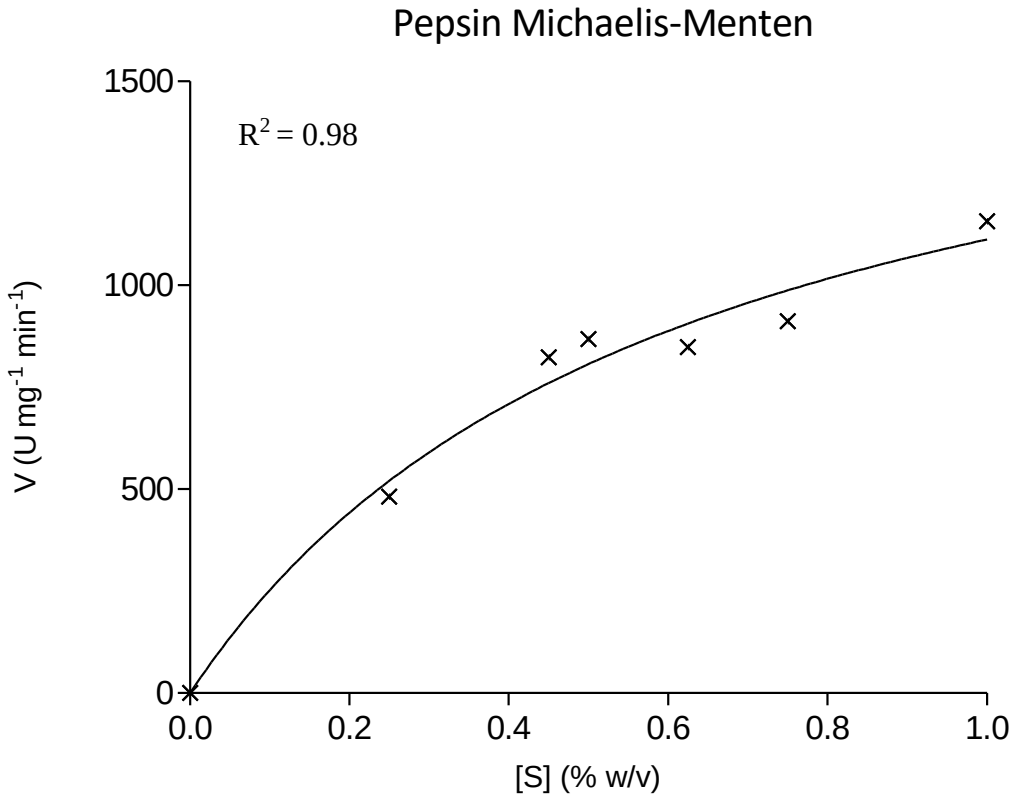

Figure 4.4 Michaelis-Menten plot for porcine pepsin at 37 °C. Haemoglobin concentration varied 0.25–1.25 % w/v, while pepsin concentration remained constant at 20 μg mL^{-1}.

The K_M and V_{max} for the plot in Figure 4.4 are 0.6099 % w/v and 1791 U mg^{-1} min^{-1}, respectively. Another method to determine the K_M and V_{max} values was developed by Hans Lineweaver and Dean Burk. This involves using the reciprocal of the Michaelis-Menten equation to obtain a linear plot called the Lineweaver-Burk plot. The lineweaver-Burk plot is also known as the double-reciprocal plot. Figure 4.5 shows the Lineweaver-Burk plot for the data plotted in the Michaelis-Menten plot in Figure 4.4.

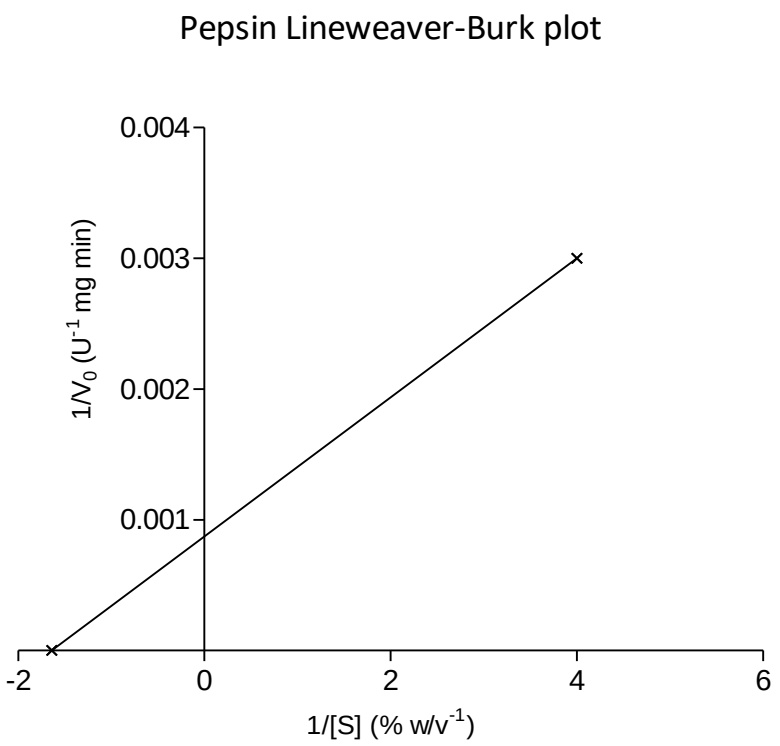

Figure 4.5 Lineweaver-Burk plot also known as the double reciprocal plot for porcine pepsin at 37 °C. Haemoglobin concentration varied 0.25–1.25 % w/v, while pepsin concentration remained constant at 20 μg mL^{-1}.

Once the values were plotted, the regression line of the Lineweaver-Burk plot was extrapolated using GraphPad Prism® software. The software determined the y intercept, which equates to 1/ V_{max} and the x intercept, which equates to -1/ K_M. From the x and y intercept values V_{max} and K_M was calculated to be 1149 U mg^{-1} min^{-1} and 0.6099 % w/v, respectively. It can be seen that the K_M value for both the Michaelis-Menten plot and the Lineweaver-Burk plot are the same. The V_{max} value for the Lineweaver-Burk plot was 642 U^{-1} mg min lower than that for the Michaelis-Menten plot. The K_M and V_{max} are unique to each enzyme and substrate. Therefore, once it has been ascertained if the pepsin released from the hydrogel has enzymatic activity then another Michaelis-Menten and Lineweaver-Burk plot will be produced using the released pepsin to determine if there is any change in pepsins enzyme kinetics.

PVA-borate hydrogels (PVA 6.0 % w/w; borate 2.0 % w/w) loaded with the three concentrations of pepsin (0.05, 0.10, 0.20 % w/w) were clear and homogenous once fully re-congealed and stored in the fridge. Each pepsin-loaded hydrogel was then subject to a frequency sweep oscillating rheometry investigation to determine if incorporating the various concentrations of pepsin into the hydrogel matrix had any effect on the viscoelastic properties of the hydrogel. This was achieved by comparing the crossover modulus obtained for each pepsin-loaded hydrogel to a hydrogel of the same formulation, which had no pepsin incorporated into the gel network. It can be seen from Figure 4.6 that on incorporation of all three concentrations of pepsin, there was a significant ($p<0.01$) decrease in the crossover modulus, compared to the blank hydrogel. However, there was no significant difference in the crossover modulus when increasing the pepsin concentration from 0.05 to 0.10 % w/v ($p = 0.3384$) and from 0.10 to 0.20 % w/w ($p = 0.5425$). The lowest crossover modulus (2283 ± 79 Pa) was recorded for the 0.20 % w/w pepsin compared to the blank hydrogel with a crossover modulus of 2747 ± 91 Pa.

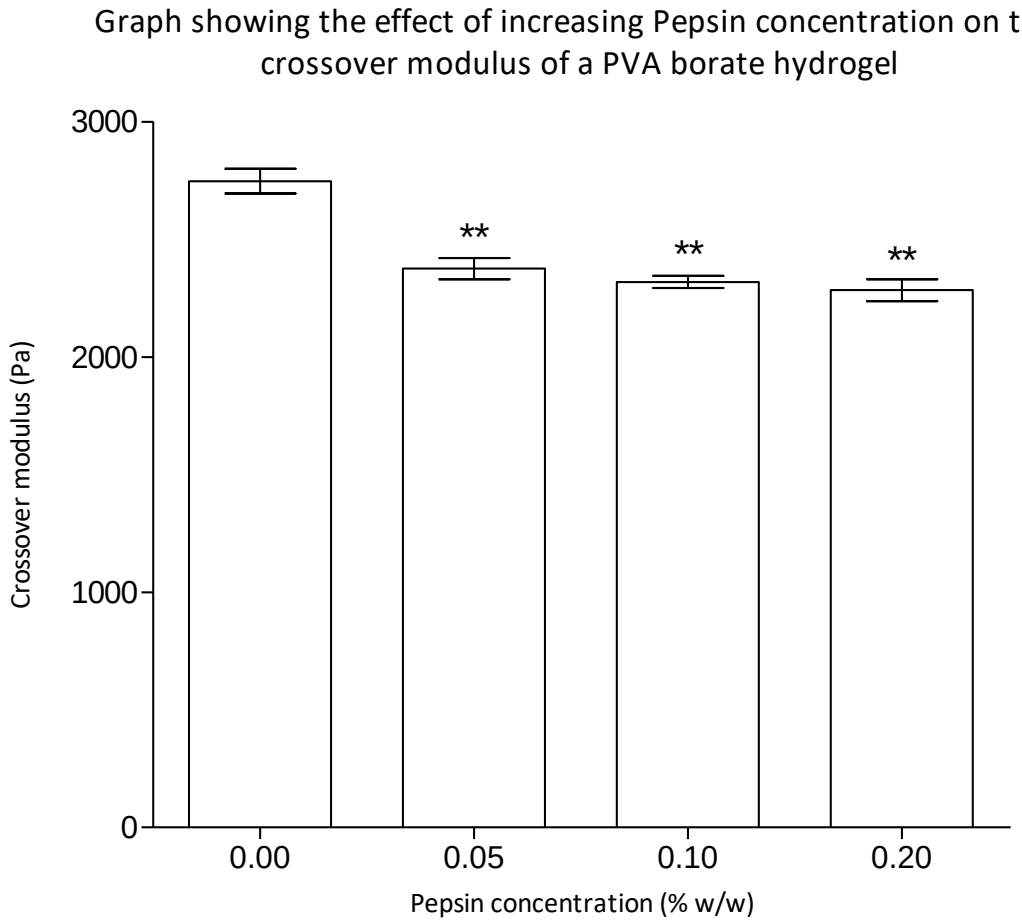

Figure 4.6 Graph showing the effect of incorporating three concentrations of pepsin into a PVA (6.0 % w/w) borate (2.0 % w/w) hydrogel has on the crossover modulus, compared to a blank hydrogel, of the same formulation. Data shown as the mean ± standard deviation (n=3). All measurements carried out at 25°C ± 0.2°C. $p < 0.05$ (*), $p < 0.01$ (**), $p < 0.001$ (***).

A BCA assay was used to detect and quantify the pepsin released from the PVA-borate hydrogel system. Figure 4.7 shows a typical BCA assay calibration plot that was used to determine the pepsin concentration in each sample. A calibration plot was carried out on each plate of samples to account for day-to-day, and plate-to-plate optical variability. As the r^2 is 0.99 the data is correlated, and confidence can be had in any values calculated using the line equation.

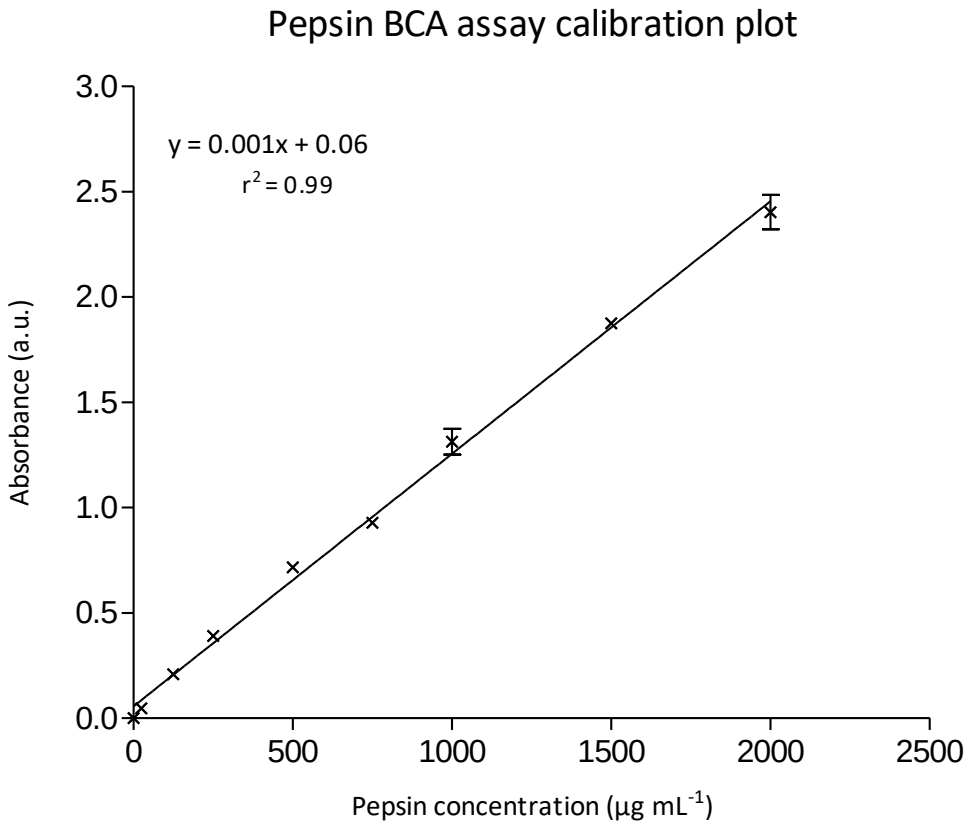

Figure 4.7 BCA assay calibration plot produced using several dilutions of a pepsin stock solution 2 mg mL^{-1}. The standard dilutions concentration range 20–2000 µg mL^{-1}. The λ = 562 nm, data shown as mean ± standard deviation (n=3).

The percentage cumulative release profiles of each of the three concentrations of pepsin from the PVA-borate hydrogel can be seen in Figure 4.8. The hydrogel loaded with 0.05 % w/w pepsin released the least amount of pepsin (71.06 ± 1.05 %), after 8 hours. The 0.10 % w/w pepsin-loaded gel released 80.37 ± 0.42 % of the loaded pepsin and the 0.20 % w/w pepsin-loaded hydrogel released the largest quantity of pepsin at 8 hours (84.84 ± 0.79 %). At the second and third hour sampling points, the 0.05 % w/w pepsin-loaded hydrogel gave a higher release of pepsin, compared to the 0.10 % w/w loaded hydrogel. However, from the fourth to eight hour, the 0.10 % w/w loaded hydrogel released a larger quantity of pepsin than the 0.05 % w/w loaded hydrogel, as seen in Figure 4.8. The general trend exhibited by all three concentrations is as time increased so did the quantity of pepsin released

from the PVA-borate hydrogels. It can also be seen from the fourth to eight hour the hydrogels containing the higher concentrations of pepsin released the largest quantity of pepsin at each time point.

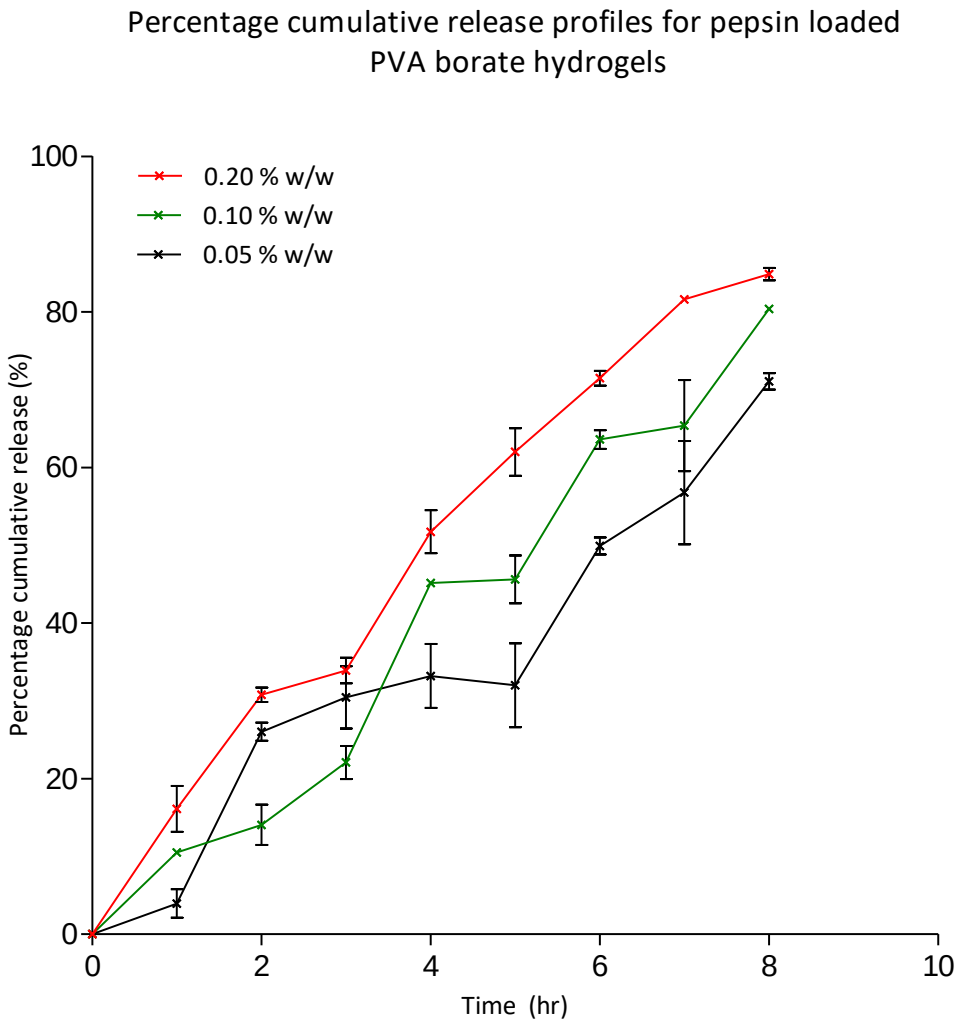

Figure 4.8 Percentage cumulative release profiles for three pepsin loaded PVA (6.0 % w/w) borate (2.0 % w/w) hydrogels of varying pepsin concentration, over 8 hours. Release studies were carried out at 37 °C using poly(carbonate) membranes with a pore size 8.0 µm, on Franz diffusion cells. Data shown as the mean ± standard deviation (n=3).

Figure 4.9 shows the resultant SDS-PAGE gel for the molecular weight of pepsin released from the PVA-borate hydrogel matrix. Pepsin released from the hydrogel can be seen in lanes 4–6 with a standard sample of pepsin of the same concentration seen in lane 3 (Figure 4.9). As the protein band seen in lane 3 for the pepsin standard is located in proximity to the 38 kDa molecular marker band of the protein ladder, it

can be assumed that this is pepsin, which has a molecular weight of 35 kDa. Furthermore, it can be seen that the pepsin samples released from the hydrogel are also in close proximity to the pepsin standard band in lane 3 and the 38 kDa molecular marker band. Therefore, the pepsin released from the PVA-borate hydrogel has not been subject to degradation, upon release or whilst in the hydrogel matrix.

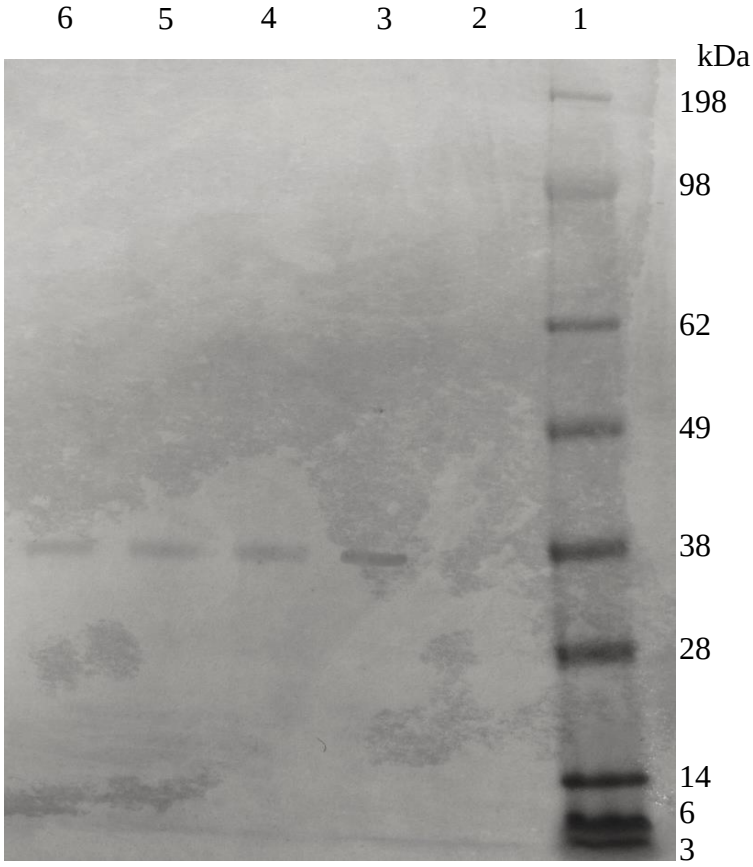

Figure 4.9 Image of the SDS-PAGE NuPAGE® Bis–Tris 4-12 % resolving gel (1.0 mm x 10 well), stained with coomassie blue for pepsin released from a hydrogel (PVA 6.0 %w/w borate 2.0 % w/w) and a pepsin standard. Lane 1 molecular markers, Lane 2 was intentionally left blank, Lanes 4–6 pepsin samples released from the PVA-borate hydrogel.

The activity of pepsin released from the hydrogel was compared to the activity of a pepsin standard of the same concentration. It can be seen from Table 4.4 that the pepsin released from the hydrogel had no activity, compared to the standard pepsin sample, which had an enzymatic activity of 3093 ± 42 U mg^{-1} min^{-1}. After 10

minutes, the pepsin standard in test tube C had broken down the haemoglobin. This is because on addition of the TCA (5 % w/v), it produced a homogenous light brown translucent solution, compared to the test tubes A and B, which contained the pepsin released from the hydrogel, as seen in Figure 4.10. On addition of TCA to test tubes A and B, the solutions became cloudy with large undigested acid-insoluble clumps of haemoglobin present at the surface and throughout the solution (Figure 4.10). This indicates visually that there is limited to no pepsin activity compared to test tube C.

Table 4.4 Activity of pepsin released from a hydrogel compared to standard stock solution. Data shown as mean values ± SD (n=3).

Test Tube	**Absorbance (a.u.)**	**Activity (U mg^{-1} min^{-1})**
A	0.0000	0
B	0.0000	0
C	0.4640 ± 0.0100	3093 ± 42

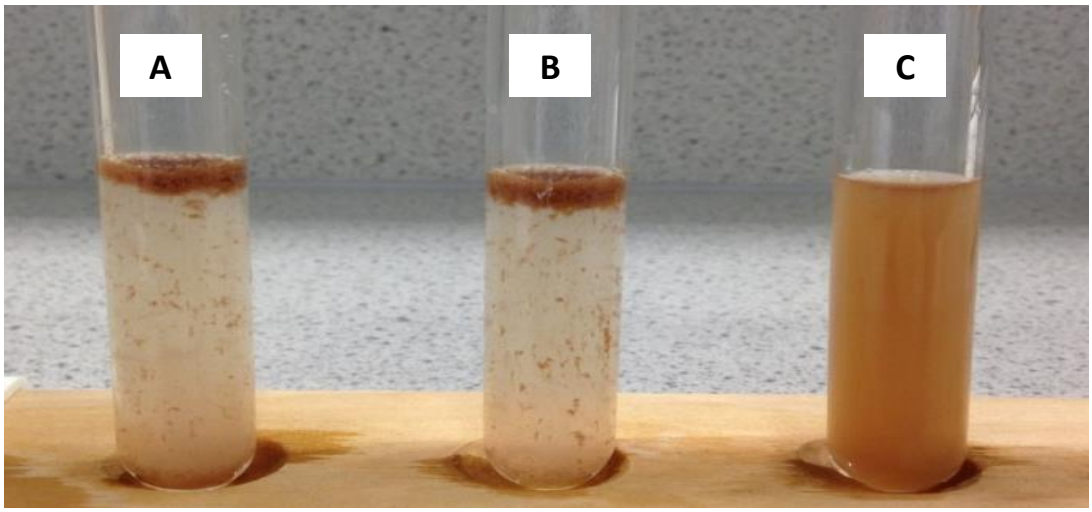

Figure 4.10 A representative photograph of one set of the three replicates of test tubes from the pepsin enzyme activity experiment. Haemoglobin concentration was 1.0 % w/w pH 2.0 ± 0.2, incubation for 10 minutes at 37 °C with 30 μg mL^{-1} pepsin. Test tubes A and B contain pepsin released from hydrogels (PVA 6.0 % w/w borate 2 % w/w) and test tube C is the pepsin standard.

To determine if the pH of the hydrogel environment that the pepsin was exposed to was a factor for no enzymatic activity, the experiment outlined in section 4.4.7 was completed. It can be seen from Figure 4.11 that pepsin showed the highest enzymatic activity (3705 ± 8 U mg^{-1} min^{-1}) at pH 2.0. On increasing the pH of the haemoglobin solution to 4.0, there was a decline in pepsin activity to 996 ± 22 U mg^{-1}. At a pH 7.0 (neutral) the enzymatic activity further decreased to 381 ± 27 U mg^{-1} min-1 and exhibiting its lowest activity, 337 ± 5 U mg^{-1} min^{-1}, at pH 9.0 (weak alkaline).

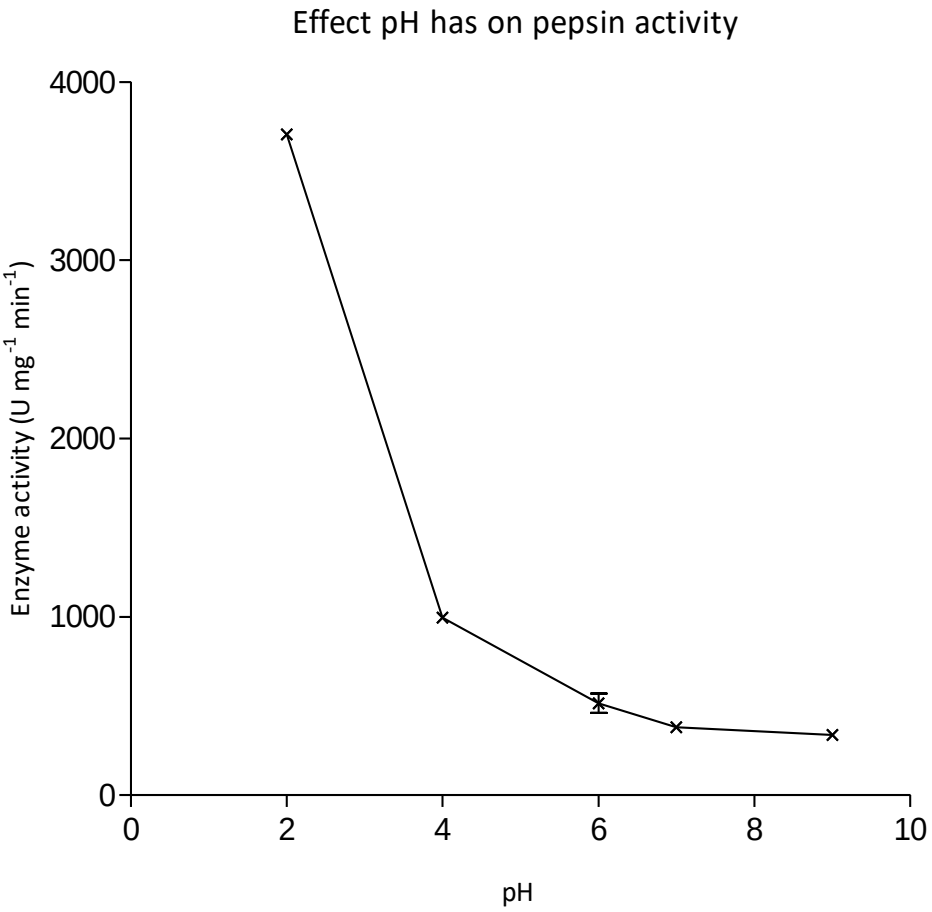

Figure 4.11 Graph showing enzymatic activity of pepsin (30 μg mL^{-1}) over a pH range of 2.0–9.0 incubated for 10 minutes with 1 % w/w haemoglobin at 37 °C. Data shown as mean ± standard deviation (n=3).

In order to try and achieve a more stable environment for the pepsin within the hydrogel, an attempt was made to lower the pH of the hydrogel system, to an acidic

environment. It can be seen from Table 4.5 that on adding 1 mL of 2.000, 1.000 and 0.050 M HCl to the hydrogel the pH was reduced from a basic (pH 8.03 ± 0.03) to an acidic (pH 1.26 ± 0.07) environment.

Table 4.5 The effect adding varying concentrations of HCl, has on the pH of a PVA 6 % w/w borate 2.0 % w/w hydrogel. Data shown as mean ± Standard Deviation (n=3).

HCl concentration (M)	**pH (Average ± SD)**
2.000	1.26 ± 0.07
1.000	1.59 ± 0.15
0.500	3.52 ± 0.16
0.250	7.25 ± 0.25
0.125	7.38 ± 0.04
0.000	8.03 ± 0.03

Although the addition of HCl to the PVA-borate hydrogel was effective at creating an acidic environment within the hydrogel, it caused the formulations to become white and cloudy in appearance (Figure 4.12), with phase separation also evident on visual inspection. On examination, it was observed that the hydrogels had de-mixed to a solid and liquid phase.

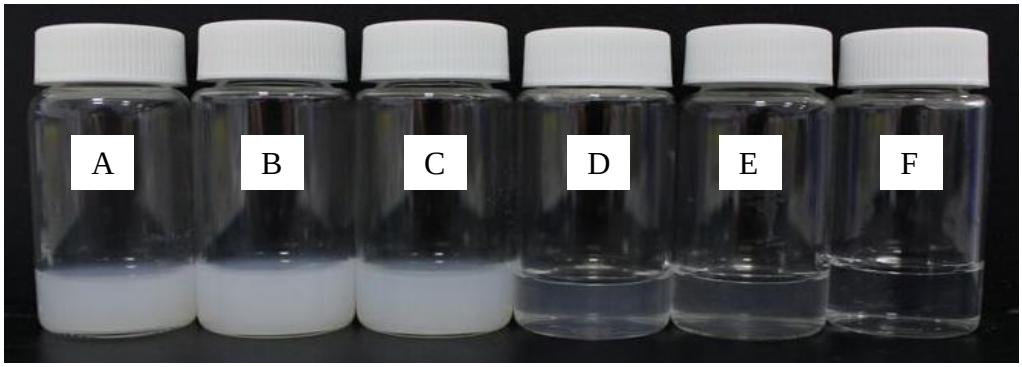

Figure 4.12 Photograph showing six glass vials containing 4.0 g of PVA-borate hydrogel (PVA 6.0 % w/w, borate 2.0 % w/w). Each vial, except vial F, contained 1 mL of HCl of varying concentration. Vial A) 2.000 M, B) 1.000 M, C) 0.500 M, D) 0.250 M, E) 0.125 M, F) Blank (no HCl).

4.6 Discussion

Utilising the PVA-borate hydrogel delivery system for administering enzymes topically is a novel application. However, a gel-based dressing has been used to deliver an enzyme, topically, to burn wounds for debridement with positive results (Klasen, 2000). Topical application of other enzymes to burns wounds for debridement has also proven to be beneficial (Durham *et al.*, 1993; Rutter *et al.*, 2000; Vellard, 2003). Therefore, the findings of this chapter may indicate worthwhile future research, whereby the PVA-borate hydrogel has the potential to deliver enzymes topically, which promote wound management and repair. The enzyme pepsin is irreversibly denatured at pH $\geq$ 8.0 and has an optimal pH of 2.0 (Piper & Fenton, 1965). The reason for choosing to deliver pepsin in this study was to determine if its enzymatic activity could be maintained during entrapment in the hydrogel and upon release from the hydrogel.

Pepsin belongs to the family of aspartic peptidases and is found in the stomach of mammals (Tang *et al.*, 1973). Its main purpose is to aid in the digestion of large proteins by hydrolysing peptide bonds. Enzymatic hydrolysis breaks down the large proteins into small peptides and single amino acids, which can be readily absorbed through the intestine mucosa. Pepsin is initially synthesised as a pro-enzyme known as pepsinogen. Pepsinogen has an extra 44 amino acid pro-peptide portion, which blocks the active site (Goodsell, 2000), as seen in Figure 4.13. This is so that the pepsin does not digest components of the cell synthesis apparatus prior to being released into the stomach. Once in the acidic environment of the stomach, the pro-peptide segment is cleaved off in an autocatalytic manner (Davies, 1990), leaving the active site free to complex with consumed protein material.

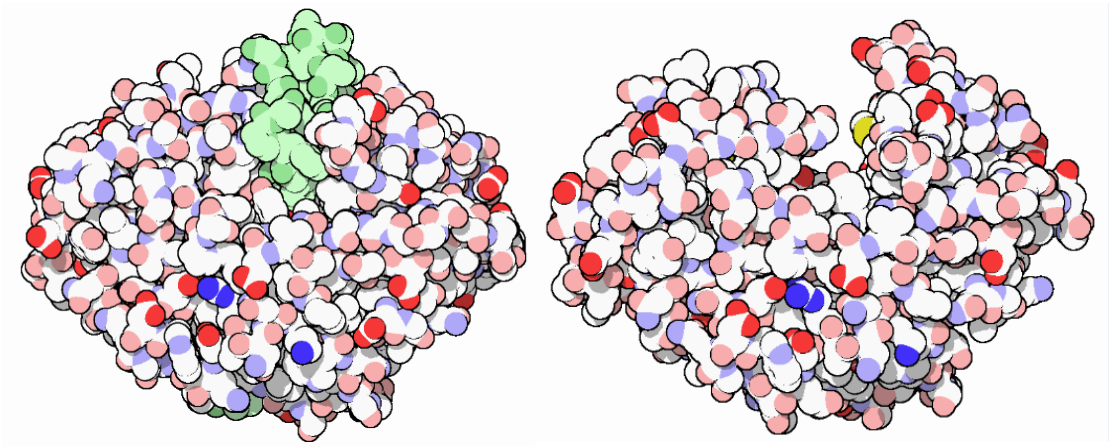

Figure 4.13 Space-filling model diagram of a) the pepsin pro-enzyme pepsinogen where the green block represents the extra 44 amino acid chain that blocks the active site and b) the active pepsin with the additional segment removed from the active site (Goodsell, 2000).

Porcine pepsin, which was used in this study, is a 327-amino acid single poly(peptide) chain folded into a 3D structure, which is strengthened by three disulphide bridges between cysteine residues at positions 45 and 50, 206 and 210, and, 250 and 283 (Tang *et al.*, 1973), as seen in Figure 4.14. The two aspartate residues situated in the active site, which are known to partake in the catalytic reaction, can be seen in Figure 4.14 (Tang *et al.*, 1973).

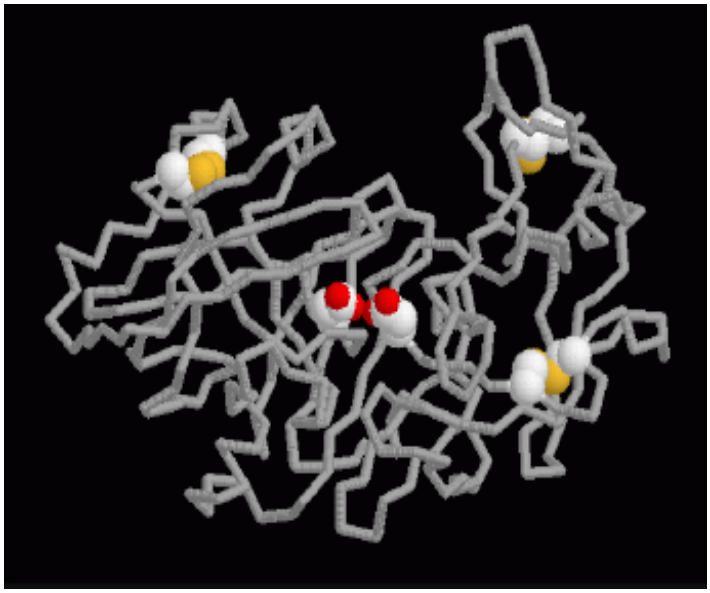

Figure 4.14 Wireframe diagram of pepsin where the red and white components represent the two aspartate residues in the active site and the yellow and white residues represent the three disulphide bridges (Goodsell, 2000).

The two aspartic residues found in a hydrophobic region of the active site at positions 32 (Asp 32) and 215 (Asp 215) play an active role in the catalytic reaction. Although structurally the same, the two aspartic groups are thought to have different pK_a values, 1.0 and 4.7, respectively (Knowles, 1970). The carboxyl groups present on each of these residues must be different for the catalytic process to occur. One carboxyl group needs to be in the ionised form and the other in the non-ionised form (Polgar, 1987). The exact mechanism of action of pepsin and other aspartic residues has been extensively studied (Fruton, 1976; Bott *et al.*, 1982; James *et al.*, 1982; James & Sielecki, 1985), however, certain aspects of the mechanism are still not fully understood. In summarising, Davies (1990) and Dunn (2002) in their review articles conclude that the majority of researchers agree that the mechanism of peptide bond hydrolysis by aspartic proteases is by general acid-base catalysis. The general acid-base mechanism proposes that Asp 215 acts as a base and removes a proton from the water molecule located between the two aspartate groups. This in turn activates the water molecule, which then carries out a nucleophilic attack on the carbonyl group of the peptide bond and at the same time Asp 32 donates a proton to the carbonyl oxygen atom, resulting in a tetrahedral intermediate (Davies, 1990). Re-configuration of this intermediate results in the protonation of the nitrogen atom in the peptide bond by Asp 215, resulting in the peptide bond (C-N) breaking and leaving the Asp 215 negatively charged to catalyse another reaction. The carboxyl product from the N-terminal side of the peptide is thought to remain hydrogen bonded to the Asp 32 (Dunn, 2002). Recent research into the aspartic proteases cleavage mechanism suggests that the water molecule is in a low-barrier hydrogen bond between the two aspartate residues, detected by nuclear magnetic resonance (NMR) (Piana & Carloni, 2000; Northrop, 2001).

In this chapter, haemoglobin was used as a substrate to determine the enzymatic activity of pepsin prior to loading into the PVA-borate hydrogel and then again on release. The use of haemoglobin as the substrate to quantity the enzymatic activity of pepsin was first developed by Anson & Mirsky in 1932. This specific method and variations of it are still widely used to determine the enzymatic activity of proteases (Sigma-Aldrich; Worthington Biochemical Corporation, 2017). Haemoglobin contains several amino acid residues that are known to be cleavage sites for pepsin at the C-terminal side of the amino acid (Scaloni *et al.*, 1998). These amino acid residues are phenylalanine, leucine, methionine, cysteine, glutamate, tyrosine and tryptophan (Tomita *et al.*, 1991; Cao *et al.*, 1997; Hamuro *et al.*, 2008). Phenylalanine and leucine are the two most favourable sites of cleavage (Hamuro *et al.*, 2008). Therefore, this explains the successful digestion of haemoglobin by pepsin to achieve the Michaelis-Menten plot and the corresponding Lineweaver-Burk plot.

The Michaelis-Menten plot is a plot of enzyme velocity against substrate concentration. The Michaelis-Menten equation was first developed in 1913, and named after the two scientists, Leoner Michaelis and Maud Leonora Menten who developed the equation (Johnson & Goody, 2011). From the plot, two values can be obtained, which are specific to each enzyme and substrate, they are the Michaelis constant (K_M) and the maximum velocity (V_{max}). K_M is the substrate concentration that corresponds to half the maximum velocity. V_{max} is the maximum velocity that the enzyme can catalyse the reaction at (Voet *et al.*, 1999). At the V_{max}, all the enzyme present has been saturated with substrate, in other words, all the active sites are occupied by substrate.

The Lineweaver-Burk plot is a linear transformation of the Michaelis-Menten plot also known as the double reciprocal plot, as seen in Equation 4.5, where V_o is initial velocity of the reaction, V_{max} is the maximum rate of the reaction, K_M is the Michaelis-Menten constant and [S] is the substrate concentration. The plot is the reciprocal of the velocity against the reciprocal of the substrate concentration. A straight line is then fitted to the data and the V_{max} is calculated by taking the reciprocal of the y intercept. K_M can be found by two methods; first by taking the value of the slope of the line and multiplying it by V_{max}; second, is by extrapolating the line back until it intercepts the x axis, the value will be $-1/K_M$ from which K_M can be calculated.

$$\frac{\mathbf{1}}{\boldsymbol{v_o}} = \left(\frac{K_M}{V_{\max}}\right)\frac{\mathbf{1}}{[\mathbf{S}]} + \frac{\mathbf{1}}{V_{\mathbf{max}}} \qquad \text{Equation 4.5}$$

It can be seen from the enzyme kinetic studies carried out in this chapter that the pepsin is enzymatically active as shown in the Michaelis-Menten plot were K_M value of 0.6099 % w/w and V_{max} value of 1791 U mg^{-1} min^{-1} was obtained. Therefore, a Lineweaver-Burk plot was also achieved, where the K_M value was 0.6099 % w/v and the V_{max} value 1149 U mg^{-1} min^{-1}. Comparing the K_M and V_{max} values obtained in this study to those in published work is difficult due to differences in experimental parameters, such as temperature, pH, origin of pepsin, substrate, concentration of pepsin, concentration of substrate and origin of substrate, which are all known to affect the enzyme activity. However, Hu *et al*. (2006) found the V_{max} value of the free pepsin used in their study to be 52 U mg^{-1} min^{-1}, which is lower than the V_{max} value found for the pepsin in this chapter. But, the origin of the pepsin in the study is not stated and, the pH (3.0) and substrate (casein) (Hu *et al.*, 2006) were different to

those used in investigation in this chapter. Altun & Cetinus. (2007) in their work used porcine pepsin and bovine haemoglobin as the substrate, similar to the work in this chapter. However, they completed the enzymatic activity experiments at 40 °C and not 37 °C. The documented V_{max} value for free pepsin, which was not bound to chitosan microbeads was 5220 U g^{-1} min^{-1} and the corresponding K_M value was 12.0 g L^{-1} (Altun & Cetinus, 2007). In similar work, Poojari *et al*. (2009) found that free pepsin, which was not bound to silicone elastomer had K_M and V_{max} values of 4.5 g L^{-1} and 14000 U mg^{-1} min^{-1}, respectively. The product specification sheet for the porcine pepsin used in this study states that its enzymatic activity should be within the range of approximately 3200–4500 U mg^{-1} min^{-1} (Sigma-Aldrich, 2015). Therefore, it can be confirmed that the pepsin was enzymatically active prior to loading into the hydrogel as values of 3094 ± 42 U mg^{-1} min^{-1} and 3705 ± 8 U mg^{-1} min^{-1} were obtained for the stock pepsin used in this investigation.

Dowds & Riggs (1965) determined and compared the K_M and V_{max} values from a Michaelis-Menten plot and Lineweaver-Burk plot. They concluded that the estimation of the two parameters using the Lineweaver-Burk plot is less reliable than the Michaelis-Menten plot. The main error in the Lineweaver-Burk plot was believed to arise when plotting the reciprocal of the enzyme velocity (v). They stated that the lowest value of v plays a crucial role in the fitting of the regression line to the data. Therefore, if there is a large error in the determination of the lowest v value then the corresponding plotted reciprocal value will be too large and lead to inaccurate placing of the regression line, thus unreliable K_M and V_{max} values. However, both models were used to determine if pepsin catalysed synthetic N-acetyl dipeptides faster with phenylalanine or tyrosine residues (Jackson *et al.*, 1965). Enzyme kinetic parameters K_M and V_{max} for the digestion of bovine β-lactoglobulin

by pepsin was also determined by plotting a Lineweaver-Burk plot, which provided reliable results (Izquierdo *et al.*, 2007). English *et al*. (2006) state that an enzyme does not catalyse reactions in the classic way set out by Michaelis and Menten, which looks solely at a large group of enzymes. With advances in technology and using single-molecule fluorescence studies several researchers have confirmed that when an enzyme catalyses a reaction it is an ever-fluctuating dynamic entity, experiencing fluctuations in catalytic rates due to temporal fluctuations in conformation (Zhuang *et al.*, 2002; van Oijen *et al.*, 2003; Velonia *et al.*, 2005; Flomenbom *et al.*, 2005; English *et al.*, 2006; Zheng & Lu, 2014). However, English *et al*. (2006) state that the Michaelis-Menten equation is still useful when determining activity of large quantities of enzymes as the fluctuation will be less significant to the overall values obtained for K_M and V_{max}. Therefore, the steady state assumption of the Michaelis-Menten equation is more feasible. Despite the Michaelis-Menten equation being over 100 years old and with a better understanding of enzymes by enzymologists, the equation and its linear transformation, the Lineweaver-Burk plot, is still used widely to quantify enzyme activity in a plethora of scientific research areas, such as biotechnology antibody fabrication (Boushaba *et al.*, 2003), bioanalytical technology (Orosco *et al.*, 2009; Ponomareva *et al.*, 2010) and the food industry (Castillo-Yanez *et al.*, 2006; Marques *et al.*, 2015).

On loading three concentrations of pepsin into the PVA-borate hydrogel, crossover modulus analysis was completed to determine if incorporation of the pepsin into the hydrogel matrix caused any changes in the viscoelastic properties of the hydrogel. All three pepsin concentrations were found to decrease the crossover modulus significantly in comparison to a hydrogel of the same formulation, which contained no pepsin. When pepsin is dissolved in deionised water and added to the

hydrogel it will have an overall negative charge, due to having an isoelectric point in the range of 2.2–3.2 (Jonsson, 1972; Chaiyasut & Tsuda, 2001). One possible explanation for the reduction in crossover modulus may be due to the interaction of the negatively charged pepsin and the Na^+ cation. The Na^+ cation is a product of the dissociation of the sodium tetraborate decahydrate and plays a role in the cross-linking and overall shape of the polymer chains. The first complex formed in the two part reaction of the PVA-borate crosslink is a negatively charged poly(electrolyte) (Loughlin *et al.*, 2008). The cation exerts a shielding effect on the poly(electrolytes), reducing the repulsion between them. This allows the polymer chains to re-orientate and reside closer together, thus, increasing polymer entanglement and cross-linking (Lin *et al.*, 2005). Therefore, if the negatively charged pepsin is interacting with the Na^+ cation then the shielding effect of the cation may be diminished resulting in less cross-linking and polymer entanglement, thus, reducing the crossover modulus. Jenson *et al.* (2002) found that on addition of BSA to a polymer hydrogel there was electrostatic repulsion between the negatively charged BSA and the negatively charged regions on the polymer. A similar occurrence was observed on addition of BSA to the PVA-borate hydrogel in chapter 3. A similar phenomena may be occurring with the addition of the negatively charged pepsin and negative regions of the PVA polymer. If complete cross-linking does not occur fully or as a result of the reversible nature of the PVA-borate cross-link there may be negatively charged regions present within the hydrogel. This would result in repulsion with the pepsin with the possibility of reducing the cross-linking density and as result reduce the gel viscosity and crossover modulus.

The three pepsin-loaded hydrogels gave sustained release profiles over 8 hours with the 0.20 % w/w hydrogel giving the highest release (84.84 ± 0.79 %).

Release studies were carried out at 37 °C, similar to those in Chapter Three, to mimic body temperature. The reason for the PVA-borate hydrogel giving a high sustained release of pepsin is most likely due to the combination of the electrostatic repulsion, between the hydrogel components and the pepsin, and the decrease in viscosity because of this repulsion. Lysozyme is an enzyme, which is used frequently as a model protein in polymeric hydrogel studies (Jensen *et al.*, 2002; Khoury *et al.*, 2003; Verheyen *et al.*, 2010; Appel *et al.*, 2012). Jensen *et al.* (2002), Verheyen *et al.* (2010) and Appel *et al*. (2012) all achieved sustained release of the enzyme lysozyme, similar to what was found in this study with pepsin. However, Jensen *et al*. (2002) did not achieve passive release of lysozyme from the chondroitin 4-sulphate hydrogel due to opposite charge interaction between the positively charged lysozyme and the negative charges in the polymeric backbone. But, they were able to achieve the release on applying a pulsating electric field across the hydrogel, driving out the lysozyme by a process known as electro-simulative release.

Sodium dodecyl sulphate poly(acrylamide) gel electrophoresis was used to determine the molecular weight of pepsin prior to loading into the PVA-borate hydrogel and after release from the hydrogel. It was found that the pepsin released from the hydrogel remained intact and had not been broken down, when compared to the pepsin standard. The enzymatic activity of the released pepsin was determined against a pepsin standard using haemoglobin as the substrate, as discussed previously. It was found that upon release from the hydrogel, the pepsin had no enzymatic activity in comparison to the pepsin standard. It was thought that the reason for no activity was due to the pepsin being exposed to a basic environment, for its duration of time encapsulated in the PVA-borate hydrogel. It was found from the pH analysis of the PVA-borate hydrogels in Chapter Two that the PVA 6.0 %

w/w borate 2.0 % w/w hydrogel, which was used in this pepsin study, had an average pH of 8.3. As mentioned at the start of this discussion, pepsin is found in the acidic environment of the stomach and, therefore, has an optimum pH of 2.0. From the pepsin activity study carried out in this chapter it was also found that the pepsin had the highest enzymatic activity at pH 2.0 and low activity at pH 8.0. It is well documented that the aspartic proteases have an optimum pH range of 2.0–4.0 (Piper & Fenton, 1965; Lin *et al.*, 1992). It was also found that hydrolysis of haemoglobin by pepsin extracted from tuna fish also had an optimum pH of 2.0 (Nalinanon *et al.*, 2008). Piper & Fenton (1965) document that pepsin has maximum activity at pH 2.0, but, on increasing to pH 4.0, the pepsin exhibited only 70 % of its maximal activity. On further increasing the pH to 8.0 it was observed that the pepsin was irreversibly inactivated and, therefore, had no enzymatic activity. It is thought that the change in pH may influence both the dissociation of the substrate and the ionisation of the aspartic residues in the active site of the pepsin, therefore, rendering it inactive (Piper & Fenton, 1965; Denniston *et al.*, 2008). Similarly, Nalinanon *et al*. (2008) found that the activity of the tuna pepsin had diminished upon the mixture reaching pH 5.0. Ruan *et al*. (2010) found that the degree and rate of hydrolysis of egg white protein by pepsin decreased on increasing the pH from 2.0 to 3.0. They also stated that if the pH of the mixture was > 5.0, the pepsin began to denature and become inactive (Ruan *et al.*, 2010). Admittedly, the pH dependent stability of pepsin should have been taken into consideration when choosing an appropriate enzyme. However, it was thought that as the pH of the hydrogel was borderline on the limit of the pepsin's irreversible denaturing pH that on returning it back to an acidic pH there was the possibility it may re-activate. Appel *et al*. (2012) achieved sustained released of the enzyme lysozyme from a PVA-viologen-

hydroxyethylcellulose-*N*-methylpyrrolidone hydrogel. Appel *et al*. (2012) also found that the lysozyme was bioactive on released from the hydrogel.

An attempt was made to lower the pH of the hydrogel using hydrochloric acid (HCl). On adding a small volume (1 mL) of HCl 0.125 M and 0.250 M to the PVA-borate hydrogel the pH did drop below 8.0. But, the addition of HCl to the hydrogel caused a similar white de-mixing, as was seen previously in Chapter Three when the hydrogel was exposed to a high concentration of NaCl. A similar phenomena was seen by Loughlin *et al*. (2008) on addition of lidocaine HCl to the PVA-Borate formulation. The de-mixing or collapse of the network is thought to be caused by an increase in the free ion concentration within the formulation (Loughlin *et al.*, 2008). The increase in the free ion concentration (H^+ and Cl^-) brought about by the addition of the HCl caused a decrease in the repulsive forces between the poly(electrolytes). This results in an increase in the complexation constant, leading to hyper-cross-linking, which leads to de-mixing and phase separation (Pezron *et al.*, 1988a; Pezron *et al*., 1989a; Pezron *et al*., 1989b).

4.7 Conclusion

The work completed in this chapter has shown that addition of all three concentrations of pepsin (0.05, 0.10 and 0.20 % w/w) resulted in significant ($p<0.01$) decreases in the crossover moduli, in comparison to a hydrogel of the same formulation, but, containing no pepsin. The change in the crossover modulus detected using oscillation rheometry indicates that the viscoelastic properties of the hydrogel have changed on addition of the pepsin, which may have aided the release.

The PVA-borate hydrogel provided a sustained release of pepsin over an 8-hour period at 37 °C, with a maximum percentage cumulative release of 84.84 ± 0.79 %

from the 0.20 % w/w pepsin-loaded hydrogel. This indicates that the PVA-borate hydrogel may be able to provide a sustained release for protein payloads of a similar molecular weight and isoelectric point. SDS-PAGE was used to analysis the molecular weight of the pepsin, which was released from the hydrogel, in comparison to a sample of the stock pepsin. It was concluded that the pepsin had not undergone degradation, in terms of changes in molecular weight, on being released from the hydrogel. This investigation showed that the enzymatic activity of the pepsin could not be maintained upon release from the PVA-borate hydrogel.

To conclude, the results from this study indicate that in moving forward with the overall aim of the project, careful consideration needs to be taken when choosing a suitable protein payload, which promotes wound management and repair. This is to ensure that the biological activity of the payload can be maintained when encapsulated in the gel matrix and upon release.

Chapter 5

Chapter 5

5 Formulation, characterisation, *in vitro* release, stability and enzymatic activity study of an IGF-1-loaded PVA-borate hydrogel.

5.1 Introduction

Based on the results in Chapter Three and Four it was decided to proceed with the incorporation and release of insulin-like growth factor-1 (IGF-1). IGF-1 is known to cause an increase in cell migration and proliferation. Therefore, research has been conducted to determine if the topical application of exogenous IGF-1 to wounds can enhance healing (Tsuboi *et al.*, 1995; Koshizuka *et al.*, 1997; Nagano *et al.*, 2003; Emmerson *et al.*, 2012; Nunes Achar *et al.*, 2014).

The structure, biological function, therapeutic use and experimental use of IGF-1 was discussed in detail in Chapter One, section 1.4.6. Briefly, IGF-1 is a 7.6 kDa poly(peptide) consisting of 70 amino acids, with an A and B chain linked together by disulphide bonds (Laron, 2001). The major source of circulating IGF-1 is the liver and its main function is to control cell differentiation (Dercole *et al.*, 1984). The majority of circulating IGF-1 (approx. 80 %) is bound with high affinity in a ternary complex with insulin-like growth factor binding protein-3 (IGFBP-3) and an acid labile glycoprotein subunit. The ternary complex prolongs the half-life of IGF-1, protecting it from proteolytic degradation (Laviola *et al.*, 2007). In order to mediate its intra-cellular effect IGF-1 binds to a 1326-amino acid tyrosine kinase transmembrane receptor, known as insulin-like growth factor-1 receptor (IGF-1R) (Jones & Clemmons, 1995).

A commercially available recombinant preparation of IGF-1 for clinical use is Increlex™. Increlex™ is indicated for the treatment of growth retardation in

children aged 2–17 years, who have severe primary IGF-1 deficiency (BNF, 2017). Increlex™ is given by subcutaneous injection with a maximum maintenance dose of 120 μg kg^{-1} twice daily. Increlex™ is to be discontinued if there is no evident response after one year of treatment (BNF, 2017).

Nunes Achar *et al*. (2014) applied creams containing IGF-1 (1 % and 3 %) to wounds on non-diabetic and diabetic rats, to evaluate the effect of topically delivered IGF-1 on wound healing. They found that both creams increased re-epithelisation in all the treated groups compared to the control group. Similarly, Provenzano *et al*. (2007) concluded that subcutaneous injection of IGF-1 to ligament wounds in rats caused increased healing in comparison to the control group and a group treated with growth hormone. IGF-1 is a potent therapeutic agent demonstrating a median effective dose (ED_{50}) of 0.3–1.5 ng mL^{-1} when used in a cell proliferation assay using MCF-7 human breast cancer cells (Karey & Sirbasku, 1988). Due to the low concentration of IGF-1 being loaded and released in this study, an enzyme-linked immunosorbent assay (ELISA) was used to detect and quantify IGF-1 released from the PVA-borate hydrogel.

ELISA is an assay-based technique, which can be used to detect and quantify a range of substances, such as proteins, peptides, hormones and antibodies (Gan & Patel, 2013). The molecule to be detected, known as the antigen, must first be immobilised. The antigen is then complexed with an antibody, which is conjugated to an enzyme. A substrate for the enzyme is then added and the product of the enzymatic reaction gives a measurable signal. The measurable signal is most commonly fluorescent or chemiluminescent, measured on a spectrometer (Crowther, 1995). There are a number of modifications to the basic ELISA procedure, such as direct assay, indirect assay and a capture assay also known as a sandwich assay (Gan

& Patel, 2013). A direct assay involves the antigen being adsorbed onto a solid surface and the primary antibody conjugated with the enzyme then attaches to the antigen (Guidi *et al.*, 2001), as seen in Figure 5.1a. The advantages of a direct assay are, (i) it is less time consuming as there is only one antibody to be added and, therefore, fewer steps in the procedure in comparison to the indirect and sandwich assay, and (ii) cross-reactivity of the secondary antibody is eliminated as there is only the primary antibody present. Disadvantages of the direct assay are, minimum signal amplification and the immunoreactivity of the primary antibody could be affected by conjugation with the enzyme, leading to reduced binding with the antigen.

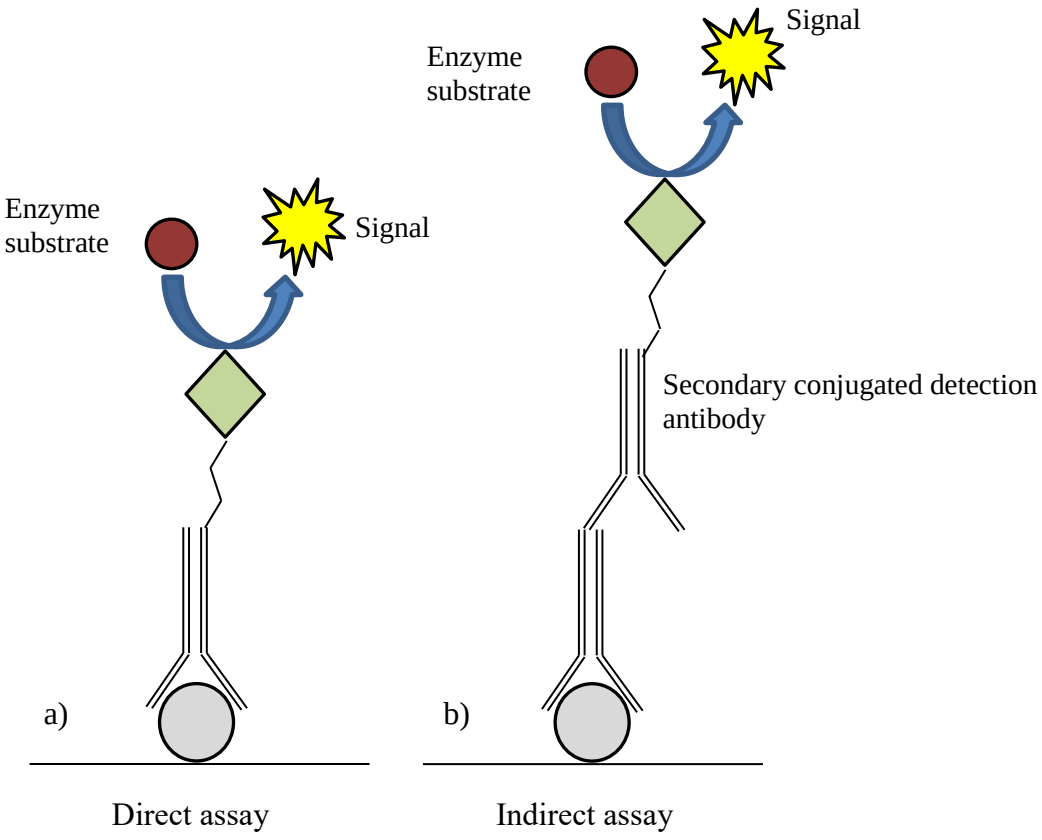

Figure 5.1 Schematic diagram showing an antigen adsorbed onto a solid plate and then assayed using a) a direct ELISA and b) an indirect ELISA.

An indirect assay also requires the adsorption of the antigen onto a solid surface prior to the binding of the primary antibody to the antigen (Crowther, 1995). However,

the primary antibody in an indirect assay is not conjugated to the enzyme. Instead, there is a secondary enzyme-conjugated antibody, which binds to the primary antibody, as seen in Figure 5.b. The advantages of the indirect assay method are (i) maximum immunoreactivity of the primary antibody is achieved due to no conjugation, (ii) increased sensitivity as each primary antibody has several binding regions for secondary conjugated antibodies, thus, increasing signal amplification, and (iii) different conjugated secondary antibodies are commercially available for use with the one primary antibody. The two main disadvantages are non-specific signalling may occur due to cross-reactivity of the secondary antibody and it is time consuming due to second antibody needing to be added. A capture or sandwich assay is similar to the indirect assay with the difference being that the antigen is captured by a third antibody, which is prefixed to a solid surface, usually a 96-well plate. The advantages and disadvantages of the sandwich assay are similar to those of the indirect assay. However, the sandwich assay gives higher specificity due to the capturing of the antigen by a highly specific third antibody (Gan & Patel, 2013). In this chapter, a modified sandwich assay was used for the detection and quantification of IGF-1. The modification was that the secondary detection antibody was eliminated, leaving the prefixed capture antibody and the enzyme conjugated detection antibody (R&D Systems, 2017), as seen in Figure 5.2.

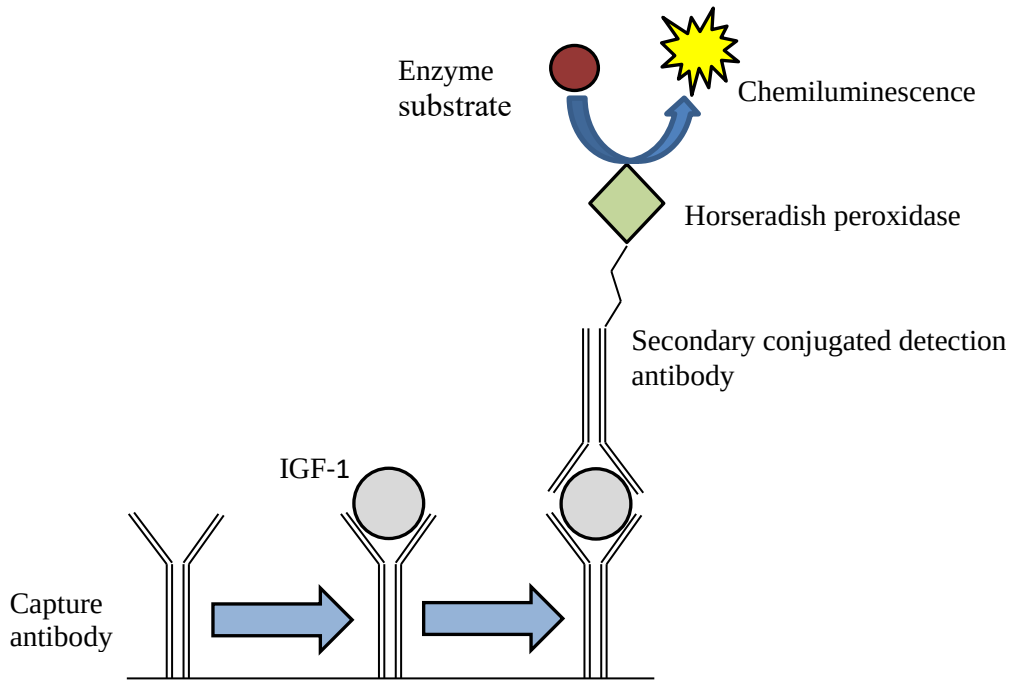

Figure 5.2 Schematic diagram illustrating the detection and quantification of the antigen, IGF-1, using a sandwich chemiluminescence ELISA.

5.2 Aims and objectives

The aim of this study was to formulate, characterise and complete *in vitro* release studies for IGF-1-loaded PVA-borate hydrogels (PVA 6.0 % w/w borate 2.0 % w/w).

Objectives;

- formulate PVA-borate hydrogels loaded with varying concentrations of IGF-1,
- characterise the viscoelastic properties of the IGF-1-loaded PVA-borate hydrogels using oscillatory rheometry,
- complete *in vitro* release studies for the IGF-1-loaded hydrogels using Franz diffusion cells,
- detect and quantify IGF-1 released from the hydrogels using an enzyme-linked immunosorbent assay (ELISA).

5.3 Materials

Chemicals and reagents

Poly(vinyl alcohol) (PVA) (Mw = 31–50 kDa, 98-99 % hydrolysed), sodium tetraborate decahydrate (ACS reagent ≥ 99.5 %), dialysis tubing cellulose membrane (Mw cut off 14 kDa, average flat width 43 mm), α-cyano-4-hydroxycinnamic acid (CHCA), sinapinic acid and trifluroacetic acid were purchased from Sigma-Aldrich Ltd. (Gillingham, Dorset, UK).

Peptide Calibration Mix 2 (LaserBio Labs, Spohia-Antipolis, Cedex, France).

Recombinant human Insulin growth-like factor-1 and Human Quantikine® ELISA kits were purchased from R & D Systems a biotechne® brand (Abingdon, UK).

All reagents were of appropriate laboratory standard and used without further purification.

Deionised water (R ≥ 18 MΩ cm) was obtained from a Purelab Ultra, purification system, Egla (Marlow, UK).

Apparatus

Kinexus Pro rheometer, Malvern instruments (Malvern, Worcestershire, UK).

FLUOstar® Omega microplate reader, BMG LABTECH Ltd. (Ortenburg, Germany).

Franz diffusion cells, Perme-Gear diffusion cells & systems. (USA) and Techne TE 10D Tempette® water bath & Pump, Bibby scientific Ltd. Staffordshire. (UK)

PerSeptive Biosystems Voyager-DE Biospectrometer (Hertfordshire, UK)

5.4 Methods

5.4.1 Formulation of IGF-1-loaded PVA-borate hydrogels

An optimum hydrogel formulation of 6.0 % w/w PVA and 2.0 % w/w borate was selected and loaded with various quantities of IGF-1 (50, 100, 200 ng). A sample (25 g) of this formulation was prepared by mixing 6.25 g of PVA stock solution (24 % w/w) and 10.00 g of borax stock solution (5 % w/w), as previously described. To a desired quantity of hydrogel the appropriate volume of the IGF-1 stock solution (1 μg mL^{-1}) was added and mixed in using a stainless steel spatula. The hydrogel was then stored in the fridge (2–8 °C) until used. Final formulations were clear and homogenous in appearance with no air bubbles present.

5.4.2 Viscoelastic analysis

Analysis of the viscoelastic properties was carried out using a Kinexus Pro rheometer (Malvern Instruments Ltd., Worcestershire, UK) on all hydrogel formulations, as described previously in sections 2.4.2. Briefly, a strain (1.0 %) controlled frequency sweep (0.1–10 Hz) was completed from which, the crossover modulus (Gc) was determined. All tests were carried out at 25 °C ± 0.2 °C, using 20 mm diameter stainless steel parallel plate geometry and a working gap of 1 mm. Three replicates were performed for each formulation (n=3). Student's t-test statistical analysis was carried out on the data.

5.4.3 *In vitro* release study

IGF-1 release studies were carried out using Franz diffusion cells (Perme Gear cells & Systems, USA) and a Techne TE 10D Tempette® water bath & Pump (Bibby scientific Ltd. Staffordshire, UK). All release studies were carried out at 37 °C using

cellulose dialysis membrane cut to size (MW cut off 14 kDa Sigma Aldrich). A sample (1.00 g) of hydrogel (PVA 6.0 % w/w borate 2.0 % w/w) containing 200 ng of IGF-1 was placed in each donor chamber at time zero. Samples (0.5 mL) were withdrawn at specified time intervals (0–8 hours) and replaced with 0.5 mL of fresh receiver phase. A blank PVA-borate hydrogel of the same formulation was ran as a control.

5.4.4 Detection and quantification of IGF-1 released from the PVA-borate hydrogel using an enzyme-linked immunosorbent assay (ELISA)

A solid phase Quantikine® ELISA kit (R & D systems, bio-techne®) was used to detect and quantify the IGF-1 in the samples taken from the receiver phase of the Franz cell. Each well of the supplied 96-well plate is pre-coated with a monoclonal capture antibody specific for IGF-1. To each well, 150 μL of assay diluent RD1-53 was added, followed by 50 μL of standards (0.094–6.000 ng mL^{-1}) or the samples to be tested. The wells were then covered with an adhesive strip and incubated at between 2–8 °C for 2 hours. Once this time had passed, all the liquid was removed from each well and washed four times with wash buffer. The plate was flicked over a sink after each wash to ensure removal of all liquid. After the fourth wash, the plate was inverted and blotted against clean tissue paper to ensure all the wash buffer was removed. Human IGF-1 conjugate polyclonal detection antibody (200 μl) was added to each well. The plate was covered with a new adhesive strip and incubated for 1 hour between 2–8 °C. All of the solution in each well was removed and each well was washed another four times, as described previously. To each well, 200 μL of substrate solution was added and incubated for 30 minutes at room temperature, wrapped in tin foil and placed in a cupboard to protect it from light. After 30

minutes, 50 µL of sulfuric acid (9.8%) was added to each well to stop the reaction and a colour change from blue to yellow occurred. The optical density of each well was read at 450 nm using a FLUOstar® Omega microplate reader, (BMG LABTECH Ltd. Ortenburg, Germany). Wavelength correction was set at 540 nm to compensate for any optical imperfections in the plate. Six replicates were completed for each sample and standard (n=6), with three optical density readings taken for each well (n=3).

5.4.5 Matrix-assisted laser desorption/ionisation time-of-flight mass spectrometry. (MALDI-TOF MS) analysis of IGF-1

MALDI-TOF MS was performed using a PerSeptive Biosystems Voyager-DE Biospectrometer (Hertfordshire, UK) equipped with a 1 m time-of-flight tube. A 10 mg mL^{-1} solution of the appropriate matrix of either α-cyano-4-hydroxycinnamic acid (α-CHCA) or sinapinic acid was prepared in 80 % acetonitrile, 20 % water with 0.1 % trifluroacetic acid. The matrix was vortexed thoroughly to mix and centrifuged for 2 minutes to ensure any undissolved matrix settled to the bottom of the tube. Only the supernatant was used. A 10 µL aliquot of matrix was vortexed with 10 µL of each sample, to mix thoroughly. A 1.5 µL aliquot of the mixture was pipetted onto a predefined well of a 100-well stainless steel plate. Once the spotted samples had dried on the plate, the plate was inserted into the MALDI-TOF. An internal mass calibration of the instrument was performed prior to sample analysis using Peptide Calibration Mix 2 (LaserBio Labs, Spohia-Antipolis, Cedex, France) containing four individual peptides; Neurotensin, ACTH fragment 18–39, Insulin bovine β-chain oxidised and Insulin bovine, with monoisotopic masses of 1672.9176, 2465.1989, 3494.6514 and 5730.6087 Da, respectively. All sample measurements

were collected in linear positive ionisation mode using 100 laser shots/spectrum. When using CHCA matrix, the accelerating voltage was maintained at 20,000 V, with the grid voltage and guide wire voltages set at 93 % and 0.05 %, respectively, of the accelerating voltage. When using sinapinic acid matrix, the accelerating voltage was maintained at 25,000 V, with the grid voltage and guide wire voltages set at 92 % and 0.3 %, respectively, of the accelerating voltage. The nitrogen laser set at 337 nm and directed toward a dense area of the sample spot. The laser intensity was adjusted to obtain the best spectral response and mass/ charge ratio (m/z) was plotted against relative abundance.

5.5 Results

Three concentrations of IGF-1 were incorporated into samples of a PVA 6.0 % w/w borate 2.0 % w/w hydrogel, after which rheological and statistical analysis were carried out. It can be seen in Figure 5.3 that the addition of 50 ng g^{-1} of IGF-1 into the hydrogel caused a small increase in the crossover modulus from 3831 ± 187 Pa to 4166 ± 116 Pa. However, this increase was not significant ($p = 0.2026$).

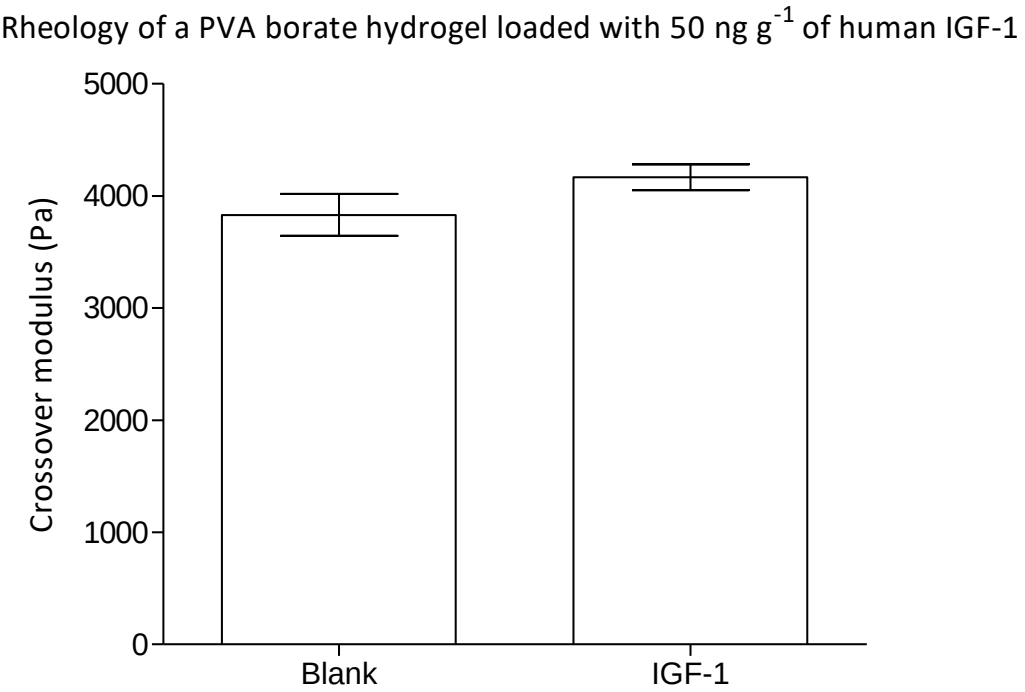

Figure 5.3 Graph showing the effect of incorporating 50 ng g^{-1} of IGF-1 into a PVA (6.0 % w/w) borate (2.0 % w/w) hydrogel has on the crossover modulus, compared to a blank hydrogel, of the same formulation. Data shown as the mean ± standard deviation (n=3). All measurements carried out at 25°C ± 0.2°C.

Figure 5.4 shows that on adding 100 ng g^{-1} of IGF-1 to the hydrogel there was again a small increase in the crossover modulus from 3524 ± 136 Pa to 3562 ± 116 Pa. A difference of 38 Pa, which is smaller than the difference (335 Pa) seen between the blank hydrogel and the hydrogel loaded with 50 ng g^{-1} of IGF-1, as seen in Figure 5.3. The increase caused by the loading of 100 ng g^{-1} of IGF-1 was not significant ($p = 0.8843$), similar, to the increase caused by the 50 ng g^{-1}.

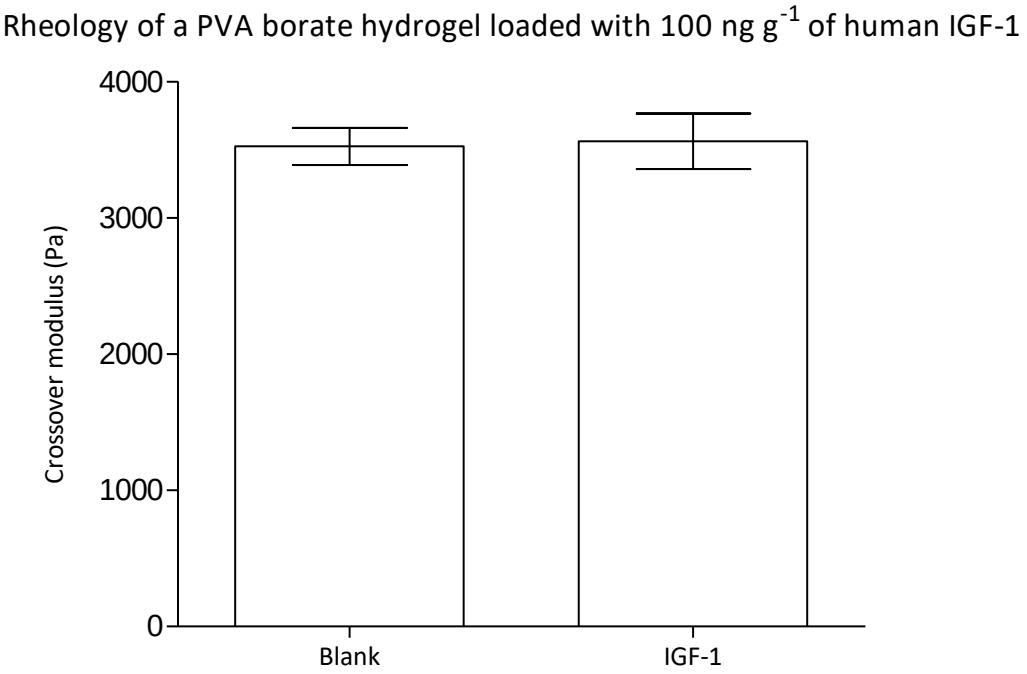

Figure 5.4 Graph showing the effect of incorporating 100 ng g^{-1} of IGF-1 into a PVA (6.0 % w/w) borate (2.0 % w/w) hydrogel has on the crossover modulus, compared to a blank hydrogel, of the same formulation. Data shown as the mean ± standard deviation (n=3). All measurements carried out at 25°C ± 0.2°C.

On adding 200 ng g^{-1} of IGF-1 to the hydrogel, the crossover modulus decreased from 2689 ± 105 Pa to 2591 ± 239 Pa. This is the opposite effect from that observed previously, when adding 50 and 100 ng g^{-1} of IGF-1 to the hydrogel. The decrease in the crossover modulus seen in Figure 5.5 is small (98 Pa) and is again not significant ($p = 0.7264$). Overall there is no general trend seen between the three concentrations and the change in the crossover modulus caused by all three concentrations are deemed not significant.

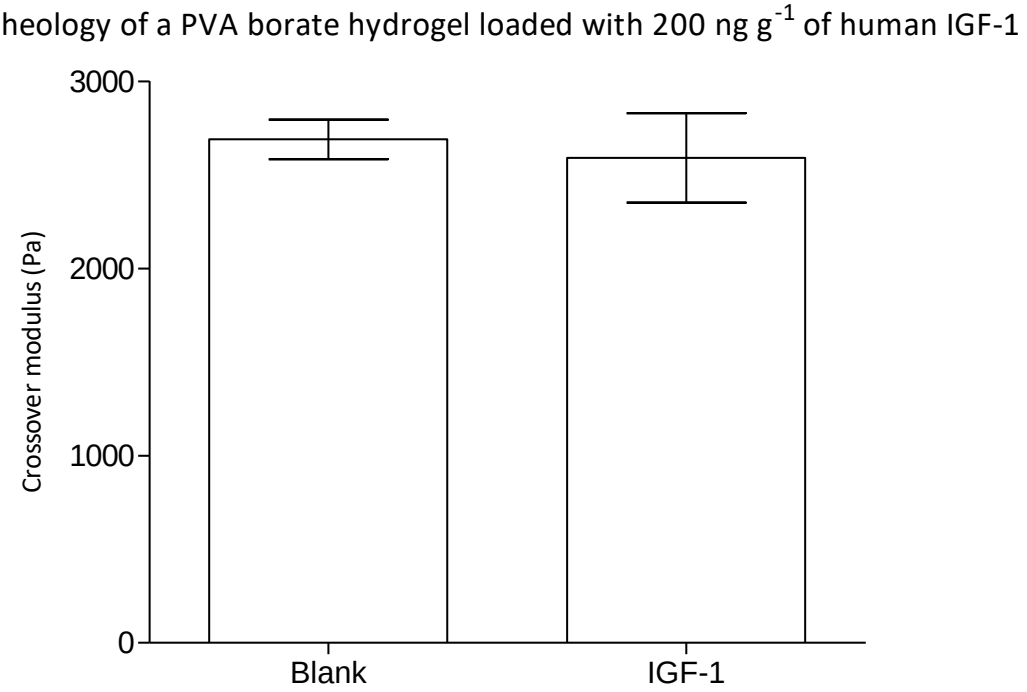

Figure 5.5 Graph showing the effect of incorporating 200 ng g^{-1} of IGF-1 into a PVA (6.0 % w/w) borate (2.0 % w/w) hydrogel has on the crossover modulus, compared to a blank hydrogel, of the same formulation. Data shown as the mean ± standard deviation (n=3). All measurements carried out at 25°C ± 0.2°C.

Having failed to detect IGF-1 released from the hydrogel in the receiver phase using HPLC and a commercially available fluorometric assay kit, due to lack of adequate sensitivity, it was decided to use an ELISA assay kit. The ELISA was both specific and highly sensitive at detecting IGF-1 in the receiver phase, having a minimum detectable concentration of 0.026 ng mL^{-1}. Figure 5.6, shows the calibration plot achieved for the Human IGF-1 ELISA assay. As seen in Figure 5.6 the r^2 value is 0.9996 showing that the data is correlated and, therefore, confidence can be had in any IGF-1 concentrations calculated using the line equation.

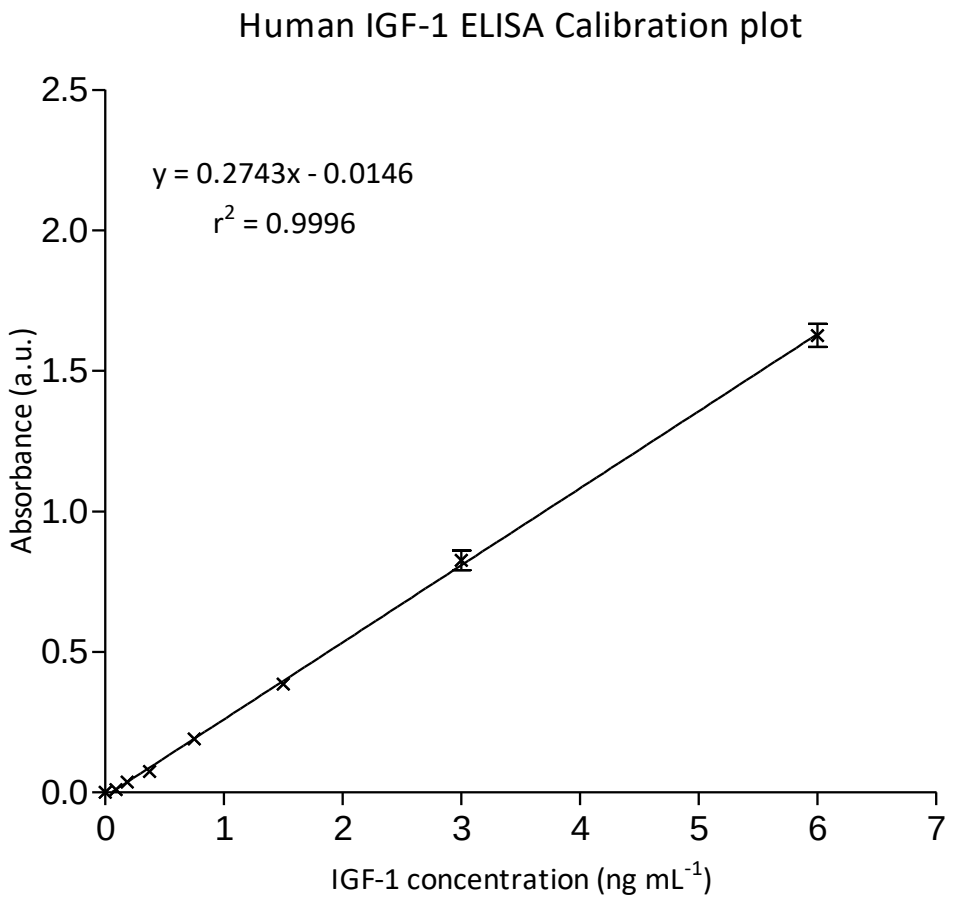

Figure 5.6 Human IGF-1 ELISA calibration plot produced using several dilutions of an IGF-1 stock solution 60 ng mL^{-1}. The standard dilutions concentration range was 0.094–6.000 ng mL^{-1}. The optical density λ = 450 nm and the wavelength correction set at 540 nm. The data is shown as mean ± standard deviation (n=6).

A percentage cumulative release profile for a PVA 6.0 % w/w borate 2.0 % w/w hydrogel loaded with 200 ng of IGF-1 can be seen in Figure 5.7. Due to the high cost of both the IGF-1 drug and the ELISA kit, only three replicates of a release profile for one concentration was achieved. However, this is the quantity of IGF-1 which will be used in the hydrogel for further cell culture studies. Therefore, it is imperative that an understanding of how this quantity of IGF-1 is released from the hydrogel over a set period of time. After 7 hours, a maximum percentage release of 58.15 ± 4.88 % was achieved equating to approximately 116.3 ng of IGF-1. The release profile shows a slower release of IGF-1 from hours 1 to 4, followed by a

period of a more rapid release from hours 4 to 6. The release profile then begins to plateau between hours 6 and 8.

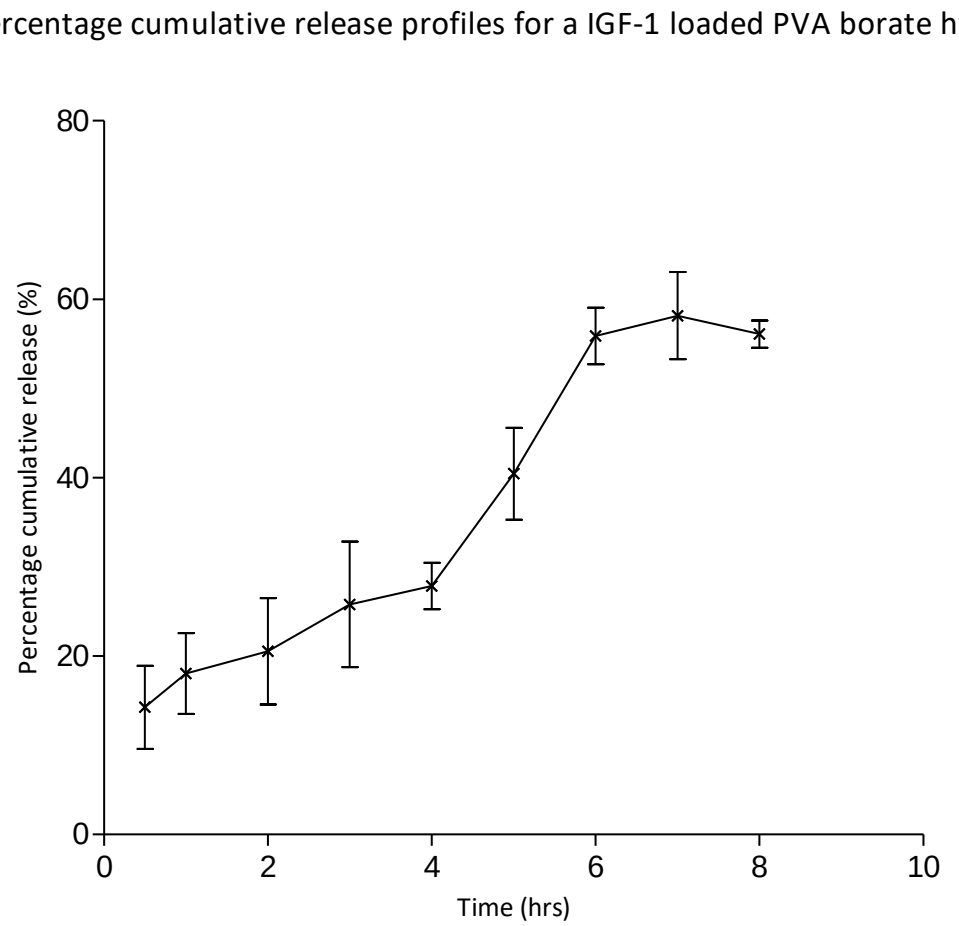

Figure 5.7 Percentage cumulative release profiles a PVA (6.0 % w/w) borate (2.0 % w/w) hydrogel loaded with 200 ng g^{-1}, over 8 hours. Release studies were carried out at 37 °C using cellulose dialysis membrane (MW cut off 14 kDa), on Franz diffusion cells. The data is shown as the mean ± standard deviation (n=3).

Samples were taking from the receiver phase of the Franz diffusion cells and subject to MALDI-TOF analysis to determine if any changes in the molecular weight of the IGF-1 had occurred during its time in the hydrogel, or during the release process. Any changes in molecular weight compared to an IGF-1 standard would be indicative of degradation of the poly(peptide). Figure 5.8 shows the MALDI-TOF spectra for the internal standard calibration. It can be seen from the spectra that the

peaks for the four proteins are found to be at the correct molecular weights as stated in method section 5.4.5 (1672.9176, 2465.1989, 3494.6514 and 5730.6087 Da).

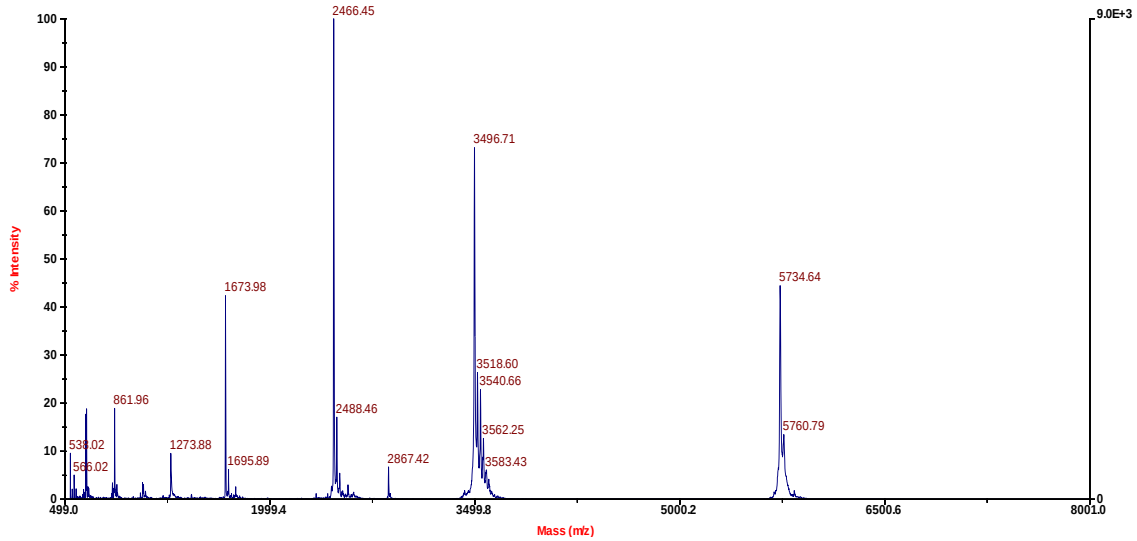

Figure 5.8 MALDI-TOF spectra for Peptide Calibration Mix 2 containing four individual peptides; Neurotensin, ACTH fragment 18–39, Insulin bovine β-chain oxidised and Insulin bovine with monoisotopic masses of 1672.9176, 2465.1989, 3494.6514 and 5730.6087 Da, respectively. A sinapinic acid matrix was used and, therefore, the accelerating voltage was maintained at 25,000 V, with the grid voltage and guide wire voltage set at 92 % and 0.3 %, respectively, of the accelerating voltage. The nitrogen laser set at 337 nm and the time-of-flight tube was 1 m.

The MALDI-TOF spectra for the IGF-1 standard can be seen in Figure 5.9. It can be seen that there is a sharp peak at 7664.41 Da, which is the same as the documented molecular weight for the IGF-1 protein (7.6 kDa), stated on the certificate of analysis. This confirms that the protein sent from the company is IGF-1 and also serves as the comparison for the released IGF-1 from the hydrogel. The peak at 7755.87 Da to the left of the main 7664.41 Da peak is thought to be a matrix cluster adduct.

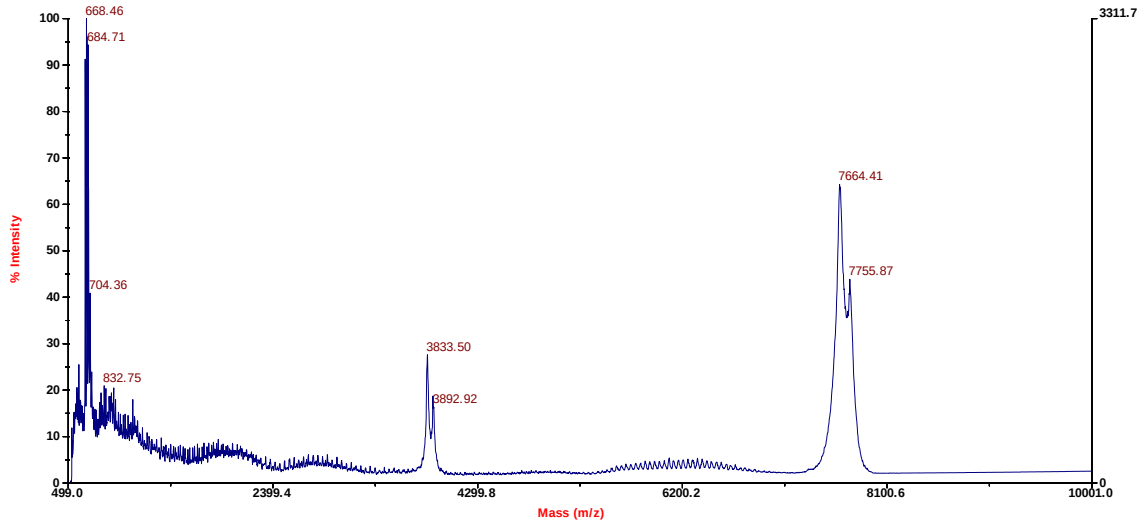

Figure 5.9 MALDI-TOF spectra for IGF-1 standard (molecular weight 7.6 kDa), using sinapinic acid matrix. The accelerating voltage was maintained at 25,000 V, with the grid voltage and guide wire voltage set at 92 % and 0.3 %, respectively, of the accelerating voltage. The nitrogen laser set at 337 nm and the time-of-flight tube was 1 m.

Figure 5.10 shows the MALDI-TOF spectra for the IGF-1 released from the hydrogel into the receiver phase of the Franz diffusion cells. It can be seen that there is a peak at 7640.49 Da, although it is not as intense as the peak seen in Figure 5.9 and is 23.92 Da less. However, confidence can be had that IGF-1 has not been subject to extensive degradation during the formulation and release process. There is also a peak of lower intensity to the left of the 7640.49 Da peak at 7676.31 Da. This is similar to what was seen in Figure 5.9 for the standard IGF-1 sample and again is thought to be a matrix cluster adduct.

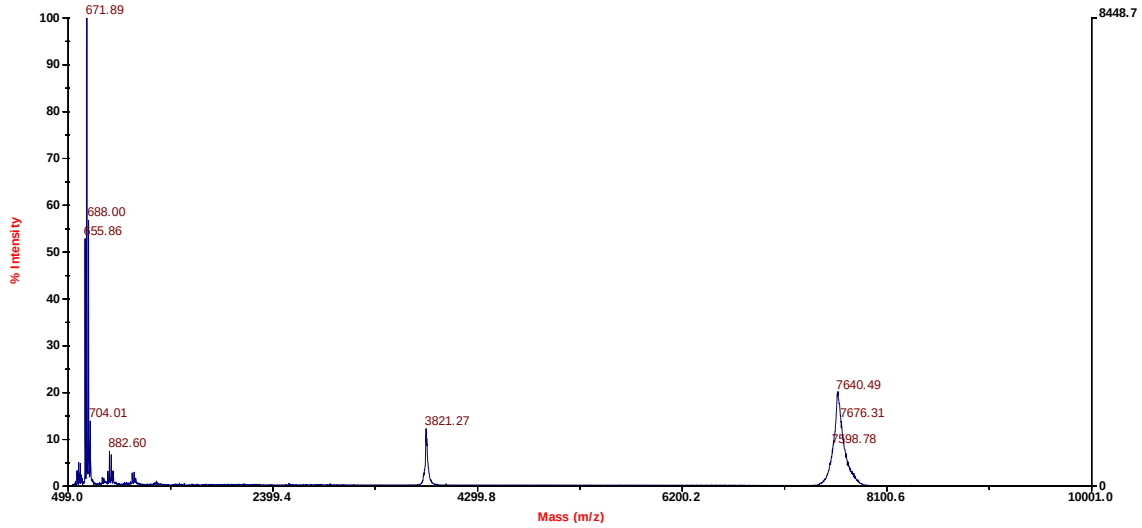

Figure 5.10 MALDI-TOF spectra for IGF-1 released from a PVA 6.0 % w/w borate 2.0 % w/w hydrogel over an 8-hour period. A sinapinic acid matrix was used and therefore, the accelerating voltage was maintained at 25,000 V, with the grid voltage and guide wire voltage set at 92 % and 0.3 %, respectively, of the accelerating voltage. The nitrogen laser set at 337 nm and the time-of-flight tube was 1 m.

5.6 Discussion

Several different delivery systems have been investigated for administration of insulin-like growth factor-1 (IGF-1), such as poly(lactic acid-co-glycolic acid) (PLGA) microspheres (Elisseeff *et al.*, 2001), alginate cross-linked biomaterial (Ruvinov *et al.*, 2011), chitosan-tripolyphosphate microspheres (Mantripragada & Jayasuriya, 2014), a topical solution (Tsuboi *et al.*, 1995), multivesicular liposomes (Katre *et al.*, 1998) and topical cream (Nunes Achar *et al.*, 2014). However, there has been no published data in relation to the use of a PVA-borate hydrogel as a sustained delivery system for growth factors, and IGF-1 in particular.

On loading three concentrations of IGF-1 (50, 100 and 200 ng g^{-1}) into samples of a PVA 6.0 % w/w borate 2.0 % w/w hydrogel, it was found that there was no significant ($p = 0.2023$, 0.8843 and 0.7264, respectively) change in the viscoelastic properties of the hydrogel, compared to a hydrogel of the same formulation with no IGF-1. IGF-1 has an isoelectric point of approximately 8.6

(Chen *et al.*, 2006) and as the pH of the PVA 6.0 % w/w borate 2.0 % w/w hydrogel is 8.3 the IGF-1 will most likely have a weak positive net charge. However, due to the pH of the hydrogel being close to the isoelectric point of IGF-1, a proportion of the IGF-1 may have no overall net charge and as a result will not have any charge interaction with the hydrogel. This may explain why there is no significant change in the viscoelastic properties of the gel. Chen *et al*. (2006) state that ionic interactions between opposite charged molecules can dissociate overtime, but, that it is statistically unlikely that they will all dissociate simultaneously. If the IGF-1 is positively charged, there is the possibility of electrostatic interaction with the negatively charge poly(electrolyte) that is formed in the complexation process of the PVA and borate (Loughlin *et al.* 2008) or, with negatively charged regions on the polymers due to the reversible nature of the PVA-borate cross-link. This may explain the small increase observed in the crossover modulus, although, as mentioned previously, it is not statistically significant. Nanogram quantities of IGF-1 were incorporated in the hydrogel, and therefore, any electrostatic interactions that do occur may be insignificant. This could be another reason why the small increase in crossover modulus is not statistically significant and has no overall effect on the viscoelastic properties of the hydrogel. If the IGF-1 has a hydrodynamic diameter smaller than the pore size of the hydrogel matrix, the IGF-1 may reside within the pores without causing any change in the viscoelastic properties of the gel itself (Mantripragada & Jayasuriya, 2014), especially if the IGF-1 has no overall net charge. This may be possible as the IGF-1 has the lowest molecular weight (7.6 kDa) of the five proteins loaded into the PVA-borate hydrogel in this thesis and is the only one which did not cause a change in the viscoelastic properties of the hydrogel. However, further work involving the measurement of the diameter of the pores

within the hydrogel and the hydrodynamic diameter of IGF-1 would need to be completed in order to confirm this theory.

Due to the high cost of the ELISA kits and difficulties obtaining data initially, only three replicates of one concentration (200 ng g^{-1}) of an IGF-1-loaded hydrogel were achieved. However, this is the concentration of IGF-1, which would be used in cell culture studies in future work. Therefore, it was important that release data was obtained for the 200 ng g^{-1} IGF-1-loaded hydrogel, to determine the quantity released over a defined period of time. The PVA-borate hydrogel delivered a sustained release of IGF-1 over 8 hours at 37 °C. The reason for the hydrogel giving a sustained release of IGF-1 is thought to be due to a combination of effects. If the IGF-1 has no overall net charge and the hydrodynamic size of the IGF-1 molecule is smaller than that of the pore size within the hydrogel matrix then it can be assumed that the IGF-1 will freely move through the gel matrix and into the receiver phase by passive diffusion. This may still partially occur if the IGF-1 has a weak positive charge, if the interactions were to dissociate gradually over a period of time, as suggested by Chen *et al*. (2006), but, this would give a slower rate of release. Mantripragada & Jayasuriya (2015) concluded that when the chitosan-tripolyphosphate cross-linking density was reduced and the delivery system was exposed to an acidic environment, the mesh size became larger than the encapsulated IGF-1 molecules, resulting in an increase in the release of IGF-1. In an acidic environment, the chitosan-tripolyphosphate complex became positively charged resulting in repulsion between protonated amino residues, enlarging the mesh size and allowing free passage of the positive charged IGF-1 through the matrix (Mantripragada & Jayasuriya, 2014). Conversely, on exposure of the chitosan-tripolyphosphate microspheres to a basic environment, the mesh size decreases due

to the chitosan molecules taking on a globular shape. This entraps the protein, decreasing the rate of release. Any release that occurred when exposed to a basic environment was deemed to be due to enzymatic degradation of the chitosan microspheres (Mantripragada & Jayasuriya, 2014). If the IGF-1 is positively charged and involved in opposite charge interaction or has a larger hydrodynamic diameter than the pore size of the hydrogel, then the release is most likely governed by degradation of the hydrogel matrix. If the loaded protein has a larger hydrodynamic radius than the polymeric matrix (Censi *et al.*, 2012) or is involved in opposite charge interaction with the delivery system (Chen *et al.*, 2006), swelling and erosion or degradation of the PVA-borate hydrogel must occur, for release to take place. From the swelling studies carried out in Chapter Two, it was determined that after 180 minutes the PVA-borate hydrogels began to disintegrate in the deionised water due to extensive swelling. This may explain why the release profile indicates a greater rate of release for 4 to 6 hours as during this time period the hydrogel began to disintegrate, increasing the IGF-1 release. Katre *et al*. (1998), Elisseeff *et al*. (2001), Chen *et al*. (2006), Ruvinov *et al*. (2011) and Mantripragada & Jayasuriya (2015) all demonstrated sustained release of IGF-1 from their respective delivery systems, similar to the PVA-borate hydrogel. They all also used ELISAs to detect and quantify the IGF-1 released from their delivery systems. This indicates that the ELISA was an appropriate technique to use for detection of low concentrations of IGF-1 (ng g^{-1}), due to the high specificity and sensitivity of the ELISA test.

The molecular weight of IGF-1 was analysed using MALDI-TOF mass spectrometry to determine if the IGF-1 was subject to degradation after release from the gel. On analysis of the spectra, it was found that there was a peak present at 7640.49 Da. The certificate of analysis for the IGF-1 states that the molecular

weight of the IGF-1, determined by MALDI-TOF, is 7.6 kDa (R&D Systems, 2015). Therefore, confidence can be had that this peak is IGF-1 and that it has not undergone any degradation according to its molecular weight. There was, however, a small discrepancy of 23.92 Da between the standard sample of IGF-1, which produced a peak at 7664.41 Da and the molecular weight of the released IGF-1. This difference (23.92 Da) is smaller than the molecular weight of a single residues of glycine (75.1 Da), which is the amino acid with the lowest molecular weight. Therefore, this would indicate that the IGF-1 released from the hydrogel has not lost any amino acid residues from its chain. A lower intensity peak at a higher molecular weight was observed on the left-hand-side of the main peak of IGF-1. This additional peak was observed for both the standard IGF-1 sample and released IGF-1 sample. These additional peaks can also be seen on some of the peptide calibration mix peaks, in particular the peak at 5734.64 Da. As these extra peaks are present in the calibration spectra and the peaks belonging to proteins within the calibration mix are all at the correct molecular weight, it could be assumed that they are characteristic to the matrix that is used. One possible explanation is protein-matrix cluster adducts, which become evident in MALDI-TOF spectra when the concentration of peptide or protein being analysed is low (Keller & Li, 2000; Zbu & Papayannopoulos, 2003). Matrix cluster adducts are thought to occur due to salts being present in the sample itself or which have been extracted from contaminated plastics and equipment used to prepare the samples or matrix (Keller & Li, 2000). Matrix cluster adducts can cause several interference peaks, peak broadening, peak tailing and increase the size of the protein (Sachon *et al.*, 2007). Other factors that can cause matrix cluster peaks are; the pH of sample, high laser intensity and the matrix used. Zbu & Papayannopoulos (2003) observed matrix clusters when using

α-cyano-4-hydroxycinnamic acid (α-CHCA) matrix and Sachon *et al*. (2007) observed matrix clusters using sinapinic acid matrix. Both these matrices were used in the analyses of IGF-1 in this chapter and also the IGF-1 stock solution was reconstituted in phosphate buffer saline (PBS).

5.7 Conclusion

It was found that upon incorporating any of the three concentrations (50, 100 and 200 ng g^{-1}) of IGF-1 into the PVA (6.0 % w/w)-borate (2.0 % w/w) hydrogel that there was no change in the viscoelastic properties. This was determined using oscillating rheometry, whereby, no significant ($p = 0.2023$, 0.8843 and 0.7264, respectively) change in the crossover moduli was observed for any of the three concentrations, in comparison to a blank hydrogel. The PVA-borate hydrogel loaded with 200 ng g^{-1} of IGF-1 was found to provide a sustained release over an 8-hour period at 37 °C. The maximum percentage cumulative release (58.15 ± 4.88 %) was observed after 7 hours. The median effective dose (ED_{50}) of the IGF-1 used in this study, in human cell lines, is 0.3-1.5 ng mL^{-1}, as stated by the manufacture in the certificate of analysis (R&D Systems, 2015). Therefore, with 58.15 ± 4.88 % cumulative release over 8 hours, confidence can be had in the PVA-borate hydrogel delivering a sufficient quantity of IGF-1 in future cell culture work to observe any effect it may have on the cells. Molecular weight analysis of the IGF-1 poly(peptide) prior to incorporation into the PVA-borate hydrogel and on release from the hydrogel confirmed that no degradation had occurred that resulted in a change in molecular weight of the growth factor. It can be concluded that the PVA-borate hydrogel has the potential to be a suitable topical delivery system for sustained release of growth factor payloads for wound management and repair.

Chapter 6

Chapter 6

6 Cell culture and cell signaling pathway investigation

6.1 Introduction

In the previous Chapter (Five), it was established that the PVA-borate hydrogel is capable of delivering a sustained release of IGF-1, over an 8-hour period at 37 °C. The key question to be answered in this chapter was to determine if the IGF-1 released from the hydrogel was biologically active. In order to do this, cell culture-based investigations were completed using two human skin cell types of keratinocyte and fibroblast origin. Both these cell types were chosen due to their dermatological role in the wound healing process.

Fibroblasts are the most common cell type found in the dermal layer of the skin and are a member of the connective tissue family (Tracy *et al.*, 2016). Fibroblasts are heterogeneous cells, changing their appearance and function depending on their location within the body (Tracy *et al.*, 2016). In the skin, the main role of the fibroblasts is to synthesise proteins, such as fibronectin, hyaluronan, proteoglycans and collagen, which are components of the extracellular matrix (ECM) (Velnar *et al.*, 2009). Therefore, without the presence of fibroblasts, there would be no ECM scaffold for keratinocytes to migrate over in the later stages of the proliferation phase (Li *et al*., 2007). Growth factors, such as TGF-β and PDGF secreted by platelets and other inflammatory cells stimulate fibroblasts to migrate into the wound from surrounding tissue (Velnar *et al*., 2009). Fibroblasts undertake a phenotype change to myofibroblasts, on completion of the secretion of ECM proteins and proliferation. The myofibroblasts aid in wound contraction, after which they are removed by apoptosis (Velnar *et al*., 2009).

Keratinocytes play an important role in the re-epithelialisation during the proliferation phase of wound healing and are regulated by keratinocyte growth factor (KGF), predominately secreted from fibroblasts (Werner, 1998). A major source of keratinocyte stem cells is from hair follicles in the dermis layer of the skin (Hirobe, 2014). As the keratinocyte stem cells begin to travel upward towards the epidermal layer, they differentiate. During differentiation, the keratinocytes produce and store keratin in their cytoplasm, a process known as keratinisation or cornification (Hirobe, 2014). The keratinised keratinocytes form the majority of the epidermis with dead keratinised keratinocytes forming the outermost layer of the skin, known as the *stratum corneum* (Martini & Nath, 2009), as seen in Figure 6.1. Therefore, the homeostasis of the epidermis is dependent on the proliferation and differentiation of keratinocytes (Hirobe, 2014). During re-epithelialisation, keratinocytes migrate over the top of the newly formed granulation tissue from the edges of the wound. The migrating edges are steered in the correct direction by binding to fibronectin in the newly formed ECM (Baum & Arpey, 2005). Once the leading edges meet, migration is stopped by a mechanism known as contact inhibition. The cells then begin to form the new basement membrane, separating the epidermis from the dermis.

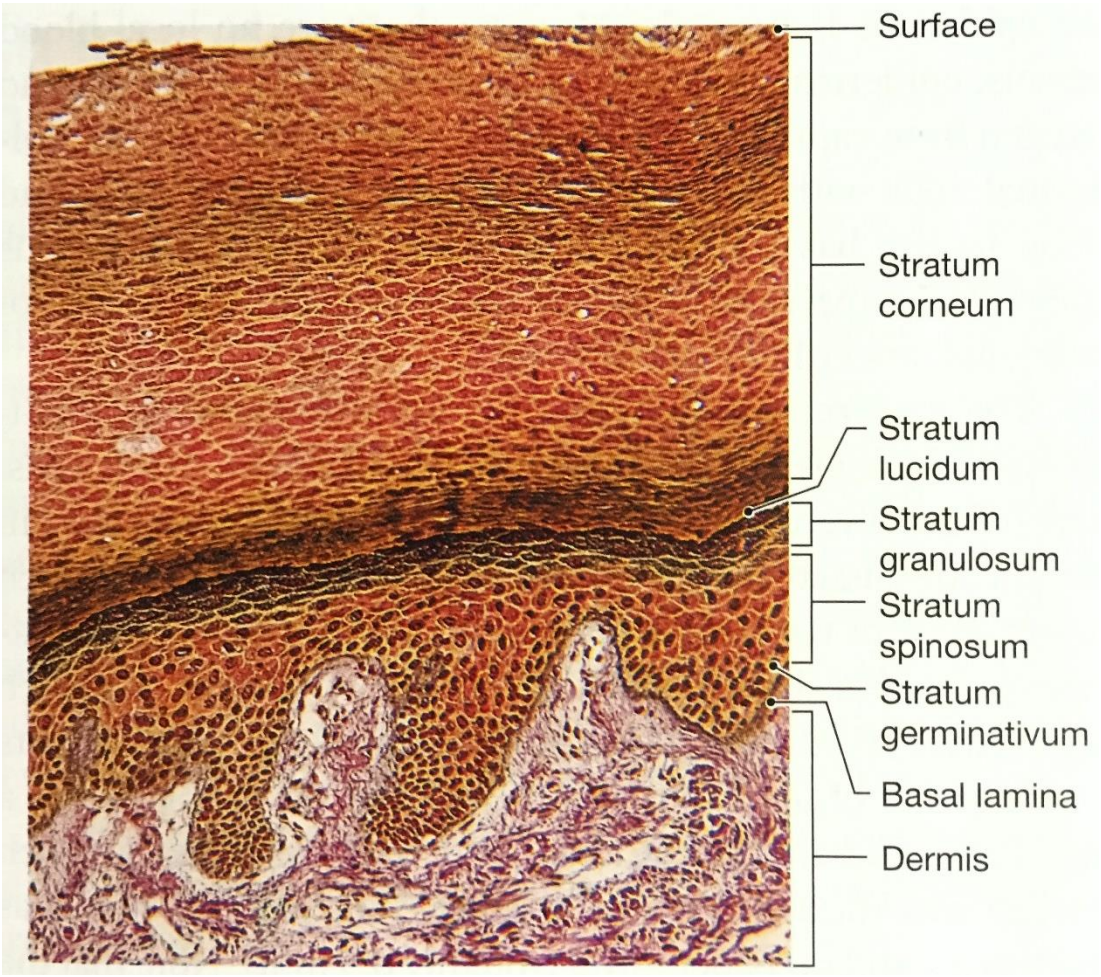

Figure 6.1 Histological picture showing the various layers of the epidermis and the beginning of the dermis. This is taken from a thick-skinned area, such as the palm of the hands or soles of the feet, as evidenced by the depth of the *stratum corneum* (approximately 0.5 mm) and the presence of the *stratum lucidum*, which is not found in thin-skinned areas. The *stratum corneum* is approximately 0.08 mm deep in thin-skinned areas, which covers most of the body (Martini & Nath, 2009). Light magnification x 210.

Current research indicates that the application of IGF-1 to wounds causes increased cell proliferation, migration and, therefore, increased wound healing (Tsuboi *et al.*, 1995; Koshizuka *et al.*, 1997; Nagano *et al.*, 2003; Emmerson *et al.*, 2012; Nunes Achar *et al.*, 2014). In addition, Loughlin *et al.* (2008), McCarron *et al.* (2011) and Murphy *et al.* (2012) conclude that the PVA-borate hydrogel is a suitable delivery system for topical application to wounds. Therefore, an IGF-1-loaded PVA-borate hydrogel may prove beneficial for the management and repair of acute and chronic wounds.

Insulin-like growth factor-1 (IGF-1) is known to trigger cell proliferation and migration. As a result of this, research has been conducted to establish if exogenous topical application of IGF-1 can stimulate wound healing (Tsuboi *et al.*, 1995; Nunes Achar *et al.*, 2014). Tsuboi *et al.* (1995) concluded that topical application of eye drops containing IGF-1 stimulates corneal epithelial wound healing in neurotrophic keratopathy in a rat model. Likewise, Nunes & Achar (2014) concluded that topical application of a cream containing IGF-1 increases the expression of myofibroblasts in skin wounds on rats, resulting in increased wound healing. Binding of IGF-1 to the transmembrane IGF-1 receptor (IGF-1R) triggers a complex interconnected network of cell signalling pathways. On activation of IGF-1R, a cascade of interactions and reactions occur, which leads to the activation of Akt and ERK (Vincent & Feldman, 2002). Stimulation of both these pathways leads to an increase in anti-apoptotic factors, such as nuclear factor-Kβ (NF-Kβ), Bcl2 and BclX, and inhibition of pro-apoptotic factors, such as caspase-9, Bad, GSK-3β, FasL and FKH (Vincent & Feldman, 2002). This was found to result in increased cell proliferation and migration. Therefore, in this chapter, an immunofluorescent chemistry technique was used to determine if IGF-1 delivered by the PVA-borate hydrogel caused upregulation of the Akt pathway in the two cell lines.

6.2 Aims and objectives

The aim of this study was to evaluate the effect that applying an IGF-1-loaded PVA-borate hydrogel had on two human skin cell lines and to determine activation of an intracellular signaling pathway by IGF-1.

Objectives;

- determine the growth rate of the HaCaT and Hs27 cell lines,
- evaluate the effect of free IGF-1 on the growth rate of both human skin cell lines,
- evaluate hydrogel toxicity towards both human skin cell lines,
- evaluate the effect of IGF-1 has on cell proliferation and migration using a scratch assay,
- determine if IGF-1 causes upregulation of the Akt cell signaling pathway, using immunofluorescent microscopy.

6.3 Materials

Chemicals and reagents

Dulbecco Modified Eagle Medium (DMEM), Foetal Bovine Serum (FBS), penicillin-streptomycin (Pen-Strep), trypsin EDTA x10, phosphate-buffered saline tablets (Dulbecco A tablets) Oxoid and goat anti-rabbit IgG secondary antibody, Alexa Fluor 488 were purchased from Thermofisher Scientific Ltd. (Paisley, UK).

Trypan blue 0.4 % solution, MTT (3-(4, 5 dimethylthiazol-2-yl)-2, 5-diphenyl-tetrazolium bromide), Triton X100, Tween® 20, bovine serum albumin (BSA), goat serum, dimethyl sulfoxide (DMSO), paraformaldehyde, phalloidin-

tetramethylrhodamine B isothiocyanate and propidium iodide solution were all purchased from Sigma-Aldrich Ltd. (Gillingham, Dorset, UK).

Recombinant human Insulin growth-like factor-1 was purchased from R & D Systems a biotechne brand (Abingdon, UK).

Phospho-AKt (Ser473) (D9E) XP® Rabbit monoclonal antibody was purchased from Cell Signaling Technology® via Brennan and Company (Dublin, Ireland).

UltraCruz® Mounting Medium was purchased from Santa Cruz Biotechnology (Heidelberg, Germany).

HaCaT and Hs27 cell lines were purchased from ATCC in partnership with LGC standards (Middlesex, UK).

All reagents were of appropriate laboratory standard and used without further purification.

Deionised water (R ≥ 18 MΩcm) was obtained from a Purelab Ultra, purification system, Egla (Marlow, UK).

Apparatus

FLUOstar® Omega microplate reader, BMG LABTECH Ltd. (Ortenburg, Germany).

Carl Zeiss Primo Vert microscope (Cambridge, UK) equipped with an Axiocam ERC 5s.

Carl Zeiss Axio Scope A1 Microscope Nikon, (Japan) and Axiovisio Rel 4.8 software (Gottingen, Germany).

Leica TCS SP2 confocal microscope (Milton Keynes, UK).

Countess™ Automated Cell Counter Invitrogen (USA).

Millicell hanging cell culture inserts, 12-well, pore size 8.0 μm, Merck (USA).

6.4 Methods

6.4.1 Culturing of human skin cells

Human skin cells, HaCaT and Hs27 were cultured in either T75 or T175 culture flasks containing 15–20 mL or 20–30 mL of DMEM media supplemented with 1 % penicillin-streptomycin and 10 % foetal bovine serum. Cells were incubated at 37 °C in an atmosphere of 5 % CO_2 until 70–80 % confluent. Once the desired confluency was reached, spent media was removed from the culture flask and discarded. Cells were washed twice using pre-warmed (37 °C) sterile PBS. Cells were then dissociated from the flask by addition of pre-warmed trypsin-EDTA solution (3 mL for T75 and 6 mL for T175) and incubated for 5 minutes at 37 °C. The cell suspension was transferred to a centrifuge tube and the trypsin neutralised by addition of an equal volume of media. Cells were centrifuged at 1200 rpm for 5 minutes, after which the supernatant was discarded and the pellet of cells re-suspended in fresh media. Cells were counted by mixing 10 µL of cell suspension with 10 µL of trypan blue solution and loading 10 µL of the mixture onto a Countess™ cell counting chamber slide. The slide was then inserted into the Countess™ Automated Cell Counter to obtain the total number of live cells per mL of media. Cells were then seeded at the desired seeding density in the required plates for experimental work.

6.4.2 Skin cell growth curves

HaCaT and Hs27 cells were seeded in 96-well plates at the following seeding densities; 1000, 2000, 4000, 6000, 8000 and 10000 cells mL^{-1}. Cells were seeded in replicates of six (n=6) on each plate and two plates were seeded for each cell line. Cells were incubated at 37 °C in an atmosphere of 5 % CO_2 in 200 µL of DMEM

media supplemented with 1 % penicillin-streptomycin and 10 % foetal bovine serum. One plate of each cell line was incubated for 24 hours and the other for 48 hours, after which an MTT (3-(4, 5 dimethylthiazol-2-yl)-2, 5-diphenyl-tetrazolium bromide) assay was carried out on the cells to determine any increase in cell quantity. After incubation, all media were removed and each well washed twice with 200 μL of sterile PBS. A sample (40 μL) of MTT solution (5 mg mL^{-1} in sterile PBS) was added to each well, in minimal light. To each well, 160 μL of complete DMEM was added to achieve a total well volume of 200 μL. The plates were wrapped in tin foil and incubated for 3 hours at 37 °C. After 3 hours, all media and MTT solution were removed from wells and 200 μL of dimethyl sulfoxide (DMSO) added to each well to dissolve the insoluble formazan. The optical density of each well was read at 570 nm using a FLUOstar® Omega microplate reader, (BMG LABTECH Ltd. Ortenburg, Germany).

6.4.3 Skin cells dose-response curve

HaCaT and Hs27 cells were seeded at a density of 4000 cells mL^{-1} in 96-well plates. Each well was treated with a different concentration of IGF-1 (1, 2, 5, 10, 20, 40, 60, 80 and 100 ng mL^{-1}). Six replicates were performed for each treatment (n=6) and a MTT assay used to determine any increase in the quantity of cells compared to the control group. Each plate was incubated for 24 hours at 37 °C in 5 % CO_2 in DMEM media, supplemented with 1 % penicillin-streptomycin and 10 % foetal bovine serum. Student's t-test statistical analysis was carried out on the data to determine any significant responses to IGF-1.

6.4.4 PVA-borate hydrogel toxicity study

HaCaT and Hs27 cells were seeded in 96-well plate at a density of 10000 cells mL^{-1} and a 24-well plate at 0.05 x 10^6 cell mL^{-1} in complete DMEM media to a final well volume of 200 µL and 500 µL, respectively. After 24 hours of incubation at 37 °C in 5 % CO_2, the spent medium was removed and the cells washed twice with sterile PBS. A sample of hydrogel was placed on top of the cells in the 24-well plate for 1 hour and then removed, after which an MTT assay was used to determine cell viability. Six replicates were performed for each treatment (n=6) and cell viability was expressed as a percentage relative to the non-treated control cells. Cells were also treated with a range of concentrations of borate (0.5, 1.0, 1.5, 2.0, 2.5 % v/v) and a range of concentrations of PVA (6.0, 8.0, 10.0, 12.0 % v/v) in the 96-well plates, diluted to the desired concentration with complete DMEM media. The cells were then incubated for 60 minutes, after which an MTT assay was used to determine cell viability. Student's t-test statistical analysis was carried out on the data.

6.4.5 Scratch assay

HaCaT and Hs27 cells were seeded at a density of 0.1 x 10^6 cells mL^{-1} in 12-well plates in complete DMEM media to a final well volume of 1.5 mL. Cells were incubated at 37 °C in 5 % CO_2 until a monolayer was formed (approximately 24 hours later). A sterile 1 mL plastic pipette tip was used to scratch the surface of the monolayer along the diameter of each well. All wells were washed twice with 1 mL of sterile PBS to remove the detached cells. A volume of 1.5 mL of complete DMEM was added to each well along with the desired treatment; i) media only, ii) 20 ng of free IGF-1, iii) 1.00 g of hydrogel loaded with 200 ng of IFG-1, iv) 1.00 g of blank hydrogel. Twelve-well hanging cell culture inserts with a poly(ethylene

terephthalate) membrane (pore size 8.0 μm) were used to deliver IGF-1 directly to the cells without the hydrogel coming in direct contact with the cells (Figure 6.2). Photographs were taken of each well using a Carl Zeiss Primo Vert microscope (Cambridge, UK) equipped with an Axiocam ERC 5s at 0, 12, 24, 36 hours for the HaCaT cell line and 0, 6, 12, 24 hours for the Hs27 cell line. The area of the scratch was then measured using ImageJ® software and the percentage scratch closure was expressed relative to the time zero area for each well. All treatments were performed in triplicate (n=3). Statistical analysis was used to determine any significant changes in the scratch area by applying two-way analysis of the variance (ANOVA) to the data.

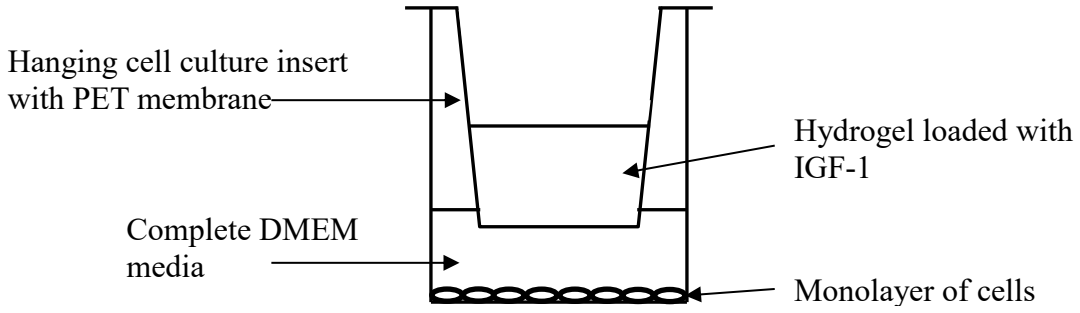

Figure 6.2 Schematic diagram of a twelve-well hanging cell culture inserts setup, used to deliver IGF-1 from PVA-borate hydrogels to the cell monolayer, without direct contact with the cells.

6.4.6 Immunofluorescent microscopy

Round glass cover slips (13 mm diameter) were placed in the bottom of each well of a 12-well tissue culture plate. HaCaT and Hs27 cells were seeded at a density of 4000 cells mL^{-1} in each well, in complete DMEM media to a final well volume of 1.5 mL. The seeded cells were then incubated at 37 °C in 5 % CO_2 for approximately 24 hours. After 24 hours, the desired treatment comprising; i) media only, ii) 20 ng of free IGF-1, iii) 1.00 g of hydrogel loaded with 200 ng of IFG-1, iv) 1.00 g of blank hydrogel were added to the appropriate wells. Twelve-well hanging cell culture

inserts with a poly(ethylene terephthalate) membrane (pore size 8.0 μm) were used to deliver IGF-1 directly to the cells without the hydrogel coming in direct contact with the cell, as seen in Figure 6.2 in section 6.4.5. After a further 4 hours of incubation with each treatment at 37 °C in 5 % CO_2, the cells were fixed with 4 % paraformaldehyde (PFA) at room temperature for 30 minutes. Each well was then washed three times with PBS for approximately 15 minutes (5 minutes for each wash). The fixed cells were then permeabilised with 0.5 % Triton X-100 in PBS for 40 minutes at room temperature. Each well was washed three times for a total of 15 minutes (5 minutes each wash), first with PBS, second with PBS-Tween 20 and third with PBS. A 1 mL aliquot of blocking buffer, consisting of 10 % goat serum and 1 % BSA diluted in PBS, was added to each well and left for one hour at room temperature. Remaining blocking buffer solution was removed after the hour had passed. An aliquot of 100 μL of a 1:100 dilution of the primary antibody, Phospho-Akt (Ser473) rabbit monoclonal antibody in 1 % BSA dissolved in PBS, was added to each well. A small piece of parafilm was cut and placed on top of each slide to keep the antibody in contact with the cells at all times and help maintain a humidified environment. Each plate was wrapped in tin foil and placed in the fridge (2–8 °C) overnight. The plates were removed from the fridge the following morning and left for 45 minutes at room temperature. Each well was washed three times for a total of 15 minutes (5 minutes each wash), first with PBS, second with PBS-Tween 20 and third with PBS. A 100 μL aliquot of goat anti-rabbit IgG secondary antibody Alexa fluor 488, diluted 1:1000 in 1 % BSA dissolve in PBS, was added to each well and covered with a small piece of parafilm. Each plate was wrapped in tin foil and incubated at 37 °C for 1 hour. After the hour had passed, any remaining secondary antibody solution was removed and each well washed three times as previously

mentioned with PBS and PBS-Tween 20, for a total of 15 minutes. A small volume of phalloidin solution was added to each well and incubated for 15 minutes at room temperature. Excess stain was removed and all wells washed three times with PBS. This process was repeated for propidium iodide stain. Each cover slip was removed from the well and placed cell side down on top of a single drop of mounting media on a glass microscope slide. Excess mounting solution was blotted off using clean tissue paper. Each slide was labelled and left to dry for approximately 30 minutes. The edge of each cover slip was sealed using nail polish and left to dry for 2–3 hours, wrapped in tin foil. Images of each slide were then take using Leica TCS SP2 confocal microscope (Milton Keynes, UK) and a Carl Zeiss Axio Scope A1 Microscope Nikon, (Japan).

6.5 Results

To determine the seeding densities for further experiments, two growth curves were produced to ascertain the rate at which both cell lines proliferate. Each cell line was seeded in a 96-well plate at a range of seeding densities (1000–10000 cells mL^{-1}) for 24 and 48 hours.

Figure 6.3 shows that the keratinocytes (HaCaT cells) proliferate faster, in both a 24-hour and 48-hour period, in comparison to the fibroblasts (Hs27 cells), as seen in Figure 6.4. It can also be seen that there is a greater increase in proliferation at all the seeding densities between the 24-hour and 48-hour plates for the HaCaT cells, compared to the Hs27 cells.

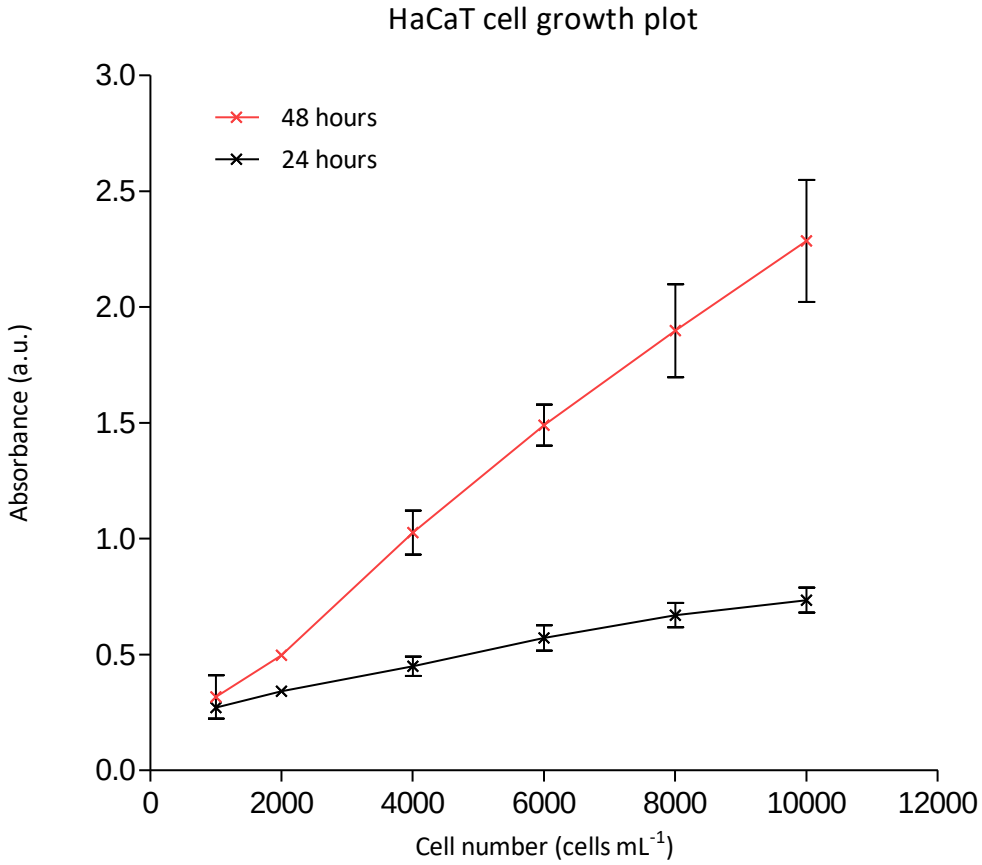

Figure 6.3 Graph showing MTT assay absorbance values, which are representative of HaCaT cell proliferation at different cell seeding densities (1000–10000 cells mL^{-1}) over a 24-hour and 48-hour period. The cells were cultured in DMEM media supplemented with 1 % penicillin-streptomycin and 10 % foetal bovine serum. Cells were incubated at 37 °C in an atmosphere of 5 % CO_2. Data shown as mean ± standard deviation (n=6).

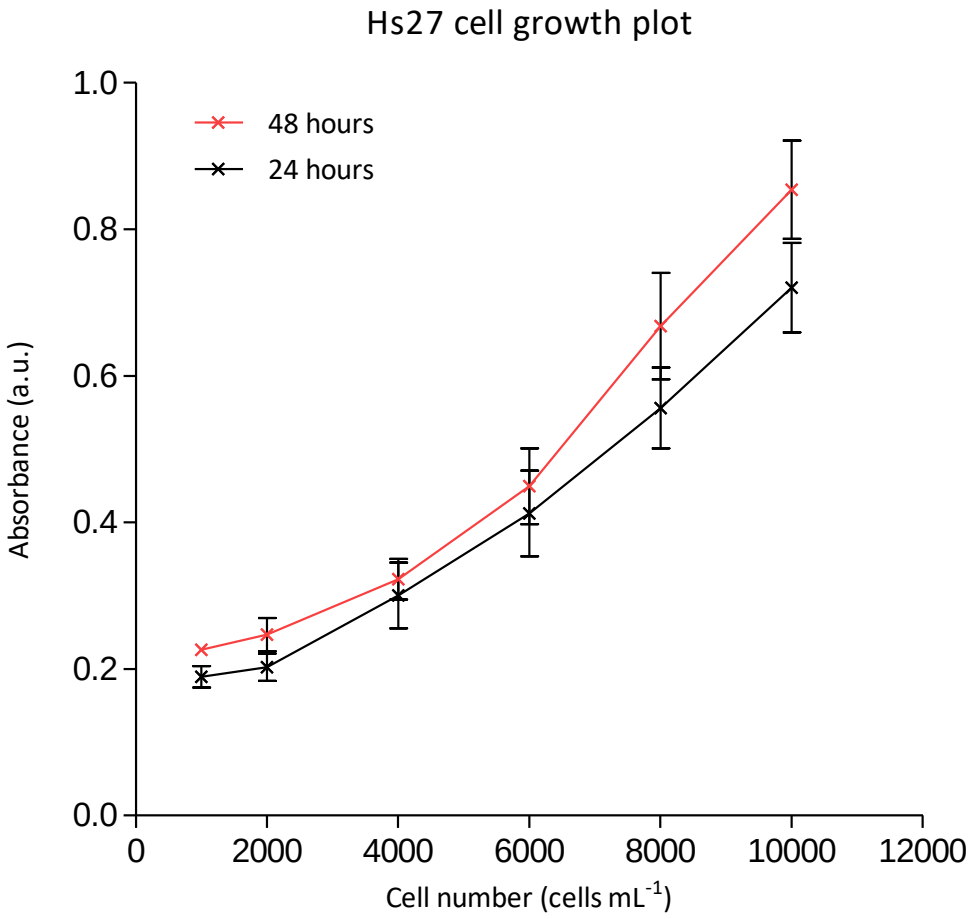

Figure 6.4 Graph showing MTT assay absorbance values, which are representative of Hs27 cell proliferation at different cell seeding densities (1000–10000 cells mL^{-1}) over a 24-hour and 48-hour period. The cells were cultured in DMEM media supplemented with 1 % penicillin-streptomycin and 10 % foetal bovine serum. Cells were incubated at 37 °C in an atmosphere of 5 % CO_2. Data shown as mean ± standard deviation (n=6).

A range of IGF-1 concentrations were added to a constant number of cells for both cell lines in order to obtain a dose-response curve. It can be seen from Figure 6.5 that all the concentrations of IGF-1 (2–100 ng mL^{-1}) caused a significant ($p<0.01$) increase in the MTT assay absorbance values, compared to the non-treated HaCaT cells. A high absorbance value corresponds to a large number of viable cells being present. For the HaCaT cells, the general trend seen was as the concentration of IGF-1 increased so did the absorbance value. Figure 6.6 shows that on addition of IGF-1 to the Hs27 cells there was an increase in the MTT absorbance value indicating an increase in cell proliferation. Similarly, addition of IGF-1

concentrations (2–80 ng mL^{-1}) caused a significant ($p<0.05$) increase in the number of viable Hs27 cells. However, the 100 ng mL^{-1} concentration (0.618 ± 0.115 a.u.) did not cause a significant ($p = 0.3850$) increase in the absorbance value compared to the control group, which had an absorbance of 0.535 ± 0.092 a.u. The Hs27 cells do not show any general trend in response to increasing the IGF-1 concentration.

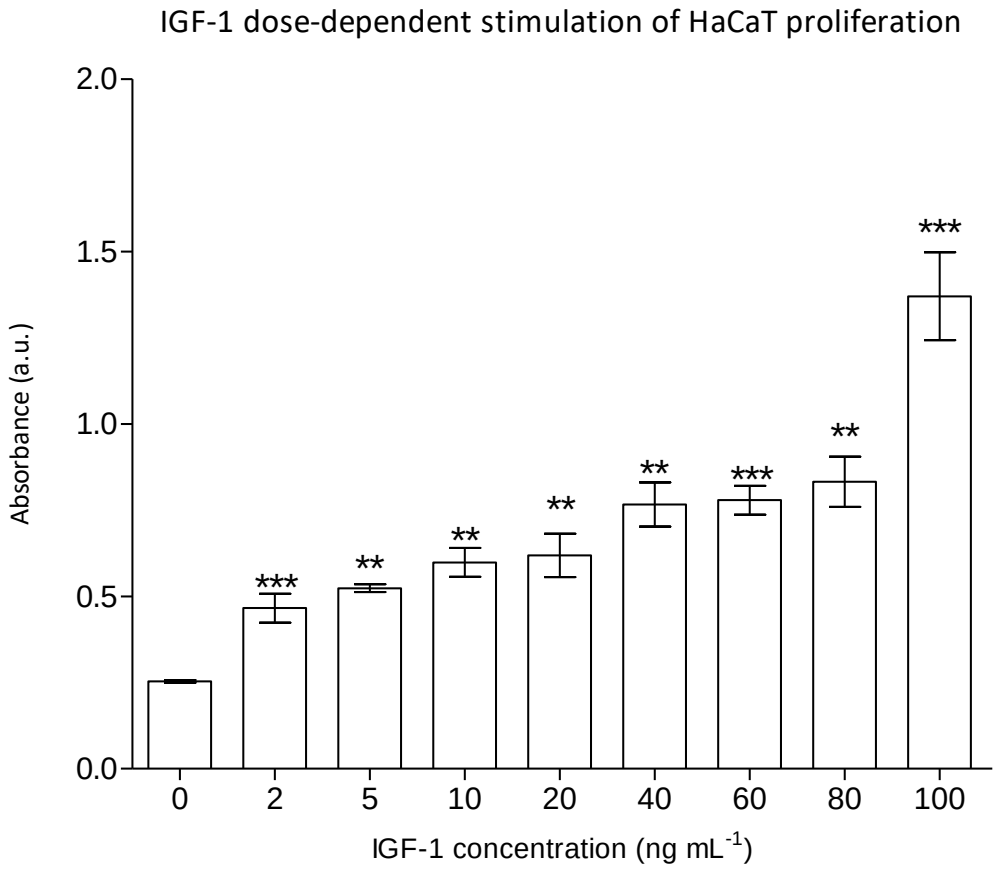

Figure 6.5 Graph showing MTT assay absorbance values, which are representative of HaCaT cell proliferation at a cell seeding density of 4000 cells mL^{-1} while varying the concentration of IGF-1 (2–100 ng mL^{-1}). The cells were cultured in DMEM media supplemented with 1 % penicillin-streptomycin and 10 % foetal bovine serum. Cells were incubated for 24 hours at 37 °C in an atmosphere of 5 % CO_2. Data shown as mean ± standard deviation (n=6), $p < 0.05$ (*), $p < 0.01$ (**), $p < 0.001$ (***).

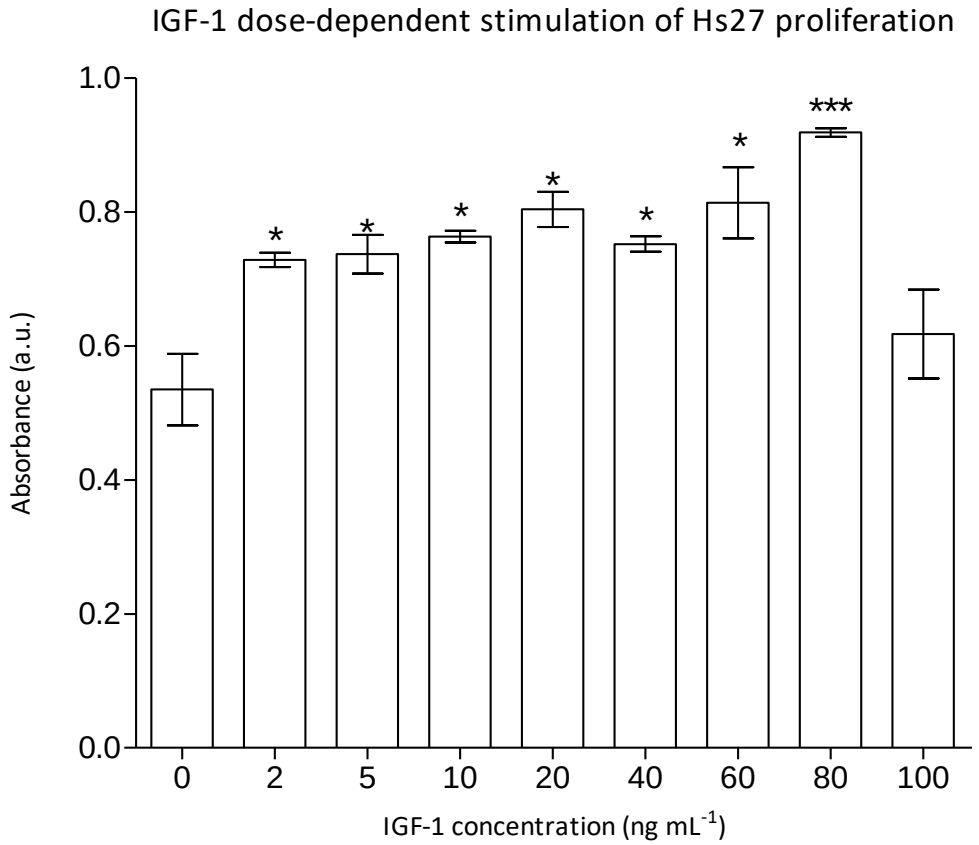

Figure 6.6 Graph showing MTT assay absorbance values, which are representative of Hs27 cell proliferation at a cell seeding density of 4000 cells mL^{-1} while varying the concentration of IGF-1 (2–100 ng mL^{-1}). The cells were cultured in DMEM media supplemented with 1 % penicillin-streptomycin and 10 % foetal bovine serum. Cells were incubated for 24 hours at 37 °C in an atmosphere of 5 % CO_2. Data shown as mean ± SD (n=6).), $p < 0.05$ (*), $p < 0.01$ (**), $p < 0.001$ (***).

The toxicity of the PVA-borate hydrogel towards each cell line was tested before applying IGF-1-loaded hydrogels to the cells. On applying a sample of the hydrogel directly on top of the cells for 1 hour, it was found to decrease cell viability significantly (HaCaT $p<0.01$ and Hs27 $p<0.001$) for both cell lines, as seen in Figure 6.7 and 6.8. The HaCaT cell viability decreased from 100.0 % to 28.9 ± 1.2 % and the Hs27 viability decreased from 100.0 % to 20.0 ± 0.8 %. Cells were also seeded on top of the hydrogel, but did not survive reaching zero viability within an hour. An alternative method was tried, whereby, the hydrogel was in contact with the media rather than in direct contact with the cells, as seen in Figure 6.2 in section 6.4.5. In using cell culture inserts, this mimicked the set up seen in the Franz diffusion cell

apparatus. The cell viability still decreased for both cells lines, but not to the same extent as it did on direct contact with the hydrogel. The HaCaT and Hs27 cell viability decreased to 62.0 ± 4.3 % and 48.0 ± 1.2 %, respectively on using a cell insert.

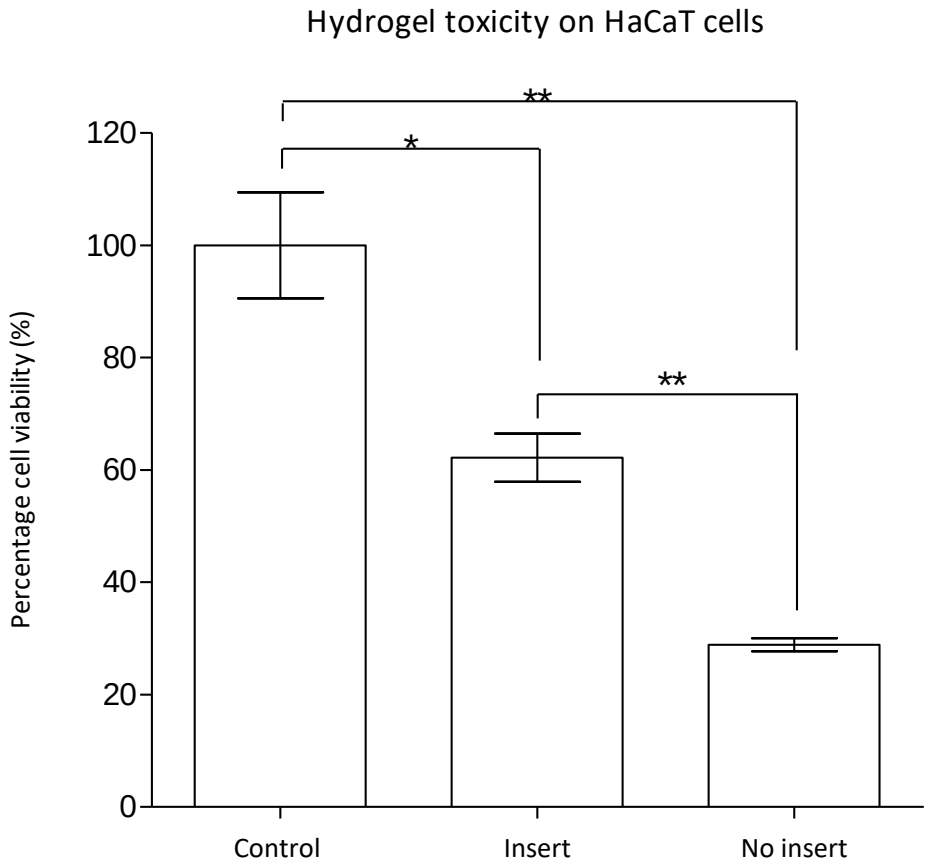

Figure 6.7 Graph showing hydrogel toxicity towards HaCaT cells when applied directly onto the cells (without insert) and non-direct contact (with insert). The cells were cultured in DMEM media supplemented with 1 % penicillin-streptomycin and 10 % foetal bovine serum. Cells were incubated at 37 °C in an atmosphere of 5 % CO_2. A PVA 6.0 % w/w borate 2.0 % w/w hydrogel was used. Data shown as mean ± standard deviation (n=6), $p < 0.05$ (*), $p < 0.01$ (**), $p < 0.001$ (***).

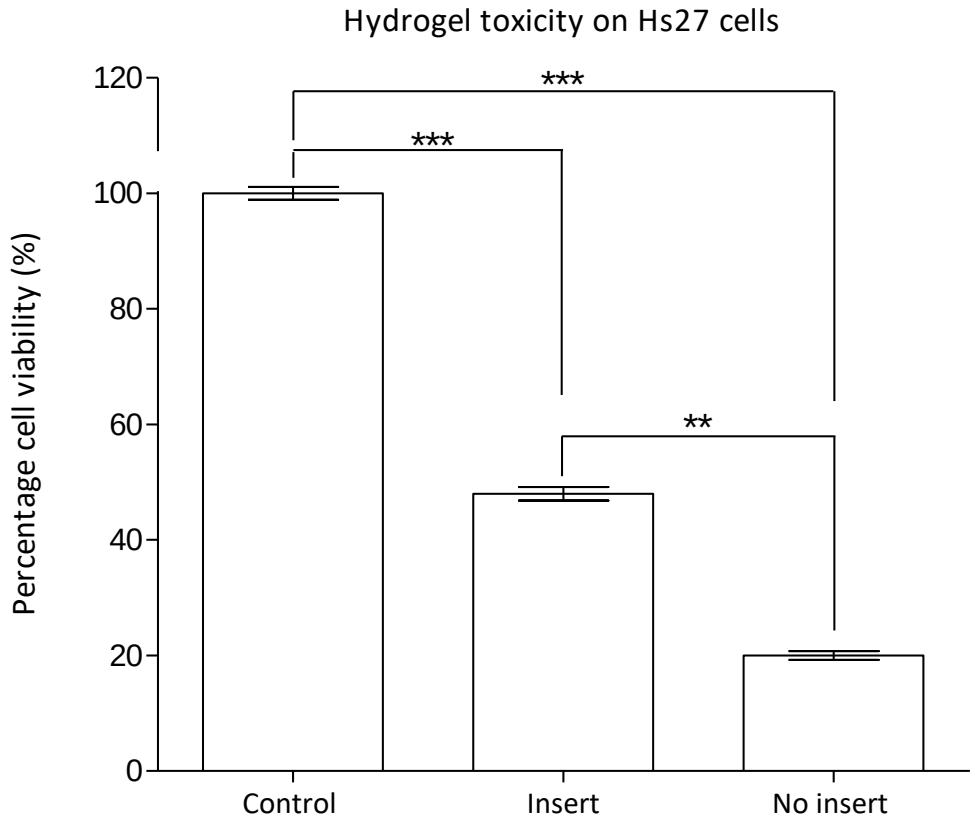

Figure 6.8 Graph showing hydrogel toxicity towards Hs27 cells when applied directly onto the cells (without insert) and non-direct contact (with insert). A PVA 6.0 % w/w borate 2.0 % w/w hydrogel was used. The cells were cultured in DMEM media supplemented with 1 % penicillin-streptomycin and 10 % foetal bovine serum. Cells were incubated at 37 °C in an atmosphere of 5 % CO_2. Data shown as mean ± standard deviation (n=6), $p < 0.05$ (*), $p < 0.01$ (**), $p < 0.001$ (***).

As a result of the findings seen in Figure 6.7 and 6.8, the decision was made to split the hydrogel into its two main components to investigate further if one had a more detrimental effect than the other. It can be seen in Figure 6.9 that as the PVA concentration in the media was increased from 8.0–12.0 % w/w the HaCaT cell percentage viability increased to a maximum of 146.4 ± 9.6 % relative to the control at 100.0 ± 9.5 %. However, on addition of 6.0 % w/w PVA the percentage cell viability decreased to 81.0 ± 5.1 %, but it is not a significant decrease ($p = 0.0788$). PVA 10.0 and 12.0 % w/w both caused significant increases with p values of 0.0051 and 0.0149, respectively.

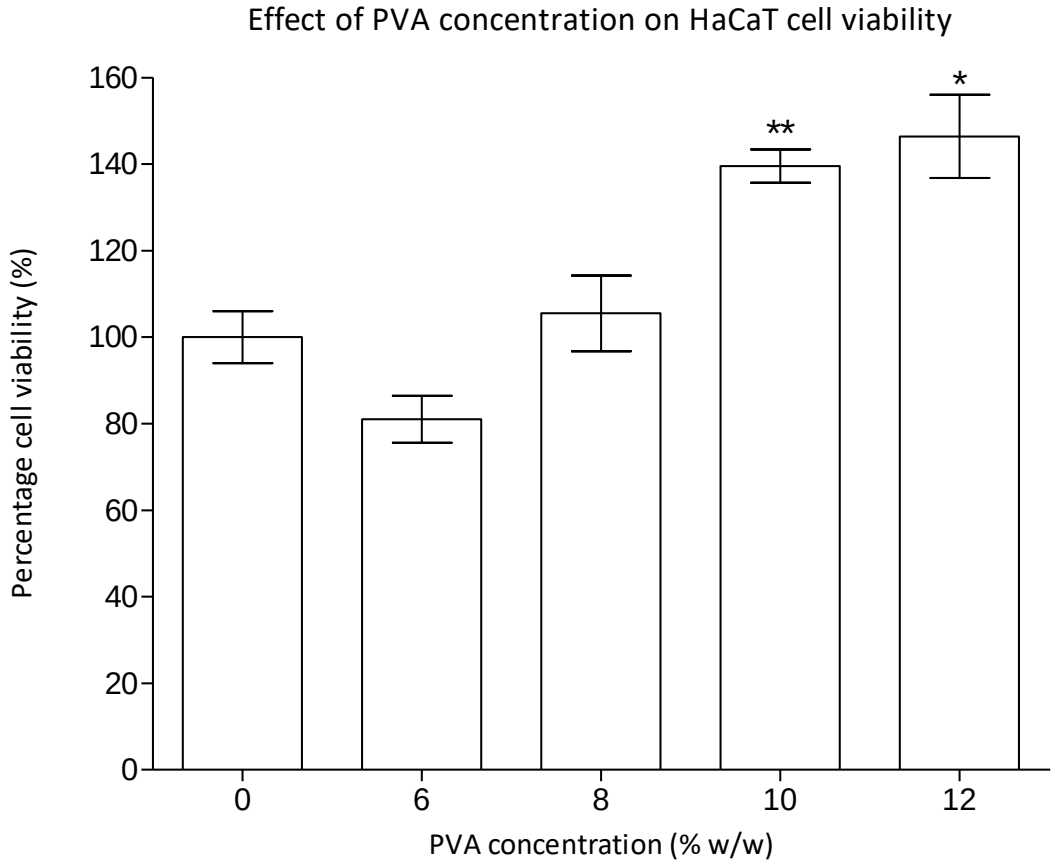

Figure 6.9 Graph showing the effect PVA concentration (6.0–12.0 % w/w) had on HaCaT cell viability when mixed directly into the media and incubated for 60 minutes. Cells were incubated at 37 °C in an atmosphere of 5 % CO_2. Data shown as mean ± standard deviation (n=6), $p < 0.05$ (*), $p < 0.01$ (**), $p < 0.001$ (***).

PVA had the same effect on the Hs27 cells but to a lesser extent (Figure 6.10). Only the 10.0 and 12.0 % w/w PVA concentrations caused an increase in percentage cell viability (110.7 ± 1.8 % and 128.5 ± 18.1 %), compared to the control group. Both the 6.0 and 8.0 % w/w PVA concentrations caused a decrease in cell viability 88.2 ± 6.3 % and 96.6 ± 9.5 %, respectively, compared to the control group. However, none of the changes were statistically significant ($p>0.05$). Therefore, it would seem that PVA being present in the media has less of an effect on the Hs27 cell viability, compared to the HaCaT cell viability.

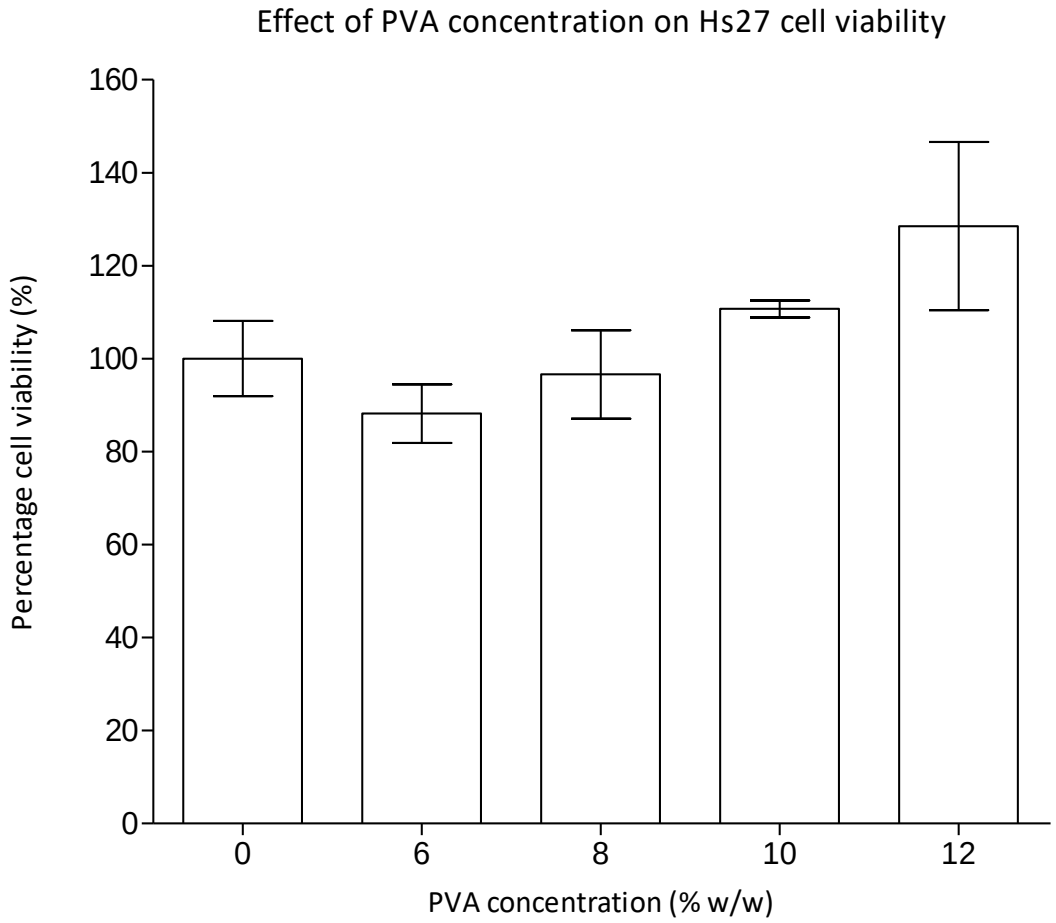

Figure 6.10 Graph showing the effect PVA concentration (6.0–12.0 % w/w) had on Hs27 cell viability when mixed directly into the media and incubated for 60 minutes. Cells were incubated at 37 °C in an atmosphere of 5 % CO_2. Data shown as mean ± standard deviation (n=6), $p < 0.05$ (*), $p < 0.01$ (**), $p < 0.001$ (***).

Borate, the second component of the hydrogel system, was added to the media in the same way as the PVA in a range of concentrations (0.5–2.5 % w/w). It was found that as the borate concentration increased in the media, the HaCaT percentage cell viability decreased significantly ($p<0.01$), as seen in Figure 6.11. The highest concentration of borate (2.5 % w/w) gave the largest decrease in percentage cell viability from 100.0 ± 6.0 % for the control group to 12.4 ± 0.1 %. The same trend was seen for the Hs27 cell line (Figure 6.12), with increasing borate concentration the cell viability decreased. Again, the largest decrease was observed in the group treated with 2.5 % w/w borate, which reduced the cell viability from 100.0 ± 8.1 %

to 38.7 ± 6.5 %. However, the decrease in percentage cell viability was not as significant across all the borate concentrations in the Hs27 cell line as it was for the HaCaT cells. Therefore, it would seem that borate also has a lesser effect on the Hs27 cells, compared to the HaCaT cells, the same trend seen for PVA.

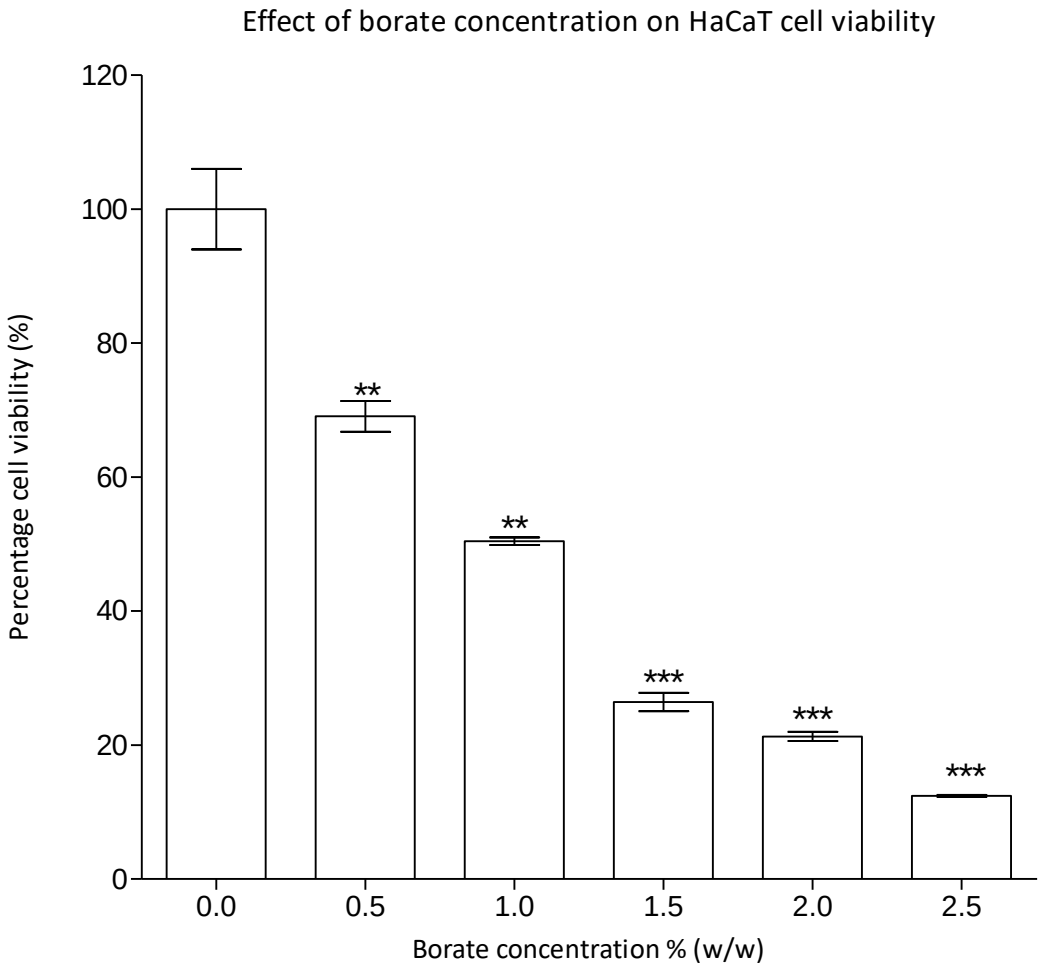

Figure 6.11 Graph showing the effect borate concentration (1.0–2.5 % w/w) had on HaCaT cell viability when mixed directly into the media and incubated for 60 minutes. Cells were incubated at 37 °C in an atmosphere of 5 % CO_2. Data shown as mean ± standard deviation (n=6), $p < 0.05$ (*), $p < 0.01$ (**), $p < 0.001$ (***).

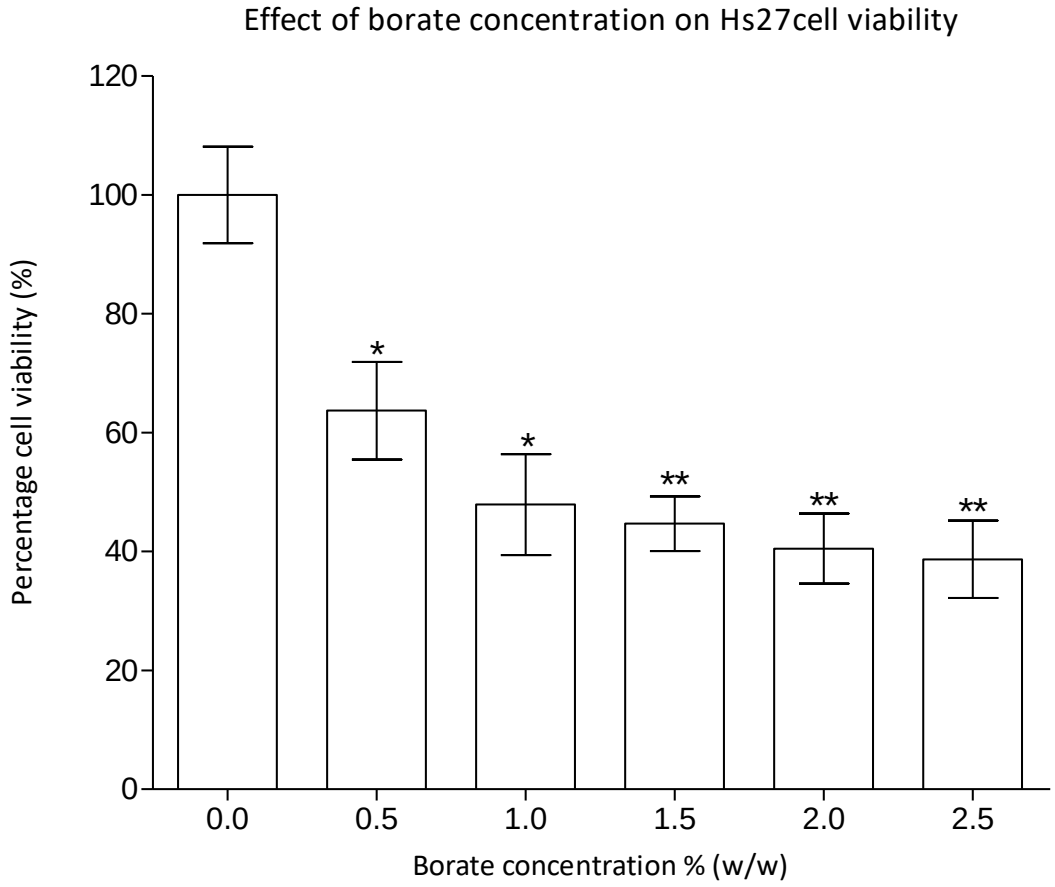

Figure 6.12 Graph showing the effect borate concentration (1.0–2.5 % w/w) had on Hs27 cell viability when mixed directly into the media and incubated for 60 minutes. Cells were incubated at 37 °C in an atmosphere of 5 % CO_2. Data shown as mean ± standard deviation (n=6), $p < 0.05$ (*), $p < 0.01$ (**), $p < 0.001$ (***).

Scratch assays were carried out on monolayers of both cell lines and treated with the appropriate treatments, as stated in the method section 6.4.5. Figure 6.13 shows the rate at which the HaCaT cells closed the scratch when exposed to each of the treatments. It can be seen that free IGF-1 (20 ng) caused the scratch to close within 24 hours post scratching. The IGF-1-loaded hydrogel had almost closed the scratch within 24 hours as only as small part at either end of the scratch remained not closed (Figure 6.13). However, the scratch treated with the IGF-1-loaded hydrogel had completely closed by hour 36. The blank hydrogel closed the scratch faster than the negative control, but, slower than the IGF-1-loaded hydrogel. A larger portion of the scratch had not closed at 24 hours for the blank hydrogel treated cells, compared to

the IGF-1-loaded hydrogel. Interestingly, the blank hydrogel did cause the scratch to be completely closed by hour 36, in comparison to the control group, which was still partially open at hour 36.

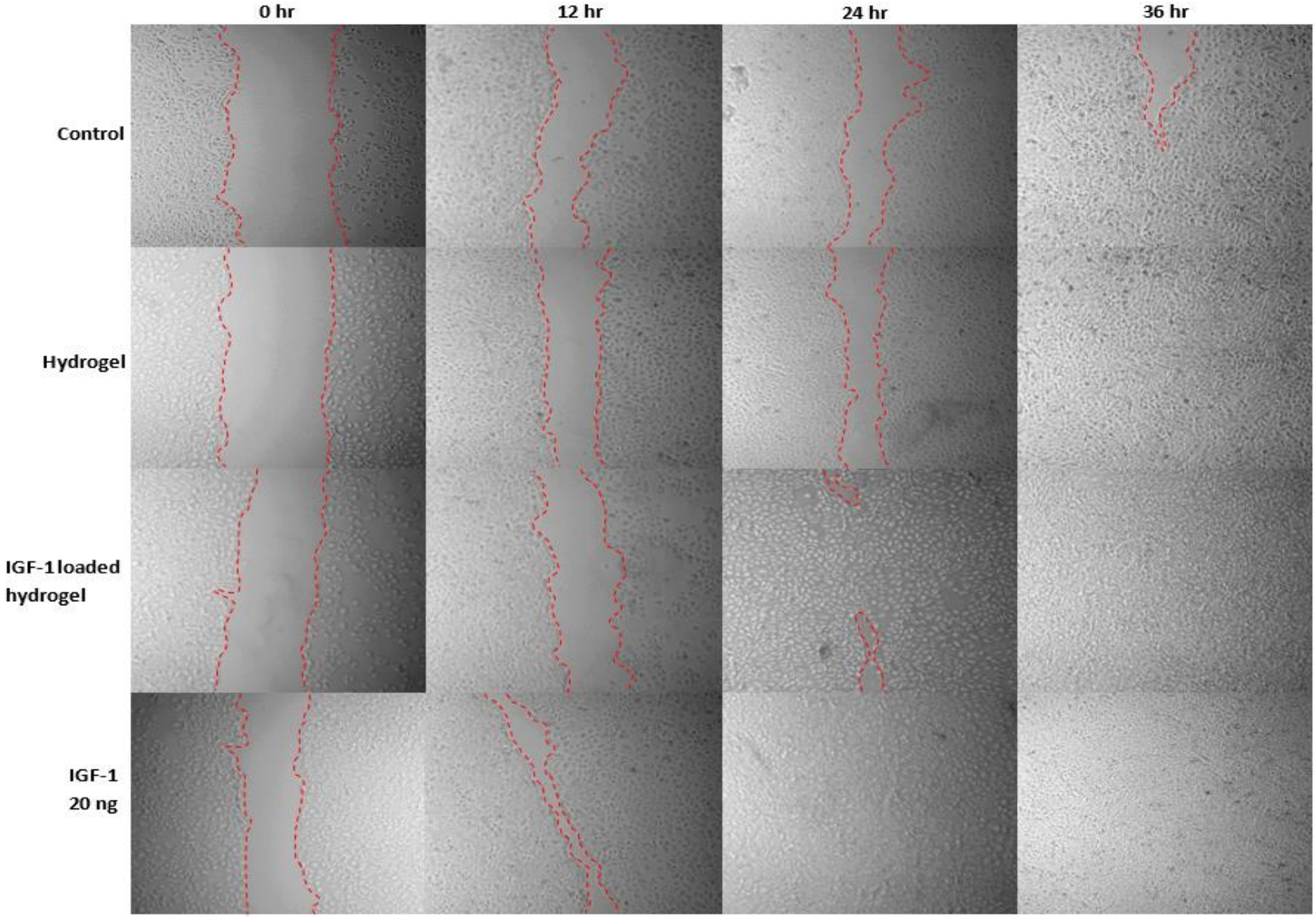

Figure 6.13 Representative images at each time point for each of the four treatment groups of a scratch assay study on HaCaT cells. Cells were incubated for 36 hours at 37 ℃ in an atmosphere of 5 % CO_2.

Figure 6.14 quantifies the qualitative data seen in Figure 6.13. After 12 hours, the free IGF-1 and IGF-1-loaded hydrogel had closed 97.32 ± 0.27 % and 96.32 ± 0.13 % of the scratch, respectively, compared to the control, which had achieved 50.00 ± 10.08 % closure after 12 hours. The blank hydrogel had closed 38.06 ± 6.48 % of the scratch, which was less than the control at 12 hours. By 24 hours, the rate of closure slowed down, with the HaCaT scratch treated with the IGF-1-loaded hydrogel only closing a further 1.40 % to a total closure of 98.72 ± 0.32 %. The cells treated with free IGF-1 achieved a scratch closure of 97.54 ± 0.27 %, at 24 hours.

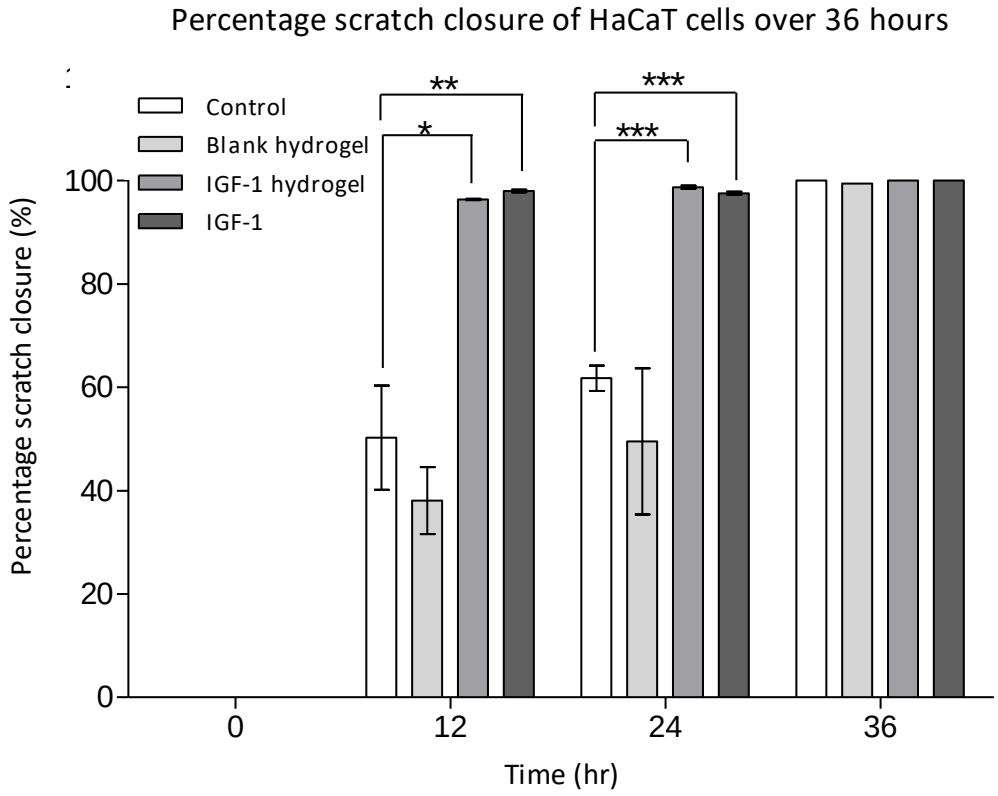

Figure 6.14 Graph showing percentage scratch closure HaCaT cells over a 36-hour period when exposed to three different treatments. Cells were incubated at 37 °C in an atmosphere of 5 % CO_2. Data shown as mean ± standard deviation (n=3).), $p < 0.05$ (*), $p < 0.01$ (**), $p < 0.001$ (***).

The Hs27 fibroblasts closed the scratch faster than the HaCaT keratinocytes. It can be seen in Figure 6.15 that by 24 hours, all 4 treatment groups had achieved 100.00 % scratch closure, compared to the HaCaT cells, which took 36 hours. The Hs27

cells followed the same general pattern as the HaCaT cells with the free IGF-1 and IGF-1-loaded hydrogel achieving the quickest scratch closure, in comparison to the blank hydrogel and control group. By hour 12, the free IGF-1 and IGF-1-loaded hydrogel had caused the cells to achieve 100.00 % scratch closure with the blank hydrogel and control group achieving 100 % closure by hour 24.

The graph seen in Figure 6.16 quantifies the qualitative data seen in Figure 6.15. It can be seen that at 6 hours the hydrogel loaded with IGF-1 and the free IGF-1 drug had caused 62.31 ± 2.28 % and 77.91 ± 2.51 % of the scratch to close, respectively, compared to the control group, which had achieved 44.34 ± 6.51 % closure. By hour 12, the free IGF-1 and the hydrogel loaded with IGF-1 had both achieved complete scratch closure. The cells treated with the blank hydrogel had achieved 86.42 ± 13.58 % closure, compared to the control group, which had 54.42 ± 8.69 % closure at 12 hours. At 24 hours, these two treated groups had reached 100.00 % closure. Therefore, in comparison to the HaCaT cells, the Hs27 cells achieved total scratch closure over a shorter time period. The free IGF-1 and IGF-1-loaded hydrogel treated HaCaT groups reached 100.00 % closure by 24 and 36 hours, respectively, compared to the Hs27 groups, which reached 100 % closure by 12 and 24 hours for the same treatment groups. The Hs27 cell group treated with blank hydrogel and the control group both achieved 100.00 % scratch closure by 24 hours. Whereas, the HaCaT group treated with blank hydrogel took 36 hours to reach 100.00 % closure.

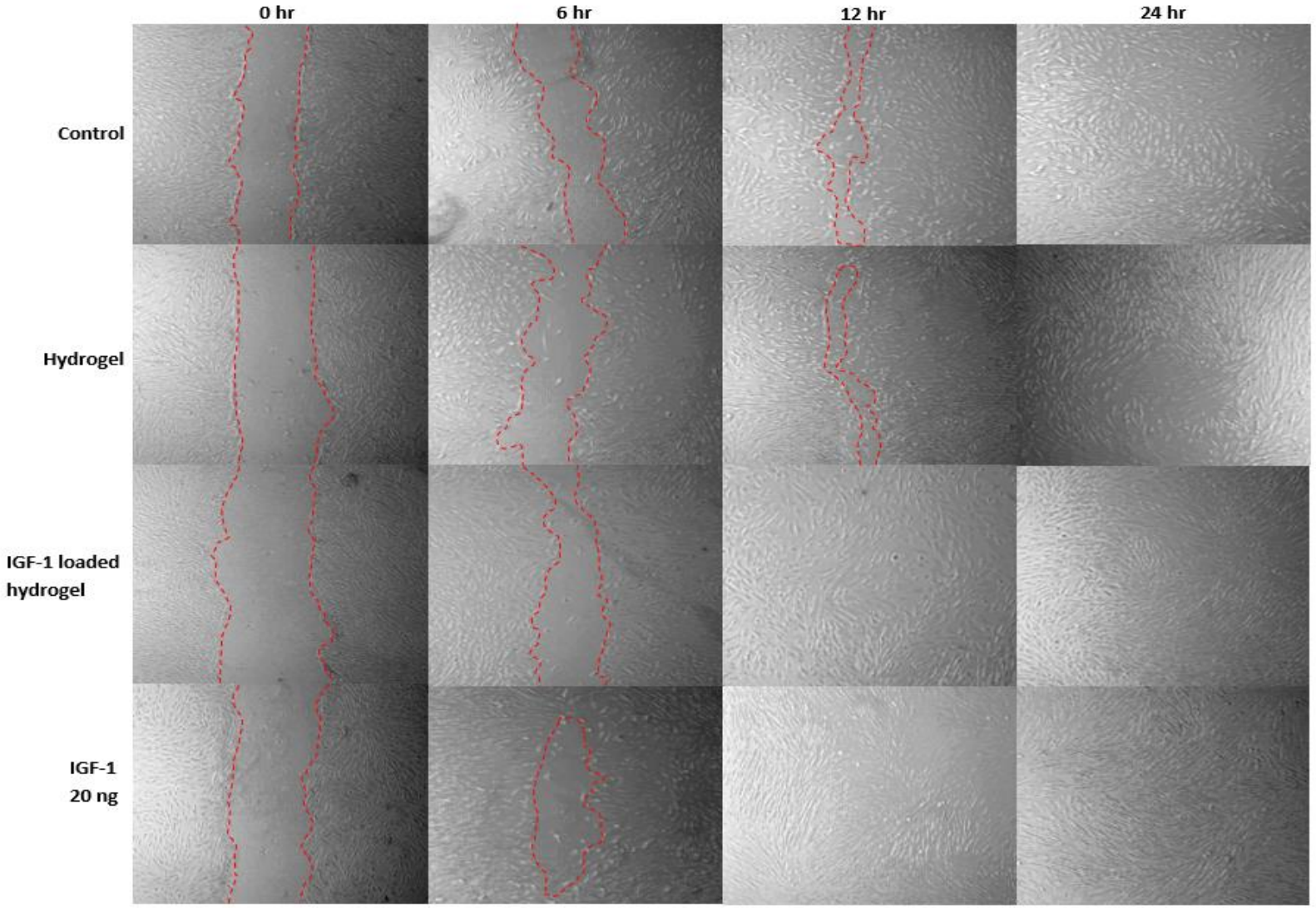

Figure 6.15 Representative images at each time point for each of the four treatment groups of a scratch assay study on Hs27 cells. Cells were incubated for 36 hours at 37 °C in an atmosphere of 5 % CO_2.

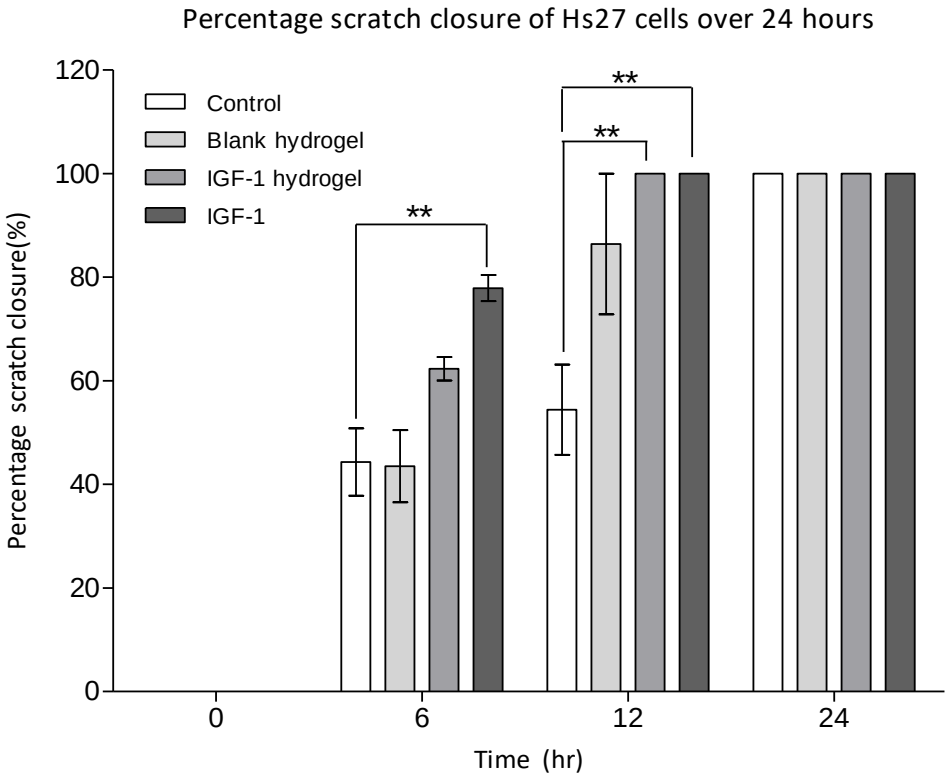

Figure 6.16 Graph showing percentage scratch closure Hs27 cells over a 36-hour period when exposed to three different treatments. Cells were incubated at 37 °C in an atmosphere of 5 % CO_2. Data shown as mean ± standard deviation (n=3).), $p < 0.05$ (*), $p < 0.01$ (**), $p < 0.001$ (***).

Immunofluorescent chemistry was used to determine if IGF-1 caused upregulation of the Akt cell signalling pathway. Figure 6.17 shows that HaCaT cells treated with raw IGF-1 (20 ng) displayed an increase in expression of phospho-Akt (p-Akt) protein, represented by green fluorescence, compared to the non-treated cells. It can be seen in Figure 6.18 that HaCaT cells treated with an IGF-1-loaded hydrogel also showed an increase in p-AKt expression, compared to the control, but to a lesser extent than the raw IGF-1 treated cells. Interestingly, it was also seen that the blank hydrogel used as another control also caused expression of p-AKt although less than the IGF-1-loaded hydrogel (Figure 6.18).

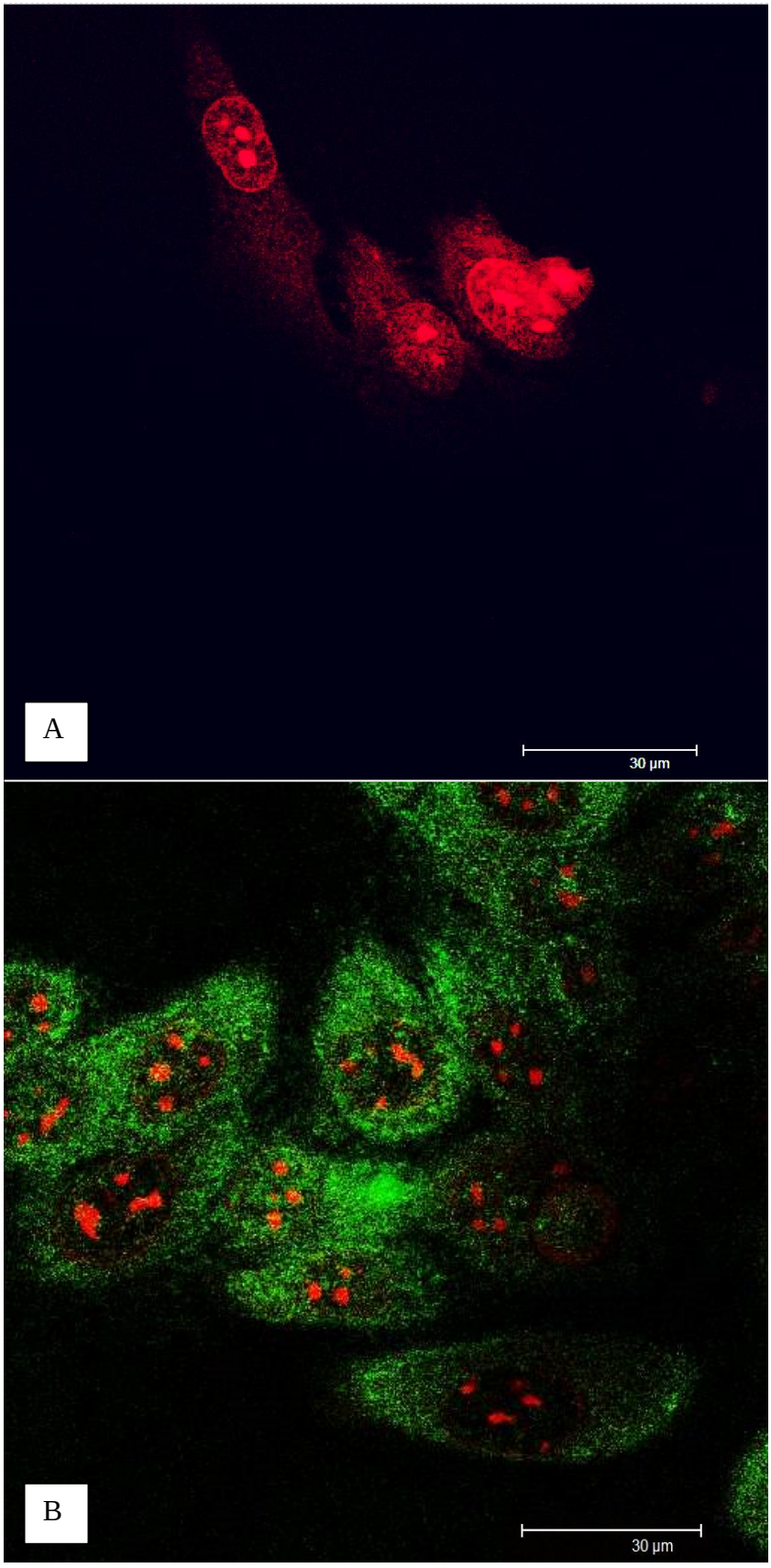

Figure 6.17 representative confocal immunofluorescent images of HaCaT cells A) no treatement and B) treated with 20 ng of raw IGF-1. Phospho-AKt (Ser473) (D9E) XP® rabbit mAb (green), actin filaments labelled with phalloidin (red) and nuclear label propidium iodide (red).

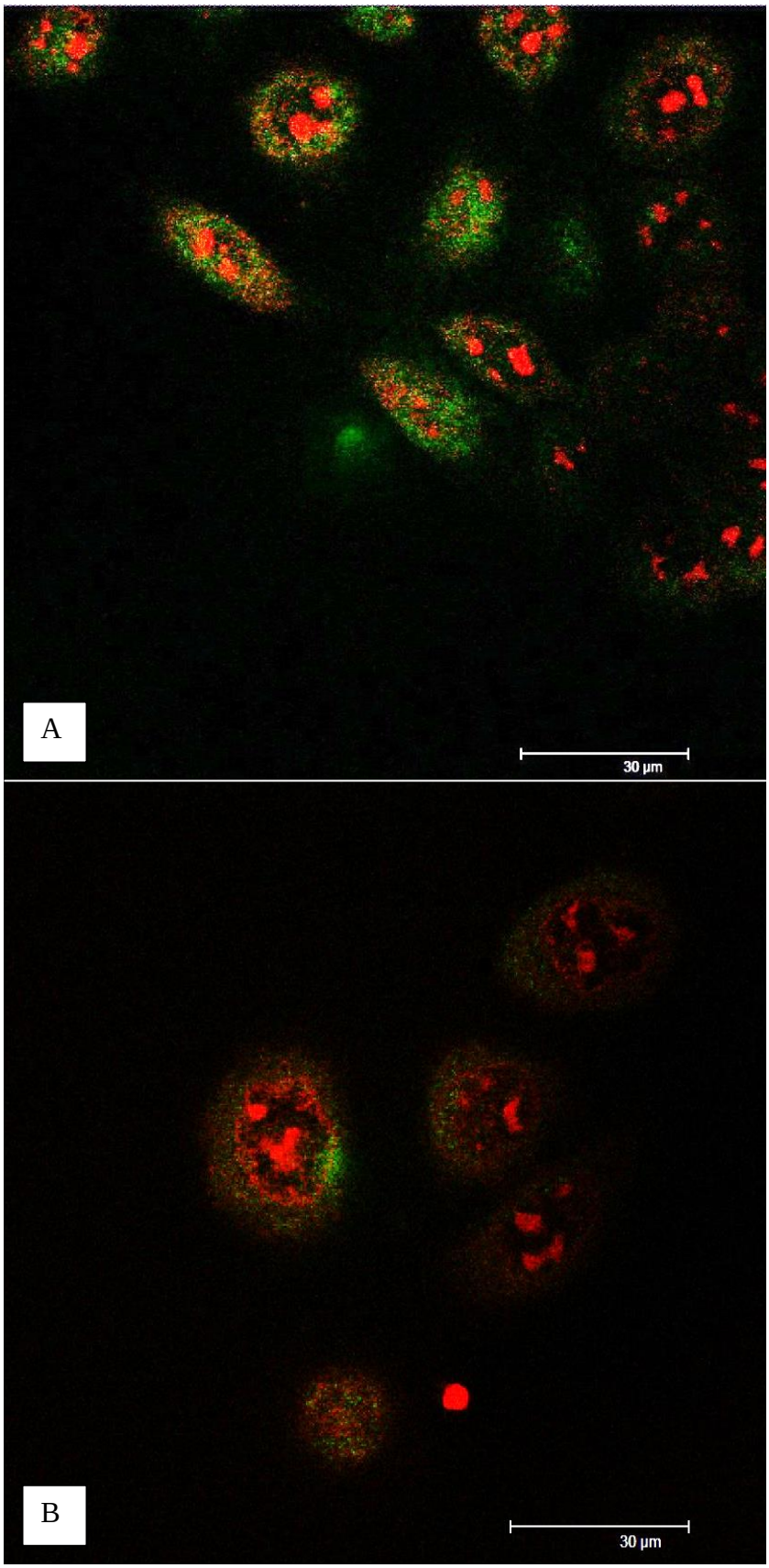

Figure 6.18 representative confocal immunofluorescent images of HaCaT cells A) treated with an IGF-1-loaded hydrogel and B) treated with blank hydrogel. Phospho-AKt (Ser473) (D9E) XP® rabbit mAb (green), actin filaments labelled with phalloidin (red) and nuclear label propidium iodide (red).

There was no green fluorescence exhibited by any of the Hs27 cell groups. Therefore, either there was experimental error or IGF-1 triggers a different cell signaling pathway in fibroblast cells, compared to the HaCaT cells. Representative images taken of each the different treated groups of the Hs27 fibroblasts can be seen in Figures 6.19.

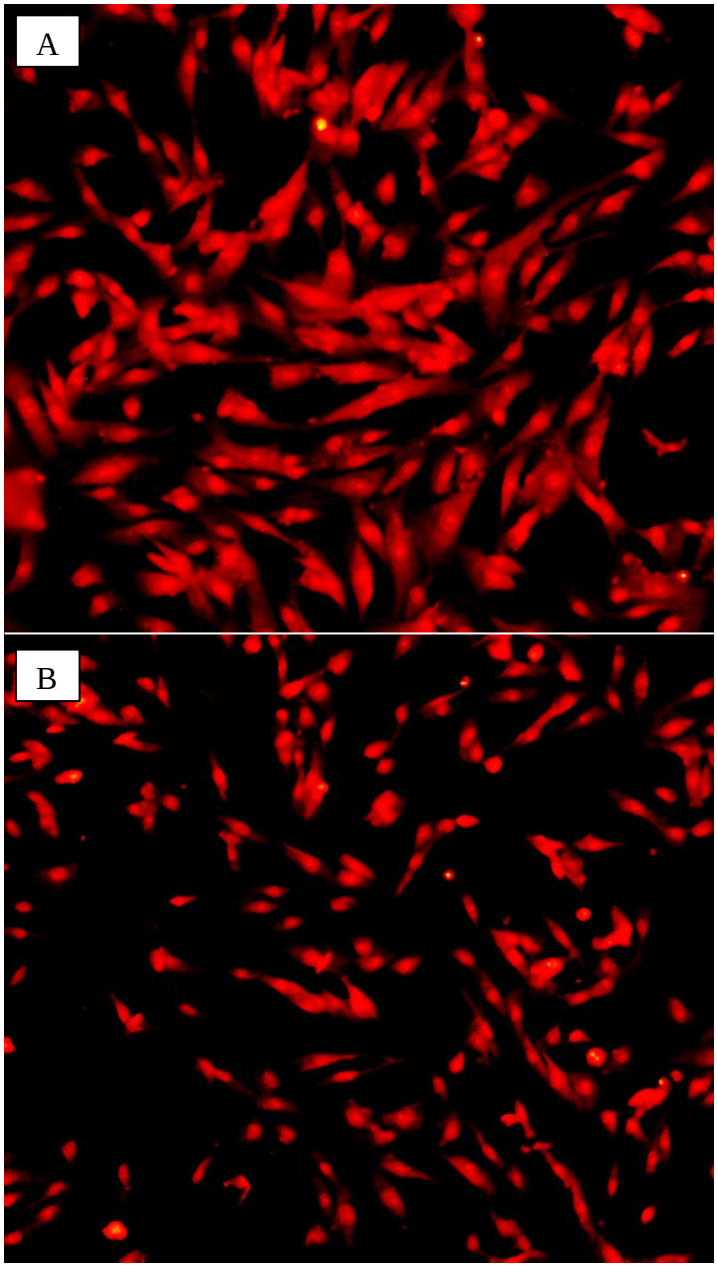

Figure 6.19 representative confocal immunofluorescent microscope images of Hs27 cells A) treated with 20 ng of raw IGF-1 and B) no treatment. Phospho-AKt (Ser473) (D9E) XP® rabbit mAb (green), actin filaments labelled with phalloidin (red) and nuclear label propidium iodide (red).

6.6 Discussion

Insulin-like growth factor-1 has been studied extensively in cell cultures as a potential therapeutic drug to aid wound healing due to its ability to stimulate cell proliferation and migration (Ando & Jensen, 1993; Bhora *et al.*, 1995; Beckert *et al.*, 2005; Lee *et al.*, 2006). In this chapter, the aim was to determine if the PVA-borate hydrogel could deliver biologically active IGF-1 to keratinocytes and fibroblasts, stimulating an increase in cell proliferation and migration.

The keratinocytes (HaCaT) and fibroblasts (Hs27) used in this study both demonstrated time-dependent proliferation in serum-supplemented media. This was an expected finding, as the longer the cells are incubated, the more time they have to proliferate. On completion of a dose-response curve, it was found that as the concentration of IGF-1 increased (2–100 ng mL^{-1}) so did HaCaT cell proliferation. This indicates that stimulation of proliferation by IGF-1 is dose-dependent for HaCaT cells. Similarly, Pozzi *et al.* (2004) demonstrated IGF-1 dose-dependent HaCaT proliferation. Pozzi *et al.* (2004) used an IGF-1 concentration range of 1–100 ng mL^{-1}, with the increase in proliferation not significant until 5 ng mL^{-1} was reached (Pozzi *et al.*, 2004). In comparison, there was a significant ($p<0.001$) increase in cell proliferation by the HaCaT cells in this investigation at 2 ng mL^{-1}. The Hs27 cells displayed a significant ($p<0.01$) increase in cell proliferation on addition of 2–80 ng mL^{-1} of IGF-1. However, the general trend seen for the HaCaTs was not observed for the Hs27 cells. The 100 ng mL^{-1} IGF-1 concentration did not cause a significant ($p = 0.3850$) increase in Hs27 proliferation compared to the control. Yet, Telasky *et al*. (1998) found 100 ng mL^{-1} of IGF-1 to cause a significant ($p<0.05$) increase in proliferation of human dermal fibroblast cells over a period of 5 days. IGF-1 was found to increase cell proliferation of the MCF-7 breast cancer cell line in a dose-

dependent manner, indicating that increased levels of IGF-1 promotes the metastasis, survival and motility of cancer cells (Surmacz *et al.*, 1998; Borowiec *et al.*, 2007).

PVA is used widely in the pharmaceutical industry due to it being a biocompatible polymer (Kadajji & Betageri, 2011). Hans *et al*. (2014) and Loughlin *et al*. (2008) both state the PVA-borate hydrogel is a non-toxic, biocompatible delivery system. However, on application of a sample of PVA-borate hydrogel directly on top of the keratinocytes and fibroblasts used in this work, both cell types exhibited a significant ($p<0.01$ and $p<0.001$, respectively) decrease in cell viability. An explanation for this may be due to the unique viscoelastic flow properties of the PVA-borate hydrogel. It may be that on application to the top of the cells, the hydrogel began to flow over the cells until flow was inhibited by the edge of the well. This would result in the cells being completely starved of oxygen as gas exchange could no longer take place efficiently. Also, as the hydrogel is denser than the DMEM media the gel sank down to the bottom of the well on top of the cells displacing the media. This meant that the media was no longer in contact with the cells, starving them of vital nutrients. Another reason may be due to the leaching of borate from the hydrogel into the media. Murphy *et al.* (2012) documented that boron species do diffuse out of the PVA-borate hydrogel over a period of time, when in contact with a liquid phase. However, the quantity released was deemed to be not toxic to humans (Murphy *et al.*, 2012). Nevertheless, cells are fragile in comparison to the whole human body. Therefore, if a small quantity of borate is diffusing into the media it may kill the cells directly or through changing the pH of the media. Borate is a low toxic mineral, which can exhibit toxicity towards cell cultures and to humans if ingested in large quantities (Pongsavee, 2009). An experiment was devised, whereby, the hydrogel was indirectly in contact with cells via the media,

rather than being directly in contact with the cells themselves. This was achieved using cell culture inserts, as seen in Figure 6.2, section 6.4.5. Interestingly, this approach was found to reduce the decrease in cell viability observed in both cell lines caused by direct contact. Likewise, Smith *et al*. (2006) found that when a poly(*N*-vinylpyrrolidinone) (PNVP) gel was in contact with the media and not in direct contact with the cells, the drop in cell viability was also reduced. Smith *et al*. (2006) proposed two reasons why the gel may increase cell proliferation and maintain cell viability when not in direct contact with the cells. First, the gel may uptake small quantities of nutrients from the media and mitogenic factors released from the cells. The gel may then release these at a later time, or, as the gel uptakes mitogens, it stimulates more mitogens to be released by the cells resulting in the gel acting as a mitogen factor reservoir (Smith *et al.*, 2006). Second, the gel may be acting as a filter, removing metabolic waste from the media across a concentration gradient, helping to maintain a favourable environment for cell survival and proliferation (Smith *et al.*, 2006).

The hydrogel was split into its two components, PVA and borate, and added to both cell types separately. This was to ascertain if one component was more toxic towards either of the cell types than the other. It was observed that on increasing the PVA concentration, the cell viability of both the cell types increased, indicating an increase in cell proliferation. In a similar manner, PNVP was found to have a stimulatory effect on the proliferation of human dermal fibroblasts (Smith *et al.*, 2006). Yang *et al*. (2010) stated that extracts of a PVA-ws-chitosan-glycerol hydrogel when applied to L929 mouse fibroblasts show no toxicity and increases the cell viability. Addition of PVA to the culture media of 3T3 mouse fibroblast cells, which were then incubated for 24 hours was found to have no toxic effect towards

the fibroblasts and have no negative effect on mitochondrial activity (Oliveira *et al.*, 2014). Similarly in this study, PVA was found to have no toxic effect on Hs27 human fibroblast or HaCaT keratinocytes.

On adding a range of concentrations of borate to both cell types, it was found that on increasing the borate concentration, the cell viability decreased for both cell lines. Therefore, this suggests that it is the borate within the hydrogel that is causing the cytotoxic effects of the PVA-borate hydrogel. Pongsavee (2009) found that borate concentrations of 0.1–0.6 mg mL^{-1} causes a decrease in lymphocyte cell proliferation and changes within the DNA of lymphocytes.

From the scratch assays, it was confirmed that free IGF-1, IGF-1-loaded PVA-borate hydrogel and, interestingly, the blank hydrogel all closed the scratch faster than the control, for both cell lines. Topical application of a PVA-ws-chitosan-glycerol hydrogel, containing no therapeutic drug, to full-thickness wounds on Sprague-Dawlrey rats was found to increase the rate of wound healing in comparison to a normal gauze dressing (Yang *et al.*, 2010). The increase in wound healing is thought to be attributed to the hydrogel's ability to maintain adequate moisture in the wound, which is thought to increase the migration of the cells in the epidermis (Yang *et al.*, 2010). Chitosan is also believed to stimulate fibroblast migration and inflammatory cells, enhancing wound healing (Yang *et al.*, 2010). However, in this investigation, the scratch in the cells was already kept hydrated, due to the liquid media and also there was no chitosan present. Another explanation could be that the PVA from the hydrogel is leaching into the media as the hydrogel begins to swell and disintegrate. However, as previously mentioned, boron species will also be present, most likely as boric acid (Murphy *et al.*, 2012). As the scratch assays are carried out in larger 12-well plates, the volume of media required in each well is

more than that required for the 96-well plates that the PVA and borate toxicity studies where completed in. Therefore, the borate that is released into this larger volume of media may result in a lower borate concentration in the media. A lower concentration of borate may not affect the cell viability to the same extent as higher concentrations in the toxicity studies. If this is the case, then the stimulatory effect seen by the PVA in the toxicity study may have a greater effect on the cells than the toxic effect of the borate. Thus, explaining why the rate of the scratch closure was faster for the blank hydrogel than the control group.

The free IGF-1 and IGF-1-loaded hydrogels both exhibited a greater reduction in the scratch area over the allocated time, compared to the blank hydrogel and control group, for both cell types. Similarly, Ando & Jensen (1993) found that addition of IGF-1 (1–50 ng mL^{-1}) to keratinocyte cells caused a dose-dependent increase in migration of the keratinocyte cells, compared to the control group. Therefore, this indicates that IGF-1 is causing a stimulatory effect on cell migration and, as a result, covering the scratch area faster than the control group. Likewise, Haase *et al*. (2003) found that adding 100 ng mL^{-1} of IGF-1 to primary human keratinocytes caused an increase in the rate of the scratch closure in comparison to the non-treated group. Human corneal epithelial cells (HCEC) were cultured until a monolayer formed and where then scratched in a similar manner to the method used in this investigation (Lee *et al.*, 2006). The HCEC were treated with 10 and 50 ng mL^{-1} of IGF-1 and incubated for 12 hours. Similar to what was found in this chapter, Lee *et al*. (2006) found that addition of IGF-1 to the scratched HCEC monolayer resulted in increased migration and proliferation in comparison to the control group. They also found that IGF-1 stimulated the release of LN-5, an ECM component that aids in epithelial cell migration and adhesion (Lee *et al.*, 2006). Emmerson *et al*.

(2012) carried out scratch assays on monolayers of primary human epidermal keratinocytes and dermal fibroblast, concluding that addition of IGF-1 to the media of both cell types resulted in an increase in the percentage closure of the scratch compared to the control group. Beckert *et al*. (2005) found that addition of IGF-1 released from a PVA film and methylcellulose gel to L929 mouse fibroblasts caused an increase in cell proliferation. Topical administration of IGF-1 released from a PVA film, which was attached to a hydrogel dressing and applied to full-thickness wounds on Sprague-Dawley rats was also found to cause an increase in wound healing (Beckert *et al.*, 2005). The findings from the study in this chapter and Beckert *et al.* (2005) would indicate that a topical PVA based delivery system for IGF-1 may be beneficial for wound healing. Other *in vivo* wound healing experiments, which involved the administration of IGF-1 to enhance wound healing have been carried out by several researchers (Tsuboi *et al.*, 1995; Koshizuka *et al.*, 1997; Provenzano *et al.*, 2007; Nunes Achar *et al.*, 2014). All of these studies concluded that administration of IGF-1 alone or in combination with other growth factors increased the rate of wound healing in comparison to the non-treated control groups. Interestingly, Tsuboi *et al*. (1997) found that co-administering insulin-like growth factor binding protein-1 (IGFBP-1) along with IGF-1, further enhanced the healing of full-thickness skin wounds in diabetic mice and normal rabbits, compared to IGF-1 alone. IGFBPs are a family of binding proteins, whose main function in the body are to increase the half-life of circulating IGF-1 from a few minutes to 30 minutes by preventing proteolytic degradation of the IGF-1 (Laviola *et al*., 2007). Once the IGF-1 is bound to the IGFBP, a third component known as the acid labile subunit can also bind forming a tertiary complex (Laron, 2001). This further extends the half-life of the IGF-1 to approximately 12–15 hours (Rosenfeld *et al*., 1999).

IGF-1 is thought to stimulate cell proliferation and migration through different intracellular signaling pathways, but mainly by way of the Akt pathway (Vincent & Feldman, 2002). In this investigation, immunofluorescent chemistry was used to detect if the Akt pathway within the keratinocyte and fibroblast cells was up-regulated and, therefore, the reason for increased cell proliferation and migration of the cells on addition of IGF-1. Akt was found to be phosphorylated in the keratinocyte cells on addition of both free IGF-1 and IGF-1 that was released from the PVA-borate hydrogel, in comparison to the negative control group. Also, there was a modest phosphorylation of Akt in HaCaT cells treated with the blank hydrogel. This is in keeping with the scratch closure results mentioned previously. However, the exact mechanism of how the blank hydrogel is activating the Akt pathway is unknown. But, as discussed previously, it may due to the PVA, which was also seen to cause an increase in cell proliferation when added alone to the media. It is unlikely, but, not impossible, that the PVA is activating one of the many cell surface receptors as these are ligand-specific receptors. IGF-1 causes phosphorylation of Akt through a cascade of events, which occurs on binding of IGF-1 to the IGF-1 transmembrane receptor. Several adaptor molecules interact with the activated IGF-1R, mainly insulin receptor substrate-1 and 2 (IRS-1 and 2) (Laviola *et al.*, 2007). On interaction with the receptor, the IRS becomes phosphorylated and activates phosphoinositide 3-kinase (PI3K). PI3K leads to the production of membrane-associated inositol, which also undergo phosphorylation (Stitt *et al.*, 2004). The inositol then attracts and activates phosphoinositide-dependent kinases (PDKs), which activates Akt protein kinase B (Stitt *et al.*, 2004). Akt then stimulates protein synthesis and gene transcription leading to cell proliferation and migration (Laviola *et al.*, 2007). Similar to the results found in this investigation, IGF-1 was found to

upregulate the Akt pathway via phosphorylation in primary human keratinocytes (Haase *et al.*, 2003), HCECs (Lee *et al.*, 2006), MCF-7 breast cancer cells (Dufourny *et al.*, 1997; Borowiec *et al.*, 2007) and mouse lung-tumour epithelial cells (Fritz *et al.*, 2011). Lee *et al*. (2006) also document that the ERK pathway was already phosphorylated on addition of IGF-1, but, that IGF-1 increased ERK phosphorylation.

It is uncertain if IGF-1 caused phosphorylation of the Akt pathway in the Hs27 fibroblast cells as no phosphorylated Akt (pAkt) was detected in the immunofluorescent visualisation. This may have been due to error in the experimental procedure. However, the experiment was repeated several times using the exact same protocol as for the HaCaT keratinocyte cells. Another possibility is that the fibroblast cells utilise another intracellular pathway to trigger cell proliferation, differentiation and migration. Activation of the IGF-1 receptor has been shown to trigger other pathways, such as the ERK and MAPK pathways (Vincent & Feldman, 2002; Lee *et al*. 2006; Laviola *et al*., 2007; Fritz *et al*., 2011). Both these cell signaling pathways are known to promote cell migration and proliferation (Vincent & Feldman, 2002). Vincent & Feldman (2002) concluded in their review of the IGF signaling pathways that activation of the IGF-1R leads to activation of multiple signaling pathways through phosphorylation, to promote cell survival. However, IGF-1 was found to phosphorylate Akt through PI3K in human foetal lung fibroblast (Chetty *et al.*, 2006). But, it is hard to compare this to skin fibroblast cells as fibroblast cells found in different body tissue and, indeed, within the same tissue have different characteristics and differentiate differently (Tracy *et al.*, 2016).

The Hs27 fibroblasts displayed a faster rate of closure for the IGF-1-loaded hydrogel, blank hydrogel and control groups, compared to the HaCaT keratinocytes. Likewise, Walter *et al*. (2010) found that L929 mouse fibroblasts closed the scratch area faster than HaCaT keratinocytes in both the treated and non-treated groups. It was also found that in co-culturing of both cell types the fibroblast cells still migrated into the scratch area before the keratinocytes (Walter *et al.*, 2010).

Haase *et al*. (2003) state that keratinocyte cells migrate by a crawling-like process known as lamellipodial locomotion. Lamellipodial locomotion of the keratinocytes involves the extension of the plasma membrane at the front of the cell and contraction of the cell body at the rear of the cell (Sixt, 2012). In order to crawl effectively, Haase *et al*. (2003) concluded from their investigation that there needs to be both IGF-1 and epidermal growth factor (EGF) present in adequate concentrations. They state that IGF-1 triggers the plasma membrane extension, facilitating cell spreading and EGF stimulates the contraction at the rear of the cell. Haase *et al*. (2003) deduced that IGF-1 primarily activates the PI3K/Akt signaling pathway and EGF activates the MAPK/ERK pathway. However, they found that IGF-1 on its own did cause an increase in random cell migration of the primary human keratinocytes, but, concluded that for a complex process of *in vivo* wound re-epithelisation both growth factors would need to be present in adequate amounts (Haase *et al.*, 2003). Restricted crawling leading to reduced random migration may explain why the HaCaT cells took longer to achieve complete scratch closure for the IGF-1-loaded hydrogel, blank hydrogel and control group compared to the same treatment groups of Hs27 fibroblast cells. It is documented that fibroblast cells migrate into the scratch as single non-clustering cells (Monsuur *et al.*, 2016). Fibroblasts present as spindle-shape, from which several cytoplasmic projections

extend outwards providing anchoring points for wound contraction (Velnar *et al.*, 2009; Trepat *et al.*, 2012). As a result of this, the fibroblasts may be able to cover the scratch area faster than the keratinocytes due to their ability to spread out over a large area. This may explain why the fibroblasts closed the scratch quicker, yet, in the growth curve study showed to be slower at proliferating than the keratinocytes. Alternatively, the keratinocyte cells are more rounded in shape and are known in an *in vivo* wound to migrate as one continuous edge (Baum & Arpey, 2005). Baum & Arpey (2005) state that the leading edge of keratinocyte cells differentiate to inhibit temporarily their ability to proliferate and that a close knitted layer of proliferation cells is laid down behind the leading edge. Fibroblast are known to be activate in wound healing prior to the re-epithelisation by keratinocytes (Velnar *et al.*, 2009). Fibroblasts are involved in the synthesis of extracellular matrix components, secretion of keratinocyte growth factor and the formation of granulation tissue (Li *et al.*, 2007; Enoch & Leaper, 2008). The keratinocytes begin to migrate over the granulation tissue as it is formed, re-epithelising the wound. As a result of this, some researchers have seeded keratinocytes on top of a fibroblast feeder layer, which have had their ability to proliferate inhibited to investigate the highly complex cross-talk and interactions between the two cell types and better replicate wound healing *in vivo* (Werner *et al.*, 2007). Despite this, no single cell culture or animal model can fully replicate the highly orchestrated, complex nature of the wound healing process as it occurs in the human body.

Pastar *et al*. (2018) state in their review of pre-clinical models for wound healing that two-dimensional cell culture models are unable to replicate, completely, biological events, such as the immune response, cell-cell interaction and cell-matrix interaction that occurs during wound healing *in vivo*. However, in recent year's

development of human skin equivalent three-dimensional organotypic models have shown to be a beneficial improvement on the two-dimensional model. The three-dimensional organotypic human wound model allows the recreation of the fundamental skin layers including the stratified epidermis (Pastar *et al.,* 2018). These cell models have shown to be able to maintain complex activities, such as hair follicle formation and migration (Oh *et al.,* 2013). Organotypic cell cultures display a basal keratinocyte proliferation rate similar to an *in vivo* wound (Garlick & Taichman, 1994). Despite these advantageous properties these models still lack the complexity of an *in vivo* human wound and cannot replicate complex processes, such as angiogenesis and inflammation (Oh *et al.,* 2013; Pastar *et al.,* 2018). Organotypic models are produced by seeding layers of fibroblasts harvested from human donors onto a dermal substrate. After several days of incubation, human harvested epidermal keratinocyte cells are then seeded on top of the fibroblast layer (Boutrand *et al.,* 2017). As a result, these 3D organotypic models can be fabricated from keratinocytes and fibroblasts harvested from chronic wounds, such as diabetic foot ulcers (Maione *et al.,* 2016) and keloids (Butler *et al.,* 2008). This provides *in vitro* models whereby the cells have the characteristic traits of the *in vivo* cells in the chronic wound from which they were harvested. MatTek Corporation sell a readily available 3D human skin equivalent model, called EpiDerm™. Miyana & Hughes (2016) used EpiDerm™ to assess the irritant effects of metallic nanoparticles towards the skin. EpiDerm™ is a reconstructed human epidermis consisting of human-derived epidermal keratinocytes for research use in academic and pharmaceutical settings (MatTek Corporation, 2018). Organotypic human skin equivalence models can be produced rapidly using a 3D bioprinter, as demonstrated by Cubo *et al,* (2016). They demonstrated that 100 cm^2 of 3D printed skin is

achievable in less than 35 minutes in comparison to several weeks when cultured manually (Cubo *et al.*, 2017). Human *ex vivo* skin wound models have also been used successfully to assess a wide variety of pharmaceutical agents on epithelialisation, such as EGF (Pastar *et al.*, 2018). The human skin isolates used in these models are obtained from reduction surgeries with the patients consent. As a result, these skin isolates can be expensive to acquire and are not readily available. Human skin isolates are advantageous over the previously mentioned models as the basement membrane integrity is maintained, the defined layers of the skin are maintained and they have similar gene expression patterns to human *in vivo* wounds (Andrew Chan *et al.*, 2008; Roupe *et al.*, 2010; Xu *et al.*, 2012). However, ultimately they still do not fully replicate an *in vivo* wound due to the lack of a blood supply and, therefore, immune cell infiltration (Pastar *et al.*, 2018).

6.7 Conclusion

On completion of the experimental work in this chapter, it was found that several concentrations of IGF-1 (2–100 ng mL^{-1}) caused an increase in cell proliferation in a dose-dependent manner for both HaCaT keratinocyte and Hs27 fibroblast cell lines. It was found that both cell lines did not tolerate the PVA-borate hydrogel being in direct contact, indicated by the significant ($p<0.05$ and $p<0.001$) decrease in cell viability. However, both cell lines tolerated the hydrogel being in contact with the media, evident by a smaller decrease in the cell viability. On further investigation, it was found that the PVA showed no toxic effects towards either cell line and caused an increase in cell proliferation. However, the borate species at all concentrations (0.5–2.5 % w/w) was found to be toxic towards both cell lines. Application of free IGF-1 and IGF-1 released from the hydrogel to the HaCaT keratinocytes showed to

increase the scratch closure rate (100 % closed by 24 hours and 36 hours, respectively), in comparison to the control group (>36 hours to achieve 100 % closure). Likewise, for Hs27 fibroblasts, the free IGF-1 and IGF-1 released from the hydrogel caused an increase in the rate of closure of the scratch area. Both these treated groups had achieved 100 % closure by 12 hours in comparison to the control group, which took 24 hours. Interestingly, all the groups of the fibroblast cells closed the scratch area faster in comparison to the corresponding groups of the HaCaT cells. This is believed to be due to a combination of factors, such as migration, proliferation and function of the cell types. On immunofluorescent analysis of the treated cells, it was found that IGF-1 caused activation of the Akt intracellular pathway in the HaCaTs, which is linked to stimulation of cell survival, migration and proliferation. However, it is uncertain if the IGF-1 stimulated the Akt pathway in the Hs27 fibroblasts due to no detection of phosphorylated Akt. However, IGF-1 is known to activate other intracellular signalling pathway such as, ERK and MAPK. Therefore, the fibroblasts may utilise one of these pathways, which can also stimulate cell survival, migration and proliferation. It was shown that the PVA-borate hydrogel is capable of delivering biologically active IGF-1 to two human skin cell types, stimulating an increase in cell proliferation and migration, which is thought to be through the activation of potentially one (Akt) if not more intracellular cell signalling pathways.

Chapter 7

Chapter 7

7 General conclusion

Chronic wounds do not progress through the normal stages of healing in a timely and efficient manner. The healing may be disrupted at one or more of the widely-recognised stages, leading to a chronic state. The wound healing process can also be complicated by patient comorbidities and medication (Menke *et al*., 2007). In 2008, it was reported that 200,000 people in the UK alone had a chronic wound, costing the NHS an estimated £2.3–3.1 billion per year (Posnett & Franks, 2008).

Growth factors found to be present in wound serum are thought to have multifunctional roles in the activation of the complex, highly orchestrated, intracellular signaling network, which controls the wound healing process and the many cells involved. However, in chronic wounds, there is often a deficiency of these necessary growth factors. The main route of administration, currently, is parentally for many therapeutic proteins and growth factors. However, one drawback of parenteral administration is the need for frequent injections due to the short half-life of many proteins and peptides. Growth factors involved in wound healing act locally as they possess short diffusional distances across the extracellular matrix because they degrade within a short period of time. Platelet-derived growth factor, basic fibroblast growth factor and vascular endothelial growth factor after intravenous administration have half-lives of 2, 3 and 30 minutes, respectively (Edelman *et al*., 1993; Lee, 2000; Eppler *et al*., 2002). The high frequency of injections required to maintain an adequate growth factor concentration within a defined therapeutic window will lead to reduced patient compliance and concordance (Li *et al*., 1998). Therefore, there is a need for an alternative controlled release delivery system, which is capable of enhancing the pharmacodynamics and

pharmacokinetic properties of the therapeutic protein or peptide being delivered. Therefore, the overall aim of this thesis was to investigate the ability of the PVA-borate hydrogels to deliver, topically, a sustained release of a bioactive peptide for wound management and repair.

The viscoelastic properties of the sixteen PVA-borate hydrogels formulated were investigated using oscillating rheometry. It was concluded from the rheological characterisation that the viscoelastic properties could be modified by varying the PVA and borate concentrations. The hydrogel formulation, PVA 6.0 % w/w borate 2.0 % w/w was deemed to be the optimum formulation. The optimum formulation was deemed to be a hydrogel that displayed the correct balance between elastic cohesiveness and liquid-like flow, while showing low adhesive properties. The optimum gel when physically manipulated retained its shape for several seconds before flowing at an acceptable speed. Theses viscoelastic properties exhibited by the PVA-borate hydrogel are advantageous for topical drug delivery in wound management and repair. The viscoelastic properties allow the PVA-borate hydrogel to flow into the wound crevasses, providing maximum wound-hydrogel contact, for drug delivery. Yet, they retain enough cohesive integrity to be removed fully intact from the wound. The low adhesiveness of the PVA-borate hydrogel facilitates removal from the wound with minimal disturbance to the new tissue. The PVA-borate hydrogels demonstrated the ability to uptake and carry small volumes (10.00g approximately 1–2 mL) of deionised water, making them advantageous for wound management and potentially suitable for application to lightly exuding wounds.

Physically mixing the desired quantity of payload to a pre-formed PVA-borate hydrogel was found to be a sufficient method to obtain a homogenous mix of heat-sensitive payloads throughout the hydrogel matrix. The *in vitro* release of

several proteins was characterised using Franz diffusion cells at 37 °C. The PVA-borate hydrogel demonstrated the ability to deliver a sustained release of three concentrations of BSA and haemoglobin over 8 hours. The hydrogel provided a maximum cumulative percentage release of 58.34 ± 1.17 %, after 8 hours, from a 0.10 % w/w BSA-loaded hydrogel and a maximum cumulative percentage release of 50.62 ± 1.52 %, after 8 hours, from a 0.10 % w/w haemoglobin-loaded hydrogel. The hydrogel also displayed partial release of trypsin from 0.05% and 0.10 % w/w loaded hydrogels, after 4 hours and release from a 0.20 % w/w trypsin-loaded gel over 8 hours. However, the uncharacteristic release profiles for trypsin accompanied with large standard deviations of the mean values, may indicate certain limitations to the gels' capability of providing a sustained release of specific proteins. It has been found that addition of all three concentrations of each of the different model proteins caused changes in the viscoelastic properties of the hydrogel. On analysis of the released proteins using SDS-PAGE, it was concluded that all three proteins were released from the hydrogel without undergoing degradation in relation to changes in molecular weight. It would seem that the most suitable protein payloads for incorporation into the PVA-borate hydrogel are those which will have a net negative charge when incorporated into the hydrogel matrix. The results also indicated that high molecular weight proteins are released in a sustained manner. Therefore, it was presumed that if the hydrogel can release large bulky high molecular weight proteins then it could also release lower molecular weight proteins and poly(peptides).

Addition of three concentrations of pepsin (0.05, 0.10 and 0.20 % w/w) resulted in significant ($p<0.01$) decreases in the crossover moduli. The PVA-borate hydrogel provided a sustained release of pepsin over an 8-hour period at 37 °C, with a maximum percentage cumulative release of 84.84 ± 0.79 % from the 0.20 % w/w

pepsin-loaded hydrogel. This indicates that the PVA-borate hydrogel may be able to provide a sustained release for protein payloads of a similar molecular weight and isoelectric point. SDS-PAGE was used to analysise the molecular weight of the pepsin, which was released from the hydrogel. It was concluded that the pepsin had not undergone degradation, in terms of changes in molecular weight, on being released from the hydrogel. However, the enzymatic activity of the pepsin could not be maintained upon release from the PVA-borate hydrogel. This indicated that in moving forward with the overall aim of the project, careful consideration needed to be taken when choosing a suitable protein payload, which promotes wound management and repair. This is to ensure that the biological activity of the payload can be maintained when encapsulated in the hydrogel matrix and upon release.

IGF-1 is a 7.6 kDa poly(peptide) consisting of 70 amino acids. Its function is to control cell differentiation and, therefore, growth of body tissue (Laron, 2001). Its synthesis is stimulated by growth hormone (GH) released from the anterior pituitary gland and the major source of circulating IGF-1 in the body is the liver (Dercole *et al*., 1984). Numerous reports of topical application of IGF-1 to full-thickness skin wounds in animal models (Tsuboi *et al.*, 1995; Koshizuka *et al.*, 1997; Provenzano *et al.*, 2007; Nunes Achar *et al.*, 2014) and to scratch assays in monolayers of cells (Dufourny *et al*., 1997; Haase *et al*., 2003; Lee *et al*., 2006; Borowiec *et al*., 2007; Fritz *et al*., 2011) have demonstrated an increase in wound healing and scratch closure. IGF-1 circulating in the body has a short half-life, estimated to be a few minutes. Hence, approximately 80 % of circulating IGF-1 is bound in a tertiary complex, which increases its half-life to 12–15 hours by protecting it from proteolytic degradation (Rosenfeld *et al*., 1999). Therefore, if IGF-1 is to be delivered to chronic wounds where protease activity is high, a delivery system,

which can provide a sustained release over a prolonged period of time, should be considered. The PVA-borate hydrogel is an ideal novel delivery system to investigate the sustained release of IGF-1 as it has provided sustained release of protein payloads over an 8-hour period. In addition, McCarron *et al*. (2011) concluded that the PVA-borate hydrogel is suitable for application to wounds in a clinical setting.

It was found that upon incorporating three concentrations of IGF-1 (50, 100 and 200 ng g^{-1}) into the PVA borate hydrogel that there was no significant ($p = 0.2023$, 0.8843 and 0.7264, respectively) change in the viscoelastic properties. The PVA-borate hydrogel loaded with 200 ng g^{-1} of IGF-1 was found to provide a sustained release over an 8-hour period at 37 °C. The maximum percentage cumulative release (58.15 ± 4.88 %) was observed, after 7 hours. The median effective dose (ED_{50}) of the IGF-1 used in this study, in human cell lines, is 0.3-1.5 ng mL^{-1}, as stated by the manufacture in the certificate of analysis (R&D Systems, 2015). Therefore, with 58.15 ± 4.88 % cumulative release over 8 hours, confidence can be had in the PVA-borate hydrogel delivering a sufficient quantity of IGF-1 in cell culture work to observe any effect it may have on the cells. Molecular weight analysis, by MADLI-TOF MS of the IGF-1 poly(peptide) prior to incorporation into the PVA-borate hydrogel and on release from the hydrogel confirmed that no degradation had occurred. This would suggest that the PVA-borate hydrogel has the potential to be a suitable and stable topical delivery system for sustained release of growth factor payloads for wound management and repair.

Several concentrations of IGF-1 (2–100 ng mL^{-1}) caused an increase in cell proliferation in a dose-dependent manner for both the HaCaT keratinocyte and Hs27 fibroblast cell lines. It was found that both cell lines did not tolerate the PVA-borate

hydrogel being in direct contact, indicated by the significant ($p<0.05$ and $p<0.001$) decrease in cell viability. However, both cell lines tolerated the hydrogel being in contact with the media, evident by a smaller decrease in the cell viability. On further investigation, it was found that the PVA showed no toxic effects towards either cell line and, in fact, caused an increase in cell proliferation. However, the borate at all concentrations (0.5–2.5 % w/w) was found to be toxic towards both cell lines. Application of free IGF-1 and IGF-1 released from the hydrogel to the HaCaT keratinocytes increased the scratch closer rate (24 hours and 36 hours to achieve 100 % closure, respectively), in comparison to the control group (>36 hours to achieve 100 % closure). Likewise, for the Hs27 fibroblasts the free IGF-1 and IGF-1 released from the hydrogel caused an increase in the rate of closer of the scratched area. Both these treated groups had achieved 100 % closure by 12 hours in comparison to the control group, which took 24 hours. Interestingly, all the groups of the fibroblast cells closed the scratch area faster, in comparison to the corresponding groups of HaCaT cells. This is believed to be due to a combination of factors, such as migration, proliferation and function of the cell types. On immunofluorescent analysis of the treated cells, it was found that IGF-1 caused activation of the Akt intracellular pathway in the HaCaT cells, which is linked to stimulation of cell survival, migration and proliferation. However, it is uncertain if the IGF-1 stimulated the Akt pathway in the Hs27 fibroblasts due to no detection of phosphorylated Akt. However, IGF-1 is known to activate other intracellular signalling pathway, such as ERK and MAPK. Therefore, the fibroblasts may utilise one of these pathways, which can also stimulate cell survival, migration and proliferation.

To conclude, the experimental work completed in this thesis has shown that the PVA-borate hydrogel is capable of delivering several protein payloads and, in particular, the poly(peptide) IGF-1. IGF-1 was shown to maintain its biological activity on release from the hydrogel, stimulating an increase in cell proliferation and migration. Therefore, an IGF-1-loaded PVA-borate hydrogel could be a potential biocompatible treatment for enhancing healing of chronic wounds.

Chapter 8

Chapter 8

8 References

Abbade, L. and Lastoria, S. (2005) Venous ulcer: epidemiology, physiopathology, diagnosis and treatment. *International Journal of Dermatology,* 44(6), 449-456.

Abidin, A.Z., Puspasari, T. and Nugroho, W.A. (2012) Polymers for Enhanced Oil Recovery Technology. *International Conference on Innovation in Polymer Science and Technology,* 4, 11-16.

Aboyans, V., Criqui, M.H., Abraham, P., Allison, M.A., Creager, M.A., Diehm, C., Fowkes, F.G.R., Hiatt, W.R., Joensson, B., Lacroix, P., Marin, B., McDermott, M.M., Norgren, L., Pande, R.L., Preux, P., Stoffers, H.E.(., Treat-Jacobson, D., American Heart Assoc Council Perip, Council Epidemiology Prevention, Council Clinical Cardiology, Council Cardiovasc Nursing, Council Cardiovasc Radiology Inter and Council Cardiovasc Surg & Anesthes. (2012) Measurement and Interpretation of the Ankle-Brachial Index A Scientific Statement From the American Heart Association. *Circulation,* 126(24), 2890-2909.

Alconcel, S.N.S., Baas, A.S. and Maynard, H.D. (2011) FDA-approved poly(ethylene glycol)-protein conjugate drugs. *Polymer Chemistry,* 2(7), 1442-1448.

Altun, G.D. and Cetinus, S.A. (2007) Immobilization of pepsin on chitosan beads. *Food Chemistry,* 100(3), 964-971.

Amendt, C., Schirmacher, P., Weber, H. and Blessing, M. (1998) Expression of a dominant negative type II TGF-beta receptor in mouse skin results in an increase in carcinoma incidence and an acceleration of carcinoma development. *Oncogene,* 17(1), 25-34.

Amsden, B. (1998) Solute diffusion within hydrogels. Mechanisms and models. *Macromolecules,* 31(23), 8382-8395.

Ando, Y. and Jensen, P.J. (1993) Epidermal Growth-Factor and Insulin-Like Growth Factor-i Enhance Keratinocyte Migration. *Journal of Investigative Dermatology*, 100(5), 633-639.

Andrew Chan, K.L., Zhang, G., Tomic-Canic, M., Stojadinovic, O., Lee, B., Flach, C.R. and Mendelsohn, R. (2008) A coordinated approach to cutaneous wound healing: vibrational microscopy and molecular biology. *Journal of Cellular and Molecular Medicine,* 12(5B), 2145-54.

Appel, E.A., Loh, X.J., Jones, S.T., Dreiss, C.A. and Scherman, O.A. (2012) Sustained release of proteins from high water content supramolecular polymer hydrogels. *Biomaterials,* 33(18), 4646-4652.

Ashcroft, G., Yang, X., Glick, A., Weinstein, M., Letterio, J., Mizel, D., Anzano, M., Greenwell-Wild, T., Wahl, S., Deng, C. and Roberts, A. (1999) Mice lacking Smad3 show accelerated wound healing and an impaired local inflammatory response. *Nature Cell Biology,* 1(5), 260-266.

Aulton, M.E. ed. (2007) *Aultons's Pharmaceutics, The design and manufacture of medicines.* 3rd ed. Churchhill Livingstone Elsevier.

Balasubramanian, V., Onaca, O., Enea, R., Hughes, D.W. and Palivan, C.G. (2010) Protein delivery: from conventional drug delivery carriers to polymeric nanoreactors. *Expert Opinion on Drug Delivery,* 7(1), 63-78.

Barrientos, S., Stojadinovic, O., Golinko, M.S., Brem, H. and Tomic-Canic, M. (2008) Growth factors and cytokines in wound healing. *Wound Repair and Regeneration,* 16(5), 585-601.

Baum, C.L. and Arpey, C.J. (2005) Normal cutaneous wound healing: Clinical correlation with cellular and molecular events. *Dermatologic Surgery,* 31(6), 674-686.

Bauters, C., Asahara, T., Zheng, L., Takeshita, S., Bunting, S., Ferrara, N., Symes, J. and Isner, J. (1994) Physiological Assessment of Augmented Vascularity Induced by

Vegf in Ischemic Rabbit Hindlimb. *American Journal of Physiology-Heart and Circulatory Physiology*, 267(4), H1263-H1271.

Bauters, C., Asahara, T., Zheng, L., Takeshita, S., Bunting, S., Ferrara, N., Symes, J. and Isner, J. (1995) Site-Specific Therapeutic Angiogenesis After Systemic Administration of Vascular Endothelial Growth-Factor. *Journal of Vascular Surgery*, 21(2), 314-325.

Beckert, S., Hierlemann, H., Muschenborn, N., Witte, M., Ranke, M. and Coerper, S. (2005) Experimental ischemic wounds: Correlation of cell proliferation and insulin-like growth factor I expression and its modification by different local IGF-I release systems. *Wound Repair and Regeneration*, 13(3), 278-283.

Bharat Biotech. (2015) *Regen-D.* India: Bharat Biotech. Available at: http://www.bharatbiotech.com/products/bio-therapeutic/regen-d/ [Accessed 16/08/17].

Bhora, F., Dunkin, B., Batzri, S., Aly, H., Bass, B., Sidawy, A. and Harmon, J. (1995) Effect of Growth-Factors on Cell-Proliferation and Epithelialization in Human Skin. *Journal of Surgical Research*, 59(2), 236-244.

Black, J., Cuddigan, J., Langemo, D., Ratliff, C. and NPUAP. (2007) National Pressure Ulcer Advisory Panel's Updated Pressure Ulcer Staging System. *Advances in Skin & Wound Care*, 20(5), 269-274.

BNF. (2017) *British National Forumlary 74 September 2017 to March 2018.* UK: Pharmaceutical Press. Available at: https://www.medicinescomplete.com/mc/bnfc/current/DMD12101411000001108.htm?q=increlex&t=search&ss=text&tot=1&p=1#DMD12101411000001108 [Accessed 04/09/17].

Borowiec, A., Hague, F., Harir, N., Guenin, S., Guerineau, F., Gouilleux, F., Roudbaraki, M., Lassoued, K. and Ouadid-Ahidouch, H. (2007) IGF-1 activates hEAG k(+) channels through an akt-dependent signaling pathway in breast cancer cells: Role in cell proliferation. *Journal of Cellular Physiology*, 212(3), 690-701.

Bott, R., Subramanian, E. and Davies, D.R. (1982) Three-dimensional structure of the complex of the Rhizopus chinensis carboxyl proteinase and pepstatin at 2.5-A resolution. *Biochemistry*, 21(26), 6956-6962.

Bottinger, E., Letterio, J. and Roberts, A. (1997) Biology of TGF-beta in knockout and transgenic mouse models. *Kidney International*, 51(5), 1355-1360.

Boushaba, R., Kumpalume, P. and Slater, N. (2003) Kinetics of whole serum and prepurified IgG digestion by pepsin for F(ab ')(2) manufacture. *Biotechnology Progress*, 19(4), 1176-1182.

Bouten, C., Oomens, C., Baaijens, F. and Bader, D. (2003) The etiology of pressure ulcers: Skin deep or muscle bound? *Archives of Physical Medicine and Rehabilitation*, 84(4), 616-619.

Boutrand, L., Thepot, A., Muther, C., Boher, A., Robic, J., Guere, C., Vie, K., Damour, O. and Lamartine, J. (2017) Repeated short climatic change affects the epidermal differentiation program and leads to matrix remodeling in a human organotypic skin model. *Clinical Cosmetic and Investigational Dermatology*, 10, 43-50.

Bowcher, T. and Dawber, J. (1989) C-13 and B-11 Nuclear Magnetic-Resonance Study of the Reaction of Polyvinyl-Alcohol) with the Tetrahydroxyborate Ion. *Polymer Communications*, 30(7), 215-217.

Briscoe, B., Luckham, P. and Zhu, S. (2000) The effects of hydrogen bonding upon the viscosity of aqueous poly(vinyl alcohol) solutions. *Polymer*, 41(10), 3851-3860.

British Heart Foundation. (2016) *Atherosclerosis.* Available at: https://www.bhf.org.uk/heart-health/conditions/atherosclerosis

Bucalo, B.F.V. (1993) Inhibition of cell proliferation by chronic wound fluid. *Wound Repair and Regeneration*, 1, 181-186.

Bullen, E., Longaker, M., Updike, D., Benton, R., Ladin, D., Hou, Z. and Howard, E. (1995) Tissue Inhibitor of Metalloproteinases-1 is Decreases and Activated

Gelatinases are Increased in Chronic Wounds. *Journal of Investigative Dermatology*, 104(2), 236-240.

Burnand, K.G., Whimster, I., Naidoo, A. and Browse, N.L. (1982) Pericapillary fibrin in the ulcer bearing skin of the leg: the cause of lipodermatosclerosis and venous ulceration. *British Medical Journal*, 285, 1071-1072.

Butler, P.D., Ly, D.P., Longaker, M.T. and Yang, G.P. (2008) Use of organotypic coculture to study keloid biology. *American Journal of Surgery*, 195(2), 144-148.

Cakir, A., Ak Azem, F. and Ungan, G. (2011) Use of Polyvinyl alcohol to improve adhesion properties of hap coating on Ti-6Al-4V. *Journal of Biomechanics*, 44, 21.

Callam, M. (1992) Prevalence of Chronic Leg Ulceration and Severe Chronic Venous Disease in Western Countries. *Phlebology*, 7, 6-12.

Cao, Y., Chen, A., An, S., Ji, R., Davidson, D., Cao, Y. and Llinas, M. (1997) Kringle 5 of plasminogen is a novel inhibitor of endothelial cell growth. *Journal of Biological Chemistry*, 272(36), 22924-22928.

Cappuzzo, F., Hirsch., F.R., Rossi, E., Bartolini, S., Ceresoli, G.L., Bemis, L., Haney, J., Witta, S., Danenberg, K., Domenichini, I., Ludovini, V., Magrini, E., Gregorc, V., Doglioni, C., Sidoni, A., Tonato, M., Franklin, W.A., Crino, L., Bunn, J., P.A. and Varella-Garcia, M. (2005) Epidermal Growth Factor Receptor Gene and Protein and Gefitinib Sensitivity in Non-Small-Cell Lung Cancer. *Journal of the National Cancer Institute*, 97(9), 643-655.

Carretti, E., Grassi, S., Cossalter, M., Natali, I., Caminati, G., Weiss, R.G., Baglioni, P. and Dei, L. (2009) Poly(vinyl alcohol)-Borate Hydro/Cosolvent Gels: Viscoelastic Properties, Solubilizing Power, and Application to Art Conservation. *Langmuir*, 25(15), 8656-8662.

Castillo-Yanez, F., Pacheco-Aguilar, R., Garcia-Carreno, F., Navarrete Del Toro, M. and Lopez, M. (2006) Purification and biochemical characterization of chymotrypsin from the viscera of Monterey sardine (Sardinops sagax caeruleus). *Food Chemistry*, 99(2), 252-259.

Censi, R., Di Martino, P., Vermonden, T. and Hennink, W.E. (2012) Hydrogels for protein delivery in tissue engineering. *Journal of Controlled Release,* 161(2), 680-692.

Chaiyasut, C. and Tsuda, T. (2001) Isoelectric points estimation of proteins by electroosmotic flow: pH relationship using physically adsorbed proteins on silica gel. *Chromatography,* 22(2), 91-95.

Cheison, S.C., Brand, J., Leeb, E. and Kulozik, U. (2011) Analysis of the Effect of Temperature Changes Combined with Different Alkaline pH on the beta-Lactoglobulin Trypsin Hydrolysis Pattern Using MALDI-TOF-MS/MS. *Journal of Agricultural and Food Chemistry,* 59(5), 1572-1581.

Chen, P., Xie, H., Chandra Sekar, M., Gupta, K. and Wells, A. (1994a) Epidermal Growth Factor Receptor-mediated Cell Motility: Phospholipase C Activity Is Required, but Mitogen-activated Protein Kinase Activity Is Not Sufficient for Induced Cell Movement. *The Journal of Cell Biology,* 127(3), 847-857.

Chen, F., Zhao, Y., Wu, H., Deng, Z., Wang, Q., Zhou, W., Liu, Q., Dong, G., Li, K., Wu, Z. and Jin, Y. (2006) Enhancement of periodontal tissue regeneration by locally controlled delivery of insulin-like growth factor-I from dextran-co-gelatin microspheres. *Journal of Controlled Release,* 114(2), 209-222.

Chen, P., Gupta, K. and Wells, A. (1994b) Cell-Movement Elicited by Epidermal Growth-Factor Receptor Requires Kinase and Autophosphorylation but is Separable from Mitogenesis. *Journal of Cell Biology,* 124(4), 547-555.

Chetty, A., Cao, G. and Nielsen, H.C. (2006) Insulin-like growth factor-I signaling mechanisms, type I collagen and alpha smooth muscle actin in human fetal lung fibroblasts. *Pediatric Research,* 60(4), 389-394.

Choi, J.S., Leong, K.W. and Yoo, H.S. (2008) In vivo wound healing of diabetic ulcers using electrospun nanofibers immobilized with human epidermal growth factor (EGF). *Biomaterials,* 29(5), 587-596.

Claesson-Welsh, L. (2016) VEGF receptor signal transduction - A brief update. *Vascular Pharmacology,* 86, 14-17.

Coffey, R., Bascom, C., Sipes, N., Gravesdeal, R., Weissman, B. and Moses, H. (1988) Selective-Inhibition of Growth-Related Gene-Expression in Murine Keratinocytes by Transforming Growth Factor-Beta. *Molecular and Cellular Biology,* 8(8), 3088-3093.

Cohen, S. (1962) Isolation of a mouse submaxillary gland protein accelerating incisor eruption and eye-lid opening in the new-born animal. *Journal of Biological Chemistry,* 237, 1555-1562.

Cohen, S. (1986) Epidermal Growth-Factor. *Bioscience Reports,* 6(12), 1017-1028.

Coleridge Smith, P.D., Thomas, P., Scurr, J.H. and Dormandy, J.A. (1988) Causes of venous ulceration: a new hypothesis. *British Medical Journal (Clinical Research Ed.),* 296(6638), 1726-1727.

Cox, J. (2011) Predictors of Pressure ulcer development in adult critical care patients. *American Journal of Critical Care,* 20(5), 364-374.

Cross, M., Dixelius, J., Matsumoto, T. and Claesson-Welsh, L. (2003) VEGF-receptor signal transduction. *Trends in Biochemical Sciences,* 28(9), 488-494.

Crowther, J.R. (1995) *ELISA: theory and practice.* Totowa, N.J. Humana Press.

Cubo, N., Garcia, M., del Canizo, J.F., Velasco, D. and Jorcano, J.L. (2017) 3D bioprinting of functional human skin: production and in vivo analysis. *Biofabrication,* 9(1), 015006.

Daniel, R., Priest, D. and Wheatley, D. (1981) Etiologic Factors in Pressure Sores - an Experimental-Model. *Archives of Physical Medicine and Rehabilitation,* 62(10), 492-498.

Davies, D. (1990) The Structure and Function of the Aspartic Proteinases. *Annual Review of Biophysics and Biophysical Chemistry,* 19, 189-215.

Dawber, J.G. and Green, S.I.E. (1986) An B-11 nuclear-magnetic-resonance study of the reaction of the tetrahydroxyborate ion with polyhydroxy compounds. *Journal of the Chemical Society-Faraday Transactions I,* (82), 3407-3413.

de Oliveira Gonzalez, A.C., Costa, T.F., Andrade, Z.d.A. and Alves Peixoto Medrado, A.R. (2016) Wound healing - A literature review. *Anais Brasileiros De Dermatologia,* 91(5), 614-620.

Denniston, K.J., Topping, J.J. and Caret, R.L. (2008) Enzymes. *In:* Anon.*General, Organic, and Biochemistry.* Sixth ed. USA: McGraw-Hill, 651-685.

Dercole, A., Stiles, A. and Underwood, L. (1984) Tissue Concentrations of Somatomedin-C - further Evidence for Multiple Sites of Synthesis and Paracrine Or Autocrine Mechanisms of Action. *Proceedings of the National Academy of Sciences of the United States of America-Biological Sciences,* 81(3), 935-939.

Dimmeler, S., Fleming, I., Fisslthaler, B., Hermann, C., Busse, R. and Zeiher, A. (1999) Activation of nitric oxide synthase in endothelial cells by Akt-dependent phosphorylation. *Nature,* 399(6736), 601-605.

Dirks, R. and Bloemers, H. (1996) Signals controlling the expression of PDGF. *Molecular Biology Reports,* 22(1), 1-24.

Donnelly, R.F., Cassidy, C.M., Loughlin, R.G., Brown, A., Tunney, M.M., Jenkins, M.G. and McCarron, P.A. (2009) Delivery of Methylene Blue and meso-tetra (N-methyl-4-pyridyl) porphine tetra tosylate from cross-linked poly(vinyl alcohol) hydrogels: A potential means of photodynamic therapy of infected wounds. *Journal of Photochemistry and Photobiology B-Biology,* 96(3), 223-231.

Dowd, S.E., Sun, Y., Secor, P.R., Rhoads, D.D., Wolcott, B.M., James, G.A. and Wolcott, R.D. (2008) Survey of bacterial diversity in chronic wounds using Pyrosequencing, DGGE, and full ribosome shotgun sequencing. *Bmc Microbiology,* 8, 43.

Drinkwater, S., Smith, A., Sawyer, B. and Burnand, K. (2002) Effect of venous ulcer exudates on angiogenesis in vitro. *British Journal of Surgery,* 89(6), 709-713.

Dufourny, B., Alblas, J., van Teeffelen, H.A.A.M., van Schaik, F.M.A., van der Burg, B., Steenbergh, P.H. and Sussenbach, J.S. (1997) Mitogenic signaling of insulin-like growth factor I in MCF-7 human breast cancer cells requires phosphatidylinositol 3-kinase and is independent of mitogen-activated protein kinase. *Journal of Biological Chemistry,* 272(49), 31163-31171.

Dunn, B. (2002) Structure and mechanism of the pepsin-like family of aspartic peptidases. *Chemical Reviews,* 102(12), 4431-4458.

Durham, D., Fortney, D.Z. and Nanney, L. (1993) **Preliminary Evaluation of Vibriolysin, a Novel Proteolytic Enzyme Composition Suitable for the Debridement of Burn Wound Eschar**. *Journal of Burn Care & Research,* 14, 544-551.

Edelman, E., Nugent, M. and Karnovsky, M. (1993) Perivascular and Intravenous Administration of Basic Fibroblast Growth-Factor - Vascular and Solid Organ Deposition. *Proceedings of the National Academy of Sciences of the United States of America,* 90(4), 1513-1517.

Edmonds, M. (2006) Daibetic Foot Ulcers. *Drugs,* 66(7), 913-929.

Elisseeff, J., McIntosh, W., Fu, K., Blunk, T. and Langer, R. (2001) Controlled-release of IGF-I and TGF-beta 1 in a photopolymerizing hydrogel for cartilage tissue engineering. *Journal of Orthopaedic Research,* 19(6), 1098-1104.

El-Kader, K., Hamied, S., Mansour, A., El-Lawindy, A. and El-Tantaway, F. (2002) Effect of the molecular weights on the optical and mechanical properties of poly(vinyl alcohol) films. *Polymer Testing,* 21(7), 847-850.

Emmerson, E., Campbell, L., Davies, F.C.J., Ross, N.L., Ashcroft, G.S., Krust, A., Chambon, P. and Hardman, M.J. (2012) Insulin-Like Growth Factor-1 Promotes Wound Healing in Estrogen-Deprived Mice: New Insights into Cutaneous IGF-1R/ER alpha Cross Talk. *Journal of Investigative Dermatology,* 132(12), 2838-2848.

English, B., Min, W., van Oijen, A., Lee, K., Luo, G., Sun, H., Cherayil, B., Kou, S. and Xie, S. (2006) Ever-fluctuating single enzyme molecules: Michaelis-Menten equation revisited (vol 2, pg 87, 2006). *Nature Chemical Biology,* 2(3), 168-168.

Enoch, S. and Leaper, D. (2008) Basic science of wound healing. *Surgery Oxford International Edition,* 26(2), 31-37.

Eppler, S., Combs, D., Henry, T., Lopez, J., Ellis, S., Yi, J., Annex, B., McCluskey, E. and Zioncheck, T. (2002) A target-mediated model to describe the pharmacokinetics and hemodynamic effects of recombinant human vascular endothelial growth factor in humans. *Clinical Pharmacology & Therapeutics,* 72(1), 20-32.

Eriksson, A., Siegbahn, B., Westermark, C., Heldin, C.H. and Claesson-Welsh, L. (1992) PDGF a- and b-receptors activate unique and common signal transduction pathways. *The EMBO Journal,* 11, 543-550.

Eswarakumar, V., Lax, I. and Schlessinger, J. (2005) Cellular signaling by fibroblast growth factor receptors. *Cytokine & Growth Factor Reviews,* 16(2), 139-149.

Etufugh, C.N. and Phillips, T.J. (2007) Venous ulcers. *Clinics in Dermatology,* 25(1), 121-130.

Falanga, V. (2004) The chronic wound: impaired healing and solutions in the context of wound bed preparation. *Blood Cells Molecules and Diseases,* 32(1), 88-94.

Falk, E. (2006) Pathogenesis of atherosclerosis. *Journal of the American College of Cardiology,* 47(8), C7-C12.

Ferrara, N., Gerber, H. and LeCouter, J. (2003) The biology of VEGF and its receptors. *Nature Medicine,* 9(6), 669-676.

Ferrara, N. and Henzel, W. (1989) Pituitary Follicular Cells Secrete a Novel Heparin-Binding Growth-Factor Specific for Vascular Endothelial-Cells. *Biochemical and Biophysical Research Communications,* 161(2), 851-858.

Flomenbom, O., Velonia, K., Loos, D., Masuo, S., Cotlet, M., Engelborghs, Y., Hofkens, J., Rowan, A., Nolte, R., Van der Auweraer, M., de Schryver, F. and Klafter, J. (2005) Stretched exponential decay and correlations in the catalytic activity of fluctuating single lipase molecules. *Proceedings of the National Academy of Sciences of the United States of America*, 102(7), 2368-2372.

Friedman, B., Hubbard, S. and Rasmussen, J. (1993) Development of a Recombinant Form of Ceredase(r) (Glucocerebrosidase) for the Treatment of Gaucher Disease. *Glycoconjugate Journal*, 10(4), 257-257.

Fritz, J.M., Dwyer-Nield, L.D. and Malkinson, A.M. (2011) Stimulation of neoplastic mouse lung cell proliferation by alveolar macrophage-derived, insulin-like growth factor-1 can be blocked by inhibiting MEK and PI3K activation. *Molecular Cancer*, 10, 76.

Frosech, E.R., Burgi, H., Ramseier, E.B., Bally, P. and Labhart, A. (1963) Antibody-suppressible and nonsuppressible insulin-like activitied in human serum and their physiological significance. An insulin assay with adipose tissue of increased precision and specificity. *The Journal of Clinical Investigation*, 42(11), 1816-1834.

Fruton, J.S. (1976) The mechanism of the catalytic action of pepsin and related acid proteinases. *Enzymology and Related Areas of Molecular Biology*, 44, 1-36.

Fulton, D., Gratton, J., McCabe, T., Fontana, J., Fujio, Y., Walsh, K., Franke, T., Papapetropoulos, A. and Sessa, W. (1999) Regulation of endothelium-derived nitric oxide production by the protein kinase Akt. *Nature*, 399(6736), 597-601.

Gailit, J., Welch, M.P. and Clark, R.A.F. (1994) TGF-β1 Stimulates Expression ofKeratinocyte Integrins During Re-Epithelialization . of Cutaneous Wounds. *The Journal of Investigative Dermatology*, 103, 221-227.

Galiano, R., Tepper, O., Pelo, C., Bhatt, K., Callaghan, M., Bastidas, N., Bunting, S., Steinmetz, H. and Gurtner, G. (2004) Topical vascular endothelial growth factor accelerates diabetic wound healing through increased angiogenesis and by mobilizing and recruiting bone marrow-derived cells. *American Journal of Pathology*, 164(6), 1935-1947.

Gan, S.D. and Patel, K.R. (2013) Enzyme Immunoassay and Enzyme-Linked Immunosorbent Assay. *Journal of Investigative Dermatology*, 133(9), E10-E12.

Garlick, J.A. and Taichman, L.B. (1994) Fate of Human Keratinocytes during Reepithelialization in an Organotypic Culture Model. *Laboratory Investigation*, 70(6), 916-924.

Gehrke, S., Uhden, L. and McBride, J. (1998) Enhanced loading and activity retention of bioactive proteins in hydrogel delivery systems. *Journal of Controlled Release*, 55(1), 21-33.

Gilbertson, D., Duff, M., West, J., Kelly, J., Sheppard, P., Hofstrand, P., Gao, Z., Shoemaker, K., Bukowski, T., Moore, M., Feldhaus, A., Humes, J., Palmer, T. and Hart, C. (2001) Platelet-derived growth factor C (PDGF-C), a novel growth factor that binds to PDGF alpha and beta receptor. *Journal of Biological Chemistry*, 276(29), 27406-27414.

Goetz, H., Kuschel, M., Wulff, T., Sauber, C., Miller, C., Fisher, S. and Woodward, C. (2004) Comparison of selected analytical techniques for protein sizing, quantitation and molecular weight determination. *Journal of Biochemical and Biophysical Methods*, 60(3), 281-293.

Goldberg, M.T., Han, Y., Yan, C., Shaw, M.C. and Garner, W.L. (2007) TNF-alpha suppresses alpha-smooth muscle actin expression in human dermal fibroblasts: An implication for abnormal wound healing. *Journal of Investigative Dermatology*, 127(11), 2645-2655.

Goodsell, D. (2000) *Pepsin.* RCSB Protein Data Base. Available at: http://pdb101.rcsb.org/motm/12 [Accessed 23/11/2017].

Gordois, A., Scuffham, P., Shearer, A. and Oglesby, A. (2003) The healthcare costs of diabetic peripheral neuropathy in the UK. (Cost-of-illness study). *The Diabetic Foot*, 6(2), 62-73.

Greenhalgh, D., Sprugel, K., Murray, M. and Ross, R. (1990) PDGF and FGF Stimulate Wound-Healing in the Genetically Diabetic Mouse. *American Journal of Pathology,* 136(6), 1235-1246.

Grey, J.E., Enoch, S. and Harding, K.G. (2006) ABC of wound healing - Pressure ulcer. *British Medical Journal,* 332(7539), 472-475.

Grey, J., Enoch, S. and Harding, K. (2006) ABC of wound healing - Venous and arterial leg ulcers. *British Medical Journal,* 332(7537), 347-350.

Guha, N., Cowan, D.A., Soenksen, P.H. and Holt, R.I.G. (2013) Insulin-like growth factor-I (IGF-I) misuse in athletes and potential methods for detection. *Analytical and Bioanalytical Chemistry,* 405(30), 9669-9683.

Guidi, A., Laricchia-Robbio, L., Gianfaldoni, D., Revoltella, R. and Del Bono, G. (2001) Comparison of a conventional immunoassay (ELISA) with a surface plasmon resonance-based biosensor for IGF-1 detection in cows' milk. *Biosensors & Bioelectronics,* 16(9-12), 971-977.

Guler, H., Zapf, J. and Froesch, E. (1987) Short-Term Metabolic Effects of Recombinant Human Insulin-Like Growth Factor-i in Healthy-Adults. *New England Journal of Medicine,* 317(3), 137-140.

Guo, S. and DiPietro, L.A. (2010) Factors Affecting Wound Healing. *Journal of Dental Research,* 89(3), 219-229.

Haase, I., Evans, R., Pofahl, R. and Watt, F.M. (2003) Regulation of keratinocyte shape, migration and wound epithelialization by IGF-1- and EGF-dependent signalling pathways. *Journal of Cell Science,* 116(15), 3227-3238.

Hafner, J., Schaad, I., Schneider, E., Seifert, B., Burg, G. and Cassina, P. (2000) Leg ulcers in peripheral arterial disease (arterial leg ulcers): Impaired wound healing above the threshold of chronic critical limb ischemia. *Journal of the American Academy of Dermatology,* 43(6), 1001-1008.

Hamuro, Y., Coales, S.J., Molnar, K.S., Tuske, S.J. and Morrow, J.A. (2008) Specificity of immobilized porcine pepsin in H/D exchange compatible conditions. *Rapid Communications in Mass Spectrometry,* 22(7), 1041-1046.

Han, J., Lei, T. and Wu, Q. (2014) High-water-content mouldable polyvinyl alcohol-borax hydrogels reinforced by well-dispersed cellulose nanoparticles: Dynamic rheological properties and hydrogel formation mechanism. *Carbohydrate Polymers,* 102, 306-316.

Hardwicke, J., Schmaljohann, D., Boyce, D. and Thomas, D. (2008) Epidermal Growth Factor Therapy and wound healing - past, present and future perspectives. *The Surgeon,* 6(3), 172-177.

Hassan, C.M. and Peppas, N.A. (2000) Structure and applications of Poly(vinyl alcohol) hydrogels produce by conventional cross linkin or by freezing/thawing methods. *Advance in Polymer Science,* 153, 37-65.

Heldin, C.H. and Westermark, B. (1999) Mechanism of Action and In Vivo Role of Platelet-Derived Growth Factor. *Physiological Reviews,* 79(4), 1283-1316.

Heldin, C., Eriksson, U. and Ostman, A. (2002) New members of the platelet-derived growth factor family of mitogens. *Archives of Biochemistry and Biophysics,* 398(2), 284-290.

Hirobe, T. (2014) Keratinocytes regulate the function of melanocytes. *Dermatologica Sinica,* 32(4), 200-204.

Holloway, J.L., Spiller, K.L., Lowman, A.M. and Palmese, G.R. (2011) Analysis of the in vitro swelling behavior of poly(vinyl alcohol) hydrogels in osmotic pressure solution for soft tissue replacement. *Acta Biomaterialia,* 7(6), 2477-2482.

Holowka, E.P. and Bhatia, S.K. (2014) Controlled-Release systems. *In:* Anon.*Drug Delievery: Materials Design anf Clinical.* New York: Springer Science+Business Media, 7-62.

Hu, J., Li, S. and Liu, B. (2006) Properties of immobilized pepsin on Modified PMMA microspheres. *Biotechnology Journal,* 1, 75-79.

Huang, X. and Brazel, C.S. (2001) On the importance and mechanisms of burst release in matrix-controlled drug delivery systems. *Journal of Controlled Release,* 71, 121-136.

Huang, X., Chestang, B. and Brazel, C. (2002) Minimization of initial burst in poly(vinyl alcohol) hydrogels by surface extraction and surface-preferential crosslinking. *International Journal of Pharmaceutics,* 248(1-2), 183-192.

Igarashi, M., Finch, P. and Aaronson, S. (1998) Characterization of recombinant human fibroblast growth factor (FGF)-10 reveals functional similarities with keratinocyte growth factor (FGF-7). *Journal of Biological Chemistry,* 273(21), 13230-13235.

Igartua, M., Hernandez, R., Esquisabel, A., Gascon, A., Calvo, M. and Pedraz, J. (1998) Stability of BSA encapsulated into PLGA microspheres using PAGE and capillary electrophoresis. *International Journal of Pharmaceutics,* 169(1), 45-54.

Iglesias, C., Nelson, E., Cullum, N., Torgerson, D. and VenUS I Collaborators. (2010) Economic analysis of VenUS I, a randomized trial of two bandages for treating venous leg ulcers. *British Journal of Surgery,* 35(4), 322-332.

Iizaka, S., Sanada, H., Nakagami, G., Koyanagi, H., Konya, C. and Sugama, J. (2011) Quantitative estimation of exudate volume for full-thickness pressure ulcers: the ESTimation method. *Journal of Wound Care,* 20(10), 453-+.

Izquierdo, F.J., Alli, I., Yaylayan, V. and Gomez, R. (2007) Microwave-assisted digestion of beta-lactoglobulin by pronase, alpha-chymotrypsin and pepsin. *International Dairy Journal,* 17(5), 465-470.

Jackson, W.T., Schlamowitz, M. and Shaw, A. (1965) Kinetics of the pepsin-catalyzed hydrolysis of N-acetyl-L-phenylalanyl-L-diiodotyrosine. *Biochemistry,* 4(8), 1537-1543.

James, M.N.G., Sielecki, A., Salituro, F., Rich, D.H. and Hofmann, T. (1982) Conformational Flexibility in the Active-Sites of Aspartyl Proteinases Revealed by a Pepstatin Fragment Binding to Penicillopepsin. *Proceedings of the National*

Academy of Sciences of the United States of America-Biological Sciences, 79(20), 6137-6141.

James, M.N.G. and Sielecki, A.R. (1985) Stereochemical Analysis of Peptide-Bond Hydrolysis Catalyzed by the Aspartic Proteinase Penicillopepsin. *Biochemistry,* 24(14), 3701-3713.

Jeffcoate, W. and Harding, K. (2003) Diabetic foot ulcers. *Lancet,* 361(9368), 1545-1551.

Jeha, S., Kantarjian, H., Irwin, D., Shen, V., Shenoy, S., Blaney, S., Camitta, B. and Pui, C. (2005) Efficacy and safety of rasburicase, a recombinant urate oxidase (Elitek (TM)), in the management of malignancy-associated hyperuricemia in pediatric and adult patients: final results of a multicenter compassionate use trial. *Leukemia,* 19(1), 34-38.

Jenkins, M.G., Murphy, D.J., Little, C., McDonald, J. and McCarron, P.A. (2014) A Non-Inferiority Randomized Controlled Trial Comparing the Clinical Effectiveness of Anesthesia Obtained by Application of a Novel Topical Anesthetic Putty With the Infiltration of Lidocaine for the Treatment of Lacerations in the Emergency Department. *Annals of Emergency Medicine,* 63(6), 704-710.

Jensen, M., Hansen, P., Murdan, S., Frokjaer, S. and Florence, A. (2002) Loading into and electro-stimulated release of peptides and proteins from chondroitin 4-sulphate hydrogels. *European Journal of Pharmaceutical Sciences,* 15(2), 139-148.

Jiang, C., Magnaldo, T., Ohtsuki, M., Freedberg, I., Bernerd, F. and Blumenberg, M. (1993) Epidermal Growth-Factor and Transforming Growth-Factor-Alpha Specifically Induce the Activation-Associated and Hyperproliferation-Associated Keratin-6 and Keratin-16. *Proceedings of the National Academy of Sciences of the United States of America,* 90(14), 6786-6790.

Johnson, K.A. and Goody, R.S. (2011) The Original Michaelis Constant: Translation of the 1913 Michaelis-Menten Paper. *Biochemistry,* 50(39), 8264-8269.

Jones, D.S. (1999) Dynamic mechanical analysis of polymeric systems of pharmaceutical and biomedical significance. *International Journal of Pharmaceutics,* 179(2), 167-178.

Jones, D.S., Tian, Y., Abu-Diak, O. and Andrews, G.P. (2012) Pharmaceutical applications of dynamic mechanical thermal analysis. *Advanced Drug Delivery Reviews,* 64(5), 440-448.

Jones, D., Brown, A. and Woolfson, A. (2001) Rheological characterization of bioadhesive, antimicrobial, semisolids designed for the treatment of periodontal diseases: Transient and dynamic viscoelastic and continuous shear analysis. *Journal of Pharmaceutical Sciences,* 90(12), 1978-1990.

Jones, J. and Clemmons, D. (1995) Insulin-Like Growth-Factors and their Binding-Proteins - Biological Actions. *Endocrine Reviews,* 16(1), 3-34.

Jonsson, M. (1972) Isoelectric spectra of native and base denatured crystallised swine pepsin. *Acta Chemica Scandinavica,* 26, 3435-3440.

Jorissen, R., Walker, F., Pouliot, N., Garrett, T., Ward, C. and Burgess, A. (2003) Epidermal growth factor receptor: mechanisms of activation and signalling. *Experimental Cell Research,* 284(1), 31-53.

Kadajji, V.G. and Betageri, G.V. (2011) Water Soluble Polymers for Pharmaceutical Applications. *Polymers,* 3(4), 1972-2009.

Kanety, H., Karasik, A., Klinger, B., Silbergeld, A. and Laron, Z. (1993) Long-Term Treatment of Laron Type Dwarfs with Insulin-Like Growth Factor-i Increases Serum Insulin-Like Growth Factor-Binding Protein-3 in the Absence of Growth-Hormone Activity. *Acta Endocrinologica,* 128(2), 144-149.

Karey, K. and Sirbasku, D. (1988) Differential Responsiveness of Human-Breast Cancer Cell-Lines Mcf-7 and T47d to Growth-Factors and 17-Beta-Estradiol. *Cancer Research,* 48(14), 4083-4092.

Katre, N.V., Asherman, J., Schaefer, H. and Hora, M. (1998) Multivesicular liposome (DepoFoam) technology for the sustained delivery of insulin-like Growth Factor-I (IGF-I). *Journal of Pharmaceutical Sciences,* 87(11), 1341-1346.

Keller, B. and Li, L. (2000) Discerning matrix-cluster peaks in matrix-assisted laser desorption/ionization time-of-flight mass spectra of dilute peptide mixtures. *Journal of the American Society for Mass Spectrometry*, 11(1), 88-93.

Keyt, B., Berleau, L., Nguyen, H., Chen, H., Heinsohn, H., Vandlen, R. and Ferrara, N. (1996) The carboxyl-terminal domain (111-165) of vascular endothelial growth factor is critical for its mitogenic potency. *Journal of Biological Chemistry*, 271(13), 7788-7795.

Khoury, C., Adalsteinsson, T., Johnson, B., Crone, W.C. and Beebe, D.J. (2003) Tunable microfabricated hydrogels - A study in protein interaction and diffusion. *Biomedical Microdevices,* 5(1), 35-45.

Kim, S.W., Bae, Y.H. and Okano, T. (1992) Hydrogels - Swelling, Drug Loading, and Release. *Pharmaceutical Research,* 9(3), 283-290.

Kim, S., Lee, K., Kim, I., Lee, Y. and Kim, S. (2003) Swelling kinetics of modified poly(vinyl alcohol) hydrogels. *Journal of Applied Polymer Science,* 90(12), 3310-3313.

Klasen, H. (2000) A review on the nonoperative removal of necrotic tissue from burn wounds. *Burns*, 26(3), 207-222.

Knowles, J.R. (1970) A discussion on the structure and function of proteolytic enzymes. *Philosophical Transactions of the Royal Society of London, Series B, Biological Science,* 257(813), 135-146.

Koch, S. and Claesson-Welsh, L. (2012) Signal Transduction by Vascular Endothelial Growth Factor Receptors. *Cold Spring Harbor Perspectives in Medicine*, 2(7), a006502.

Koetting, M.C. and Peppas, N.A. (2014) pH-Responsive poly(itaconic acid-co-N-vinylpyrrolidone) hydrogels with reduced ionic strength loading solutions offer

improved oral delivery potential for high isoelectric point-exhibiting therapeutic proteins. *International Journal of Pharmaceutics,* 471(1-2), 83-91.

Kolluri, R. (2014) Management of venous ulcers. *Techniques in Vascular and Interventional Radiology,* 17(2), 132-8.

Koseoglu, S.T., Harmatz, P., Turbeville, S. and Nicely, H. (2009) Reversed papilledema in an MPS VI patient with galsulfase (Naglazyme) therapy. *International Ophthalmology,* 29(4), 267-269.

Koshizuka, S., Kanazawa, K., Kobayashi, N., Takazawa, I., Waki, Y., Shibusawa, H. and Shumiya, S. (1997) The beneficial effects of recombinant human insulin-like growth factor-I (IGF-I) on wound healing in severely wounded senescent mice. *Surgery Today-the Japanese Journal of Surgery,* 27(10), 946-952.

Koshland, D. (1994) The Key-Lock Theory and the Induced Fit Theory. *Angewandte Chemie-International Edition,* 33(23-24), 2375-2378.

Kouhara, H., Hadari, Y., SpivakKroizman, T., Schilling, J., BarSagi, D., Lax, I. and Schlessinger, J. (1997) A lipid-anchored Grb2-binding protein that links FGF-receptor activation to the Ras/MAPK signaling pathway. *Cell,* 89(5), 693-702.

Kuhn, R.J., Gelrud, A., Munck, A. and Caras, S. (2010) CREON (Pancrelipase Delayed-Release Capsules) for the Treatment of Exocrine Pancreatic Insufficiency. *Advances in Therapy*, 27(12), 895-916.

Laidler, K.J. and Peterman, B.F. (1979) Temperature Effects in Enzyme Kinetics. *Methods in Enzymology,* 63, 234-257.

Laing, P. (1994) Diabetic Foot Ulcers. *The American Journal of Surgery,* 167(1A), 31-36.

LaRochelle, W.J., Jeffers, M., McDonald, W.F., Chillakuru, R.A., Giese, N.A., Lokker, N.A., Sullivan, C., Boldog, F.L., Yang, M., Vernet, C., Burgess, C.E., Fernandes, E., Deegler, L.L., Rittman, B., Shimkets, J., Shimkets, R.A., Rothberg, J.M. and Lichenstein, H.S. (2001) PDGF-D, a new protease-activated growth factor. *Nature Cell Biology,* 3(5), 517-521.

Laron, Z. (2001) Insulin-like growth factor 1 (IGF-1): a growth hormone. *Journal of Clinical Pathology-Molecular Pathology,* 54(5), 311-316.

Laviola, L., Natalicchio, A. and Giorgino, F. (2007) The IGF-I signaling pathway. *Current Pharmaceutical Design,* 13(7), 663-669.

Lee, H.K., Lee, J.H., Kim, M., Kariya, Y., Miyazaki, K. and Kim, E.K. (2006) Insulin-like growth factor-1 induces migration and expression of laminin-5 in cultured human corneal epithelial cells. *Investigative Ophthalmology & Visual Science,* 47(3), 873-882.

Lee, S. (2000) Cytokine delivery and tissue engineering. *Yonsei Medical Journal,* 41(6), 704-719.

Li, J., Chen, J. and Kirsner, R. (2007) Pathophysiology of acute wound healing. *Clinics in Dermatology,* 25(1), 9-18.

Li, J., Wang, N. and Wu, X. (1998) Poly(vinyl alcohol) nanoparticles prepared by freezing-thawing process for protein/peptide drug delivery. *Journal of Controlled Release,* 56(1-3), 117-126.

Li, X., Ponten, A., Aase, K., Karlsson, L., Abramsson, A., Uutela, M., Backstrom, G., Hellstrom, M., Bostrom, H., Li, H., Soriano, P., Betscholtz, C., Heldin, C., Alitalo, K., Ostman, A. and Eriksson, U. (2000) PDGF-C is a new protease-activated ligand for the PDGF alpha-receptor. *Nature Cell Biology,* 2(5), 302-309.

Lin, H., Liu, Y., Yo, T.L., Liu, W. and Rwei, S. (2005) Light scattering and viscoelasticity study of poly (vinyl alcohol)-borax aqueous solutions and gels. *Polymer,* 46, 5541-5549.

Lin, Y., Fusek, M., Lin, X., Hartsuck, J., Kezdy, F. and Tang, J. (1992) Ph-Dependence of Kinetic-Parameters of Pepsin, Rhizopuspepsin, and their Active-Site Hydrogen-Bond Mutants. *Journal of Biological Chemistry,* 267(26), 18413-18418.

Liu, Y.C., Margolis, D.J. and Isseroff, R.R. (2011) Does Inflammation Have a Role in the Pathogenesis of Venous Ulcers?: A Critical Review of the Evidence. *Journal of Investigative Dermatology,* 131(4), 818-827.

Loughlin, R.G., Tunney, M.M., Donnelly, R.F., Murphy, D.J., Jenkins, M. and McCarron, P.A. (2008) Modulation of gel formation and drug-release characteristics of lidocaine-loaded poly(vinyl alcohol)-tetraborate hydrogel systems using scavenger polyol sugars. *European Journal of Pharmaceutics and Biopharmaceutics*, 69(3), 1135-1146.

Lyttle, D., Fraser, K., Fleming, S., Mercer, A. and Robinson, A. (1994) Homologs of Vascular Endothelial Growth-Factor are Encoded by the Poxvirus Orf Virus. *Journal of Virology*, 68(1), 84-92.

MacArthur, C., Lawshe, A., Xu, J., Santos-Ocampo, S., Heikinheimo, M., Chellaiah, A. and Orntiz, D. (1995) Fgf-8 Isoforms Activate Receptor Splice Forms that are Expressed in Mesenchymal Regions of Mouse Development. *Development*, 121(11), 3603-3613.

Maione, A.G., Smith, A., Kashpur, O., Yanez, V., Knight, E., Mooney, D.J., Veves, A., Tomic-Canic, M. and Garlick, J.A. (2016) Altered ECM deposition by diabetic foot ulcer-derived fibroblasts implicates fibronectin in chronic wound repair. *Wound Repair and Regeneration*, 24(4), 630-643.

Mantripragada, V.P. and Jayasuriya, A.C. (2014) IGF-1 release kinetics from chitosan microparticles fabricated using environmentally benign conditions. *Materials Science & Engineering C-Materials for Biological Applications*, 42, 506-516.

Markham, A. (2017) Cerliponase Alfa: First Global Approval. *Drugs*, 77(11), 1247-1249.

Marques, M.R., Manolio Soares Freitas, R.A., Correa Carlos, A.C., Siguemoto, E.S., Fontanari, G.G. and Gomes Areas, J.A. (2015) Peptides from cowpea present antioxidant activity, inhibit cholesterol synthesis and its solubilisation into micelles. *Food Chemistry*, 168, 288-293.

Martin, P. (1997) Wound healing - Aiming for the perfect skin regeneration. *Science*, 276, 75-81.

Martini, F. and Nath, J.L. (2009a) Chapter 21 Blood vessels and circulation. *In:* Anon.*Fundamentals of Anatomy & Physiology.* 8th ed. San Francisco: Pearson Benjamin Cummings, 750-759.

Martini, F. and Nath, J.L. (2009b) Chapter 5 The Integumentary system, Section 5-1. *In:* Anon.*Fudamentals of Anatomy & Physiology*. 8th ed. San Francisco: Pearson Benjamin Cummings, 159-162.

Massague, J. (1990) The Transforming Growth-Factor-Beta Family. *Annual Review of Cell Biology,* 6, 597-641.

Matsumoto, T. and Claesson-Welsh, L. (2001) *VEGF Receptor signal transduction.* AAAS: Science Signaling. Available at: http://stke.sciencemag.org/content/2001/112/re21.full [Accessed 23/08/17].

MatTek Corporation. (2018) *EpiDerm™.* Ashland USA: MatTek Corporation. Available at: https://www.mattek.com/products/epiderm/ [Accessed 22/04/18].

Mazzieri, R., Jurukovski, V., Obata, H., Sung, J., Platt, A., Annes, E., Karaman-Jurukovska, N., Gleizes, P. and Rifkin, D. (2005) Expression of truncated latent TGF-beta-binding protein modulates TGF-beta signaling (vol 118, pg 2177, 2005). *Journal of Cell Science,* 118(11), 2545-2545.

McCarron, P.A., Murphy, D.J., Little, C., McDonald, J., Kelly, O.J. and Jenkins, M.G. (2011) Preliminary Clinical Assessment of Polyvinyl Alcohol-Tetrahydroxyborate Hydrogels as Potential Topical Formulations for Local Anesthesia of Lacerations. *Academic Emergency Medicine,* 18(4), 333-339.

McSwiggan, R. (2011) *Local wound assessment, Treatment objectives, 'The ideal dressing' NI Wound Care Formulary.* Tissue Viability Nurse Specialist, Northern Health and Social Care Trust.

Mellott, M., Searcy, K. and Pishko, M. (2001) Release of protein from highly cross-linked hydrogels of poly(ethylene glycol) diacrylate fabricated by UV polymerization. *Biomaterials,* 22(9), 929-941.

Menke, N.B., Ward, K.R., Witten, T.M., Bonchev, D.G. and Diegelmann, R.F. (2007) Impaired wound healing. *Clinics in Dermatology,* 25(1), 19-25.

Mezger, T.G. (2014) *The Rheology Handbook.* 4th ed. Vincentz Network.

Miller, G. and Seale, J. (1981) Lymphatic Clearance during Compressive Loading. *Lymphology*, 14(4), 161-166.

Mitra, R. and Khar, A. (2004) Suppression of macrophage function in AK-5 tumor transplanted animals: role of TGF-beta1. *Immunology Letters,* 91, 189-195.

Mitri, Z., Constantine, T. and O'Regan, R. (2012) The HER2 receptor in breast cancer: pathophysiology, clinical use and new advances in therapy. *Chemotherapy Research and Practice,* 2012, 1-7.

Miyani, V.A. and Hughes, M.F. (2017) Assessment of the in vitro dermal irritation potential of cerium, silver, and titanium nanoparticles in a human skin equivalent model. *Cutaneous and Ocular Toxicology,* 36(2), 145-151.

Moasser, M.M. (2007) The oncogene HER2: its signaling and transforming functions and its role in human cancer pathogenesis. *Oncogene,* 26(45), 6469-6487.

Mohan, V.K. (2007) Recombinant human epidermal growth factor (REGEN-DTM 150): Effect on healing of diabetic foot ulcers. *Diabetes Research and Clinical Practice,* 78, 405-411.

Monsuur, H.N., Boink, M.A., Weijers, E.M., Roffel, S., Breetveld, M., Gefen, A., van den Broek, L.J. and Gibbs, S. (2016) Methods to study differences in cell mobility during skin wound healing in vitro. *Journal of Biomechanics,* 49(8), 1381-1387.

Murphy, D.J., Sankalia, M.G., Loughlin, R.G., Donnelly, R.F., Jenkins, M.G. and McCarron, P.A. (2012) Physical characterisation and component release of poly(vinyl alcohol)–tetrahydroxyborate hydrogels and their applicability as potential topical drug delivery systems. *International Journal of Pharmaceutics,* 423(2), 326-334.

Murthy, N., Thng, Y., Schuck, S., Xu, M. and Frechet, J. (2002) A novel strategy for encapsulation and release of proteins: Hydrogels and microgels with acid-labile acetal cross-linkers. *Journal of the American Chemical Society*, 124(42), 12398-12399.

Nagai, M. and Embil, J. (2002) Becaplermin: recombinant platelet derived growth factor, a new treatment for healing diabetic foot ulcers. *Expert Opinion on Biological Therapy*, 2(2), 211-218.

Nagano, T., Nakamura, M., Nakata, K., Yamaguchi, T., Takase, K., Okahara, A., Ikuse, T. and Nishida, T. (2003) Effects of substance P and IGF-1 in corneal epithelial barrier function and wound healing in a rat model of neurotrophic keratopathy. *Investigative Ophthalmology & Visual Science*, 44(9), 3810-3815.

Nagase, H., Visse, R. and Murphy, G. (2006) Structure and function of matrix metalloproteinases and TIMPs. *Cardiovascular Research*, 69(3), 562-573.

Nalinanon, S., Benjakul, S., Visessanguan, W. and Kishimura, H. (2008) Tuna pepsin: Characteristics and its use for collagen extraction from the skin of threadfin bream (Nemipterus spp.). *Journal of Food Science*, 73(5), C413-C419.

National Institute for Health and Care Excellence. (2014) *Pressure Ulcers: prevention and management.* Available at: https://www.nice.org.uk/guidance/cg179

National Pressure Ulcer Advisory Panel. (1989) Pressure ulcer prevelance, cost, and risk assessment: consensus developement conference statement. *Decubitus*, 2(2), 24-28.

Nelzen, O., Bergqvist, D. and Lindbagen, A. (1994) Venous and non-venous leg ulcers: clinical history and appearance in a population study. *British Journal of Surgery*, 81, 182-187.

Nesargikar, P.N., Spiller, B. and Chavez, R. (2012) The complement system: history, pathways, cascade and inhibitors. *European Journal of Microbiology & Immunology*, 2(2), 103-11.

Neufeld, G., Cohen, T., Gengrinovitch, S. and Poltorak, Z. (1999) Vascular endothelial growth factor (VEGF) and its receptors. *Faseb Journal,* 13(1), 9-22.

Northrop, D. (2001) Follow the protons: A low-barrier hydrogen bond unifies the mechanisms of the aspartic proteases. *Accounts of Chemical Research,* 34(10), 790-797.

Nugent, M. and Iozzo, R. (2000) Fibroblast growth factor-2. *International Journal of Biochemistry & Cell Biology,* 32(2), 115-120.

Nunes Achar, R.A., Silva, T.C., Achar, E., Martines, R.B. and Martins Machado, J.L. (2014) Use of insulin-like growth factor in the healing of open wounds in diabetic and non-diabetic rats. *Acta Cirurgica Brasileira,* 29(2), 125-131.

Ogiso, H., Ishitani, R., Nureki, O., Fukai, S., Yamanaka, M., Kim, J., Saito, K., Sakamoto, A., Inoue, M., Shirouzu, M. and Yokoyama, S. (2002) Crystal structure of the complex of human epidermal growth factor and receptor extracellular domains. *Cell,* 110(6), 775-787.

Oh, J.W., Hsi, T., Guerrero-Juarez, C.F., Ramos, R. and Plikus, M.V. (2013) Organotypic Skin Culture. *Journal of Investigative Dermatology,* 133(11), E14-E17.

Oliveira, R.N., Rouze, R., Quilty, B., Alves, G.G., Soares, G.D.A., Thire, R.M.S.M. and McGuinness, G.B. (2014) Mechanical properties and in vitro characterization of polyvinyl alcohol-nano-silver hydrogel wound dressings. *Interface Focus,* 4(1), 20130049.

Ornitz, D.M. and Itoh, N. (2001) Fibroblast growth factors. *Genome Biology,* 2(3), 3005.1.

Orosco, M.M., Pacholski, C. and Sailor, M.J. (2009) Real-time monitoring of enzyme activity in a mesoporous silicon double layer. *Nature Nanotechnology,* 4(4), 255-258.

Orrurtreger, A., Bedford, M., Burakova, T., Arman, E., Zimmer, Y., Yayon, A., Givol, D. and Lonai, P. (1993) Developmental Localization of the Splicing

Alternatives of Fibroblast Growth-Factor Receptor-2 (Fgfr2). *Developmental Biology,* 158(2), 475-486.

Pajusola, K., Aprelikova, O., Pelicci, G., Weich, H., Claesson-Welsh, L. and Alitalo, K. (1994) Signalling properties of FLT4, a proteolytically processed receptor tyrosine kinase related to two VEGF receptors. *Oncogene,* 9(12), 3545-3555.

Park, H., Kong, B. and Oh, E. (2011) Effect of high adhesive polyvinyl alcohol binder on the anodes of lithium ion batteries. *Electrochemistry Communications,* 13(10), 1051-1053.

Pastar, I., Liang, L., Sawaya, P.A., Wikramanayake, T.C., Glinos, G.D., Drakulich, S., Chen, V., Stojadinovic, O., Davis, S.C. and Tomic-Canic, M. (2018) Preclinical models for wound-healing studies. *Skin Tissue Models, ,* 223-253.

Pastores, G.M. (2008) Laronidase (Aldurazyme (R)): enzyme replacement therapy for mucopolysaccharidosis type I. *Expert Opinion on Biological Therapy,* 8(7), 1003-1009.

Patton, J. and Palmer, A. (2006) Physical properties of hemoglobin-poly(acrylamide) hydrogel-based oxygen carriers: Effect of reaction pH. *Langmuir,* 22(5), 2212-2221.

Pecoraro, R., Reiber, G. and Burgess, E. (1990) Pathways to Diabetic Limb Amputation - Basis for Prevention. *Diabetes Care,* 13(5), 513-521.

Peirce, S., Skalak, T. and Rodeheaver, G. (2000) Ischemia-reperfusion injury in chronic pressure ulcer formation: A skin model in the rat. *Wound Repair and Regeneration,* 8(1), 68-76.

Penn, J.W., Grobbelaar, A.O. and Rolfe, K.J. (2012) The role of the TGF-β family in wound healing, burns and scarring: a review. *International Journal of Burns and Trauma,* 2(1), 18-28.

Penn, S., Hu, H., Brown, P. and Lebrilla, C. (1997) Direct analysis of sugar alcohol borate complexes in plant extracts by matrix-assisted laser desorption/ionization Fourier transform mass spectrometry. *Analytical Chemistry,* 69(13), 2471-2477.

Peppas, N.A., Bures, P., Leobandung, W. and Ichikawa, H. (2000) Hydrogels in pharmaceutical formulations. *European Journal of Pharmaceutics and Biopharmaceutics,* 50(1), 27-46.

Pepper, M.S. (1997) Transforming growth factor-beta: Vasculogenesis, angiogenesis, and vessel wall integrity. *Cytokines and Growth Factor Reviews,* 8(1), 21-43.

Pezron, E., Leibler, L., Ricard, A. and Audebert, R. (1988) Reversible Gel Formation Induced by Ion Complexation .2. Phase-Diagrams. *Macromolecules,* 21(4), 1126-1131.

Pezron, E., Leibler, L., Ricard, A., Lafuma, F. and Audebert, R. (1989) Complex-Formation in Polymer Ion Solutions .1. Polymer Concentration Effects. *Macromolecules,* 22(3), 1169-1174.

Piana, S. and Carloni, P. (2000) Conformational flexibility of the catalytic Asp dyad in HIV-1 protease: an ab initio study on the free enzyme. *Proteins-Structure Function and Genetics,* 39(1), 26-36.

Pierce, G.F., Mustoe, T.A., Altrock, B.,W., Deuel, T.F. and Thomason, A. (1991) Role of Platelet-Derived Growth-Factor in Wound-Healing. *Journal of Cellular Biochemistry,* 45(4), 319-326.

Pinkas-Kramarski, R., Shelly, M., Guarino, B., Wang, L., Lyass, L., Alroy, I., Alimandi, M., Kuo, A., Moyer, J., Lavi, S., Eisenstein, M., Ratzkin, B., Seger, R., Bacus, S., Pierce, J., Andrews, G. and Yarden, Y. (1998) ErbB tyrosine kinases and the two neuregulin families constitute a ligand-receptor network (vol 18, pg 6090, 1998). *Molecular and Cellular Biology,* 18(12), 7602-7602.

Piper, D.W. and Fenton, B.H. (1965) pH stability and activity curves of pepsin with special reference to their clinical importance. *Gut,* 6(5), 506-8.

Polgar, L. (1987) The Mechanism of Action of Aspartic Proteases Involves Push-Pull Catalysis. *FEBS Letters,* 219(1), 1-4.

Pongsavee, M. (2009) Effect of borax on immune cell proliferation and sister chromatid exchange in human chromosomes. *Journal of Occupational Medicine and Toxicology*, 4(27), 1-6.

Ponomareva, E.A., Kartuzova, V.E., Vlakh, E.G. and Tennikova, T.B. (2010) Monolithic bioreactors: Effect of chymotrypsin immobilization on its biocatalytic properties. *Journal of Chromatography B-Analytical Technologies in the Biomedical and Life Sciences*, 878(5-6), 567-574.

Posnett, J. and Franks, P.J. (2008) The burden of chronic wounds in the UK. *Nursing Times*, 104(3), 44-45.

Pozzi, G., Guidi, M., Laudicina, F., Marazzi, M., Falcone, L., Betti, R., Crosti, C., Muller, E.E., DiMattia, G.E., Locatelli, V. and Torsello, A. (2004) IGF-I stimulates proliferation of spontaneously immortalized human keratinocytes (HACAT) by autocrine/paracrine mechanisms. *Journal of Endocrinological Investigation*, 27(2), 142-149.

Provenzano, P.P., Alejandro-Osorio, A.L., Grorud, K.W., Martinez, D.A., Vailas, A.C., Grindeland, R.E. and Vanderby Jr, R. (2007) Systemic administration of IGF-I enhances healing in collagenous extracellular matrices: evaluation of loaded and unloaded ligaments. *Biomedical Central Physiology*, 7(2), 1-17.

Puntis, J.W.L. and Zamvar, V. (2015) Congenital sucrase-isomaltase deficiency: diagnostic challenges and response to enzyme replacement therapy. *Archives of Disease in Childhood*, 100(9), 869-871.

Quan, J., Tiddens, H., Sy, J., McKenzie, S., Montgomery, M., Robinson, P., Wohl, M., Konstan, M. and Pulmozyme Early Intervention Trial. (2001) A two-year randomized, placebo-controlled trial of dornase alfa in young patients with cystic fibrosis with mild lung function abnormalities. *Journal of Pediatrics*, 139(6), 813-820.

R&D Systems. (2015) *Recombinant Human IGF-1 Certificate of Analysis.* UK: R&D Systems. Available at: https://www.rndsystems.com/products/recombinant-human-igf-i-protein-cf_291-g1 [Accessed 07/12/2017].

R&D Systems. (2017) *Quantikine® ELISA Human IGF-1* . Adingdon, UK: R&D Systems a biotechne® brand.

Raffetto, J.D. (2009) Dermal pathology, cellular biology, and inflammation in chronic venous disease. *Thrombosis Research,* 123, S66-S71.

Rauser, S., Marquardt, C., Balluff, B., Deininger, S., Albers, C., Belau, E., Hartmer, R., Suckau, D., Specht, K., Ebert, M.P., Schmitt, M., Aubele, M., Hoefler, H. and Walch, A. (2010) Classification of HER2 Receptor Status in Breast Cancer Tissues by MALDI Imaging Mass Spectrometry. *Journal of Proteome Research,* 9(4), 1854-1863.

Reddy, N., Chen, L., Zhang, Y. and Yang, Y. (2014) Reducing environmental pollution of the textile industry using keratin as alternative sizing agent to poly(vinyl alcohol). *Journal of Cleaner Production,* 65, 561-567.

Reddy, N., Cochran, G. and Krouskop, T. (1981) Interstitial Fluid-Flow as a Factor in Decubitus Ulcer Formation. *Journal of Biomechanics,* 14(12), 879-881.

Rees, R., Robson, M., Smiell, J., Perry, B. and Pressure Ulcer Study Grp. (1999) Becaplermin gel in the treatment of pressure ulcers: a phase II randomized, double-blind, placebo-controlled study. *Wound Repair and Regeneration,* 7(3), 141-147.

Reiber, G., Lipsky, B. and Gibbons, G. (1998) The burden of diabetic foot ulcers. *American Journal of Surgery,* 176(2A), 5S-10S.

Righetti, P. (2004) Determination of the isoelectric point of proteins by capillary isoelectric focusing. *Journal of Chromatography A,* 1037(1-2), 491-499.

Rinderknecht, E. and Humbel, R.E. (1976) Polypeptides with nonsuppressible insulin-like and cell-growth promoting activities in human serum: isolation, chemical characterization, and some biological properties of forms I and II. *Proceedings of the National Academy of Sciences of the United States of America,* 73, 2365-2369.

Ritger, P.L. and Peppas, N.A. (1987) A simple equation for description of solute release II. Fickian and anomalous release from swellable devices. *Journal of Controlled Release,* 5, 37-42.

Roberts, A.B., Sporn, M.B., Assoian, R.K., Smith, J.M., Roche, N.S., Wakefield, L.M., Heine, U.I., Liotta, L.A., Falanga, V. and Kehrl, J.H. (1986) Transforming growth factor type beta: rapid induction of fibrosis and angiogenesis in vivo and stimulation of collagen formation in vitro. *Proceedings of the National Academy of Sciences of the United States of America,* 83, 4167-4171.

Roberts, A. (1998) Molecular and cell biology of TGF-beta. *Mineral and Electrolyte Metabolism,* 24(2-3), 111-119.

Robson, M.C. (1997) The role of growth factors in the healing of chronic wounds. *Wound Repair and Regeneration,* 5, 12-17.

Robson, M.C., Phillip, L.G., Cooper, D.M., Lyle, W.G., Robson, L.E., Odom, L.,Hanham, A.F. and Ksander, G.A. (1995) Safety and effect of transforming growth factor-β2 for treatment of venous stasis ulcers. *Wound Repair and Regeneration,* 3(2), 157-167.

Robson, M. (1997) Wound infection - A failure of wound healing caused by an imbalance of bacteria. *Surgical Clinics of North America,* 77(3), 637-&.

Robson, M. and Heggers, J. (1969) Bacterial quantification of open wounds. *Military Medicine,* 134, 19-24.

Robson, M., Phillips, L., Lawrence, W., Bishop, J., Youngerman, J., Hayward, P., Broemeling, L. and Heggers, J. (1992) The Safety and Effect of Topically Applied Recombinant Basic Fibroblast Growth-Factor on the Healing of Chronic Pressure Sores. *Annals of Surgery,* 216(4), 401-408.

Robson, M., Phillips, T., Falanga, V., Odenheimer, D., Parish, L., Jensen, J. and Steed, D. (2001) Randomized trial of topically applied, repifermin (recombinant human keratinocyte growth factor-2) to accelerate wound healing in venous ulcers. *Wound Repair and Regeneration,* 9(5), 347-352.

Rolfe, K.J., Richardson, J., Vigor, C., Irvine, L.M., Grobbelaar, A.O. and Linge, C. (2007) A role for TGF-beta 1-Induced cellular responses during wound healing of

the non-scarring early human fetus? *Journal of Investigative Dermatology*, 127(11), 2656-2667.

Rosenbloom, A.L. (2009) Mecasermin (recombinant human insulin-like growth factor I). *Advances in Therapy,* 26(1), 40-54.

Rosenfeld, R., Hwa, V., Wilson, L., Lopez-Bermejo, A., Buckway, C., Burren, C., Choi, W., Devi, G., Ingermann, A., Graham, D., Minniti, G., Spagnoli, A. and Oh, Y. (1999) The insulin-like growth factor binding protein superfamily: New perspectives. *Pediatrics,* 104(4), 1018-1020.

Ross, R., Glomset, J., Kariya, B. and Harker, L. (1974) A platelet-dependent serum factor that stimulates the proliferation of arterial smooth muscle cells in vitro. *Proceedings of the National Academy of Sciences of the United States of America,* 71, 1207-1210.

Roupe, K.M., Nybo, M., Sjobring, U., Alberius, P., Schmidtchen, A. and Sorensen, O.E. (2010) Injury Is a Major Inducer of Epidermal Innate Immune Responses during Wound Healing. *Journal of Investigative Dermatology,* 130(4), 1167-1177.

Ruan, C., Chi, Y. and Zhang, R. (2010) Kinetics of Hydrolysis of Egg White Protein by Pepsin. *Czech Journal of Food Sciences,* 28(5), 355-363.

Rubin, I. and Yarden, Y. (2001) The basic biology of HER2. *Annals of Oncology*, 12, 3-8.

Rudolph, R. and Vande Berg, J. (2005) Hypertrophic scar fibroblasts have increased connective tissue growth factor expression after transforming growth factor-beta stimulation. *Plastic and Reconstructive Surgery,* 116(5), 1391-1392.

Rutter, P.M., Carpenter, B., Hill, S.S. and Locke, I.C. (2000) Varidase: the science behind the medicament. *Journal of Wound Care*, 9(5), 223-226.

Ruvinov, E., Leor, J. and Cohen, S. (2011) The promotion of myocardial repair by the sequential delivery of IGF-1 and HGF from an injectable alginate biomaterial in a model of acute myocardial infarction. *Biomaterials,* 32(2), 565-578.

Saaristo, A., Tammela, T., Farkkila, A., Karkkainen, M., Suominen, E., Yla-Herttuala, S. and Alitalo, K. (2006) Vascular endothelial growth factor-C accelerates diabetic wound healing. *American Journal of Pathology*, 169(3), 1080-1087.

Sachon, E., Clodic, G., Blasco, T. and Bolbach, G. (2007) Protein desolvation in UV matrix-assisted laser desorption/ionization (MALDI). *Journal of the American Society for Mass Spectrometry*, 18(10), 1880-1890.

Salmon, W.D.J. and Daughaday W. (1957) A hormonally controlled serum factor which stimulates sulfate incorporation by cartilage in vitro. *Journal of Laboratory and Clinical Medicine*, 49, 825-836.

Sanford, M. and Lo, J.H. (2014) Elosulfase alfa: First Global Approval. *Drugs*, 74(6), 713-718.

Scaloni, A., Pieragostini, E., Malorni, A., Ferrara, L. and Di Luccia, A. (1998) Bovine hemoglobin alpha-globin chain polymorphism: Primary structure determination of two new genetic variants by mass spectrometry and amino acid sequencing. *Biochimie*, 80(4), 333-338.

Schlessinger, J. (2000) Cell signaling by receptor tyrosine kinases. *Cell*, 103(2), 211-225.

Schlessinger, J., Plotnikov, A., Ibrahimi, O., Eliseenkova, A., Yeh, B., Yayon, A., Linhardt, R. and Mohammadi, M. (2000) Crystal structure of a ternary FGF-FGFR-heparin complex reveals a dual role for heparin in FGFR binding and dimerization. *Molecular Cell*, 6(3), 743-750.

Schroeder, F., Diehm, N., Kareem, S., Ames, M., Pira, A., Zwettler, U., Lawall, H. and Diehm, C. (2006) A modified calculation of ankle-brachial pressure index is far more sensitive in the detection of peripheral arterial disease. *Journal of Vascular Surgery*, 44(3), 531-536.

Schultz, G., Rotatori, D. and Clark, W. (1991) Egf and Tgf-Alpha in Wound-Healing and Repair. *Journal of Cellular Biochemistry*, 45(4), 346-352.

Sellheyer, K., Bickenbach, J., Rothnagel, J., Bundman, D., Longley, M., Krieg, T., Roche, N., Roberts, A. and Roop, D. (1993) Inhibition of Skin Development by Overexpression of Transforming Growth-Factor-Beta-1 in the Epidermis of Transgenic Mice. *Proceedings of the National Academy of Sciences of the United States of America*, 90(11), 5237-5241.

Shah, A., Dinwiddie, R., Madge, S., Prescott, P. and Hudson, G. (1993) High-Dose Nutrizym-22 in Cystic-Fibrosis. *European Journal of Pediatrics*, 152(9), 763-764.

Shalaby, W., Abdallah, A., Park, H. and Park, K. (1993) Loading of Bovine Serum-Albumin into Hydrogels by an Electrophoretic Process and its Potential Application to Protein Drugs. *Pharmaceutical Research*, 10(3), 457-460.

Shaw, J. and Boulton, A. (1997) The pathogenesis of diabetic foot problems - An overview. *Diabetes*, 46, S58-S61.

Shewan, H.M. and Stokes, J.R. (2013) Review of techniques to manufacture micro-hydrogel particles for the food industry and their applications. *Journal of Food Engineering*, 119(4), 781-792.

Shim, A.H., Liu, H., Focia, P.J., Chen, X., Lin, P.C. and He, X. (2010) Structures of a platelet-derived growth factor/propeptide complex and a platelet-derived growth factor/receptor complex. *Proceedings of the National Academy of Sciences of the United States of America*, 107(25), 11307-11312.

Shiraha, H., Glading, A., Gupta, K. and Wells, A. (1999) IP-10 inhibits epidermal growth factor-induced motility by decreasing epidermal growth factor receptor-mediated calpain activity. *Journal of Cell Biology*, 146(1), 243-253.

Sieggreen, M.Y. and Kline, R.A. (2004) Arterial Insufficiency and Ulceration: Diagnosis and Treatment Options. *Advances in Skin & Wound Care*, 17(3), 242-253.

Sigma-Aldrich. *Pepsin from porcine gastric mucosa product information.* UK: Sigma-Aldrich. Available at: https://www.sigmaaldrich.com/content/dam/sigma-aldrich/docs/Sigma/Product_Information_Sheet/1/p6887pis.pdf [Accessed 23/11/2017].

Sigma-Aldrich. (2015) *Product specification pepsin from porcine gastric mucosa P6887.* USA: Sigma-Aldrich. Available at: https://www.sigmaaldrich.com/Graphics/COfAInfo/SigmaSAPQM/SPEC/P6/P6887/P6887-BULK_____SIGMA____.pdf [Accessed 07/12/2017].

Sigma-Aldrich. (2017) *Poly(vinyl alcohol) (PVA).* UK: Sigma-Aldrich. Available at: http://www.sigmaaldrich.com/materials-science/material-science-products.html?TablePage=112435902 [Accessed 07/09/2017].

Simon, D.A., Dix, F.P. and McCollum, C.N. (2004) Management of venous leg ulcers. *British Medical Journal,* 328(7452), 1358-1362.

Singer, A.J., Taira, B.R., Anderson, R., McClain, S.A. and Rosenberg, L. (2011) Reepithelialization of Mid-dermal Porcine Burns After Rapid Enzymatic Debridement With Debrase (R). *Journal of Burn Care & Research,* 32(6), 647-653.

Sinton, S.W. (1987) Complexation chemistry of sodium borate with poly(vinyl alcohol) and small diols: a boron-11 NMR study. *Macromolecules,* 20(10), 2430-2441.

Sixt, M. (2012) Cell migration: Fibroblasts find a new way to get ahead. *Journal of Cell Biology,* 197(3), 346-348.

Smith & Nephew. (2015) *Regranex® Gel.* USA: Smith & Nephew. Available at: http://www.regranex.com/

Smith, L., Rimmer, S. and MacNeil, S. (2006) Examination of the effects of poly(N-vinylpyrrolidinone) hydrogels in direct and indirect contact with cells. *Biomaterials,* 27(14), 2806-2812.

Soker, S., Takashima, S., Miao, H., Neufeld, G. and Klagsbrun, M. (1998) Neuropilin-1 is expressed by endothelial and tumor cells as an isoform-specific receptor for vascular endothelial growth factor. *Cell,* 92(6), 735-745.

Soppirnath, K. and Aminabhavi, T. (2002) Water transport and drug release study from cross-linked polyacrylamide grafted guar gum hydrogel microspheres for the

controlled release application. *European Journal of Pharmaceutics and Biopharmaceutics,* 53(1), 87-98.

Sorg, H., Tilkorn, D.J., Hager, S., Hauser, J. and Mirastschijski, U. (2017) Skin Wound Healing: An Update on the Current Knowledge and Concepts. *European Surgical Research,* 58(1-2), 81-94.

Stadelmann, W., Digenis, A. and Tobin, G. (1998) Physiology and healing dynamics of chronic cutaneous wounds. *American Journal of Surgery,* 176(2A), 26S-38S.

Steed, J.W., Atwood, J.L. and Gale, P.A. (2012) *Supramolecular Chemistry: From Molecules to Nanomaterials.* John Wiley & Sons Ltd.

Stephens, P., Cook, H., Hilton, J., Jones, C.J., Haughton, M.F., Wyllie, F.S., Skinner, J.W., Harding, K.G., Kipling, D. and Thomas, D.W. (2003) An analysis of replicative senescence in dermal fibroblasts derived from chronic leg wounds predicts that telomerase therapy would fail to reverse their disease-specific cellular and proteolytic phenotype. *Experimental Cell Research,* 283, 22-35.

Stitt, T., Drujan, D., Clarke, B., Panaro, F., Timofeyva, Y., Kline, W., Gonzalez, M., Yancopoulos, G. and Glass, D. (2004) The IGF-1/PI3K/Akt pathway prevents short article expression of muscle atrophy-induced ubiquitin ligases by inhibiting FOXO transcription factors. *Molecular Cell,* 14(3), 395-403.

Sun, W., Lin, H., Xie, H., Chen, B., Zhao, W., Han, Q., Zhao, Y., Xiao, Z. and Dai, J. (2007) Collagen membranes loaded with collagen-binding human PDGF-BB accelerate wound healing in a rabbit dermal ischemic ulcer model. *Growth Factors,* 25(5), 309-318.

Surmacz, E., Guvakova, M., Nolan, M., Nicosia, R. and Sciacca, L. (1998) Type I insulin-like growth factor receptor function in breast cancer. *Breast Cancer Research and Treatment,* 47(3), 255-267.

Takeshita, S., Zheng, L., Brogi, E., Kearney, M., PU, L., Bunting, S., Ferrara, N., Symes, J. and Isner, J. (1994) Therapeutic Angiogenesis - a Single Intraarterial Bolus

of Vascular Endothelial Growth-Factor Augments Revascularization in a Rabbit Ischemic Hind-Limb Model. *Journal of Clinical Investigation*, 93(2), 662-670.

Tang, J., Sepulveda, P., Marciniszyn, J., Chen, K., Huang, W., Tao, N., Liu, D. and Lanier, J. (1973) Amino-Acid Sequence of Porcine Pepsin. *Proceedings of the National Academy of Sciences of the United States of America*, 70(12), 3437-3439.

Tietze, W. (1953) Molecular kinetic properties of crystalline trypsinogen. *Journal of Biological Chemistry*, 204(1), 1-11.

Tomita, M., Bellamy, W., Takase, M., Yamauchi, K., Wakabayashi, H. and Kawase, K. (1991) Potent Antibacterial Peptides Generated by Pepsin Digestion of Bovine Lactoferrin. *Journal of Dairy Science*, 74(12), 4137-4142.

Toy, L.W. and Macera, L. (2011) Evidence-based review of silver dressing use on chronic wounds. *Journal of the American Academy of Nurse Practitioners*, 23(4), 183-192.

Tracy, L.E., Minasian, R.A. and Caterson, E.J. (2016) Extracellular Matrix and Dermal Fibroblast Function in the Healing Wound. *Advances in Wound Care*, 5(3), 119-136.

Trepat, X., Chen, Z. and Jacobson, K. (2012) Cell Migration. *Comprehensive Physiology*, 2(4), 2369-2392.

Tsuboi, R., Shi, C., Sato, C., Cox, G.N. and Ogawa, H. (1995) Co-Administration of Insulin-Like Growth Factor (IGF)-I and IGF-Binding Protein-l Stimulates Wound Healing in Animal Models. *The Journal of Investigative Dermatology*, 104(2), 199-203.

Tsuboi, K. and Yamamoto, H. (2012) Clinical observation of patients with Fabry disease after switching from agalsidase beta (Fabrazyme) to agalsidase alfa (Replagal). *Genetics in Medicine*, 14(9), 779-786.

Tyrone, J., Marcus, J., Bonomo, S., Mogford, J., Xia, Y. and Mustoe, T. (2000) Transforming growth factor beta(3) promotes fascial wound healing in a new animal model. *Archives of Surgery*, 135(10), 1154-1159.

Ulubayram, K., Cakar, A., Korkusuz, P., Ertan, C. and Hasirci, N. (2001) EGF containing gelatin-based wound dressings. *Biomaterials*, 22(11), 1345-1356.

van Oijen, A., Blainey, P., Crampton, D., Richardson, C., Ellenberger, T. and Xie, X. (2003) Single-molecule kinetics of lambda exonuclease reveal base dependence and dynamic disorder. *Science*, 301(5637), 1235-1238.

Vascular Society of Great Britain and Ireland. (2017) *Arterial Ulcer*. Available at: https://www.vascularsociety.org.uk/patients/conditions/12/arterial_ulcer

Vassalli, J., Sappino, A. and Belin, D. (1991) The Plasminogen-Activator Plasmin System. *Journal of Clinical Investigation*, 88(4), 1067-1072.

Vazquez, R. and Larson, D.F. (2013) Plasma protein denaturation with graded heat exposure. *Perfusion-Uk*, 28(6), 557-559.

Vellard, M. (2003) The enzyme as drug: application of enzymes as pharmaceuticals. *Current Opinion in Biotechnology*, 14(4), 444-450.

Velnar, T., Bailey, T. and Smrkoli, V. (2009) The Wound Healing Process: an Overview of the Cellular and Molecular Mechanisms. *Journal of International Medical Research*, 37(5), 1528-1542.

Velonia, K., Flomenbom, O., Loos, D., Masuo, S., Cotlet, M., Engelborghs, Y., Hofkens, J., Rowan, A., Klafter, J., Nolte, R. and de Schryver, F. (2005) Single-enzyme kinetics of CALB-catalyzed hydrolysis. *Angewandte Chemie-International Edition*, 44(4), 560-564.

Verheyen, E., Delain-Bioton, L., van der Wal, S., el Morabit, N., Barendregt, A., Hennink, W.E. and van Nostrum, C.F. (2010) Conjugation of Methacrylamide Groups to a Model Protein via a Reducible Linker for Immobilization and Subsequent Triggered Release from Hydrogels. *Macromolecular Bioscience*, 10(12), 1517-1526.

Vermonden, T., Censi, R. and Hennink, W.E. (2012) Hydrogels for Protein Delivery. *Chemical Reviews*, 112(5), 2853-2888.

Vincent, A.M. and Feldman, E.L. (2002) Control of cell survival by IGF signaling pathways. *Growth Hormone and IGF Research*, 12(4), 193-197.

Voet, D., Voet, J.G. and Pratt, C.W. (1999) Enzyme Kinetics, Inhibition, and Regulation. *In:* Anon.*Fundamentals of Biochemistry.* USA: JohnWiley & Sons, Inc, 322-347.

WADA. (2017) *The World Anti-Doping Code: The International Standard Prohibited List January 2017.* WADA. Available at: https://www.wada-ama.org/sites/default/files/resources/files/2016-09-29_-_wada_prohibited_list_2017_eng_final.pdf [Accessed 04 September 2017].

Wagner, F.W. (1981) The dysvascular foot: a system for diagnosis and treatment. *Foot Ankle International,* 2, 64-122.

Walder, C., Errett, C., Bunting, S., Lindquist, P., Ogez, J., Heinsohn, H., Ferrara, N. and Thomas, G. (1996) Vascular endothelial growth factor augments muscle blood flow and function in a rabbit model of chronic hindlimb ischemia. *Journal of Cardiovascular Pharmacology*, 27(1), 91-98.

Walsh, K.A. (1970) Trypsinogens and trypsins of various species. *Methods in Enzymology*, 19, 41-63.

Walter, M.N.M., Wright, K.T., Fuller, H.R., MacNeil, S. and Johnson, W.E.B. (2010) Mesenchymal stem cell-conditioned medium accelerates skin wound healing: An in vitro study of fibroblast and keratinocyte scratch assays. *Experimental Cell Research*, 316(7), 1271-1281.

Weinreb, N., Barranger, J., Packman, S., Prakash-Cheng, A., Rosenbloom, B., Sims, K., Angell, J., Skrinar, A. and Pastores, G.M. (2007) Imiglucerase (Cerezyme((R))) improves quality of life in patients with skeletal manifestations of Gaucher disease. *Clinical Genetics*, 71(6), 576-588.

Weitz, J., Byrne, J., Clagett, G., Farkouh, M., Porter, J., Sackett, D., Strandness, D. and Taylor, L. (1996) Diagnosis and treatment of chronic arterial insufficiency of the lower extremities: A critical review. *Circulation*, 94(11), 3026-3049.

Werner, S. (1998) Keratinocyte growth factor: A unique player in epithelial repair processes. *Cytokine & Growth Factor Reviews,* 9(2), 153-165.

Werner, S. and Grose, R. (2003) Regulation of wound healing by growth factors and cytokines. *Physiological Reviews,* 83(3), 835-870.

Werner, S., Krieg, T. and Smola, H. (2007) Keratinocyte-fibroblast interactions in wound healing. *Journal of Investigative Dermatology,* 127(5), 998-1008.

White, L., Mitchell, T. and Brinckerhoff, C. (2000) Transforming growth factor beta inhibitory element in the rabbit matrix metalloproteinase-1 (collagenase-1) gene functions as a repressor of constitutive transcription. *Biochimica Et Biophysica Acta-Gene Structure and Expression,* 1490(3), 259-268.

Williams, R.M., McDonald, A., O'Savage, M. and Dunger, D.B. (2008) Mecasermin rinfabate: rhIGF-I/rhIGFBP-3 complex: iPLEX (TM). *Expert Opinion on Drug Metabolism & Toxicology,* 4(3), 311-324.

Witte, M. and Barbul, A. (2005) General principles of wound healing. *Surgical Clinics of North America,* 77(3), 509-528.

Woolfson, A.D., Malcolm, R.K., Campbell, K., Jones, D.S. and Russell, J.A. (2000) Rheological, mechanical and membrane penetration properties of novel dual drug systems for percutaneous delivery. *Journal of Controlled Release,* 67(2–3), 395-408.

Worthington Biochemical Corporation. (2017) *Worthington pepsin assay.* Lakewood, NJ: Worthington Biochemical Corporation. Available at: http://www.worthington-biochem.com/pm/assay.html [Accessed 24/11/2017].

Wu, S.C., Driver, V.R., Wrobel, J.S. and Armstrong, D.G. (2007) Foot ulcers in the diabetic patient, prevention and treatment. *Vascular Health and Risk Management,* 3(1), 65-76.

Wysocki, A.B. (2002) Evaluating and managing open skin wounds: colonization versus infection. *AACN Clinical Issues,* 13(3), 382-397.

Xu, W., Hong, S.J., Jia, S., Zhao, Y., Galiano, R.D. and Mustoe, T.A. (2012) Application of a partial-thickness human ex vivo skin culture model in cutaneous wound healing study. *Laboratory Investigation,* 92(4), 584-599.

Yager, D., Zhang, L., Liang, H., Diegelmann, R. and Cohen, I. (1996) Wound fluids from human pressure ulcers contain elevated matrix metalloproteinase levels and activity compared to surgical wound fluids. *Journal of Investigative Dermatology,* 107(5), 743-748.

Yang, X., Yang, K., Wu, S., Chen, X., Yu, F., Li, J., Ma, M. and Zhu, Z. (2010) Cytotoxicity and wound healing properties of PVA/ws-chitosan/glycerol hydrogels made by irradiation followed by freeze-thawing. *Radiation Physics and Chemistry,* 79(5), 606-611.

Yates, C.C., Hebda, P. and Wells, A. (2012) Skin Wound Healing and Scarring: Fetal Wounds and Regenerative Restitution. *Birth Defects Research Part C-Embryo Today-Reviews,* 96(4), 325-333.

Zbu, X. and Papayannopoulos, I.A. (2003) Improvement in the Detection of Low Concentration Protein Digests on a MALDI TOF/TOF Workstation by Reducing alpha-Cyano-4-hydroxycinnamic Acid Adduct Ions. *Journal of Biomolecular Techniques,* 14, 298-307.

Zeng, G., McCue, H., Mastrangelo, L. and Millis, A. (1996) Endogenous TGF-beta activity is modified during cellular aging: Effects on metalloproteinase and TIMP-1 expression. *Experimental Cell Research,* 228(2), 271-276.

Zhang, X., Ibrahimi, O., Olsen, S., Umemori, H., Mohammadi, M. and Ornitz, D. (2006) Receptor specificity of the fibroblast growth factor family - The complete mammalian FGF family. *Journal of Biological Chemistry,* 281(23), 15694-15700.

Zheng, D. and Lu, H.P. (2014) Single-Molecule Enzymatic Conformational Dynamics: Spilling Out the Product Molecules. *Journal of Physical Chemistry B,* 118(31), 9128-9140.

Zhuang, X., Kim, H., Pereira, M., Babcock, H., Walter, N. and Chu, S. (2002) Correlating structural dynamics and function in single ribozyme molecules. *Science*, 296(5572), 1473-1476.